(20)

Hydrofoil Ship
Structural Design Criteria Study

FINAL REPORT
Contract NObs-4791

MARTIN

(3) Martin Co., Baltimore, Md.

(6) (Upper Case)

Hydrofoil Ship

Structural Design Criteria Study.

(7) FINAL REPORT.

(15) [redacted] NObs-74791

(14) ER-13727

(11) Feb[redacted]65,

(12) 10

(8)

MARTIN
BALTIMORE DIVISION
BALTIMORE, MARYLAND 21203

FOREWORD

A previous report on the Hydrofoil Craft Structural Design Study (Martin Engineering Report 11706) had been prepared for the Bureau of Ships under Contract NObs-4376 in 1961. A subsequent review of that report in 1964 indicated the need for extensive revision, and this has been accomplished under Contract NObs-4791.

This report completely supersedes the earlier report.

CONTENTS

CONTENTS (continued)

CONTENTS (continued)

1.0 SUMMARY

A study has been made of environmental conditions and the corresponding vehicle response characteristics to develop a rational method for determining structural design criteria for hydrofoil ships. While the methods are relatively general, application is made to a specific 280-ton hydrofoil ship ~~(similar to PCH)~~ in ASW missions in the North Atlantic environment.

Loading conditions are analyzed for both hullborne and foilborne conditions to determine statistical distributions of the pressures and loads which may be expected on various areas of the hull. These loadings are compared with existing seaplane loading specifications and interpreted in terms of past experience in seaplane design. Analysis of typical structures for the overall hull bending, bottom plating and stringers and decks and supporting structure is carried out for static strength, fatigue life and stiffness under the loading conditions. Statistical loadings for the struts and foils are determined, but evaluation of the controlled ship response and detail foil and strut structure is not included as a part of this study.

It is concluded from the analysis of the structure that both static strength and fatigue life must be considered in the design of hydrofoil ship structure. In the particular example ship, design fatigue life is the determining factor for overall hull bending and local design of forward areas of the hull bottom, while static strength or stiffness is of most importance on midship and after areas of the hull and the deck structure. Very low deadrise angles (5 to 6°) lead to very large local pressures and high landing accelerations which may become critical for static strength determination of overall hull bending.

Recommendations for continued work are developed on the basis of the study results. Experimental work is necessary to more clearly establish the relation between static strength design and the highly transient loading represented by low deadrise impacts, and specific fatigue life characteristics should be determined for typical welded aluminum hull bottom structure. Measurements of the slamming behavior and sinking speeds in the landing approach should be made in actual service conditions representative of ASW tactical operation.

2.0 INTRODUCTION

The structural design of a hydrofoil ship for open sea operation is a challenging problem. Efficient exploitation of the high speed capabilities of the hydrofoil places a premium on lightweight structure, yet the conditions of operation in both hullborne and foilborne modes may impose large loads on the structure.

In classes of vehicles where there is a long background of experience, the criteria for structural design have often been condensed to simple statements of maneuver load factors (as for aircraft), working allowables in terms of 1 g loads (as in ships, bridges, etc.) or other "rule of thumb" design guides. This assumes that the actual future loading conditions and material characteristics will be within the bounds of the previous experience. In the design of high performance aircraft and missile systems, such as approach is already outmoded due to dissimilarities of design and the relatively increased importance of repeated loads.

Particularly, the rapid advances in large hydrofoil ship design without a substantial background of applicable operational experience require a rational analysis system for the establishment of suitable structural design criteria. It is the purpose of this report to examine the environmental and structural characteristics of the hydrofoil ship in both hullborne and foilborne operation in the open sea to determine a rational buildup of design loads criteria and show by examples how these may be applied to a typical design.

3.0 GENERAL DESIGN CONSIDERATIONS

3.1 SUMMARY

In order to proceed with a finite study of such a broad field as structural design for hydrofoil craft, it becomes necessary to limit the investigation. For this reason the approach which follows is a combination of specific and general factors. To provide concrete examples a particular ship and mission have been defined as the example design, the typical environment of the North Atlantic has been assumed, and fairly simple analyses have been used to determine the ship responses to loads. However, the methods of determination of the loading spectrums and the reactions in the ship structure are believed to be representative and applicable to much broader classes of hydrofoil ships.

3.2 THE STUDY SHIP

The particular design selected for the study example is an outgrowth of the PC(H). The general hull form and foil configuration have been followed while increasing the gross weight to 280 tons.

In sizing the configuration for minimum weight, one of the influencing parameters to study is the density value, the total displacement divided by the volume (lb/cu ft). A comparison of density values of the 110-ton PC(H) and other craft disclosed that the PC(H) was on the low side with room for loading growth. Subsequent studies and evaluation of the extent to which density of the PC(H) could be increased resulted in the determination that it could be doubled.

Comparison of Vehicle Density

	lb/cu ft
PC(H) 110-ton version, BuShips	8.1
Hydrofoil boat--80 ton, Maritime Administration	11.8
Patrol craft-type vessel	22.0
Destroyers	23.0
Seaplane--large type	21.6
PC(H) 110-ton densified to 195 ton (study)	17.6

This study included rearrangement of crew living and working areas to accommodate additional personnel, adaptation to a modern weapon system, space provisions for future ASW electronic equipment, an investigation into maximum fuel capacity increases possible by utilizing the voids under the platform decks as tanks, a review of various propulsion systems capable of satisfying the requirements of increased weight resulting from density increases, and finally, a reappraisal of the hull, foil and strut structure for the increased weight. These data, coupled with experience in aircraft applications, resulted in the choice of a density value of 14 lb/cu ft which represents a compromise with regard to the maximum attainable value of 17.6 lb/cu ft estimated to be possible

in the PC(H) design.

A volumetric size for the 280-ton hydrofoil craft was established based on this value of 14 lb/cu ft and resulted in the following dimensions:

Length	130 ft between perpendiculars
Beam	35 ft molded maximum
Depth	16 ft midships

The hull form configuration is identical to that of the BuShips 110-ton PC(H). An interior arrangement study showed that this configuration has enough available space for 30 days of continuous sea operation for 37 crew members, sufficient fuel capacity below the platform deck for at least 30% of the loaded weight and space for various combinations of gas turbine and diesel machinery.

A canard foil configuration with a 70% to 30% load distribution, a loading of 1150 psf and a foil aspect ratio of 4.0 is used as a representative system. This system is similar to that of the PC(H) design in the arrangement of the struts and foils, but differs in the aspect ratio of the foils. The aspect ratio of 4.0 was chosen as a good compromise based on hydrodynamic, structural, lightweight, handling and docking considerations.

At 45-kn design speed this foil configuration gives a design lift coefficient of:

$$C_{L_{\text{design 45}}} = 1150/(76)^2 = 0.2, \quad 1150 = GW/545$$

and the lift curve slope is estimated to be:

$$C_{L_{\alpha 45}} = 4.3/\text{rad} = 0.075/\text{deg}$$

The foil configuration for the 100 knot design is estimated to be roughly similar but with supercavitating foils at much higher loading:

$$C_{L_{\text{design 100}}} = 2850/(168.5)^2 = 0.1, \quad 2850 = GW/221$$

$$C_{L_{\alpha 100}} = 3.44/\text{rad} = 0.060/\text{deg}$$

The example reference configuration is shown in Figs. 3-1 and 3-2. The mission chosen for the study is the ASW patrol mission. It will be recognized that such a choice does not explicitly define the detail operational history of a particular ship or even the average of a class of ships since the use of a new type vehicle can be expected to lead to new techniques. However, for the purposes of the study the following characteristics have been selected as representative of the actual operational requirements for hydrofoil ships used in ASW missions:

1. Operational availability 60% of time
2. Hullborne operation 90% x 60% = 54% of time
3. Foilborne 10% x 60% = 6% of time
4. Maximum hullborne speed 15 kn
5. Design foilborne speed 45 and 100 kn
6. Autopilot and control system designed for operation in Sea State 5
7. Distribution of hullborne operation speeds as shown in Fig. 3-3

3.3 ENVIRONMENT

The North Atlantic is assumed to be a representative area in which to operate a hydrofoil craft on barrier ASW missions. The "Climatological and Oceanographic Atlas for Mariners" (Ref. 1) presents cumulative frequency distributions of the North Atlantic surface wave heights and periods, for specific observation stations, in the format shown in Figure 3-4. These curves provide the basis for the computation of wave heights and lengths for this study. The data from six selected representative observation posts were selected for inclusion in this study:

(a) 26° to 30° N; 70° to 84° W
(b) 35° to 37° N; 68° to 70° W
(c) 40° to 44° N; 66° to 70° W
(d) 33° to 35° N; 48° to 50° W
(e) 43° to 45° N; 40° to 42° W
(f) 50° to 52° N; 36° to 38° W

The yearly cumulative frequency distributions of wave heights and periods from these six stations, covering the four seasons of the year, represent a fair average of the North Atlantic surface conditions from the southern sector to the northern sector. However, it is to be pointed out that wide variations can exist between these sectors and that specific designs should take due note of this fact in determination of the wave height and frequencies to be anticipated where specific operational times in given localities would yield something other than the average conditions used for demonstration purposes in this report. The differences between the northern and southern sectors are dramatically demonstrated in Figs. 3-5 and 3-10.

The data in Figs. 3-4 and 3-5 were gathered by periodic observations of wave height and frequency and therefore represent a time distribution of the surface conditions. To transform these data into frequency distributions representing numbers of waves the following procedure was used. One wave height, 5-1/2 ft, with one wave period, 8 sec, is used in the example.

(1) By using Fig. 3-4 as an example, and by considering 1-ft intervals, the percentages of time at $\geq$5 ft and $\geq$7 sec, and $\geq$5 ft $\geq$9 sec are read directly from the curves, and the difference is interpreted as the percentage of time at $\geq$5 ft waves having 8-sec periods.

Similarly, the values at $\geq$6 ft $\geq$7 sec and $\geq$6 ft $\geq$9 sec are interpreted as $\geq$6 ft waves at 8-sec periods. Then, the difference between these two percentages is interpreted as the percentage of time that waves of 5-1/2 ft in height and 8-sec periods exist at that particular observation station.

(2) The time percentage for all other stations is similarly obtained and combined on the basis of the amount of operational time to be spent in each locality. In this example an equal amount of time is assumed to be spent in each locality and hence the average of the time percentage of all stations was used.

(3) For each 1-ft interval of wave height and period, the number , N, of waves over a given length of time is obtained from

$$N = K\%(T) \times \frac{\text{Chosen period of time (sec)}}{\text{Wave period (sec)}}$$

For the example for 1 yr

$$N_{5\text{-}1/2 \text{ ft, } 8 \text{ sec}} = 1.3\% \, T_{5\text{-}1/2 \text{ ft, } 8 \text{ sec}} \times \frac{\text{(seconds per year)}}{8}$$

$$= 0.013 \times \frac{(365 \times 24 \times 60 \times 60)}{8}$$

$$= 51,100 \text{ waves/yr.}$$

Thus, in the example there are 51,100 waves which are 5-1/2 ft in height and have a period of 8 sec. Or, more correctly, since a 1-ft interval was used in the determination, there are 51,100 waves between 5 and 6 ft in height having periods between 7 and 9 sec.

(4) Since it is more convenient to use the length of the waves rather than the wave period in ship design, the empirical conversion factor (Ref. 2)

$$L_w = 3.41(T_w)^2 \quad \text{was used.} \quad T_w = \text{Wave period, sec}$$

The distribution of wave heights and lengths so determined is shown in Fig. 3-6, and is considered an average representation of the surface condition of the western North Atlantic Ocean.

Since the data presented in Ref. 1 were based primarily on visual wave observations by experienced observers, the heights are "significant heights," or the average height of 1/3 highest of the waves. The distribution of "average" and 1/10 highest waves according to the von Neumann spectrum (Ref. 2) was determined and is shown in Fig. 3-7. For the redistribution of the observed waves the spectrum is lumped in 3 groups as shown. The cumulative occurrences for each wave length, redistributed according to the von Neumann spectrum, are shown in Figs. 3-8 through 3-11 for the significant waves.

In using the wave data it should be noted that the occurrences represent numbers of waves passing a fixed point or small area. For the low speeds involved in the calculations for the displacement condition the data can be used directly. But at foilborne speeds, the number of waves encountered is determined from the relative ship speed multiplied by the time on foils divided by the wave length.

3.4 SHIP RESPONSE TO EXTERNAL LOADS

Load producing incidents are reacted by the vehicle in three basic modes: static balance of weight and impressed loads, rigid body inertial reaction to time variant loads and flexural response to rapidly applied loads or impulses. In the most general case of all, these would be considered simultaneously, but it is beyond the scope of this study to consider the flexural response mode in detail (even by itself). For the type of hull forms to be considered it is estimated that the major factors in design criteria may be evaluated in terms of the rigid body responses and that consideration of the flexural effects should be assigned to specific design analysis. This procedure has been used successfully in aircraft and missile structural specifications.

The vehicle response to static loads (buoyancy or steady foilborne) or single impact loads may be simply determined. For combinations of loads the solution of the problem is a little more devious and requires some assumption as to the location and magnitude of part of the loading system. For example, consider the rigid body supported by two forces:

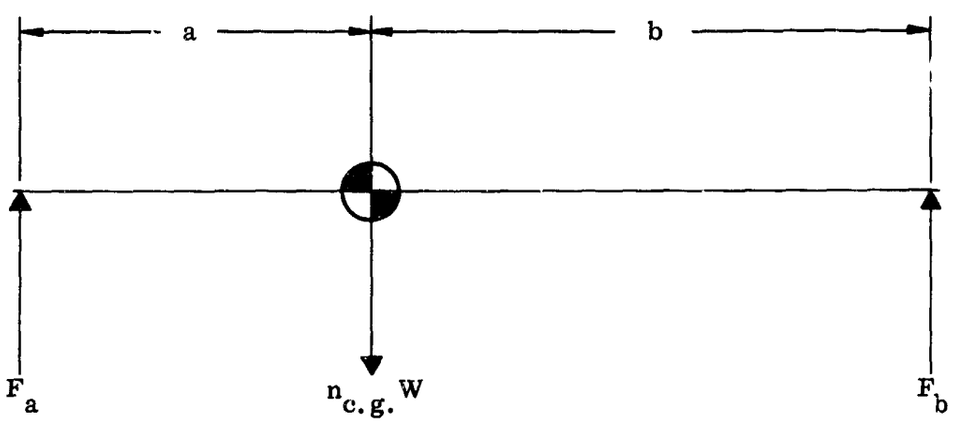

$$F_a + F_b = n_{cg}W \tag{1}$$

$$aF_a + \frac{Wk^2}{g}\ddot{\theta} = bF_b \tag{2}$$

If $F_a = 0$, then $n_{cg} = \frac{F_b}{W}$ and the load factor at b is:

$$n_b g = n_{cg} g + \ddot{\theta} b = n_{cg} g + \frac{b^2 F_b}{W k^2} g = \frac{F_b}{W} g \left(1 + \frac{b^2}{k^2}\right) \quad (3)$$

Thus, an impact at b can be treated as though a reduced mass, $\frac{W}{g} \Big/ \left(1 + \frac{b^2}{k^2}\right)$, were being subjected to the external conditions at b with a resulting increase in load factor.

If $F_a \neq 0$ and both F_a and F_b are loads due to impact, the pair of equations, Eqs (1) and (2), must be solved simultaneously. This can be done by iterative procedures, but the solution will be too sensitive to errors in approximations involved in impact formulas to be significant. Where F_a and F_b are the foil loads, they are so dependent upon the foil control laws that they must be considered as specific design problems.

When one of the forces, say F_a, is primarily constant (as from buoyancy) during an impact, the equations may be written in a combined form in the following manner:

$$F_a = B$$

$$B + F_b = n_{cg} W = n_b W - \frac{b\ddot{\theta}}{g} W \quad (1a)$$

$$aB + \frac{Wk^2}{g} \ddot{\theta} = bF_b$$

$$\frac{bW}{g} \ddot{\theta} = (bF_b - aB) \frac{b}{k^2} \quad (2a)$$

Substituting in (1a) for $\ddot{\theta}$,

$$F_b = n_b W - B - (bF_b - aB) \frac{b}{k^2} . \quad (3a)$$

For cases where B = W, this equation becomes:

$$\frac{F_b}{W} \left(1 + \frac{b^2}{k^2}\right) = n_b - 1 + \frac{ab}{k^2} \quad (4a)$$

Comparison with Eq (3) shows the increase in load, F_b, that would be necessary to give the same accelerations at b, when a buoyant force equal to the vehicle weight is acting at a distance, a, on the opposite side of the cg. When a = 0, the conditions of impact correspond to the weightlessness assumption of the simplest hydrodynamic impact formulations, and Eq (4a) is then the same as Eq (3), except that the acceleration at the point b is (load factor - 1) g.

Looking a little further to the source of these loads, we see that they arise from the extent of pressures over the hull surfaces. Hydrodynamic theory for dynamic pressures in planing and impact provides the way to determine the level of pressure and load to be expected from prescribed disturbances.

In the determination of the local pressures on the bottom, the contact conditions (normal velocity and angle) and body geometry are sufficient for the application of the general pressure formula as developed in Ref. 3.

$$\text{Peak pressure} = \frac{\rho/2 V_n^2}{\sin^2 \tau^* + \frac{4 \tan^2 \beta}{\pi^2} \cos^2 \tau^*} = \frac{\rho/2 V_n^2}{f(\theta, \tau, \phi, \beta)} \qquad (5)$$

where

ρ	=	density of water ≈ 2.
V_n	=	velocity components normal to average bottom slope including: sinking speed, v_s, component of ship speed normal to bottom slope, V_s $(\theta + \tau)$, and the wave orbital velocity.
τ^*	=	$\lvert\theta + \tau - \phi\rvert$ in rough water for the nomenclature of this report.
θ	=	angle of hull reference (positive bow up) to horizon.
τ	=	angle of butt line to hull reference (positive up toward bow).
ϕ	=	wave slope at contact with hull bottom (positive upward slope to the direction of ship motion).
β	=	deadrise angle of hull.

Average pressure is given in Fig. 3-12 as the ratio of $P_{average}$ to P_{peak} versus the range of deadrise angles. The data in Ref. 4 for 20 to 50° deadrise are extended to lower values of deadrise by fairing to the analytical values at very low deadrise angles according to the basic Wagner analysis in Ref. 5.

The determination of loads and accelerations is not a simple matter because a substantial time interval, area of bottom wetting, and ship motion are involved. Extensive work has been done with strip analysis methods to give solutions to the impact problem in great detail. However, for the present study a simpler analysis has been used based upon several approximations:

(1) The length of hull in the impacting region is treated as a constant deadrise prism in linear, two-dimensional motion (the effect of angular acceleration is accounted for by using a reduced mass of hull).

(2) The momentum exchange during the impact is between the hull and the virtual water mass moving with the bottom section without loss to the wake.

(3) The exact shape of wetted area is relatively unimportant to the maximum load level.

On the basis of the first approximation, the average pressure is uniform over the submerged area and the load will be given by $P_{average}S$. The reduced ship mass for a force applied a distance x from the cg is obtained from the rigid body response Eq (3)

$$\frac{M}{\left(1 + \frac{x^2}{k^2}\right)} = M_r, \text{ the reduced mass.} \tag{3b}$$

The load represented by $P_{average}S$ must accelerate both this mass, M_r, and the virtual water mass, M_w, involved in the impact. The acceleration at the impacting station is thus:

$$a_x = \frac{P_{average}S}{M_r + M_w} \tag{6}$$

The second approximation is common to most hydrodynamic impact theoretical analyses. It is acceptable for substantial load levels where the loss of momentum to the wake is relatively small. It relates the penetration velocity, v_n, at any time to the initial contact velocity v_{n0}.

$$v_n (M_r + M_w) = v_{n0} (M_r) \tag{7}$$

The equations of pressure, velocity and mass relationships (Eqs 5, 6 and 7) may be combined to give:

$$a_x = \frac{f(\beta)\, v_{n0}^2\, S}{M_r \left(1 + \frac{M_w}{M_r}\right)^3 f(\theta, \tau, \phi, \beta)} \tag{8}$$

The reasonableness of the third approximation may be shown by evaluation of the above equation for several possible shapes for actual impact areas: rectangular, triangular and elliptical. The virtual water mass associated with the impact is given in general form by the integral:

$$M_w = \rho \frac{\pi}{2} K \int_{x_1}^{x_2} y^2 \, dx \tag{9}$$

where

y = wetted half width at x

$\rho \frac{\pi}{2} y^2$ = mass per unit length of half circular cylinder

K = correction factor for associated water mass

$K = \frac{(1 - 2\tan\beta)}{\pi}$ (approximate for $\beta = 0°$ to $40°$)

The results of calculations for area and water mass may be shown in tabular form:

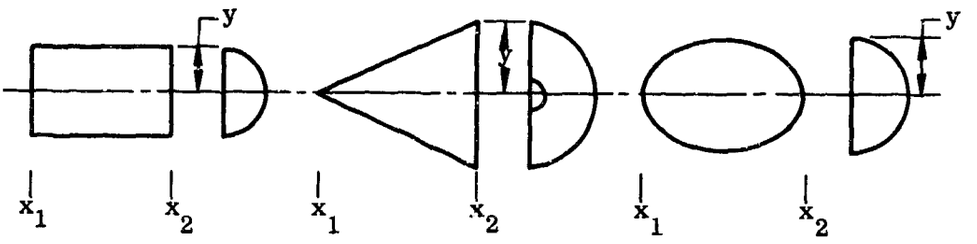

$\frac{x_1 - x_2}{2y_{max}}$ =	a =	b =	c
S =	$4ay_a^2$	$2by^2$	πcy^2
M_w =	$\rho K \pi a y^3$	$\rho K \frac{\pi}{3} b y^3$	$\rho K \frac{2\pi}{3} c y^3$
	[(for equal M_w) $y = y_1$	$y_2 = y_1 \sqrt[3]{3}$	$y_3 = y_1 \sqrt[3]{1.5}$]

It will be noted that the equation for the local acceleration, a_x, can be written as:

$$a_x = \frac{f_0\,(\text{geometry},\ v_{n0})\,y^2_{max}\ f_1\ (\text{geometry})}{M_r\left[1 + y^3_{max}\ f_2\ \ (\text{geometry},\ M_r)\right]^3} \qquad (8a)$$

where f_0, f_1 and f_2 include the factors in the peak pressure, area and virtual water mass which are invariant with time.

During the course of a given impact the immersion width, y, increases, and the area and virtual water mass both increase. At first the increase in the area is the controlling factor, and the load increases with time. However, the higher exponent of the denominator in Eq (8) eventually results in such a rapid increase that the load reaches a peak and then decreases. The peak acceleration is determined where the derivative of a_x with respect to time is zero.

when

$$\frac{d\ a_x}{dt} = 0; \qquad y^3_{max} = \frac{2}{7f_2}; \text{ and } \frac{M_w}{M_r} = \frac{2}{7}$$

and the maximum acceleration is obtained by substituting in Eq (8a)

$$a_{x_{max}} = f_0 f_1 \left(\frac{2}{7f_2}\right)^{2/3} \Big/ \ M_r \left(1 + \frac{2}{7}\right)^3 \qquad (8b)$$

$$f_1 = S/y^2$$

$$f_2 = M_w/M_r\, y^3$$

$$a_{max} = \frac{f_0}{(M_r)^{1/3}} \left(\frac{2}{7}\right)^{2/3} \frac{1}{\left(1 + \frac{2}{7}\right)^3} \frac{S}{(M_w)^{2/3}} \qquad (10)$$

	Rectangular	Triangular	Elliptical
$(\rho K)^{2/3} \left(\frac{S}{(M_w)^{2/3}}\right)$	$1.86\ a^{1/3}$	$1.95\ b^{1/3}$	$1.92\ c^{1/3}$

thus, the maximum acceleration (or load) is almost invariant with the type of wetted area shape and varies directly with the cube root of the ratio of length to width of the wetted area. This ratio must be estimated on the basis of the particular conditions of impact being investigated. Since the load varies with the cube root, only moderate variance will be introduced by errors in this estimation.

$$a_{max} = 0.25\,(f_0)\left(\frac{\text{length}}{\text{width}}\right)^{1/3}\left(\frac{1}{K}\right)^{2/3}\left(\frac{1}{M_r}\right)^{1/3} \qquad (10a)$$

$$f_0 = P_{av_0}$$

The factor $0.25 \times \frac{P_{av}}{P_p} \times \left(\frac{1}{K}\right)^{2/3}$ is a function of deadrise angle β and is plotted in Fig. 3-12. The working equation for acceleration is then written as:

$$a_{max} = \left[0.25\,\frac{P_{av}}{P_p}\,\frac{1}{\left(1 - \frac{2\tan\beta}{\pi}\right)^{2/3}}\right]\left(\frac{\text{length}}{\text{width}}\right)^{1/3}\left(\frac{1}{M_r}\right)^{1/3} P_p \qquad (10b)$$

3.5 MATERIALS

The materials selected for use in the example design are weldable, medium strength aluminum alloys, 5456-0 and 6061-T6. Alloy 5456-0 is one of the most suitable materials for welding because of its high yield strength in the as-welded condition. Alloy 6061-T6 is considered best for non-welded applications where its high strength heat-treated characteristics can be maintained. Although its corrosion resistance is not the best, alloy 7075-T6 alclad is considered in many of the examples because its static strength is great. (7075-T6 is used extensively in high performance seaplane structure.)

The general characteristics of these aluminum alloys and other materials are given in ANC-5 and various industry handbooks. For convenient reference some of these data are shown herein. The crippling stress of sections in bending is shown in Fig. 3-13. Column allowables for aluminum tubes are shown in Fig. 3-14.

Foils and struts might utilize aluminum, steel or titanium. Critical bending allowables considering skin buckling are given in Fig. 3-15 for several typical alloys.

Special design data for permanent set behavior of typical seaplane plating-stringer combinations are reported in Ref. 6. The curves in Figs. 3-16 and 3-17 give the results of the study in general form for 7075-T6 alclad and 5456 material for two stringer configurations. A considerable increase in the strength of the plating supported by the wide flange of the J type stringer is evident. It should be noted that these data were obtained at 6-in. stringer spacing and the gain in strength for the J stringer will be less at greater spacing. (The Z stringer is nearly equivalent to a line support of the plating.) The accompanying plating stress is shown as a function of applied pressure in Fig. 3-18 for values less than yield (permanent set).

An important characteristic of the structural material is its fatigue life as used to typical structure. Stress as a function of life cycles for plating bending over Z stringers is given in Fig. 3-19, and results of typical seaplane bottom plating panels are shown in Figs. 3-20 and 3-21 (see Ref. 7). A more general form of the fatigue life for a typical riveted structure of 7075-T6 aluminum is shown in Fig. 3-22.

Specific allowable fatigue data for composite structures of welded 6061 and 5456 materials are unavailable. However, for this study generalized data will suffice to determine which conditions of loading may be fatigue critical. Generalized data proven by many element and overall tests to be reliable for composite aircraft structures are presented in Fig. 3-22 (Ref. 8). The data is Fig. 3-22 is based primarily upon 7075 materials, but is presented in nondimensional form by relating the amplitude, a, and the mean, m, stress to the ultimate strength, u, of the material. In this form, fatigue strength is plotted as constant life lines in terms of the parameter a/u and m/u. Because of the great variety of repeated loadings encountered by a structure, it is not feasible to express each in terms of its own particular spectrum. All properties can be expressed in terms of constant amplitude loading and are called S-N properties. Any straight line drawn across this constant life chart represents a specific S-N curve. The fatigue data presented in Fig. 3-22 corresponds to a theoretical stress concentration factor of approximately 3 which represents notched-type structure. This may be too severe for welded-type structure but until test data become available, it will suffice.

The analysis is made in terms of cycle ratio summations, that is, the fatigue life exhausted by various numbers of cycles (n_1, n_2.....n_n) of different repeated loads (1, 2.....n) is proportional to the sum of cycle ratios (n_1/N_1 + n_2/N_2 +..... +n_n/N_n) where N_1, N_2,.....N_n is the corresponding cycle to failure. $\sum N_n/N_n = 1$, though conservative for structures whose loadings are predominantly positive mean, will be used and considered as representing fatigue failure.

3.6 LOAD DEFINITIONS

Consistent with aircraft practice the following load and strength definitions are used throughout this study.

Limit Load: Limit loads or stresses are the maximum anticipated static loads or stresses to be experienced under the design conditions required of the vehicle in its function.

Yield Load: Yield loads or stresses are limit loads or stresses multiplied by a specified yield factor of safety.

Ultimate Load: Ultimate loads or stresses are limit loads or stresses multiplied by a specified ultimate factor of safety.

Yield Factor of Safety: The yield factor of safety is a specified minimum factor by which the yield strength of the material must exceed limit load or stress.

Ultimate Factor of Safety: The ultimate factor of safety is a specified minimum factor by which the ultimate strength of the material must exceed limit load or stress.

Yield Strength: The yield strength in terms of stress is as specified in MIL-Handbook-5, the stress equivalent to a 0.2% permanent set determined by the stress-strain relationship of the material considered.

Ultimate Strength: The ultimate strength in terms of stress is, as specified in MIL-Handbook-5, the failing stresses determined on the basis of the original unloaded cross sectional area.

Fatigue Loads: Fatigue loads are expressed by loading spectrums which define the number of repeated load applications, the mean load level and the amplitudes.

Fatigue Strength: Fatigue strength is expressed as the number of repeated loadings to cause failure under particular conditions defining load level, load amplitude, and procedure of repeated load application for a specified material.

Previous page was blank, therefore not filmed.

3.7 ILLUSTRATIONS

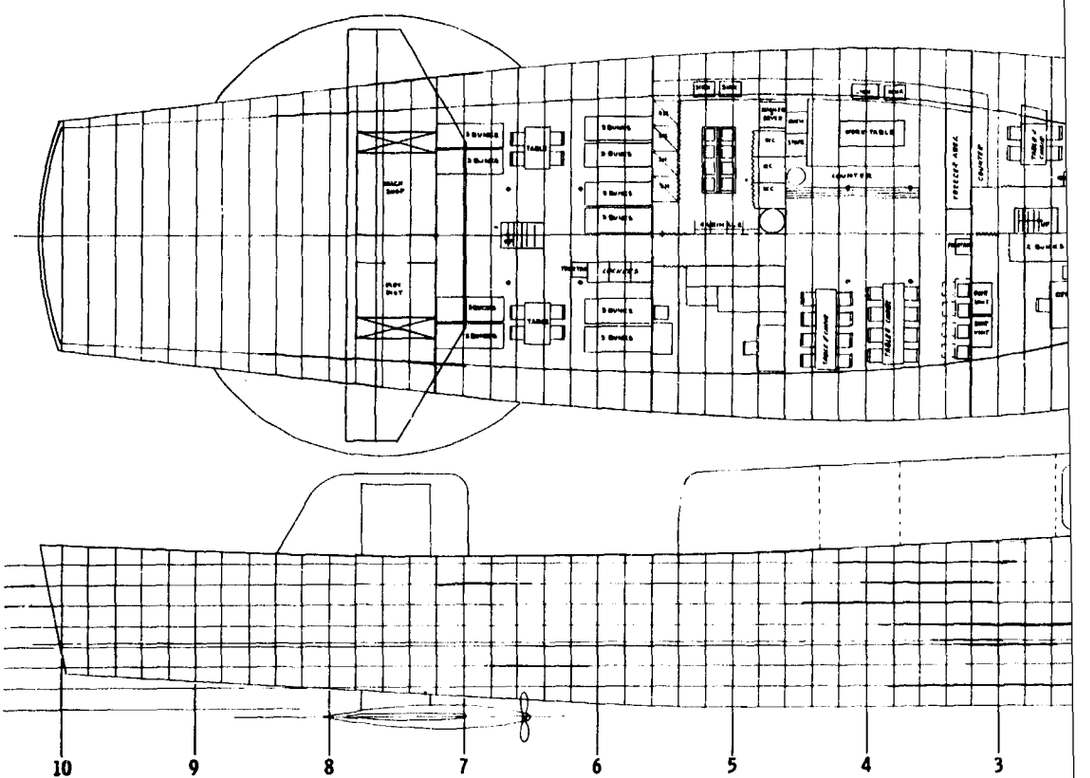
10
9
8
7
6
5
4
3

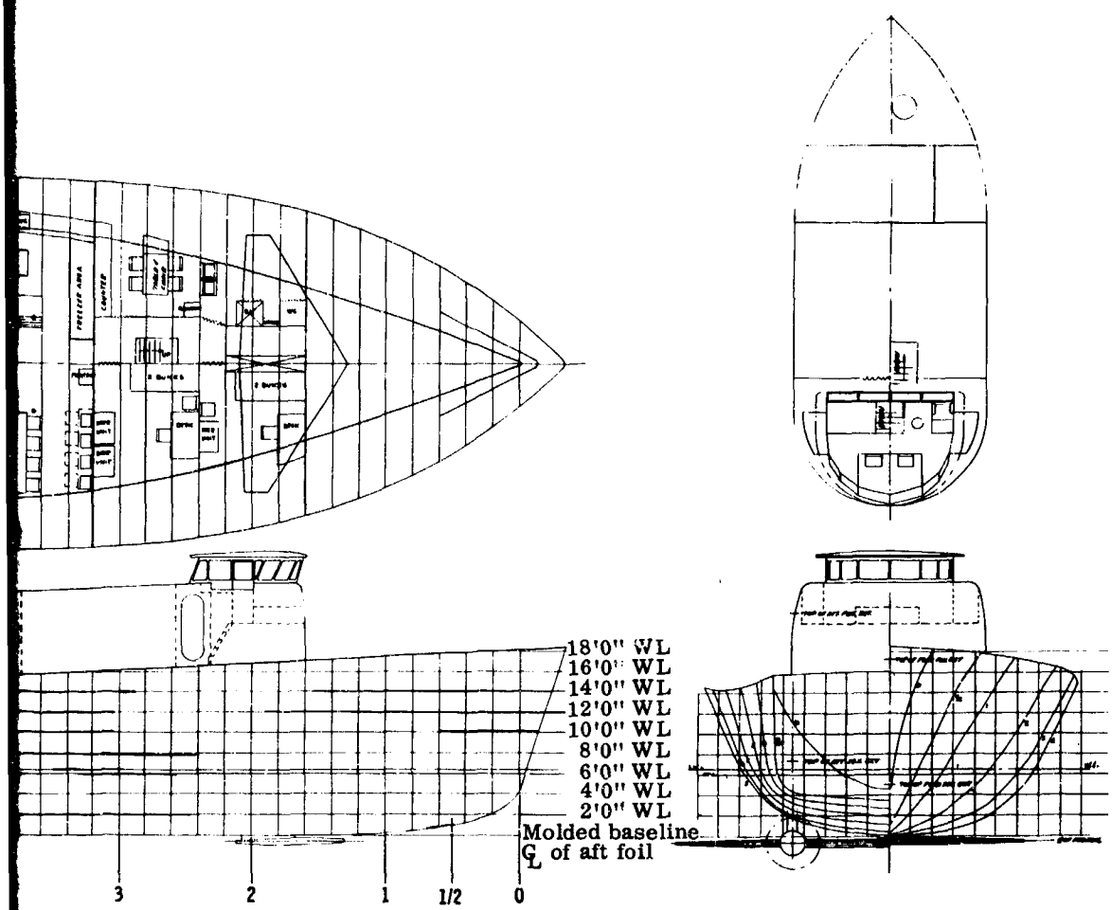

Fig. 3-1. Reference Configuration, 280-Ton Hydrofoil Craft

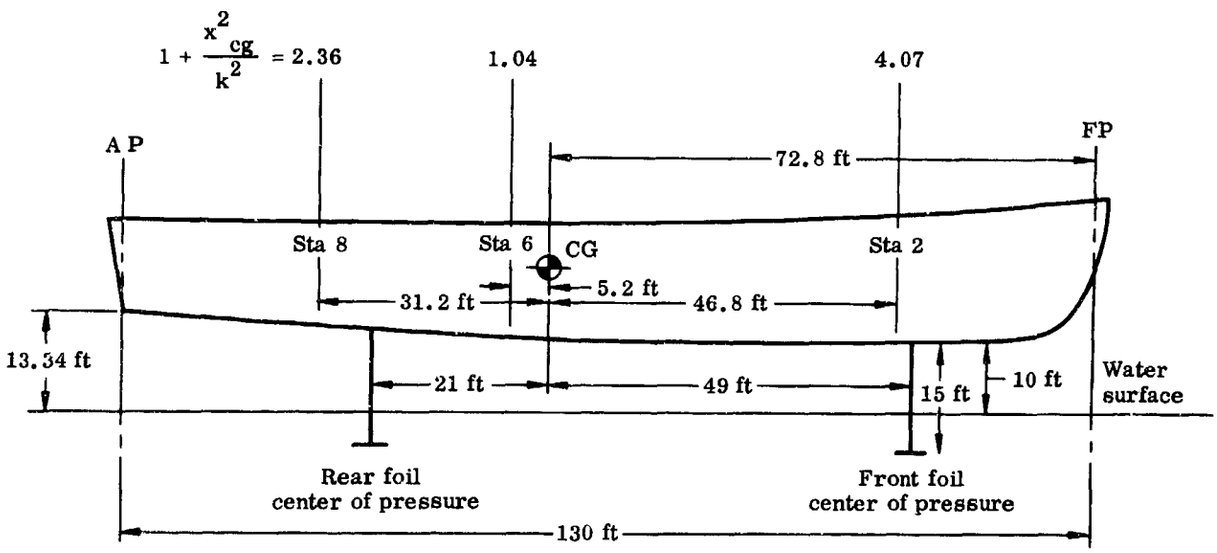

Foil Area

	Fwd.	Aft	Strut Chord
45-kn ship	165 sq ft	380 sq ft	5.0 ft
100-kn ship	66 sq ft	155 sq ft	7.5 ft

k (radius of gyration of ship's mass) = 26.7 ft

Fig. 3-2. Line Diagram of Pertinent Dimensions

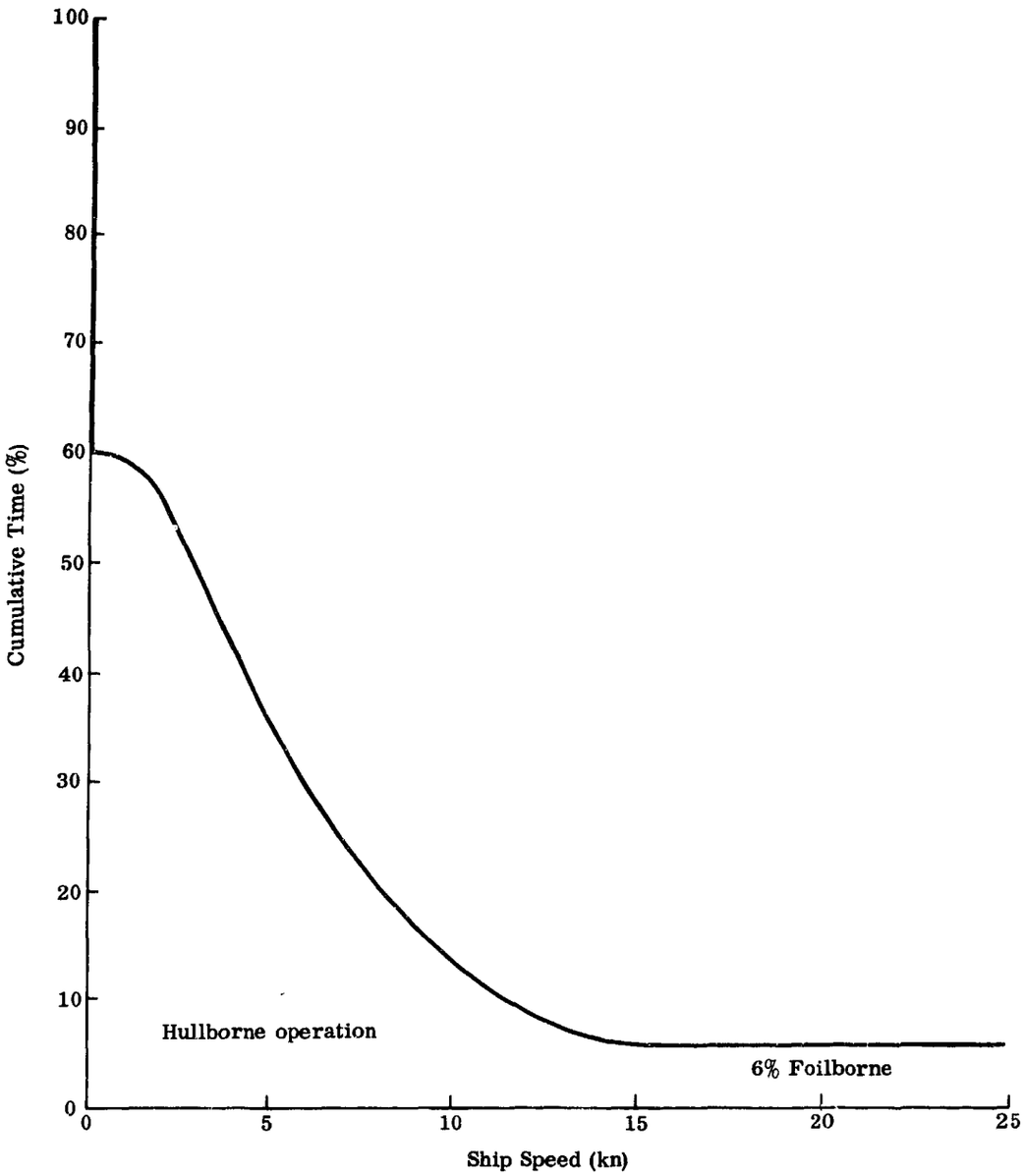

Fig. 3-3. Time (%)--Ship Speed Distribution

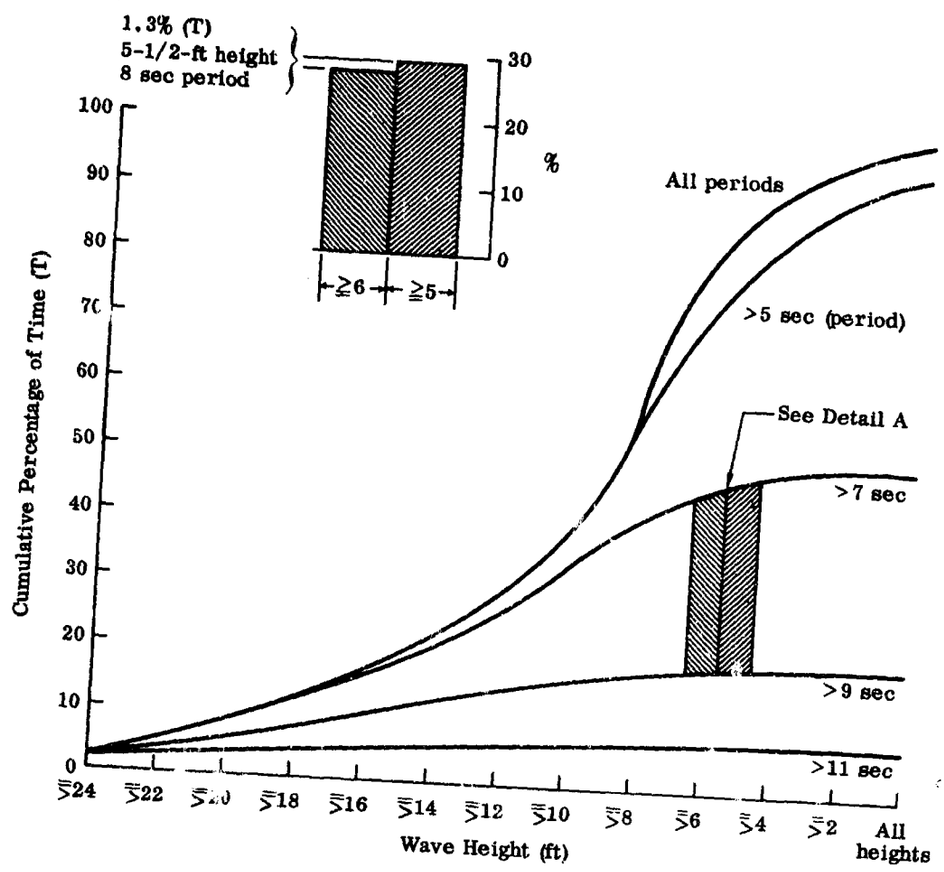

Fig. 3-4. North Atlantic Ocean Waves

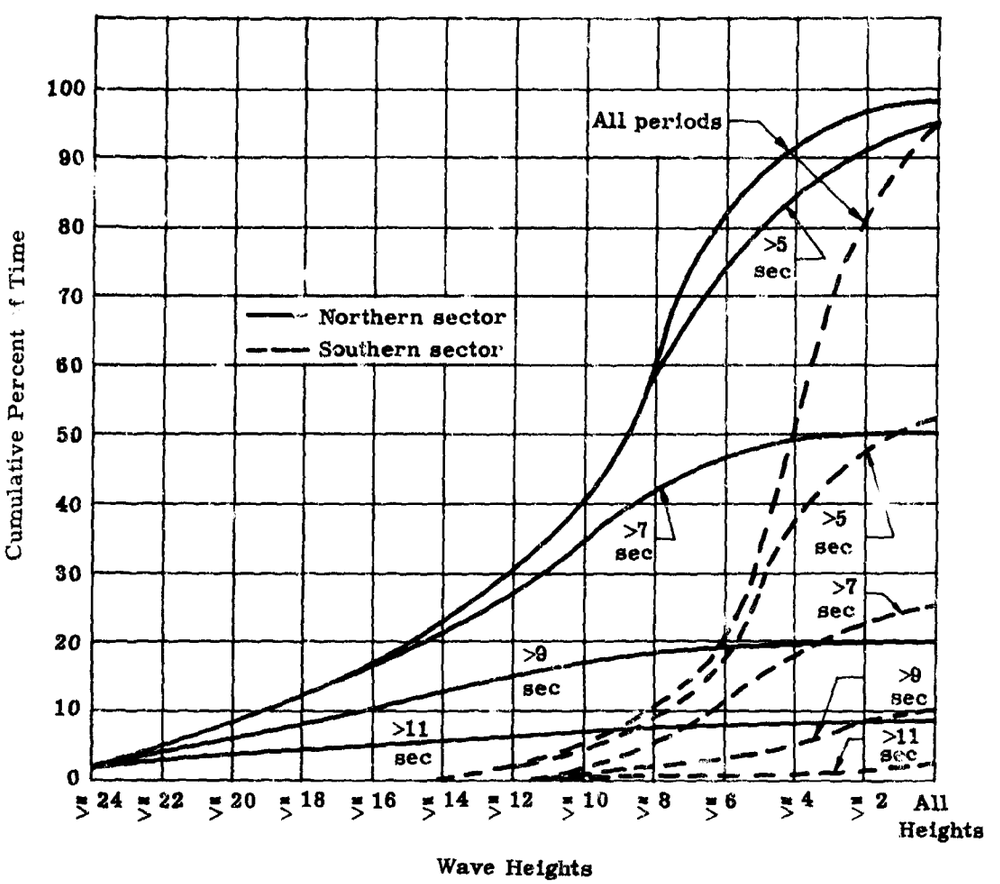

Fig. 3-5. Comparison of Waves at Two Areas in the North Atlantic

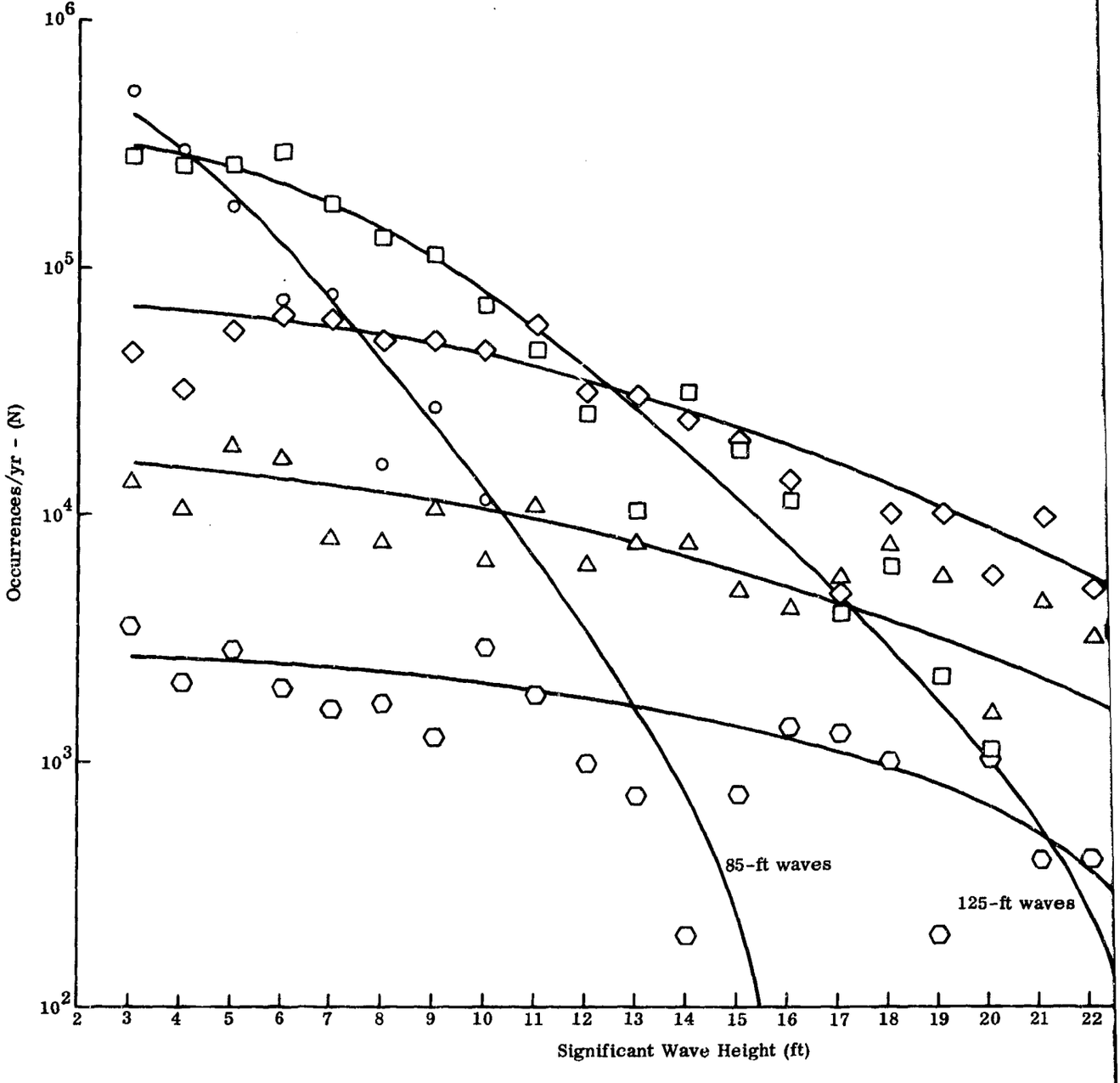

Fig. 3-6. Distribution of Wave Heights and Lengths Representative of Six Selected Areas of the North Atlantic Ocean

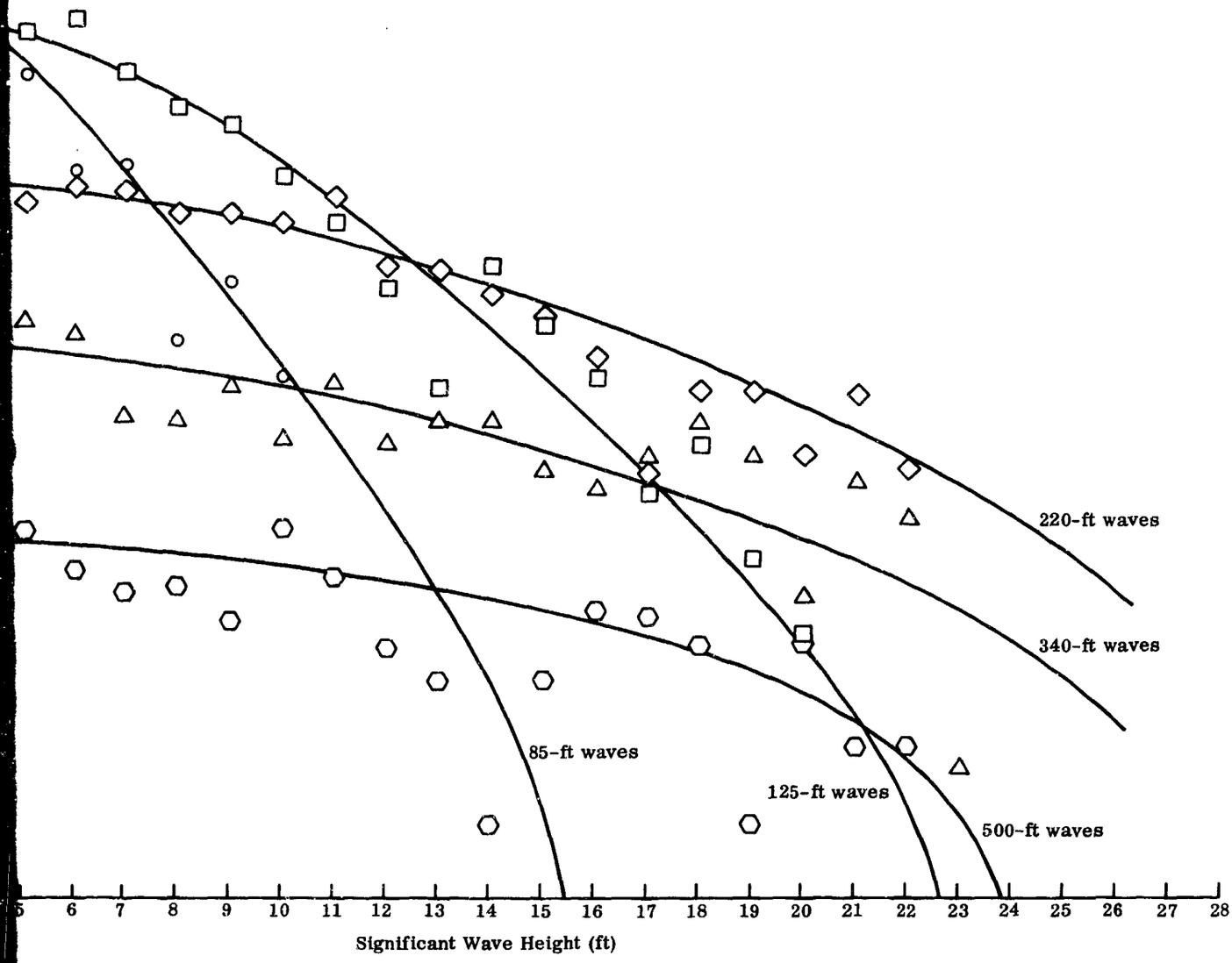

Fig. 3-6. Distribution of Wave Heights and Lengths Representative of Six Selected Areas of the North Atlantic Ocean

2

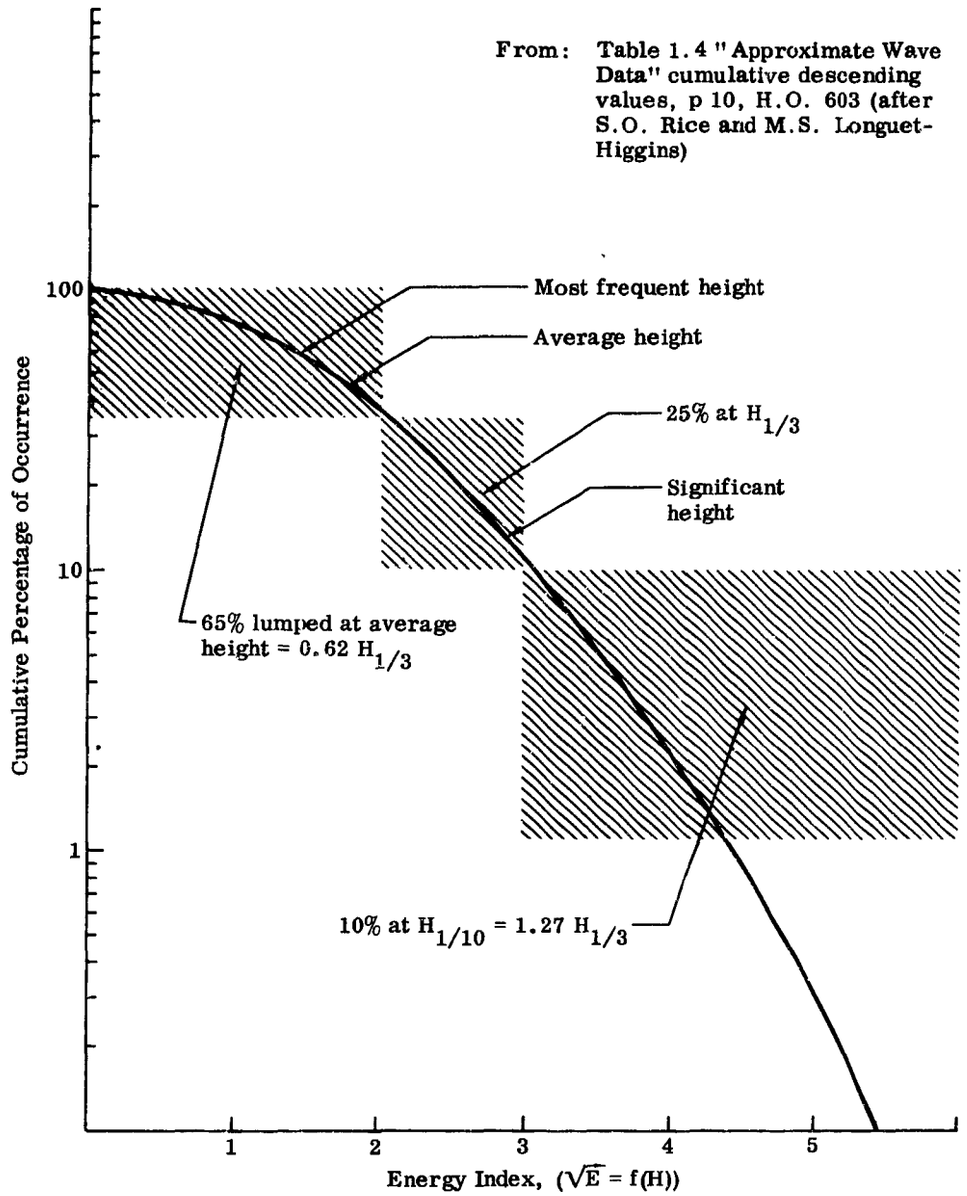

Fig. 3-7. Generalized Wave Data

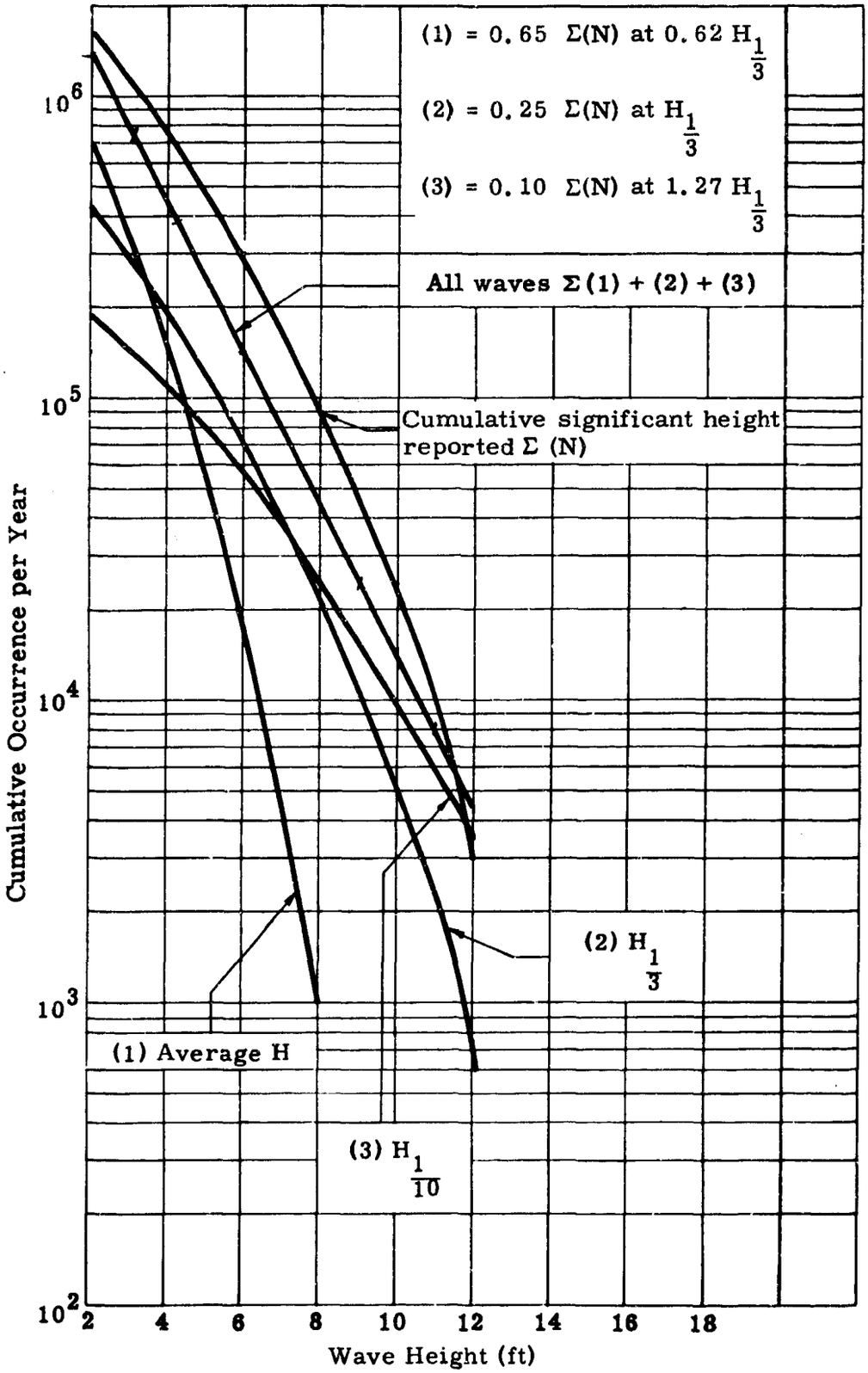

Fig. 3-8. Cumulative Wave Heights (L_w = 85 ft)

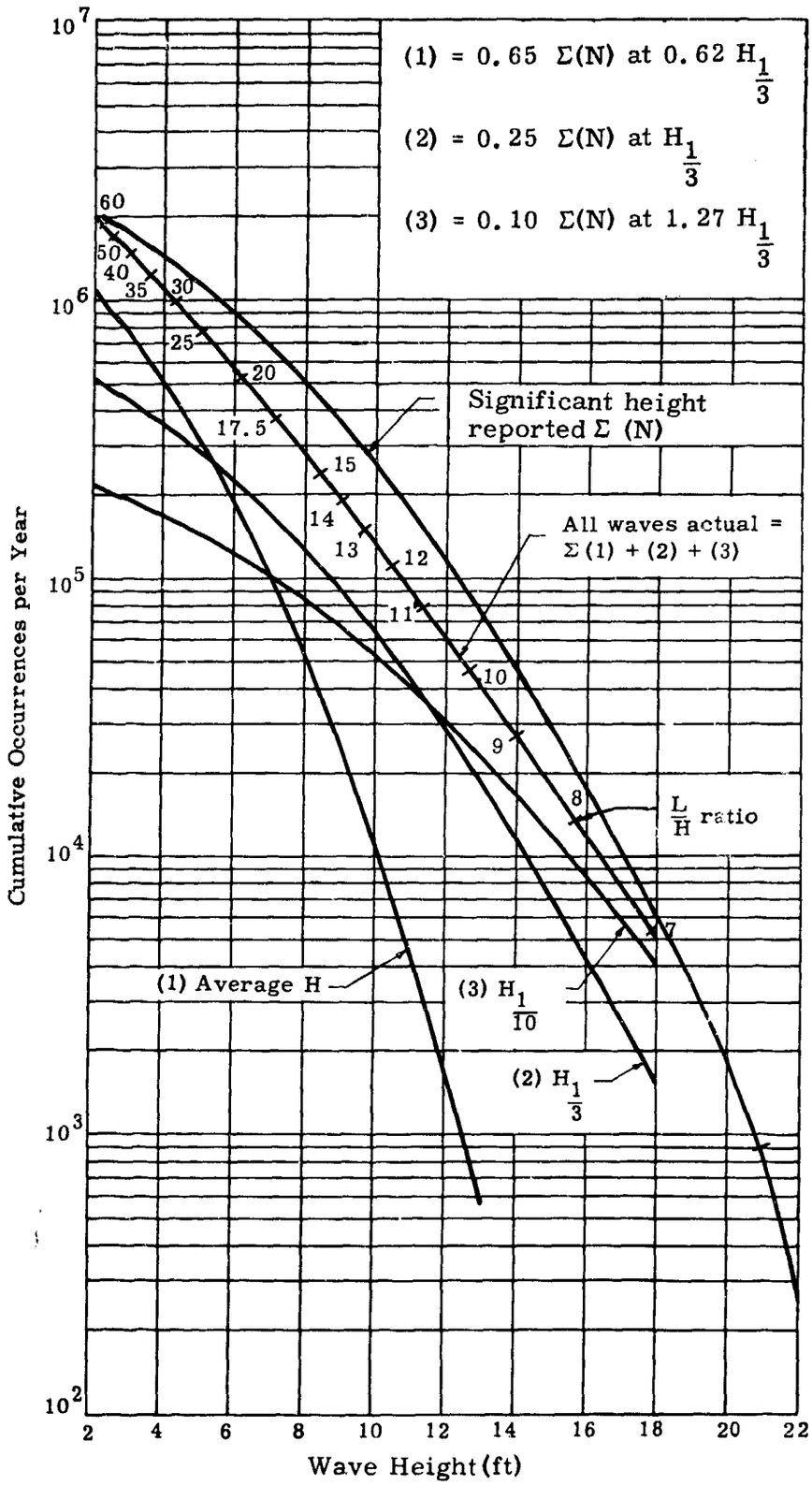

Fig. 3-9. Cumulative Wave Heights (L_w = 125 ft)

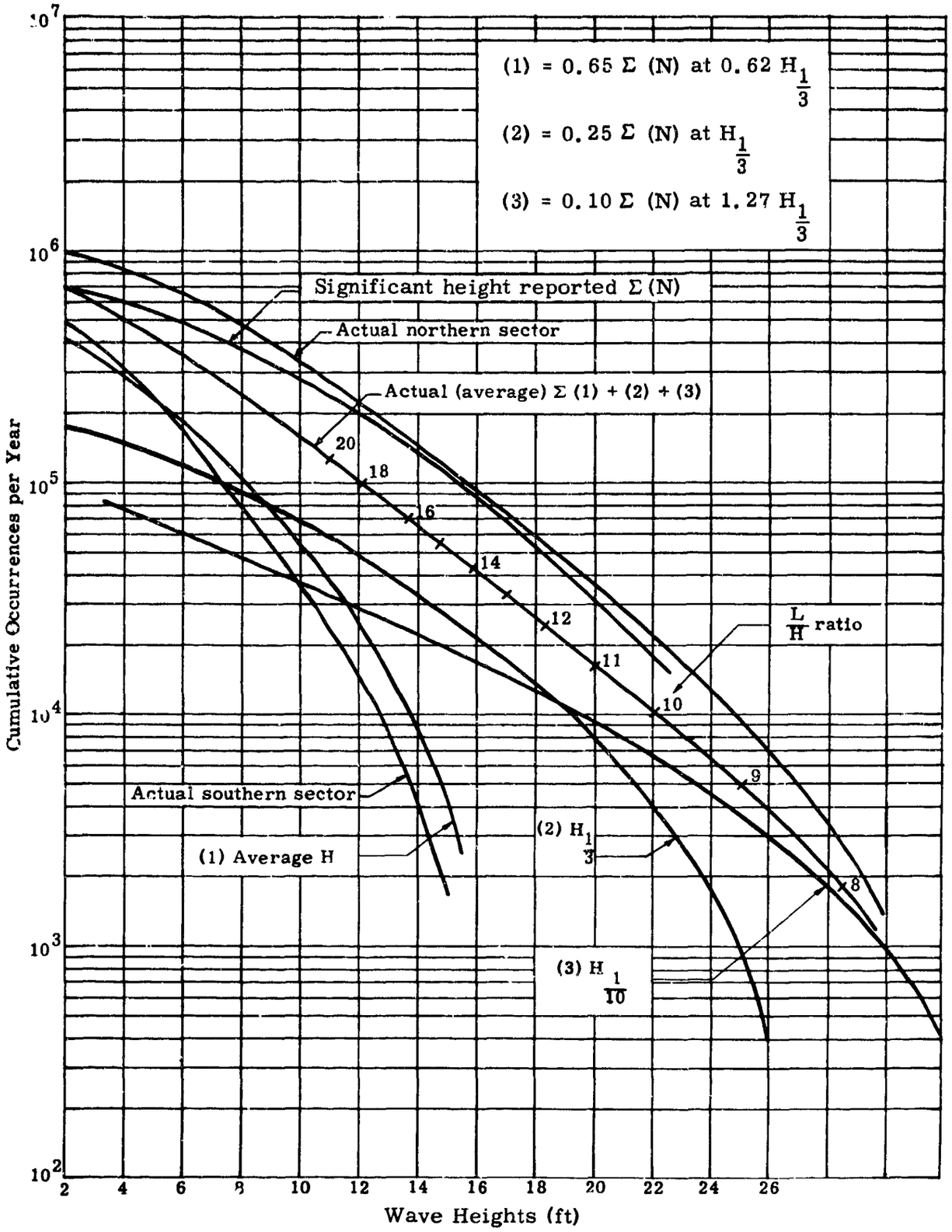

Fig. 3-10. Cumulative Wave Heights (L_w = 220 ft)

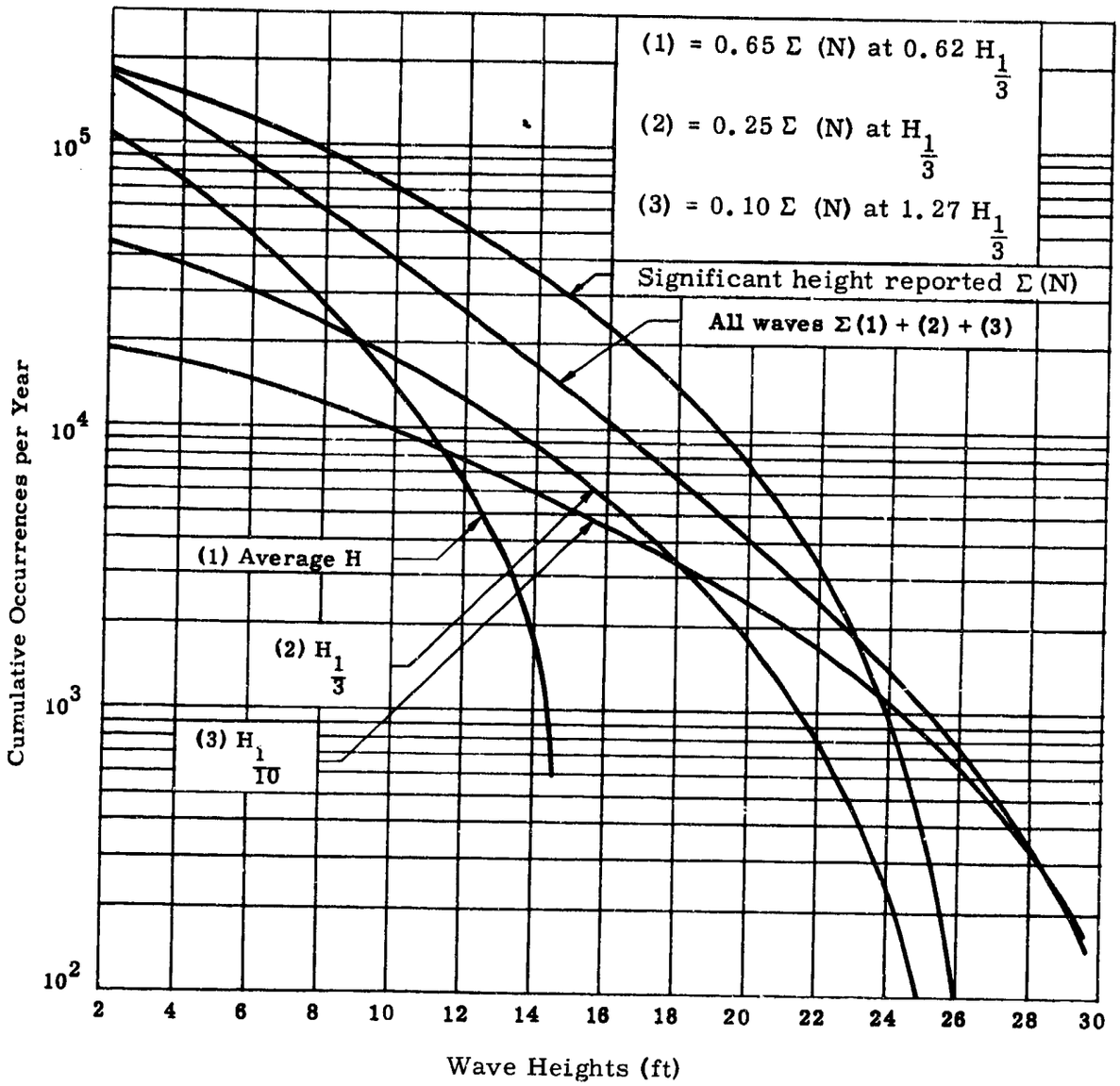

Fig. 3-11. Cumulative Wave Heights (L_w = 340 ft)

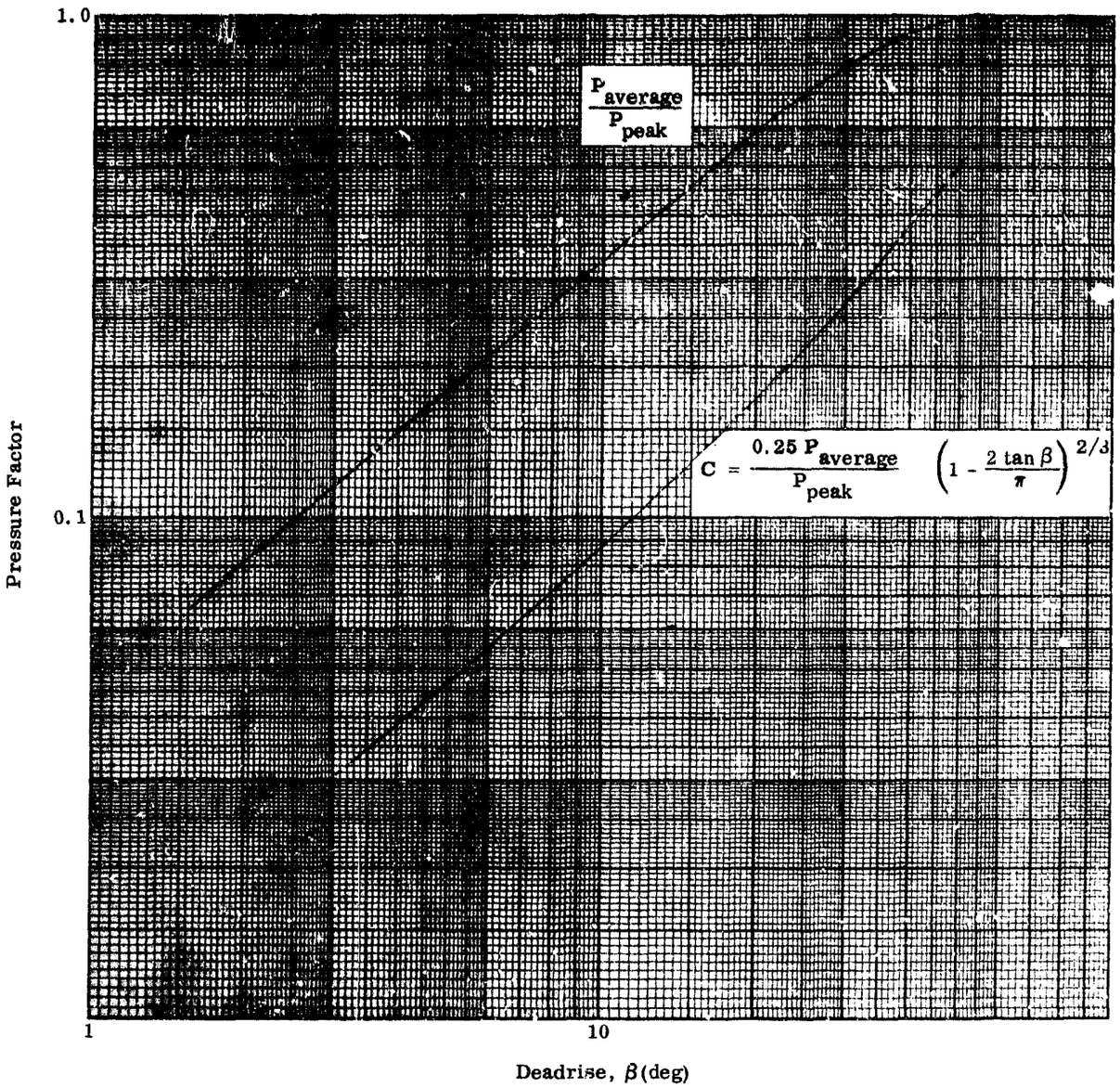

Fig. 3-12. Average Pressure Ratio and Acceleration Factor

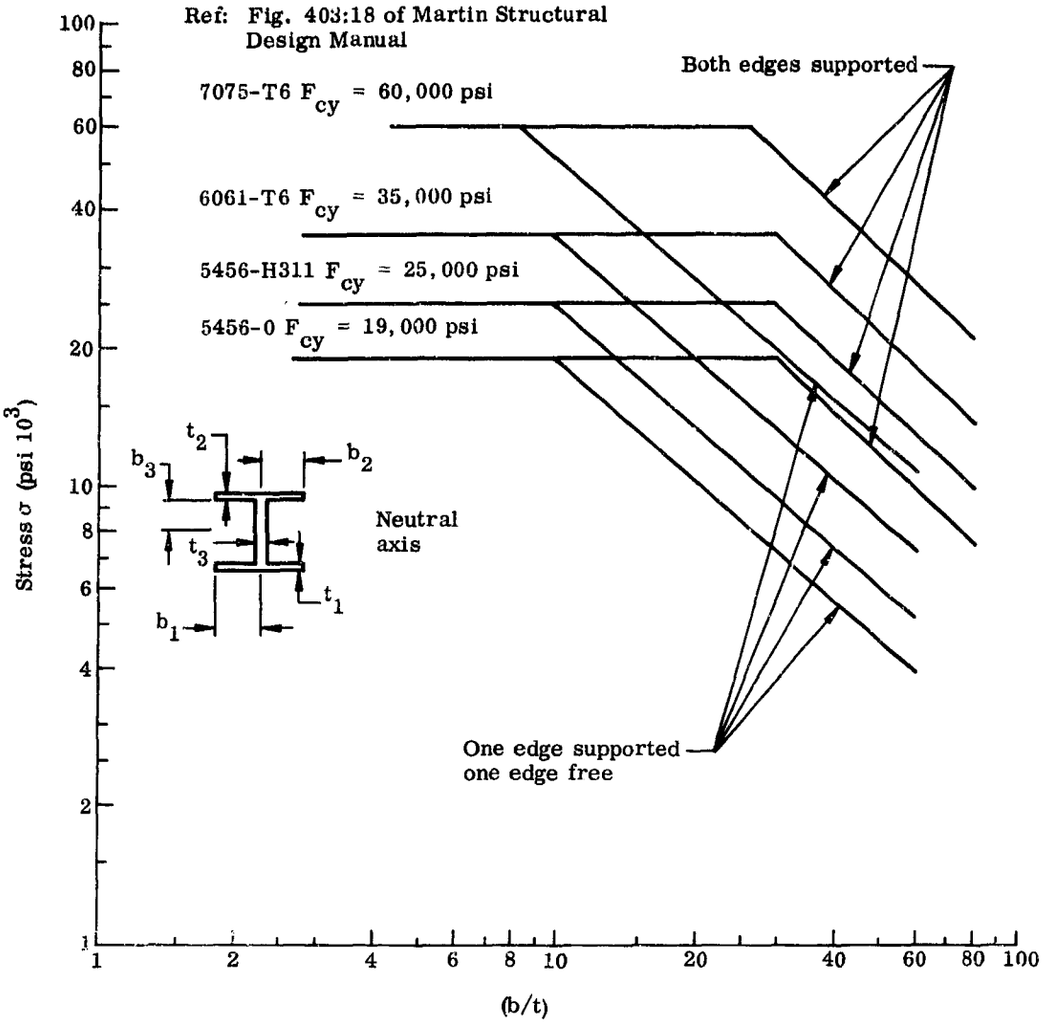

$$F_b = \sigma_{maximum} = \frac{\sigma_1 b_1 t_1 + \sigma_2 b_2 t_2 + \ldots\ldots \sigma_n b_n t_n}{b_1 t_1 + b_2 t_2 + \ldots\ldots b_n t_n}$$

F_{cy} = compression yield

Fig. 3-13. Allowable Bending Stress Based on Local Crippling of Flanges

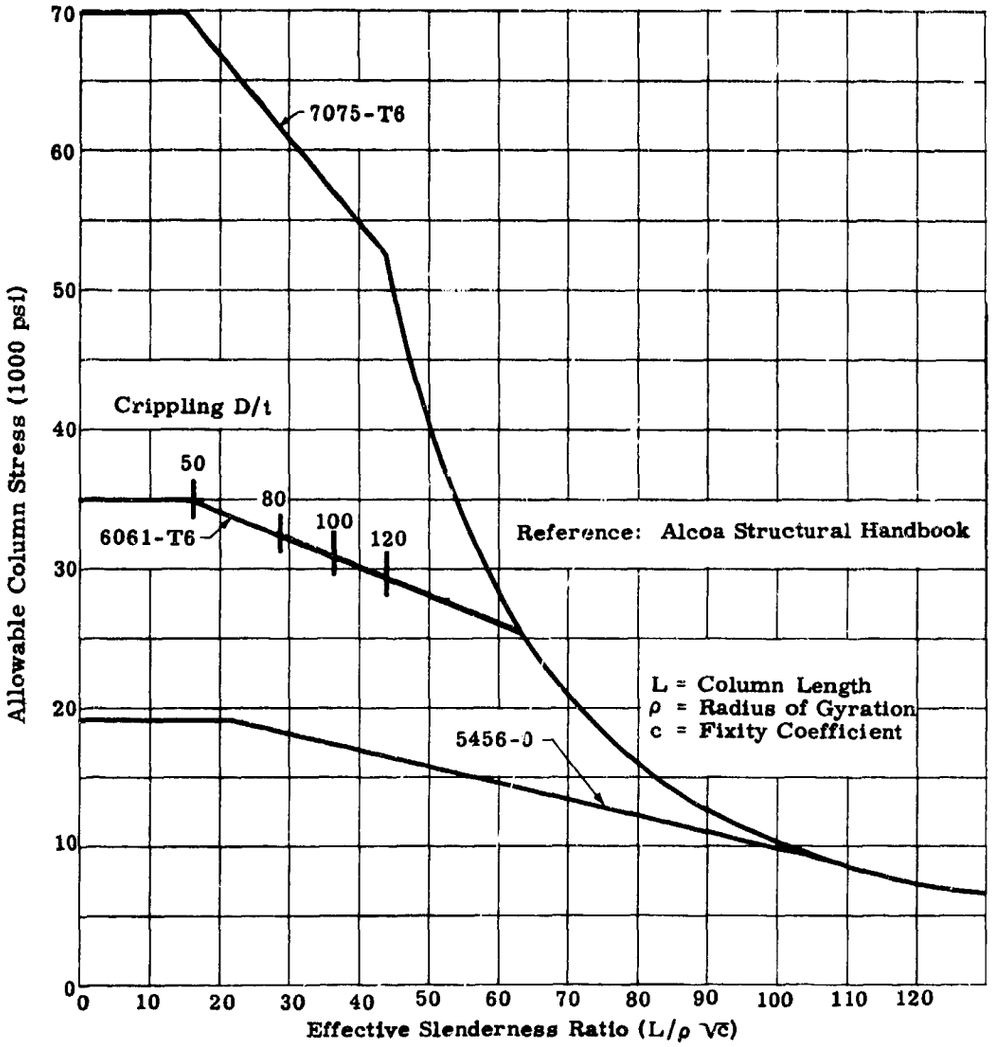

Fig. 3-14. Allowable Column Stress-Extruded Shapes

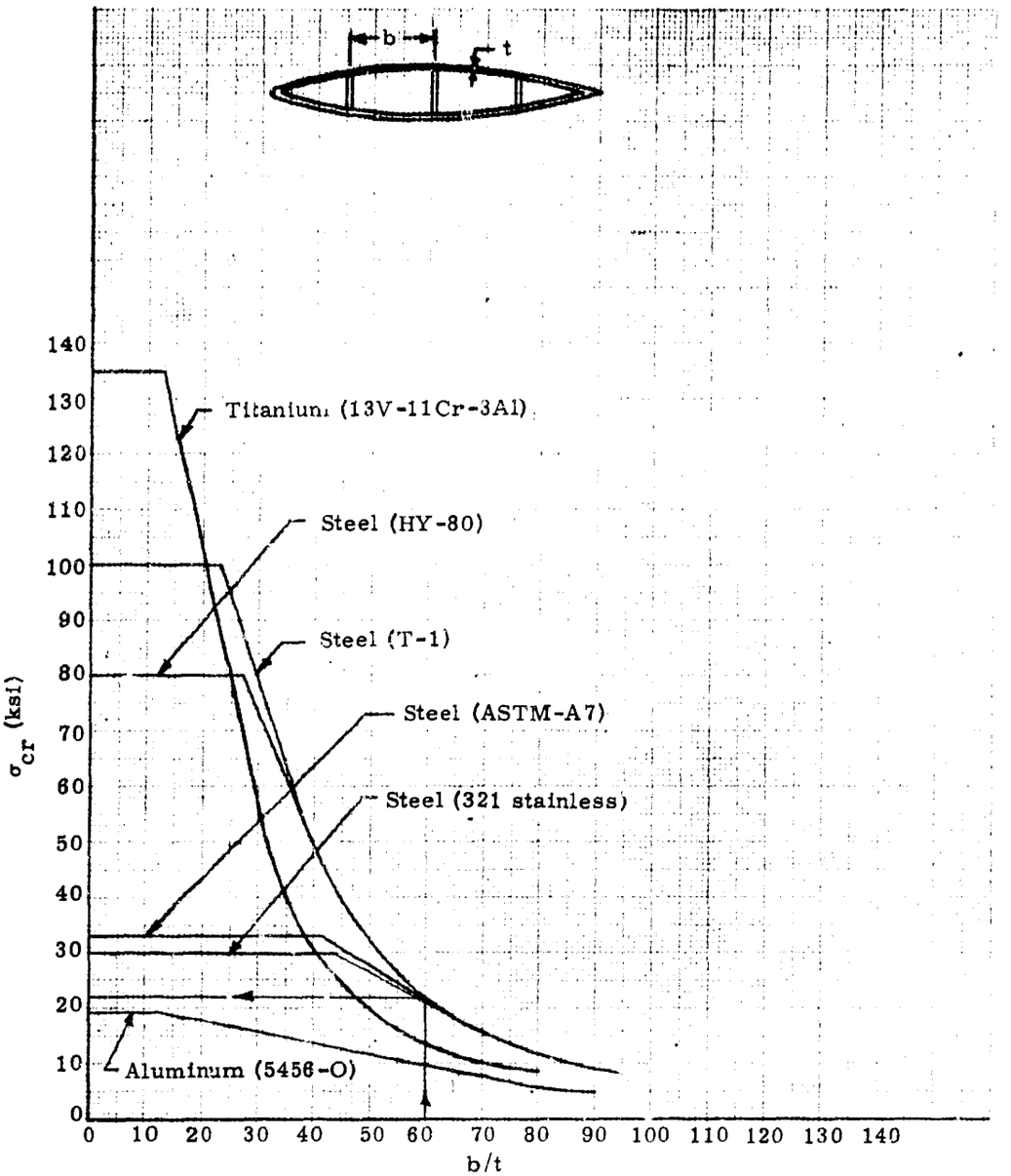

Fig. 3-15. Skin Buckling Curves

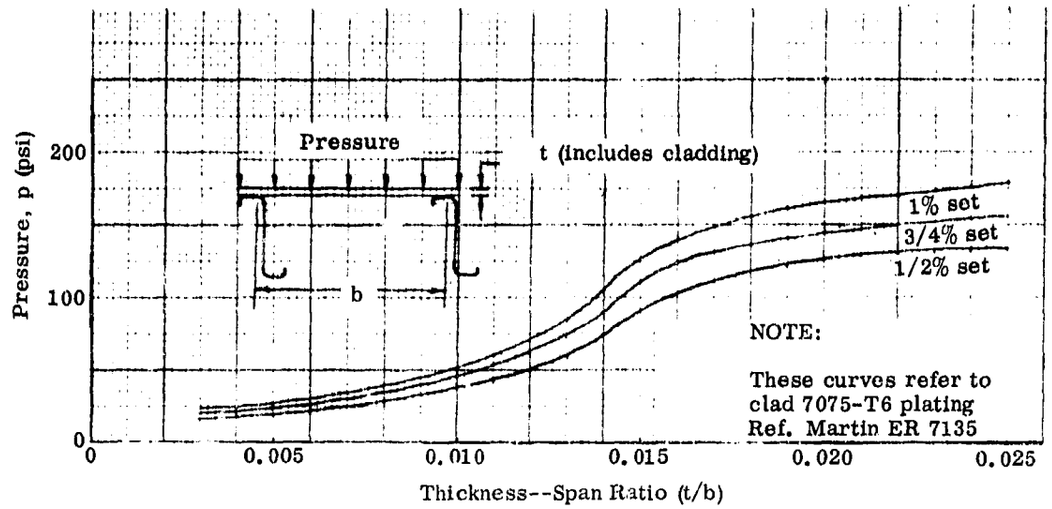

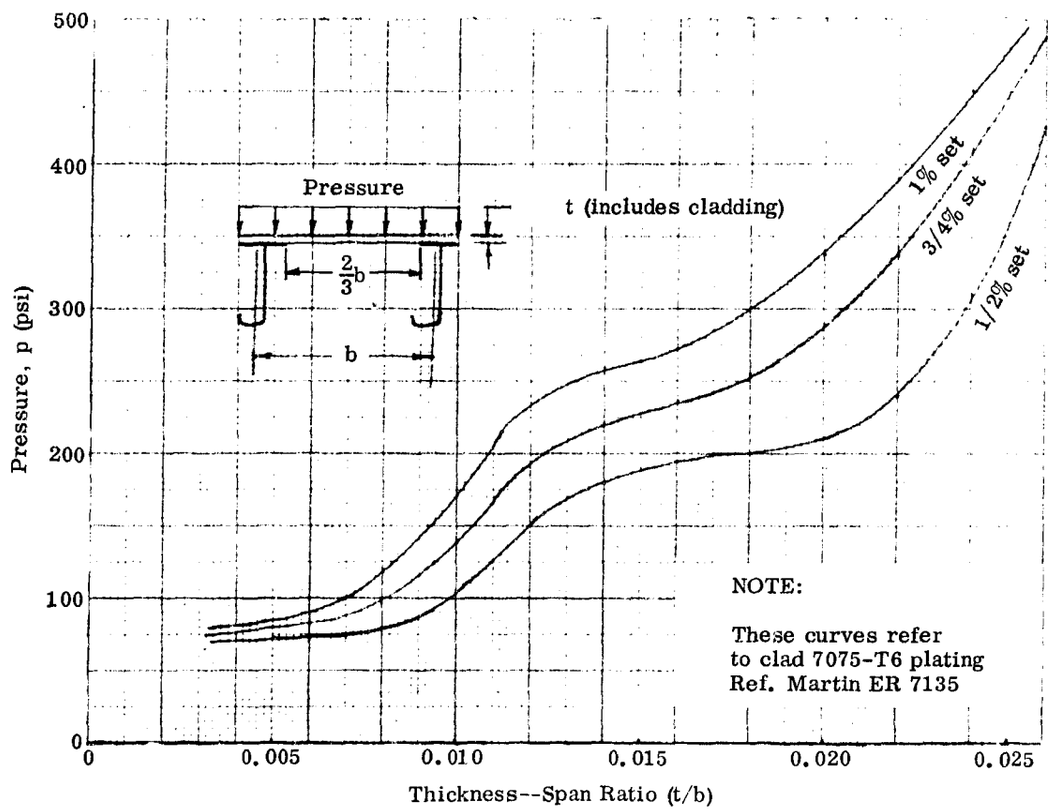

Fig. 3-16. Bottom Plating Deformation Curves--7075 Aluminum Alloy

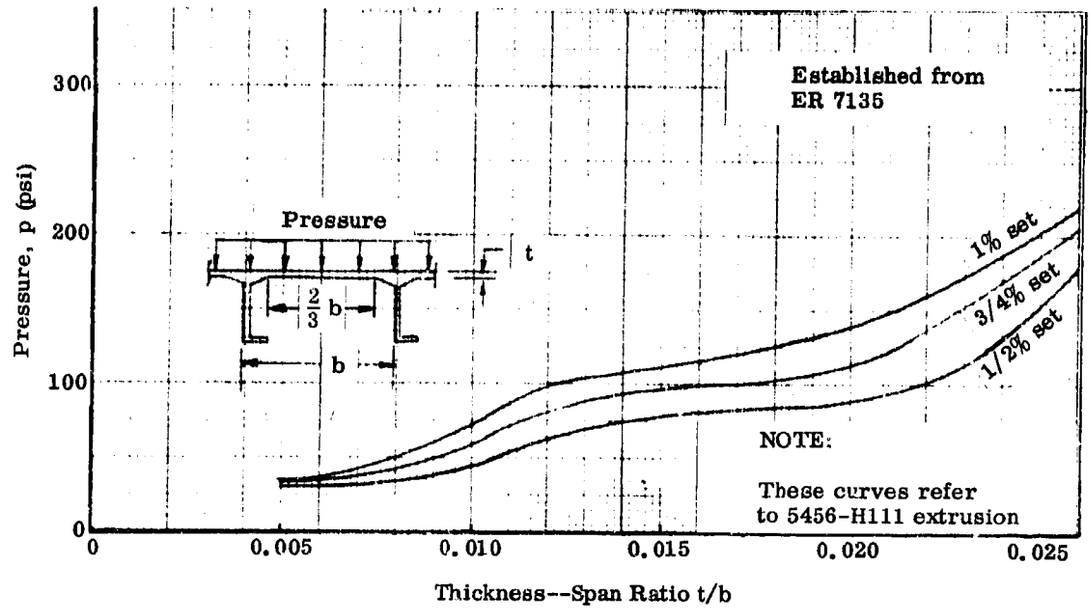

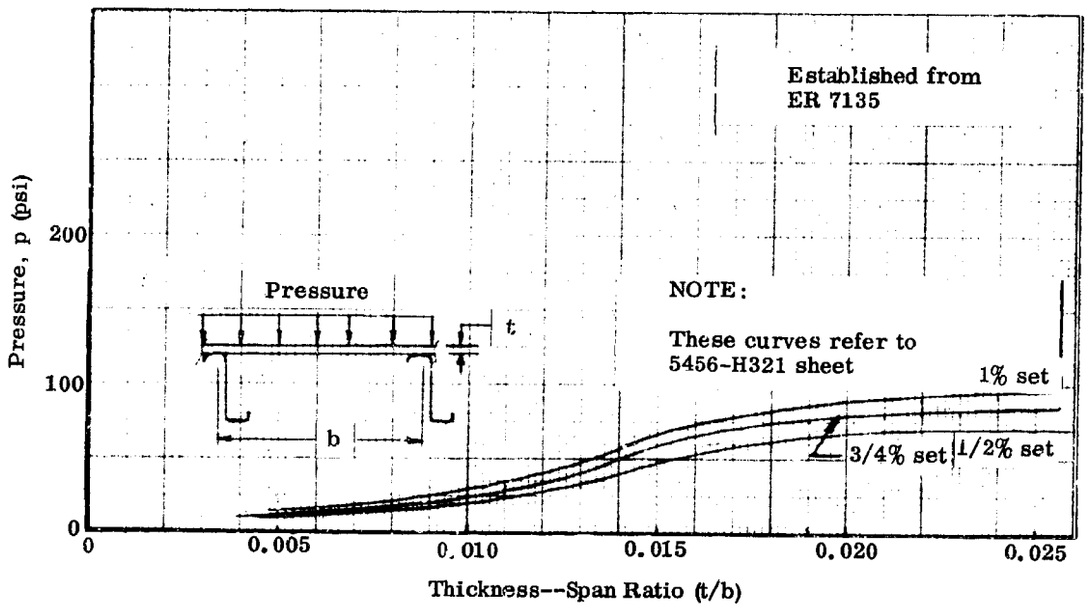

Fig. 3-17. Bottom Plating Deformation Curves--5456 Aluminum Alloy

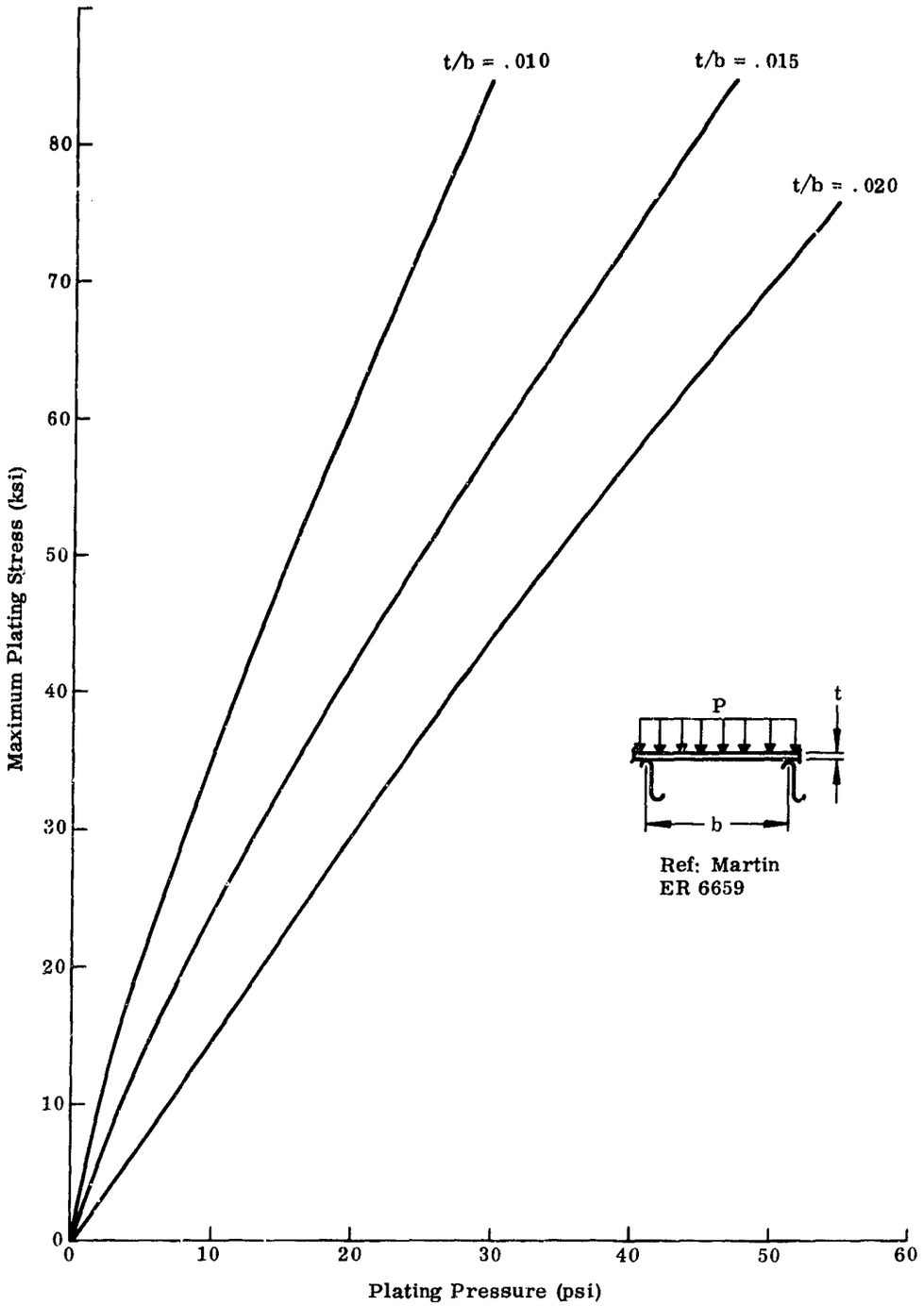

Fig. 3-18. Plating Stress as a Function of Plating Pressure

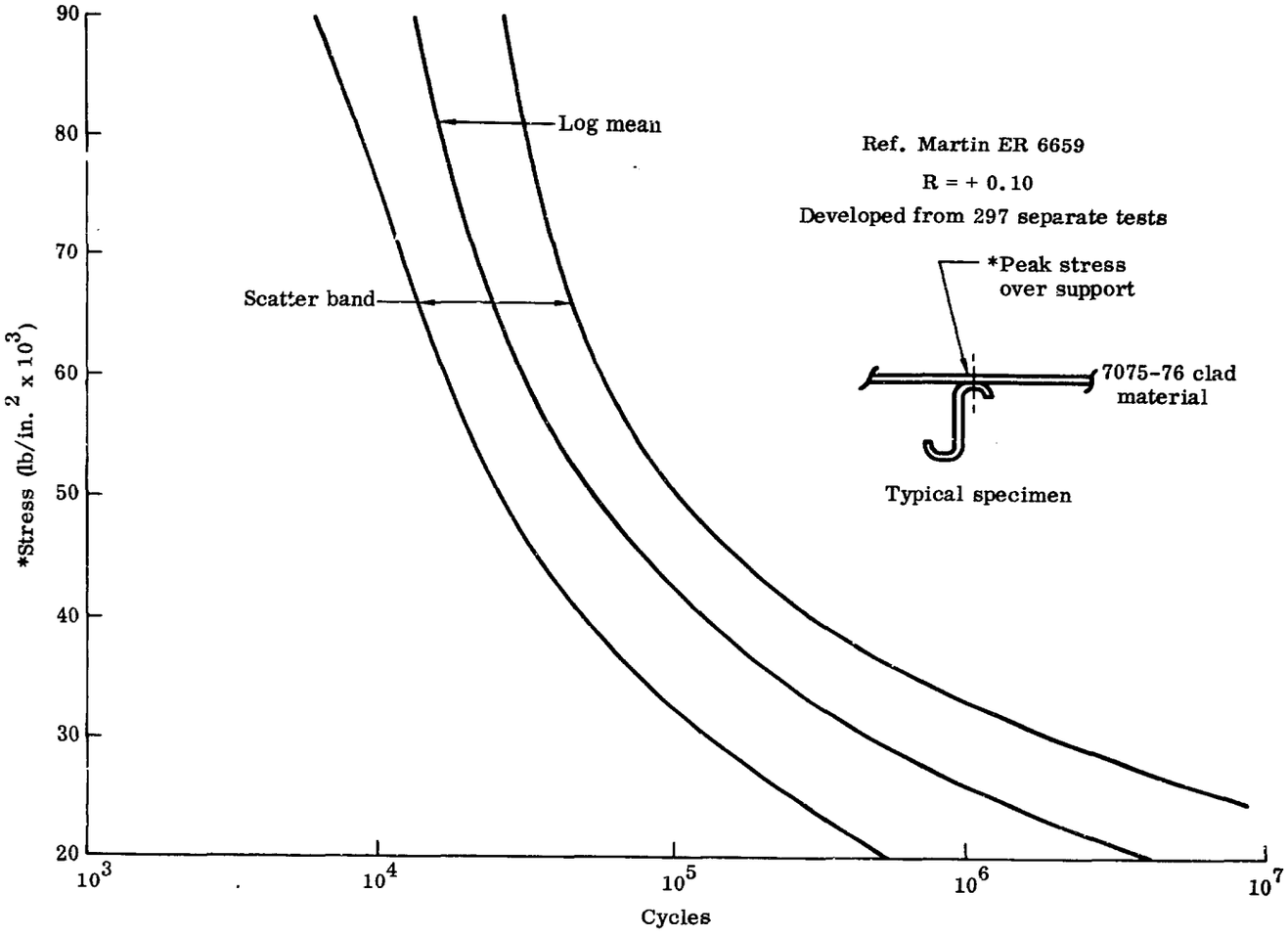

Fig. 3-19. Stress as a Function of Life Cycles for Two-Inch Hull Bottom Fatigue Specimens

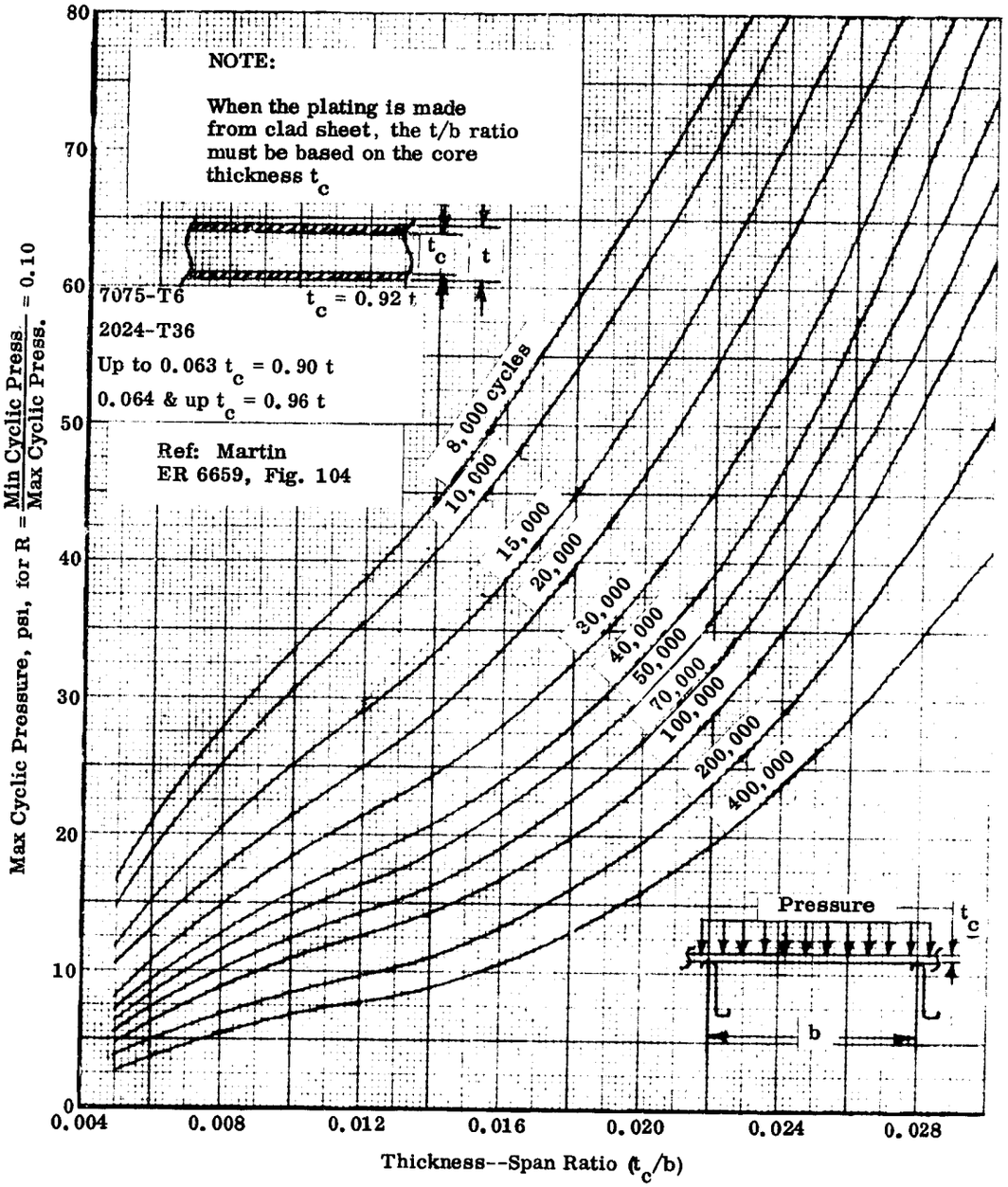

Fig. 3-20. Pressure Versus Thickness to Span Ratio for Constant Life of Hull Bottom Plating over Z-Type Stringers

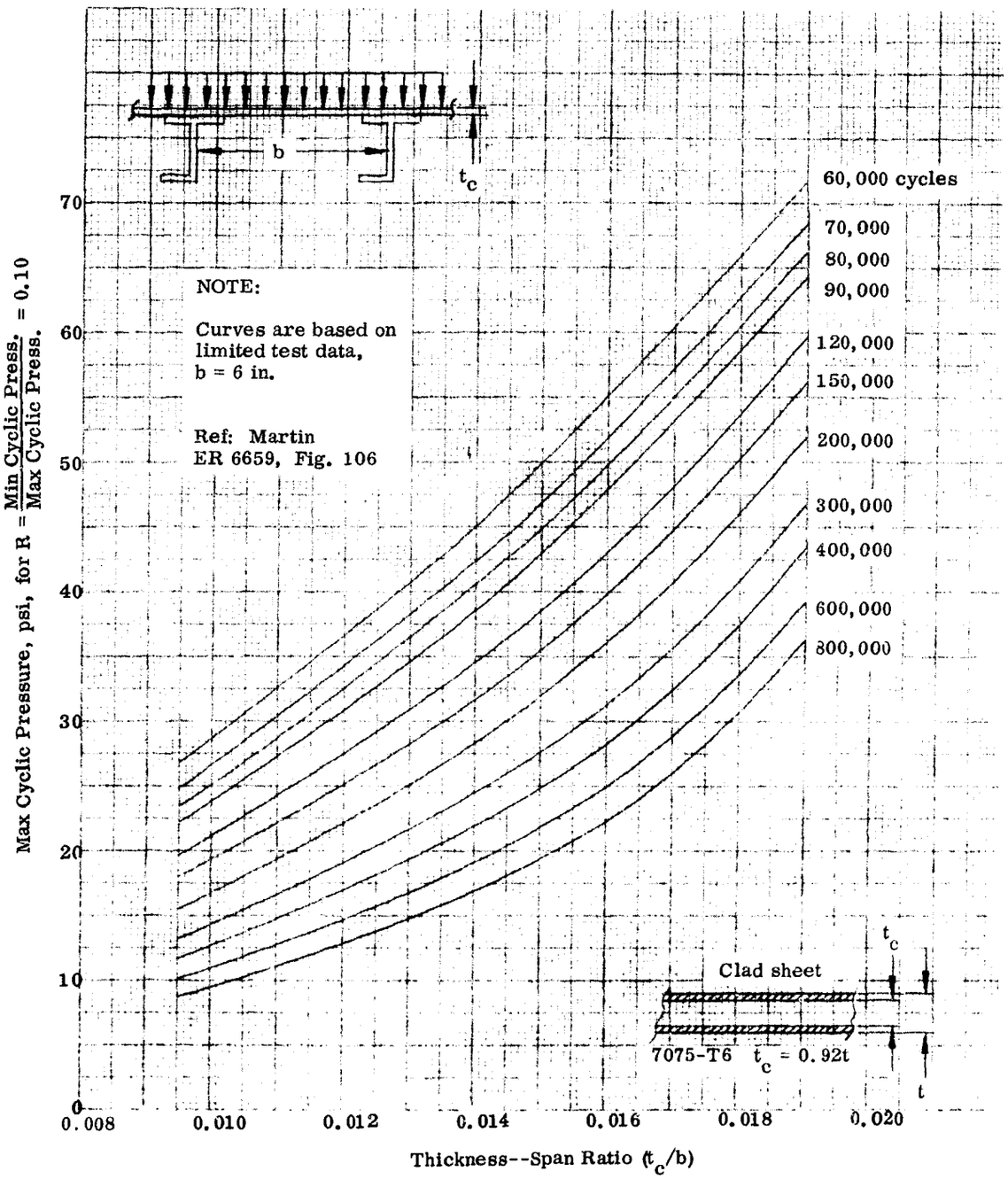

Fig. 3-21. Pressure as a Function of Thickness-to-Span Ratio for Constant Life of Hull Bottom Plating Over T- or J-Type Stringers

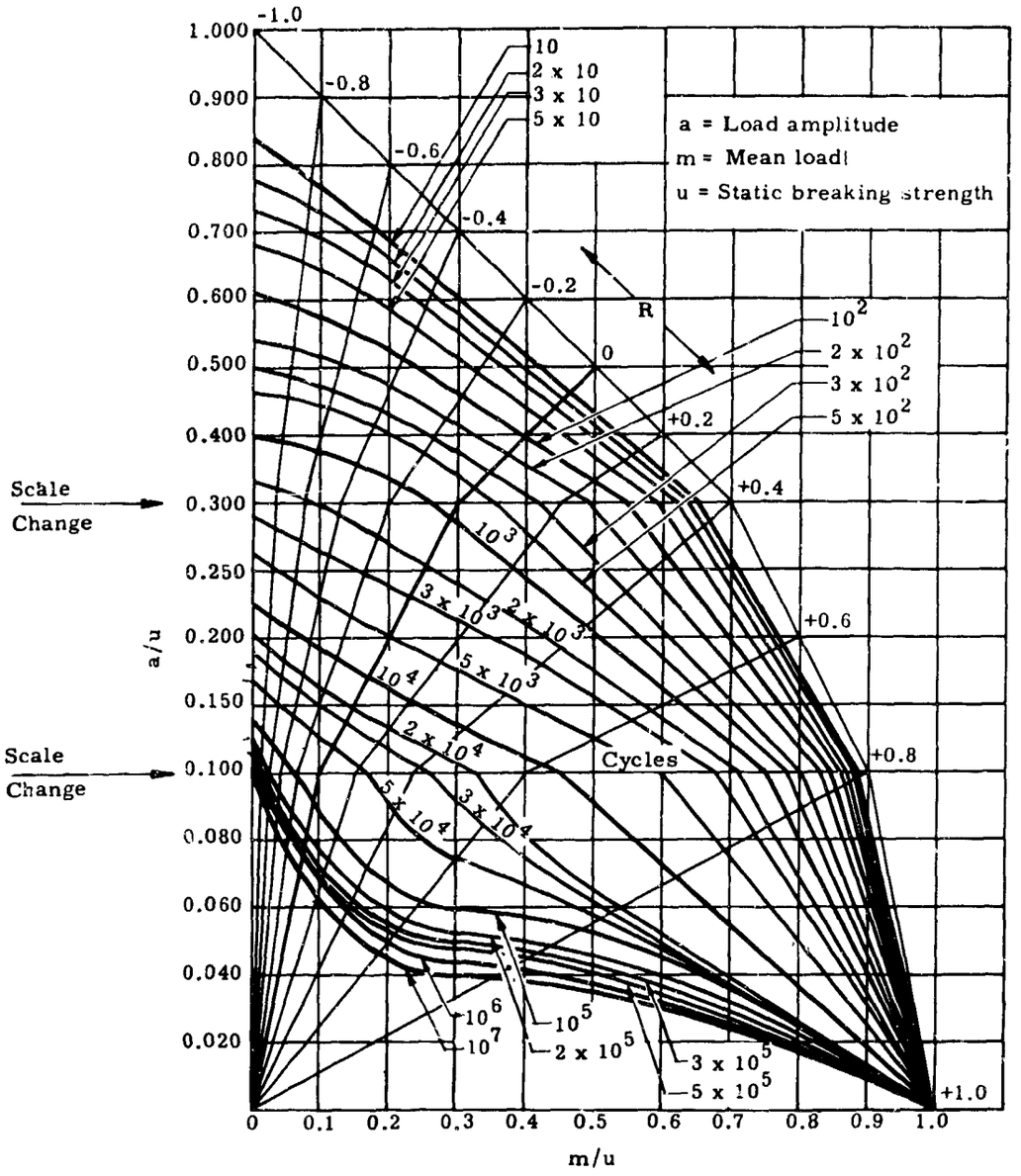

Fig. 3-22. Constant-Lifetime Fatigue Chart of Constant-Amplitude Fatigue Strenghts for 7075-T6 Aluminum Alloy Design Reference Structure

4.0 DEVELOPMENT OF DESIGN CRITERIA CONCEPTS

4.1 SUMMARY

The general design considerations of the previous section are utilized in this section to determine the structural design criteria for hydrofoil ships. The conditions of hullborne operation are investigated to give: hull loadings in the assumed operational environments, including normal buoyant forces, pressures and loads due to slamming; and deck, superstructure and all side loadings due to wave action. Foilborne loadings on the foils and struts are developed for both 45- and 100-kn example designs, and corresponding impact loads and pressures on various portions of the hull during landing are determined. In all of these conditions the loads data are presented on the basis of cumulative occurrences per year so that they may be used for both limit load static design and fatigue damage studies.

A plot of the typical results in composite form is given in Fig. 4-1. This shows the pressures on a selected bow location (Station 2) for both 45- and 100-kn designs. The effect of the design flight speed is graphically shown. For the 45-kn design the slamming condition is the major source of high bow pressures while at 100-kn the landing condition is greater. The inadequacy of typical design pressures that would have been specified by application of the seaplane design specification MIL-A-8629 is evident from comparison of the two indicated points in Fig. 4-1 with the actual loading spectrums.

In the application of the pressure and loads spectrums to the design of the structure for the hydrofoil ship it is recommended that consideration be given to the transient nature of the loadings and the actual distribution of pressures on the bottom. Experience with structural design of seaplane hulls is presented to show some of the practical aspects of the design criteria. However, the practical solution for structural design for safe response to the extreme pressures at low deadrise angles is not well defined.

4.2 HULLBORNE CONDITION LOADS

4.2.1 Summary

The hydrofoil ship in the ASW mission, as described in Section 3.2, spends most of its time in the displacement condition. A very large number of cycles of moderate pressures (due to static draft in waves) and hogging and sagging inducing loads is experienced due to the open sea nature of the assumed mission.

A method of approximating the probable slamming occurrences with the associated bow loading is developed. If the ship is operated without restriction (to avoid slamming), the bow is subjected to fairly substantial pressure levels (over 40 psi) and high local accelerations (over 4g) more than 10 times a year.

Estimates of the level of waves coming over the bow and corresponding ship motions are used to develop pressure loading criteria for the decks, superstructure and hull sides.

4.2.2 Buoyant Forces and Damping

Hull pressures or loads due to buoyancy are usually considered proportional to the vertical depth of submergence of the point considered. This is true, however, only under static conditions. When wave and/or ship motion exists, the pressures are affected to varying degrees depending upon the severity of the motions. In waves, the orbital motion of the water particles causes the buoyancy pressures to be somewhat less than expected for the depth below the wave crest and somewhat greater under the wave trough. This orbital motion, the basis of the Smith Correction, diminishes as depth of submergence increases. Ship motion in heave and pitch also affect buoyancy pressure by reason of the velocity head.

For design considerations, the buoyancy pressure should be determined neglecting the Smith Correction because the effect is small and, for greatest depth of submergence from the crest of the wave, is also conservative. Ship motion may also be neglected at low speeds because the effect is small and compensates for the omission of the Smith Correction.

The variation of the maximum buoyancy pressures along the length of the ship is dependent upon the maximum wave height at each station along the ship's length. Figure 4-2 represents for the study ship the maximum conditions at the bow and the stern under the highest wave and critical wave length to height ratio. From this figure, it can also be surmised that as the wave would proceed along the ship the depth of submergence becomes less until at the stern the wave crest is about level with the deck. Thus, at the bow the maximum keel pressure is:

$$P_K = \frac{64}{144} \times 24 = 10.7 \text{ psi (Station 1/2 to 3)}$$

and at the stern is:

$$P_K = \frac{64}{144} \times 12.5 = 5.55 \text{ psi (Station 9 to 10)}$$

The corresponding pressures in still water are:

$$P_K = \frac{64}{144} \times 6.5 = 2.9 \text{ psi (Station 1/2 to 3)}$$

and

$$P_K = \frac{64}{144} \times 2.9 = 1.3 \text{ psi (Station 9 to 10)}$$

The cumulative occurrence of these pressures can be determined from the data of Fig. 3-6 using the 85- and 125-ft waves and the assumed net utilization of 54%. Figure 4-3 presents an approximate distribution of keel pressure at the bow (Stations 1/2 to 3) and at the stern (Stations 9 and 10).

The buoyant hull pressures discussed so far have neglected the damping effects of the struts and foils upon the pitch and roll responses of the ship. These forces and their effects upon the ship motion are difficult to determine by any analytical procedures short of a complete analog solution of the problem. Such a study is beyond the scope of this effort. However, experimental data are available which give some insight into the phenomena of hydrofoil damping, and from the results of these studies it was concluded that foil damping, on the ship configuration under consideration, was negligible for design purposes.

The experimental data was obtained in conjunction with a Martin sponsored program conducted to determine the effect of length-to-beam ratio on the motions and performance of hydrofoil craft operating at displacement speeds in both smooth and rough water, Ref. 9. Two models were tested in rough water, comprised of irregular waves having a significant height of 16 ft full size. One of the models, used as a basis for comparison, closely resembles the example configuration, Fig. 3-1. The second model hull configuration tested has a length-to-beam ratio of 2 (see Fig. 4-4). The data are in the form of motion pictures and oscillograph records showing pitch, heave, wave profile and speed traces as a function of time.

Unfortunately, the quality of the oscillograph records does not permit an accurate determination of the heave and pitch rates for the desired configurations. However, a measure of the effect of foils on the ship's motion can be obtained from a comparison of ratios of pitch and heave amplitude to average wave height, for which the data suffices. Figures 4-5 and 4-6 present the results of model tests analyzed by this method. It should be noted that each point represents an average of 20 or more wave encounters, thereby minimizing the motions resulting from wave encounters having low probability of occurrence. Both records and motion pictures indicated that the craft generally followed the waves except at the higher speeds where an occasional wave would cause it to go out of synchronization for a short time.

For the reference ship, the effect of foils on heave and pitch motion is contrary to normal expectations, (Fig. 4-5). Whereas foils are usually considered as devices which will damp the action, in this case the reverse was true and pitch and heave have been increased with both foils extended. When the main or after foil is removed leaving only the bow foil, the heave is increased by a small amount while the pitch is damped, particularly at the higher speeds.

It is postulated that this effect of foils on the motions is a function of their close proximity to the water surface and their location with respect to the hull buoyancy distribution. In the first instance the foils are subject to the internal particle velocity of the waves; hence, they will tend to rise and fall with the waves. Thus, they provide a reaction which is additive to that resulting from the hull buoyancy. This gives rise to the second part of the postulation, the position

of the foils. If the foils can be so placed that they react to the waves either before or after the reaction due to buoyant forces, a damping action can result. Partial proof of this postulation is indicated by the results given in Fig. 4-6 for the low length beam ratio hull.

The hydrofoil system for the configuration having a length-to-beam ratio of 2 is similar to the reference craft in planform and load distribution, but the foils are located closer to the extremes of the hull (forward foil 10% instead of 20% of the hull length aft of the bow). For this configuration, the hydrofoils are sufficiently close to the extremes of the hull to provide some measure of damping in both pitch and heave. In this case the reaction of the bow foil occurs before the strong buoyant forces of the hull sections immediately aft come into play. Further, by the time the hull buoyant forces are becoming dominant the particle velocity on the backside of the wave may be acting downward with sufficient strength to assist in the damping. The indication that the rear hydrofoil does not contribute to pitch damping in either configuration, but seems to have an amplification effect, is seen in the increased damping in its absence. In both cases the foil is located directly beneath a section of the hull which has strong buoyancy characteristics.

A series of experiments with typical hydrofoil boat hulls fitted with feasible hydrofoil systems tested in regular wave pattern is needed for positive proof of the above postulation and to provide needed data pertaining to the effect of foil damping action.

4.2.3 Hogging and Sagging

The concept of hogging and sagging upon trochoidal waves is a well accepted procedure for ship girder design and needs no development. An expansion of the procedure, however, to include a loading spectrum for the waves of the example environment, the Western Atlantic Ocean, is presented in 5.2.2.

4.2.4. Slamming

The phenomena of slamming which results in a condition of severe impacting or pounding at the hull forefoot in certain critical wave conditions is studied, and formulas are developed for determination of the impact pressures and load factors. Loading spectrums are determined for the study ship in the assumed operational sea conditions.

Slamming is most likely to occur when the tuning factor approaches unity, Ref. 10. The tuning factor is defined as the ratio of the ship's natural period of oscillation to the period of wave encounter. The motions of the ship, at this condition, are characterized by large angles of pitch and an unfavorable relationship between maximum pitch and wave cycles. For example, in waves whose lengths approach the ship length, the bow reaches its lowest point in the wave crest and its highest point over the trough. Thus, it can be visualized that water may be shipped as the vessel proceeds through the wave crest and slamming will occur subsequent to the emergence of the forefoot.

The oscillograph records of the model tests, Ref. 9, discussed previously in the section on hydrofoil and strut damping were examined to determine the phase relationship between pitch and heave. Generally, it was found that the maximum negative pitch angles were equal in magnitude to the maximum positive pitch angles. The same can be said for heave. The data showed that maximum values of heave almost always were accompanied by zero pitch angles. Similarly, but to a lesser degree, maximum trim angles occurred when the heave was near zero. Thus, the data indicates that the example craft will generally be out of phase with the waves by 180°. This behavior is illustrated in Fig. 4-7.

It will be noted that at the point of maximum angular velocity and zero vertical velocity (zero pitch angle and maximum heave) the forefoot is about to contact the wave. Thus, angular velocity will have the greatest effect on slamming impact while the effect of vertical velocity due to heave will be negligible.

Normally, the maximum angular excursions in pitch are less than the maximum wave slope. However, the ratio of pitch angle to maximum wave slope approaches unity when the tuning factor is equal to unity. For instance, the example given in Ref. 10 shows that for the minimum value of amplitude possible, i.e., the value corresponding to large damping or to magnification factor equal to 1.0, this ratio can vary on the order of 70% for waves approximating 1.5 times the length of the boat to 100% for long waves. Since it is unlikely that large damping will be achieved (judging from the model test results for the reference configuration), the maximum amplitude in pitch, both negative and positive, is derived on the basis that the ratio of pitch angle to maximum wave slope is equal to unity.

The ship will be required to operate at any heading. At headings not directly into the waves, the ship's motion will include roll and yaw as well as pitch and heave. However, the conclusions reached in Ref. 11 are that the effect of roll and yaw on pitch and heave are very small and can be neglected.

In a given physical wave the period of encounter at oblique headings is based on an apparent length as indicated in the following sketch.

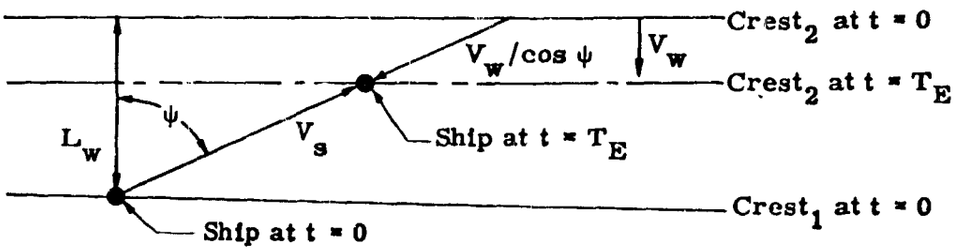

V_s = ship speed, (fps)

V_w = wave speed = $2.26\sqrt{L_w}$, (fps)

ψ = heading, (deg)

L_w = wavelength, (feet)

and, the period of encounter is

$$T_E = \frac{L_w/\cos\psi}{V_s + V_w/\cos\psi} = \frac{L_w}{V_s\cos\psi + V_w} \quad (12)$$

It should be remembered that the wave height is constant regardless of heading; thus, the maximum wave slope for oblique paths will be

$$\phi_{max} = \pi H_w/(L_w/\cos_\psi).$$

The velocities acting at the time of a slamming impact are shown in the following vector diagram. Heave is zero and the maximum angle of pitch is equal to the maximum wave slope, ϕ, as discussed previously.

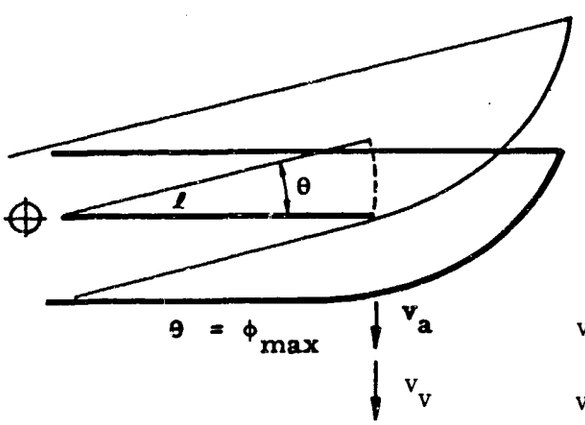

v_a = vertical velocity due to rotation

v_v = component due to wave and ship speed

The maximum angular acceleration will occur near the point of forefoot impact as shown in Fig. 4-7. Therefore, the maximum vertical velocity at distance ℓ from the point of rotation was obtained by means of the equation for harmonic motion. The center of rotation for the combined motion in heave and pitch is

not exactly defined. At the part of the cycle approaching the slam it is assumed that the rotation is about the midship station.

$$v_a = \frac{2\pi\ell}{T_E}\,\phi_{max} \tag{11b}$$

$$v_v = \left(V_{ship} + \frac{V_{wave}}{\cos\psi}\right)\phi = \frac{L_w/\cos\psi}{T_E}\,\phi_{max} \tag{13}$$

when the bow makes flat contact at the maximum slope of the wave. This most severe relationship will hold true for only the bow portion of the hull, where the upward sloping butt lines can match the wave slope.

Thus, the summation of the velocity normal to the bottom is equal to

$$v_n = \frac{L_w/\cos\psi}{T_E}\,\phi + \frac{2\pi\ell}{T_E}\,\phi\,. \tag{14}$$

Slamming occurs when the ship's period equals the period of encounter. The equation for ship's period given in Ref. 10 is:

$$T_p = 2\pi k\sqrt{\frac{(0.60 + 0.36\,B/D)}{g\,GM_L}}\,. \tag{15}$$

Where

k = radius of gyration in pitch (feet)

B = Beam (feet)

D = Draft (feet)

GM_L = Longitudinal metacentric height, (feet).

These relationships are empirical and include the entrained water mass. The radius of gyration is approximately one-fourth of the length of the hull. Further, for ships at load draft the longitudinal metacentric height is on the order of the length, Ref. 12, hence,

$$T_p = 0.277\sqrt{L_S(0.60 + 0.36\,B/D)} \tag{15a}$$

Where

L_S = ship's length, (feet).

Thus, for the slamming condition, when $T_E = T_p$ substituting Eq (15a) in Eq (14) gives

$$v_n = \phi \left[\frac{L_w/\cos\psi + 2\pi\ell}{0.277\sqrt{L_S(0.60 + 0.36\ B/D)}} \right]$$

$$v_n = \frac{\pi H_w + 2\pi^2 \ell\ H_w/(L_w/\cos\psi)}{0.277\sqrt{L_S(0.60 + 0.36\ B/D)}} \qquad (16)$$

According to Lehman, Ref. 13, the most likely area to encounter severe slamming pressures is centered at a point 20% of the length of the ship aft of the forward perpendicular (as indicated by the regions of slamming damage). Figure 4-7 indicates that typical slamming conditions can exist in the region of Station 2 and forward. For load determination the Station 2 area is treated as a constant prismatic section with a deadrise angle of 30°. An additional area centered at a point 10% of the length of the ship aft of the forward perpendicular was also considered for comparison purposes. In this case the assumed prismatic section had a deadrise of 45°.

The slamming condition has been assumed to occur when the sum of $(\theta + \tau - \phi) = 0 = \tau^*$. For this condition the pressure Eq (5)

$$\text{Peak Pressure} = \frac{\frac{\rho}{2} v_n^2}{\sin^2\tau^* + \frac{4\tan^2\beta}{\pi^2}\cos^2\tau^*}$$

becomes:

$$P_p = \frac{\rho}{2} v_n^2 \Big/ \frac{4\tan^2\beta}{\pi^2} \qquad (5a)$$

Figures 4-8 and 4-9 show peak pressures as a function of wave height and equivalent wave lengths for Stations 1 and 2, where the reference dimensions required to evaluate Eqs (16) and (5a) are:

β = 30°, 45° Beam = 35 feet

ℓ = 39 feet, 52 feet Draft = 6 feet

L_S = 130 feet

The preceding discussion relates the bottom pressures of a vessel to the wave geometry. The next step in the analysis is to determine the number of occurrences of various wave geometries which will be encountered by the reference craft when operating in the displacement condition.

It is evident that during its lifetime the vessel will travel an equal amount of time at each point of the compass, and, since waves are random, will also spend an equal time period at each oblique heading. Equation (12), for the period of encounter solved for critical ship's speed for each heading, can be used to provide the proper distribution provided the percent time spent at each displacement speed is known. Figure 3-3 is an estimate of the percent time as a function of speed expected for the subject ASW craft. It will be noted that about half of the time is spent at speeds of 2.5 to 6.0 kn (4 to 10 fps) to be consistent with ASW mission requirements. For each increment of speed the conditions for slamming, i.e., effective wave length and oblique heading can be calculated. For example, in a wave whose true length is 220 ft the heading which will produce slamming at 15 fps is obtained in the following manner.

$$V_s = \frac{L_w/\cos\psi}{T_E} - \frac{2.26\sqrt{L_w}}{\cos\psi}, \quad V_w = 2.26\sqrt{L_w} \tag{12a}$$

$$\cos\psi = \frac{220/5.2 - 2.26\sqrt{220}}{15}$$

$$\psi = 53°$$

$$L_w/\cos\psi = 367 \text{ ft}$$

Curves of critical speed versus heading, calculated in the above manner, for the wave lengths given in Fig. 3-6 are presented in polar form in Fig. 4-10. Likewise, the percentage of time the vessel operates at each speed, as given in Fig. 3-3, is shown. It should be borne in mind that the occurrences of slamming are represented in an idealized manner in Fig. 4-10. All of the waves are considered to be concentrated at discrete wave lengths of 85, 125, 220, and 340 ft. The ship speed for critical period of encounter is thus a straight horizontal line with the component of ship speed in the direction of wave travel equal to $V_s \cos\psi$. The time at heading and speed for slamming is thus given by the cross hatched bands shown in Fig. 4-10.

In the actual sea, there is a continuous distribution of length as well as height. Since the distribution of time at speed is not uniform, the actual distribution of slamming occurrences may be different from that for the idealized analysis used. However, the exact description of the sea may never be known, and the use of the lumped characteristics seems to be justified at the present time.

One exception will be made for the group of waves lumped at 125-ft length. While all the critical speed encounters in the 85-ft waves will be downwave (conditions not leading to significant slamming), a large number of the 125-ft group will be upwave. It is estimated that 1/3 of all the waves in the 125-ft band will be of lengths permissive of upwave slamming.

The percentage of the total time in which the ship will encounter slamming conditions is obtained from Fig. 4-10. For each specified true wave length (L_w = 125, 220 and 340) there will exist equivalent wave lengths equal to $L_w \cos\psi$. Each equivalent wave length has one critical slamming speed range as indicated by cross hatching. Since both speed and equivalent wave lengths represent averages of a band, it is possible to define segments of the polar which define the slamming occurrences as a percent of the total polar (see cross hatched areas in Fig. 4-10). Hence, the percent of time during which slamming will occur for each heading is

$$\% \text{ time} = \frac{2 \text{ (deg per segment)}}{360} \times \% \text{ time at speed for 220 ft at } 53°,$$

$$\text{segment } \% \text{ time} = \frac{2 \times 7.25}{360} \times 4.5 = 0.18\%.$$

The number of occurrences of the different wave heights at each true wave length ($\psi = 0°$) is obtained from Fig. 3-6. The percent time from the above equation and the number of occurrences of each of the heights for a given true wave length provides the number of occurrences of slamming conditions which the ship will experience in a prescribed period of time. Peak pressures are now obtained from Figs. 4-8 and 4-9 for each of the wave heights and equivalent length (true length/cosψ) combinations. Thus, the data are now in the form of occurrences of peak pressures. Table 4-1 is typical of this procedure.

The occurrences of the peak pressures for each true wave length are put in the form of cumulative occurrence curves by summing up the occurrences beginning with the highest pressure as shown in Table 4-2. The resulting data for each of the true wave lengths are shown in Figs. 4-11 and 4-12. The total cumulative occurrence curves shown in these plots are obtained by the direct addition of the curves for the different wave lengths. The summation curves of peak pressures for the two stations are compared in Fig. 4-13.

The peak pressures discussed above are used primarily to establish the structural requirements of the hull plating. However, by means of Eq (10b) they can be translated into local accelerations for use in determining hull bending. Equation (10b) may be written in the form

$$n = \frac{a_{max}}{32.2} = \frac{C}{32.2} \left(\frac{\text{length}}{\text{width}}\right)^{1/3} \left(\frac{1}{M_r}\right)^{1/3} P_p \qquad (10c)$$

where

P_p is in psf.

TABLE 4-1

Occurrence of Peak Pressures due to Slamming in 220-

	①	Time Factor = 0.00477 (Fig. 4-10)			Time Factor = 0.00956			Time Factor = 0.00358		
H_w	Occurrence	$\frac{L_w}{\cos\psi}$	Occurrence	P_p	$\frac{L_w}{\cos\psi}$	Occurrence	P_p	$\frac{L_w}{\cos\psi}$	Occurrence	P_p
6	6×10^4	220	286	3.1	234	573	3.0	266	215	--
7	5.6×10^4		268	4.2		535	4.0		200	3.5
8	5.3×10^4		253	5.4		506	5.1		190	4.5
9	4.8×10^4		229	6.9		459	6.4		172	5.7
10	4.4×10^4		210	7.5		420	8.0		157	7.0
11	3.9×10^4		186	10.2		373	9.5		140	8.4
12	3.5×10^4		167	12.2		334	11.4		125	10.1
13	3.0×10^4		143	14.2		286	13.3		107	11.8
14	2.6×10^4		124	16.5		248	15.4		93	13.8
15	2.2×10^4		105	19.0		210	17.7		78	15.8
16	1.9×10^4		91	21.3		182	20.0		68	17.9
17	1.6×10^4		76	24.0		153	22.5		57	20.0
18	1.3×10^4		62	27.0		124	25.0		47	22.5
19	1.05×10^4		50	30.0		100	28.0		38	25.0
20	8.5×10^3		40	33.0		81	31.0		30	27.7
21	6.9×10^3		33	36.5		66	34.0		25	30.2
22	5.5×10^3		26	40.0		53	38.0		20	33.5
Selected	From Fig. 3-6		0.00477 x ①	From Fig. 4-9						

LE 4-1

Slamming in 220-Ft Waves--Station 2

tor = 0.00358		Time Factor = 0.00364			Time Factor = 0.00187			Time Factor = 0.00086		
urrence	P_p	$\frac{L_w}{\cos\psi}$	Occurrence	P_p	$\frac{L_w}{\cos\psi}$	Occurrence	P_p	$\frac{L_w}{\cos\psi}$	Occurrence	P_p
215	--	306	218	--	368	112	--	427	52	--
200	3.5		204	3.1		105	--		48	--
190	4.5		193	4.0		99	3.4		46	3.0
172	5.7		175	5.0		90	4.3		41	3.8
157	7.0		160	6.2		82	5.3		38	4.7
140	8.4		142	7.4		73	6.3		33	5.7
125	10.1		127	8.9		66	7.6		30	6.8
107	11.8		109	10.5		56	8.9		26	8.0
93	13.8		95	12.0		49	10.3		22	9.3
78	15.8		80	14.0		41	12.8		19	10.6
68	17.9		69	15.8		36	13.5		16	12.2
57	20.0		58	17.8		30	15.2		14	13.6
47	22.5		47	20.0		24	17.0		11	15.3
38	25.0		38	22.3		20	19.0		9	17.1
30	27.7		30	24.5		16	21.0		7	19.0
25	30.2		25	27.0		13	23.0		6	20.7
20	33.5		20	29.5		10	25.5		5	23.0

2

TABLE 4-2

Cumulative Occurrences for 220-Ft Waves fro

P_p	Occurrence	Summation of Occurrence	P_p	Occurrence	Summation of Occurrence	P_p	Occurrence	S O
40	26	26	21	16	1272	13.5	36	
38	53	79	20.7	6	1278	13.3	286	
36.5	33	112	20	182	1460			
34	66	178		47	1507	12.8	41	
33.5	20	198		57	1564	12.2	167	
33	40	238	19	7	1571		16	
31	81	319		125	1696	12.0	95	
30.2	25	344	17.9	68	1764			
30	50	394	17.8	58	1822	11.8	107	
29.5	20	414	17.7	210	2032	11.4	334	
28	100	514	17.1	9	2041			
27.7	30	544	17.0	24	2065	10.6	19	
27	62	606	16.5	124	2089	10.5	109	
	25	631				10.3	49	
25.5	10	641	15.8	78		10.2	186	
25	38	679		69		10.1	125	
	124	803	15.4	248				
24.5	30	833	15.3	11		9.5	373	
24	76	909	15.2	30	2625	9.3	22	
23	5	914						
	13	927	14.2	143		8.9	127	
22.5	47	974	14	80	2848		56	
	153	1127				8.4	140	
22.3	38	1165	13.8	93		8.0	420	
21.3	91	1256	13.6	14			26	

TABLE 4-2

r 220-Ft Waves from Table 4-1--Station 2

Occurrence	Summation of Occurrence	P_p	Occurrence	Summation of Occurrence	P_p	Occurrence	Summation of Occurrence
36		7.6	66		3.8	41	
286	3277	7.5	210		3.5	200	
		7.4	142		3.4	99	
41		7.0	157	6264	3.1	286	
167						204	
16		6.9	229		3.0	573	
95	3596	6.8	20			46	11,189
		6.4	459				
107		6.3	73				
334	4037	6.2	160	7205			
19		5.7	172				
109			33				
49		5.4	253				
186		5.3	82				
125	4525	5.1	506				
		5.0	175	8426			
373							
22	4920	4.7	38				
		4.5	190				
127		4.3	90				
56		4.2	268				
140		4.0	535				
420			193	9740			
26	5689						

The length-to-width ratio of the wetted area to be used in slamming loads is 3.0. This approximation was arrived at by a rational consideration of the ship's motion through waves having periods which would produce slamming. Also, the fact is considered that the most likely area to encounter severe slamming pressures is centered at Station 2. In view of these considerations and the ship's beam at this Station 2, a length-of-width ratio of 3 appears to be the maximum applicable to slamming. The remaining constants are given below for Stations 1 and 2 together with the reduced equations for local accelerations in terms of g units.

Station 1	Station 2
$\beta = 45°$	$\beta = 30°$
$C_1 = 0.44$ (from Fig. 3-12)	$C_2 = 0.27$
$\frac{x^2}{k^2} = 5.01 \quad x_1 = 59.8$	$\frac{x^2}{k^2} = 3.07 \quad x_2 = 46.8$
$k = 26.7$	$k = 26.7$
$M_r = 3190$ (Eq (3))	$M_r = 4700$
$n_1 = 0.187\ P_p$	$n_2 = 0.103\ P_p$

where

P_p is in pounds per square inch.

The local accelerations for Stations 1 and 2 are shown in Fig. 4-14. For structural analyses these accelerations are normally referred to the center of gravity. The transfer to the center of gravity is accomplished by dividing the local acceleration by the reduced mass factor $1 + \frac{x^2}{k^2}$. This puts the acceleration in terms of total ship mass. Figure 4-15 presents the linear accelerations at the cg for loads applied at Stations 1 and 2.

4.2.5 Deck Wetting Pressure Loads

During the course of its operation a ship will encounter heavy sea conditions in which the deck will be submerged to varying depths beneath ensuing wave crests as the ship plunges and thereby is subjected to large hydrostatic pressure loads. The following investigation treats this condition using a rational analytical method to determine the order of magnitude of the highest of such loadings with the purpose of providing the designer with a better estimate of what the design loading should be for this condition. Deck pressures are determined as an example for one forebody station, Station 1/2.

Lewis in Ref. 10 indicates that the conditions for the wettest decks are the same as for slamming. However, due to the relative height of the deck above the still water level, the presence of slamming does not necessitate wet decks. Graphical representations of the ship's motions in waves such as Fig. 4-7 indicate that only the worst of the slamming conditions typified by waves of low length-to-height ratios whose length is near the ship length, will cause wet decks and hence highest pressure loads.

At the point in time that the decks are wettest (Fig. 4-2) the craft is moving forward through the wave, and is beginning to pitch upward by the bow. Thus, the deck pressures of the bow region consist of the static head of water on the deck, and the force component due to the upward acceleration.

Since the deck's loads occur as a result of the worst slamming conditions, the same basic analytical treatment may be used as for slamming. First, the main displacement buoyancy is assumed located aft on the ship ($F_a \approx W$), and secondly, the ship is considered pitching with a simple harmonic motion having a period approximately equal to the wave period (T_E). The response to the buoyant forces may be expressed by Eq (4a).

$$\frac{F_b}{W}\left(1 + \frac{b^2}{k^2}\right) = n_b - 1 + \frac{ab}{k^2}$$

The local load factor, n_b, at b, the centroid of the bow plunging load, F_b, is obtained from the second assumption, the harmonic pitching motion. Assume the pitching to take place about the cg and have angular motion equal to the maximum wave slope, then the amplitude of motion at b is equal to ($b\,\pi\,H_w/L_w$). The maximum acceleration at b is determined by:

$$n_b = \frac{\omega^2 A}{32.2} + 1 = \left(\frac{2\pi}{T_E}\right)^2 \left(b\,\pi\,\frac{H_w}{L_w}\right)\frac{1}{32.2} + 1.$$

The motion is actually a combination of pitch and heave and it should be noted that the equivalent amplitude, $(b\,\pi H_w/L_w) = A$, does not imply pure rotational motion.

A tabulation of the results of the simultaneous solution of these two equations follows. The table is based on the use of both the ship's calculated radius of gyration and the arbitrarily assumed radius of gyration of one-quarter of the ship's length, which is used (Ref. 10) to account for the damping of the attached virtual water masses. The dimensions a and b, the locations of the aft buoyant force and the bow plunging force, F_b, are estimated from Fig. 4-2.

	Without Virtual Water Mass	With Virtual Water Mass
a	27.5 ft	27.5 ft
b	46.8 ft	46.8 ft
k	26.7 ft	32.5 ft
ab/k^2	1.89	1.28
b^2/k^2	3.36	2.27
L_w/H_w	7.0	7.0
T_E	5.2 sec	5.2 sec
n_b	2.0	2.0
$F_b = W \frac{(1 + ab/k^2)}{(1 + b^2/k^2)}$	415,000 lb	437,000 lb
F_a (normal buoyancy)	627,000 lb	627,000 lb

As shown in the table the required bow forces, F_b, are approximately the same, varying by only 5%, and equal about 2/3 of the normal displacement buoyancy. With the two forces (F_b and F_a) thus determined, the ship is graphically positioned on the critical wave profile (while simultaneously satisfying both buoyancy values) to determine the height of the wave crest with respect to the deck. In Fig. 4-2, the wave crest is seen to be somewhat forward of Station 1/2 at the instant of slamming. However, it can be conceived that in the next ensuing instant the crest will be at station 1/2 with the up acceleration being approximately the same. Thus, the deck pressure for this near maximum encounter is determined as follows using a wave crest 8 ft above the deck.

$$n_{cg} = \frac{F_a + F_b}{W} = \frac{627,000 + 415,000}{627,000} = 1.66$$

$$n_{1/2} = n_{cg} + \frac{66.3}{46.8}(n_2 - n_{cg}) \quad \text{where } 66.3 = \text{distance to Sta } 1/2$$

$$= 1.66 + 1.41\,(2.0 - 1.66) = 2.14$$

and

$$P_{1/2} = 64 \times h \times n_{1/2}$$

$$P_{1/2} = 64 \times 8 \times 2.14 = 1100 \text{ psf}$$

The above procedure was followed for several wave lengths and heights shown in Fig. 3-6. It was found that by the time the lengths become 220 ft or longer and length-to-height ratio exceed 12, the stem is not likely to submerge. Waves shorter than 125 ft are also not critical.

Thus, it can be concluded that for a ship of the proportions chosen for this study the maximum deck pressures at the bow due to plunging may be as high as 1100 psf. Further investigations conducted in a similar manner would be required to determine the maximum values throughout the forebody, but these values would also have to be decreased to account for the lessening of the crest height as the wave moves aft along the ship's length and as the water flows off the deck to either side as the bow rises.

The occurrence levels in 125-ft waves at like conditions (i.e., heading, speed, wave height) will be the same for both slamming and deck wetting. However, the cutoff point will be different since slamming can occur without wet decks. For example, in Figs. 4-11 and 4-12 the conditions which give the maximum peak pressures (23 and 43 psi) are the same as those which cause the highest deck pressures at a wave length-to-height ratio of 7. The occurrence levels for deck pressures corresponding to other wave length-to height ratios were obtained in a similar manner. The resulting cumulative occurrences per year of the deck pressures are shown in Fig. 4-16.

Other parts of the deck from midship to stern will be subjected from time to time to masses of water from waves breaking over the gunwales in combination with roll action of the ship. These pressures will be less than those on the forward deck due to the lower vertical acceleration from roll and static heads. A peak pressure of 450 psf, equal to the static head of 7 ft, is estimated as the worst condition.

Thus, for the study ship the design deck pressure is assumed to vary from 1100 psf at the bow to about 450 psf amidship and is constant at 450 psf from amidship aft.

4.2.6 Superstructure Wetting Pressure Loads

Water pressure loading of a ship's superstructure is equal at the base of the side walls to the local deck pressure and decreases linearly to zero at a height equal to the crest of the highest passing wave. Thus, the design loadings are entirely dependent upon the general arrangement of the superstructure on a particular ship. However, special consideration must be given to certain areas where heavy masses of water wash with substantial velocity against such areas as the flat forward wall of a deck house or a protrusion along the longitudinal sidewall of the structure.

Considering, for example, the study ship used in this investigation it may be seen that the forward vertical wall of the pilot house at Station 1-1/2 could encounter a substantial wash of water upon emerging from a plunging condition.

The relative velocity of the water mass would be the advancing speed of the particles in the crest of the wave plus the ship's speed. (The ship will be proceeding slowly at this time.) The particle speed in the wave crest is (trochoidal wave)

$$v_w = 7.1 \sqrt{L_w} \frac{H}{L_w}$$

and since the worst conditions of plunging occur at wave lengths near the ship's length and at the highest waves ($H/L_w \approx 1/7$) the velocity of the water is

$$v_w = \frac{7.1}{7} \sqrt{125} = 11.3 \text{ fps}$$

In these wave conditions the ship could not likely exceed 15 fps. Thus, the maximum relative velocity is v = 11.3 + 15 = 26.3 fps.

The dynamic pressure, P, is determined by

$$P_D = C_D \cdot \frac{\rho}{2} \cdot V^2$$

If the forward face of the pilot house is flat, the drag coefficient, C_D, may be assumed equal to unity. Hence, the maximum dynamic pressure would be

$$P_D = (1) \left(\frac{2}{2}\right) (26.3)^2 = 690 \text{ psf}$$

In addition to this dynamic head pressure it is necessary to add the static head pressure increased by whatever heaving acceleration may also exist. The condition of wave washing against the pilot house corresponds to position 2 in Fig. 4-7. The angular acceleration is reduced to near zero by the balance of aft buoyancy and bow loading. The total acceleration on the hull will still be near maximum. The same wave and ship conditions can be expected to produce maximum deck loading and superstructure pressure loads. Thus, the heaving acceleration to be applied to the static head pressure is $n_{cg} = 1.66$ (from example in Section 4.2.5).

If the height of the crest at Station 1-1/2 is 3 ft

$$P_s = 64 \times 3 \times 1.66 = 320 \text{ psf}$$

Thus, the total pressure is

$$P_T = P_D + P_s = 690 + 320 = 1010 \text{ psf}$$

and is distributed as follows:

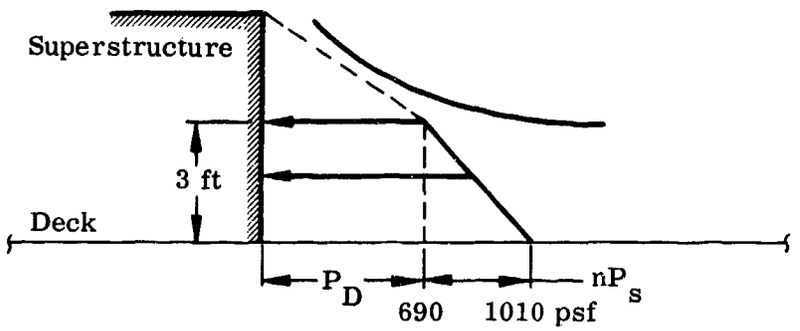

Thus, the superstructure side wall of a ship would be designed for a pressure at the deck equal to the design deck pressures decreasing to zero at the top of the passing wave crest. For regions subject to a dynamic pressure due to the velocity of a moving water mass the dynamic head pressure plus the accompanying static head should be used.

4.2.7 Side Plating Pressure Loads

In addition to ordinary buoyancy forces the side plating of a ship is subject to dynamic pressure loads resulting from the velocity head of waves breaking against the hull sides. This will occur at particular points on the hull depending upon the ship's heading and upon wave lengths. In very long waves the entire ship responds to the motion of the wave and hence it is, in local regions, only lightly affected by the wave velocity. In shorter waves the overall effect on the ship is small; the ship holds its position in space but in local areas the side plating will feel the full effect of the velocity head from the breaking waves. Now, since wave velocity is a direct function of the square root of the wave length, the longest waves which least affect the ship's motion will produce the highest local dynamic pressures. The critical wave length for this condition may be different for various locations along the hull's length and could only be determined from experimental data. However, it is likely that the critical wave length is less than that equivalent to the ship's length. Therefore, for preliminary design the designer may conservatively assume the ship's length as the critical wave for this condition. For the study ship of this investigation a 125-ft wave is chosen. In the breaking wave the top velocity approaches the wave celerity, $2.26\sqrt{L_w} = 25.3$ fps (for $L_w = 125$). The dynamic pressure loading will be 640 psf, about the same as for the superstructure.

Thus, the side plating for the study ship would be designed for a dynamic pressure of 640 psf plus the static pressure from buoyancy.

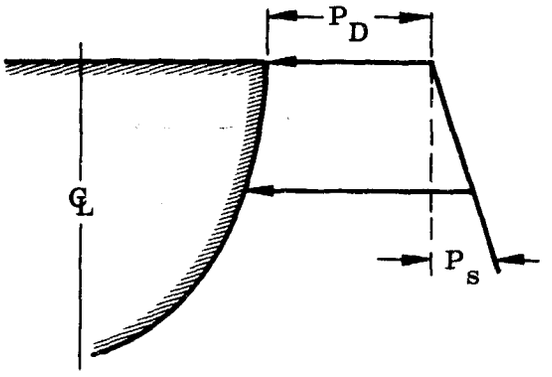

Theoretically, breaking waves occur when the length-to-height ratio is below 7.0. Figure 3-9 gives a cumulative occurrence of 5000 per year for such waves 125 ft in length. Since the craft is operational 60% of the year and is in hullborne operation 90% of the operational time, the total numbers of times the ship can be struck by these critical waves is 5000 x 0.6 x 0.9 = 2700. Because of the random heading with respect to the waves these occurrences are distributed uniformly through 360°. It follows then that the bow and after side plates (both port and starboard) each experience these pressures 675 times per year. (Any particular local area would be loaded to this level less than 1/3 of this level.)

4.3 FOILBORNE CONDITIONS LOADS

4.3.1 Summary

In the foilborne, or flying conditions, the ship is subjected to loads not encountered in the displacement condition, and the increase in ship speed is potentially a source of greatly increased loads and pressures as compared to displacement condition loadings.

The displacement condition loadings were primarily a function of the ship configuration and the operating natural environment. In the foilborne conditions (including the transition from displacement to flight, takeoff and landing) there are major factors in the environment which are under the control of the pilot. In addition, there will usually be automatic flight controls which operate to limit the attitude of the ship and the load factors to be experienced.

Since impact loads for hulls of hydrofoil craft at high speeds are similar to those experienced by water based aircraft, a comparison is made with previous seaplane experience on pressure and loads.

4.3.2 Hull Impacts

4.3.2.i Normal Landing

The attitude, forward speed and vertical velocity in takeoff and landing are under the control of the pilot within the limits of the basic ship performance and control system design restraints.

The basic ship performance restraints are partially described by the foil design operating characteristics:

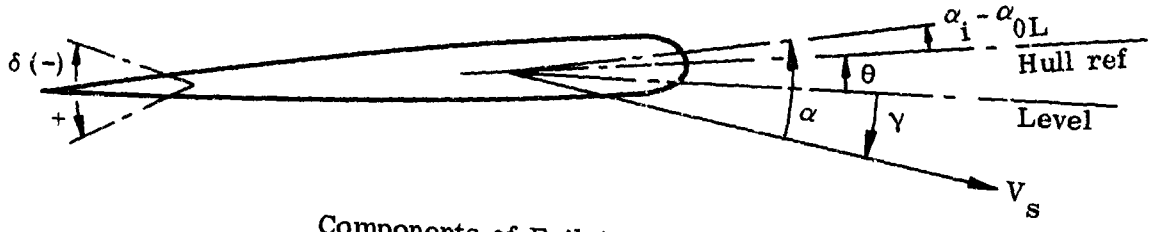

Components of Foil Angle of Attack

where

V_s = ship speed = initial speed/cos γ

γ = flight path angle

δ = flap angle

θ = ship trim angle (hull reference line, (+) up by the bow)

$\alpha_i - \alpha_{0L}$ = incidence of foil zero lift line to hull reference

$C_L = \alpha C_{L_\alpha} = \left(\alpha_i - \alpha_{0L} + \gamma + \theta + \frac{d\alpha}{d\delta} d\delta\right) C_{L_\alpha}$

C_{L_α} = lift curve slope

For equal foil loadings the total lift is:

$L = C_L \frac{\rho}{2} V_s^2$ (total foil area, S)

and, prior to initiating the takeoff or landing transient, the ship is assumed to be in steady motion (L = W).

The maximum vertical velocity of the ship that could be obtained will be limited to the flight path angle, γ, that would result in the steady state with full deflection of the control. At this condition the lift is equal to the weight and the vertical velocity is at its greatest value.

$$C_{L_{design}} \frac{\rho}{2} V_{s_{design}}^2 S = W = L_{(\delta, \gamma)_{max}} = C_L \frac{\rho}{2} V_2^2 S$$

$$\alpha_{design} C_{L_\alpha} V_{s_{design}}^2 = \alpha C_{L_\alpha} V_s^2$$

$$\alpha_{design} \left(\frac{V_{s_{design}}}{V_s} \right)^2 = \alpha_i - \alpha_{0L} + \gamma + \theta + \frac{d\alpha}{d\delta} \delta$$

$$v_v = V_s \gamma = V_s \left[\alpha_{design} \left(\frac{V_{s_{design}}}{V_s} \right)^2 - (\alpha_i - \alpha_{0L}) - \theta - \frac{d\alpha}{d\delta} \delta \right]$$

In actual practice the finite distance from the hull in the flight altitude to the water surface will put a further limitation to the sinking speed in landing:

$$v_{v_{drop\ limit}} = \sqrt{2\ a\ h}$$

where h is the drop height and a the acceleration. The downward acceleration is under control of the pilot. In either manual or automatic control it is unlikely that the negative g value would be allowed to exceed 0.5. At this acceleration,

$$v_{v_{-0.5\ g\ limit}} = \sqrt{32.2\ h}$$

The height above the water (h = 10 ft) and length of the ship also limit the maximum trim angles that can be attained to less than ±8°, and it is anticipated that the normal takeoffs and landings would be restricted to lie between ±6°.

The map of vertical velocity versus the ship speed for various trim angles for the 45- and 100-kn example ship designs is shown in Fig. 4-17. Since the maximum sinking speed for the 100-kn design can be obtained at θ = 0° with flap control (δ = -15°), it is not necessary to go to a bow-down attitude for quick landing, as it is on the 45-kn design.

An assumed distribution of attitude at landing is shown in Fig. 4-18. The ship speed at landing must be between the maximum design speed and the stall speed. For statistical purposes it is assumed that all the landings will be equally divided between two forward speed conditions 45- (or 100-) kn design speed and 25- (or 40-) kn minimum speed. The maximum sinking speeds are taken from Fig. 4-17. This combined distribution of attitude, forward speed and sinking speed may represent rather extreme conditions for the average hydrofoil ship. However, high sinking speed landings could be the normal characteristic in ASW missions.

The distribution of the landing approach conditions is used in conjunction with the sea surface conditions to determine the statistical distribution of pressures and loads which determine the structural design loading. The sea surface conditions are represented by the wave summaries in Figs. 3-8 through 3-11, cut off at the maximum operating height of 13 ft. Preliminary calculations indicated that the waves could be grouped at three height ranges without significant loss in accuracy: 6 ft (3 to 9), 10 ft (9 to 11) and 12 ft (11 to 13) for each typical length of wave. Table 4-3 gives the maximum wave slope, ϕ max, and the percentage of time that the particular range of wave heights and lengths are present with respect to all conditions suitable for foilborne operation (waves less than 13 ft estimated for the example design). The total rough water percentage adds to 75%, and the remaining 25% corresponds to relatively smooth water (waves less than 3 ft).

TABLE 4-3

H/L_w		85	125	220	340
6	ϕ	= 12.7°	8.6°	4.9°	3.2°
	t	= 16.4%	32.4%	12.0%	2.4%
	$r\omega$	= 4.63	3.81	2.88	2.32
10	ϕ	= 21.2°	14.4°	8.2°	5.3°
	t	= 0.5%	3.8%	2.5%	0.8%
	$r\omega$	= 7.70	6.35	4.78	3.85
12	ϕ	= 25.4°	17.3°	9.8°	6.4°
	t	= 0.2%	1.7%	1.5%	0.8%
	$r\omega$	= 9.25	7.62	5.75	4.63

orbital wave velocity, $r\omega = 7.1\ H/\sqrt{L_w}$ (trochoidal)

The direction of heading is assumed to be evenly distributed around the clock. Typical loading conditions are shown below:

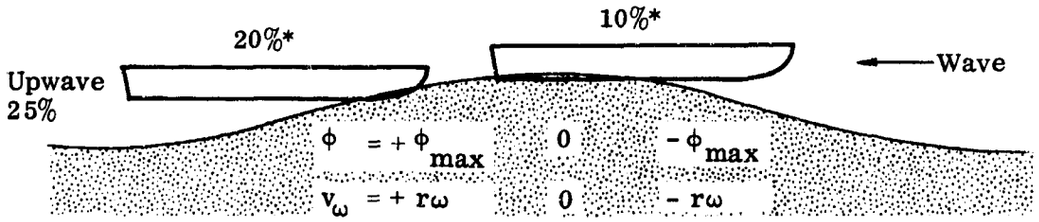

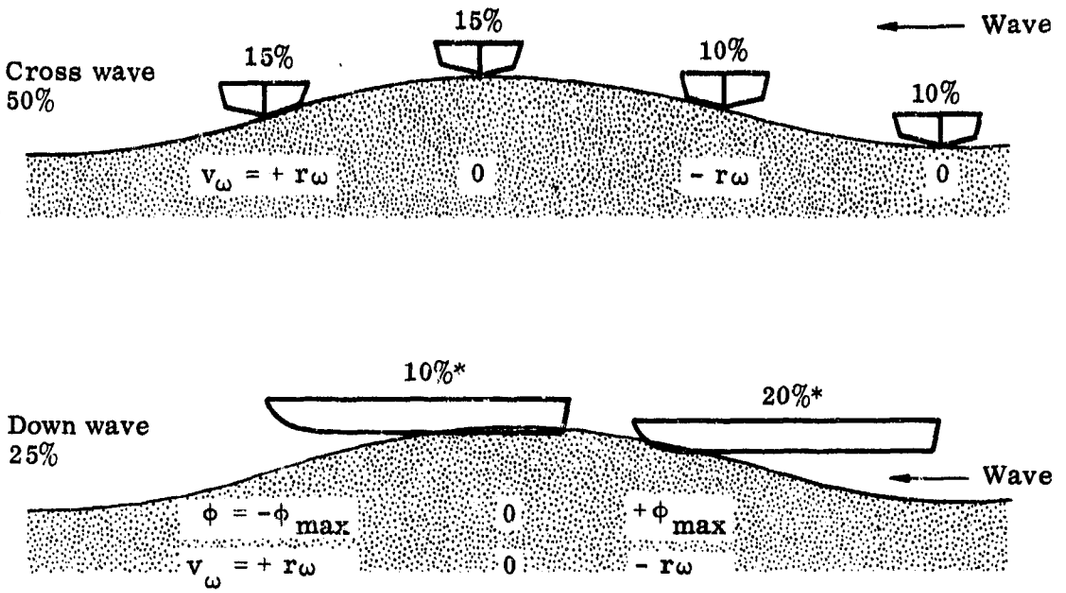

*Not mutually exclusive--bow loading may follow stern contact.

The total number of landings per year is based on the ship's availability (60%) and the percentage of time foilborne (10%). Thus, the ship is on the foils 6% of the year, 525 hr. For an average flight of 15 min, the total number of landings is 4 x 525 = 2100/year.

The number of landings for a particular set of conditions is found as in the following example:

Design speed	45 kn		100 kn		
Landing speed	45	25	100	40	
Ship attitude, θ	0	0	0	0 (selected)	
% time	30%	30%	13%	13% (Fig. 4-18)	(a)
Sinking speed	12	11	18	18 (Fig. 4-18)	
Wave range	10 ft x 125 ft 3.8% of time		$\phi_{max} = 14.4°$ (Table 4-3)		(b)
No. of landings	24	24	10	10 (a) (b) 2100/100 x 100	

The actual loadings experienced by the ship hull will depend not only upon the gross conditions described above but also on the detail condition at actual contact with the water surface. Direction of the ship motion with respect to the wave system, position of contact on the wave, roll angle and the geometry of the hull will all affect the impact pressures and loads. A complete evaluation of these factors, even for the example designs, is beyond the scope of this study. However, some consideration can be given to the direction of landing with respect to the waves as it affects the probable impact conditions.

The impact in each condition is determined by the relative normal velocity at the hull station under consideration, the hull deadrise angle and the relative trim angle between the local hull form and water surface.

Normal velocity, $v_n = v_v + V_s (\theta + \tau) + v_w$

v_v = ship sinking speed (Fig. 4-18)

θ = ship attitude (selected input to Fig. 4-18)

τ = geometric slope of hull lines to reference lines

v_w = vertical component of orbital velocity

This normal velocity, v_n, is used in Eq (5) to obtain the peak pressure acting on the hull station. This equation is plotted in Fig. 4-19 with deadrise angle, β, and effective trim angle, τ^* ($\tau^* = |\tau + \theta - \phi|$) parameters against the peak pressure divided by the normal velocity squared.

The geometric characteristics of the example hull at several typical stations are:

Station 2	$\beta = 30^\circ$	$\tau = +4^\circ$
6	6°	-2°
8	5°	-3.5°

With these hull form data, the distribution of headings and possible wave contact conditions shown and the particular set of conditions selected above for the landing attitude and wave range, it is now possible to complete the determination of the peak pressures.

v_s (knots)	45	25	100	40
(fps)	76	42.2	168.5	67.5
v_v	12	11	18	18

Case 1 bow, 20% upwave $v_w = r\omega = 7.1 \times 10/\sqrt{125} = 6.4$ fps

Station 2 $\theta + \tau = 0 + 4^\circ = 0.07$ rad

$|\theta + \tau - \phi| = 10.4^\circ$ $P_p/v_n^2 = 6.2/144$ (Fig. 4-19)

v_n (fps)	23.7	20.4	36.2	29.1
P_p (psi)	24.2	18.0	56.4	36.5
No. of occurrences	4.8 (20% of 24)	4.8 (20% of 10)	2	2

Case 2 midship and stern, cross wave 15%, upslope $v_w = 6.4$

Station 6 $\theta + \tau = 0 - 2^\circ = -0.035$

$|\theta + \tau - \phi| = 2^\circ$ $P_p/v_n^2 = 178/144$

v_n	15.7	15.9	18.5	22
P_p	306	315	424	600

Station 8 $\theta + \tau = 0 - 3.5^\circ = -0.061$

$|\theta + \tau - \phi| = 3.5^\circ$ $P_p/v_n^2 = 140/144$

v_n	13.7	14.8	14.1	20.3
P_p	183	213	194	402
No. of occurrences	3.6	3.6	1.5	1.5

Similar calculations throughout the range of conditions provide the data for the cumulative plots of peak pressure in Figs. 4-20 and 4-21.

It will be noted that the pressures on the after portion of the example hull are quite large. The primary factor is the low deadrise angle. Even though the relative normal velocity is lower in the after portion of the ship, the low trim angle at contact in combination with the small deadrise yields high pressures. Since the trim angle is largely governed by external circumstances, only change in hull form to utilize higher deadrise can relieve the high pressure conditions. The effect of such charges is indicated by the alternate lines in Fig. 4-20.

4.3.2.2 Crash Landings Due to Foil Loss

Unusual landing conditions may occur due to the loss of one or more of the main supporting hydrofoils. Lateral unbalance as a result of foil damage will result in roll-yaw motions whose analysis is beyond the scope of this study. However, complete loss of lift at either forward or aft foils may be treated as a simple body motion, assuming that the ship rotates about the undamaged foil.

The ship crashes into the water by rotating about the remaining lift vector, the weight moment being balanced by the inertia of the hull.

$$\frac{W}{g}\,(k^2 + x_{cg}^2)\,\ddot{\theta} = W x_{cg}$$

$$\ell\ddot{\theta} = g\,\ell\, x_{cg}/(k^2 + x_{cg}^2)$$

$$\ell\dot{\theta} = \sqrt{2\,(\ell\ddot{\theta})\,\ell\Delta\theta} = \ell\sqrt{2\,g\,x_{cg}\,\Delta\theta/(k^2 + x_{cg}^2)}$$

where

W = gross weight

k = radius of gyration about cg

x_{cg} = distance from cg to remaining foil

θ = pitch angle

$\Delta\theta$ = change from initial level flight condition

ℓ = distance from remaining foil to area of impact

The local acceleration, velocity and drop height at the impact area are $\ell\ddot{\theta}$, $\ell\dot{\theta}$ and $\ell\Delta\theta$, respectively.

TABLE 4-4

Impact at Station	1	2	8
ℓ	80.8	67.8	80
x_{cg}	21	21	49
k	26.7	26.7	26.7
$k^2 + x_{cg}^2$	1155	1155	3110
$\ell\dot{\theta}\sqrt{\Delta\theta}$	88.5	73.3	80.5
$\Delta\theta$	0.12 7°	0.14 8°	0.12 7°

TABLE 4-4 (continued)

Impact at Station		1	2	8
$v_v = \ell\dot{\theta}$		30.6	27.3	28
β		45°	30°	5° (12°)
τ		15°	4°	-3.5
P_p (Eq 5)	45 knot	27.0	25.0	1060.1 (330.0)
	100 knot	44.0	12.3	1450.0 (452.0)

The resulting impact pressures at Stations 1 and 2 for loss of the front foil and at Station 8 for loss of rear foils are calculated in Table 4-4 for smooth water conditions. Actually the sea will have substantial waves more than 75% of the time. Depending upon the position of impact with respect to the wave, the impact pressures will be more or less than the smooth water value in Table 4-4. Calculations of the probable distributions of the impact conditions and the resulting peak pressures were made in a manner similar to those for the normal landings, and the resulting distributions are plotted in Fig. 4-22.

4.3.2.3 Landing Loads

For the purpose of structural design, the overall load associated with the peak pressure, and its occurrence rate is needed in addition to the peak pressure distribution. This load can be found by utilization of Eq (10b).

$$a_{x_{max}} = CP_p \left(\frac{\text{length}}{\text{width}} \quad \frac{1}{M_r}\right)^{1/3}$$

where C is a constant dependent on the deadrise angle from Fig. 3-12. A reasonable approximation for the length-width relationship is length = 3 width, therefore for

		β	M_r
Station 2	$n_{x_{max}} = 0.1032\ P_p$	30°	4,800 (slugs)
Station 6	$n_{x_{max}} = 0.0130\ P_p$	6°	19,000
Station 8	$n_{x_{max}} = 0.0145\ P_p$	5°	8,300

where P_p is in psi and n_x is in g. The load is $32.2\ M_r\ n_x$.

For example, in the Case 2, Station 6 impact above, the local acceleration at Station 6 would be:

$$n_{x_{max}} = 0.0130\,(306) = 4 \text{ g for 45-kn ship at 45 kn}$$
$$(315) = 4.1 \text{ g for 45-kn ship at 25 kn}$$
$$(424) = 5.5 \text{ g for 100-kn ship at 100 kn}$$
$$(600) = 7.8 \text{ g for 100-kn ship at 40 kn}$$

It should be noted that the development of the load formulas was based upon the analysis of the weightless impact. This is basically consistent with the landing approach conditions where the maximum sinking speed was determined in most cases by the steady-state maximum glide angle. It would thus appear necessary to add 1 g to the above accelerations to get the actual load factor on the ship. At small values of the impact force and accelerations this is correct, but at the large values (> 2 g) the change in vertical velocity during the build-up to the maximum load will be sufficient to markedly change the lift on the foil system.

Since the detailed analysis of the actual ship response (including its automatic system inputs to the foil controls) is outside the scope of this analysis, it will be generally assumed that at the time of maximum impact load the foil lift is zero on the foils which experience upward acceleration and unchanged from the steady glide on foils receiving downward acceleration due to the impact. (Except that at least 1 g combined loading on hull and foils will always be assumed.)

The distributions of the local acceleration in normal landing are plotted in Figs. 4-23 and 4-24. All bow-type loadings are assumed to be centered at Station 2 while the stern and midship landings are assumed equally divided between Stations 6 and 8. Thus, the number of significant pressure occurrences and loads is the same for the bow (Station 2) but the loading occurrences are 1/2 the pressure occurrences for Stations 6 and 8 (e.g., the pressure for Station 6 at occurrence level 10 is 310 psi, and the corresponding acceleration is 4 g ($= 0.013 \times 310$) at occurrence level 5).

At low load levels there are two factors which must be added to the impact load distribution to obtain a total landing load distribution curve. The assumed glide approach on the foils will maintain the total acceleration at least to the 1 g level, and the large number of incidental wave contacts in takeoff and landing runout will increase the occurrence rate. These effects are shown in the curve extensions (dashed lines) in Figs. 4-20 through 4-24.

The impact load factors in terms of the total ship mass are determined by dividing the local impact acceleration by the reduced mass ratio, $1 + x_{cg}^2/k^2$. These load factors are plotted in Figs. 4-25 and 4-26.

4.3.3 Flying Loads--Hydrofoils

A hydrofoil system passing through a seaway is subject to loads induced by the waves. Since the foils are relatively fixed in trim and heave, the disturbing function is the vertical component of the wave internal particle velocity. The effect of this velocity on the fixed foil is to give it an effective angle of attack

$$\alpha_e = \frac{v_w}{V_s}$$

where

v_w = vertical component of internal particle velocity (fps)

V_s = ship speed (fps)

The maximum vertical velocity component is the orbital velocity. By trochoidal wave theory, the orbital velocity at depth below the surface is

$$v_{w_{max}} = r\omega = 7.1 \frac{H}{\sqrt{L_w}} e^{-\frac{2\pi h}{L_w}}$$

where

L_w = wave length (ft)

H = wave height (ft)

h = depth of submersion (ft)--assumed to be 8 for both foils

If the rate of change of the foil lift coefficient with change in angle of attack, C_{L_α}, is known, the incremental change to the lift coefficient for a change in angle of attack is

$$C_L = \alpha_e C_{L_\alpha}$$

The proportional change in foil load, defined as a load above the normal running load, is:

$$\Delta L/L = \Delta C_L/C_L = \alpha_e C_{L_\alpha}/C_L$$

At the point of maximum vertical velocity ($v_w = r\omega$) the change in foil load

$$\Delta L/L = r\omega \left(C_{L_\alpha}/C_{L_{design}}\right) V_s/V^2_{s_{design}}$$

It is anticipated that almost all of the foilborne time will be spent at the design speed. However, since speed reduction is a practical method of alleviating the loading conditions, the data will be shown for two speeds for each example ship design: 35 and 45 for the 45-kn ship and 70 and 100 for the 100-kn ship. No attempt was made to proportion the time at each speed, and the occurrence rate data are presented on the basis of either one speed or the other full time.

The sea conditions are summarized in Table 4-3, and the heading of the ship with respect to the waves is uniformly varied as in the landing analysis. Since the orbital wave velocities occur without regard to the direction of travel of the ship, the primary change with heading is the encounter rate: [see Eq (12)]

$$\text{Encounter rate} = (V_s \cos \psi + V_w)/L_w$$

which averages out to approximately $(2/3)\ V_s/L_w$.

The number of wave encounters is thus obtained for each wave group in Table 4-3 by combining the operational time foilborne with the percentages of time that the various waves occur and the wave length and ship speed.

$$\text{Occurrences/year} = (\text{seconds/year})\ (\%\ \text{foilborne})\ (\%\ \text{wave condition})\ (2/3\ V_s/L_w)$$

$$= (3.15 \times 10^7)\ (0.60 \times 0.10)\ (\%\ \text{from Table 4-3})\ (2/3\ V_s/L_w)$$

$$= 1.26 \times 10^6\ (\%\ \text{Table 4-3})\ (V_s/L_w)$$

Figures 4-27 and 4-28 show the results of operation of the fixed foil system in the assumed operating conditions.

The addition of an autopilot to the fixed foil system reduces the load to some prescribed value. A detailed analysis of an autopilot system and its function is beyond the scope of this study. Therefore, it is assumed that the autopilot will hold the load change to some prescribed level as presented by the dashed lines in Figs. 4-27 and 4-28.

Reference to Figs. 4-27 and 4-28 shows that, with fixed foil response to waves, load factors five times the desired 0.25 g load factor above normal load occur a large percentage of the time. For subcavitating foils (Fig. 4-25) a load factor of 1.5 g above normal load will occur approximately 1000 times in the course of a year. These load factors can be reduced to almost any

reasonable level by having an autopilot apply control surface reactions rather than assume a fixed foil response. If 0.25 g is the desired maximum load level, then except for some dynamic effects, the maximum load on the foil should not exceed the nominal 0.25 g above normal load. This assumes that the autopilot and the hydraulic control system are working perfectly.

The actual load level for design depends upon the reliability of the autopilot and hydraulic control systems. Analysis of each component in the hydrofoil flap hydraulic control system indicates the servo and relief valves to be the most critical components. Failure of either of these components would result in either a full up or full down flap deflection. These positions would be analogous with a rapid landing or other single cycle response rather than with the fixed foil response to waves as shown in Figs. 4-27 and 4-28.

In order to obtain the load factors due to fixed foil response, it is necessary that the control surface lock in a given position for a given wave and velocity condition. The autopilot is designed to alleviate this condition and limit the load factor to a predetermined level, e.g., 0.25 g. Analysis of the autopilot system indicates that the accelerometers and gyros are the only components in the system that would produce the condition of locked flap position just described. Using standard reliability failure rates of 0.000011 for the two rate gyros and 0.000008 for the three accelerometers, and including an operational factor of 20 for shipboard use, the combined mean time between failures is 1080 hr.

If a typical mission of one-month duration assumes 70 hr of foilborne time, the probability of successful operation (failure free) is given by:

$$P_s = e^{-t/\bar{t}}$$

where

t = operation time

$\bar{t}$ = mean time between failures (MTBF).

Using the autopilot MTBF of 1080 hr and 70 hr per mission on the foil

$$P_s = e^{-70/1080} = 0.937$$

The probability of successful operation is therefore 93.7%. (Obviously, this probability is for a given autopilot system. No attempt has been made to see what is required to increase the MTBF of the autopilot components that bear on the fixed foil response to waves.)

The effect of such a failure may be considered in several ways:

(1) The mission proceeds without limit.

(2) The particular run is completed.

(3) Landing is made as soon as practical.

In relatively smooth conditions it would be feasible to proceed with the mission if the stability of the system was not impaired. The level of actual occurrences would be determined by the portion of total time that the load control would not be working. With the failure occurring on 6.3% (100% - 93.7%) of the missions on the average, in the middle of the particular trip the number of occurrences will be 3.15% of the uncontrolled motion.

For moderate sea conditions, or where the stability of the system may have been impaired, the particular foilborne run might be completed, but further operation foilborne would be with a substitute or repaired system. The number of load occurrences would drop by another large factor

$$\text{say} \quad \frac{1/2 \text{ hr/run}}{35 \text{ hr/half mission}} = \frac{1}{70}$$

In rough sea conditions, the landing (by reducing power) would be made as soon as possible (within 1 min) after a control failure, since the unrelieved motion of the vehicle would be intolerable to the operating personnel. The number of load occurrences would be reduced to $1/30 \times 1/70 \times 3.15\% = \frac{1}{70,000}$ of the unmodified occurrence rate.

The cumulative occurrence rate for the foil loads is thus built up from the basic curves as shown in Fig. 4-29. The low level load portion of the uncontrolled motion (relatively calm water) is added in at (1) a level of 0.0315, the middle portion (3-ft to 9-ft waves) at (2) $0.0315 \times 1/70$ and the high load end at (3) $0.0315 \times 1/70 \times 1/30$. A faired curve through these three sections of occurrence rates will then approximate the cumulative effects of control failure in various sea condition, as modified by appropriate operational decisions.

4.3.4 Flying Loads--Side

Struts running through waves in any direction other than perpendicular to or effectively parallel with the wave crest will experience side loads due to the motion of the water particles within the waves. By trochoidal wave theory, the maximum horizontal velocity component will occur at the crest and trough of the wave. These velocities are equal in magnitude, but opposite in direction, such that passing through a wave will cause loads in both directions. The magnitude of the velocity, $r\omega$, is tabulated with the other wave parameters in Table 4-3.

Since the strut is a symmetrical airfoil, side loads will occur only when the strut has an effective angle of attack. This angle of attack is:

$$\alpha_e = \frac{r\omega \sin \psi}{V_s + r\omega \cos \psi}$$

where

α_e = effective angle of attack (deg)

V_s = ship velocity (fps)

ψ = ship heading (deg) (0° heading into waves)

$$F_s = \alpha_e C_{L_\alpha} A_s \frac{\rho}{2} V_R^2$$

where

F_s = lift = side load on strut (lb)

C_{L_α} = lift curve slope

V_R = effective velocity = $\sqrt{V_s^2 + 2 V_s\, r\omega \cos \psi + (r\omega)^2}$

A_s = submerged side area of the strut (ft^2) = $(\text{draft} \pm \frac{H}{2})\, \overline{C}$

$\overline{C}$ = strut chord (ft)

This analysis assumes the forcing function acts as a sharp edge gust, with no relief from movement of the affected surface. The boat will actually tend to roll and yaw in some fashion. The autopilot will attempt to overcome this tendency, and will, to some extent. It is beyond the scope of this study, however, to determine the actual motion of the autopilot-stabilized boat in waves; therefore, no correction is applied to the loads.

For example, assume the forward strut traveling at normal draft, 8 ft, at 45 kn parallel (at the crest) with 10-ft waves having a wavelength of 125 ft:

$\overline{C}$ = 5 ft

V_s = 76 fps

$r\omega$ = 6.4 fps

A_s = (8 + 10/2) 5 = 65

$$C_L = 4.3/\text{rad}$$

$$\psi = 90°$$

$$V_R = \sqrt{(76)^2 + (6.4)^2} = 76.5$$

$$F_s = \left(\frac{6.4}{76 + 0}\right) 4.3\,(65)\,(76.5)^2 = 140{,}000 \text{ lb}$$

In most cases, as in this example the wave speed is less than 10% of the ship speed so that the force is approximated by

$$\frac{F_s}{C_{L_\alpha}\,(A_s)\,V_s} = r\omega \sin\psi$$

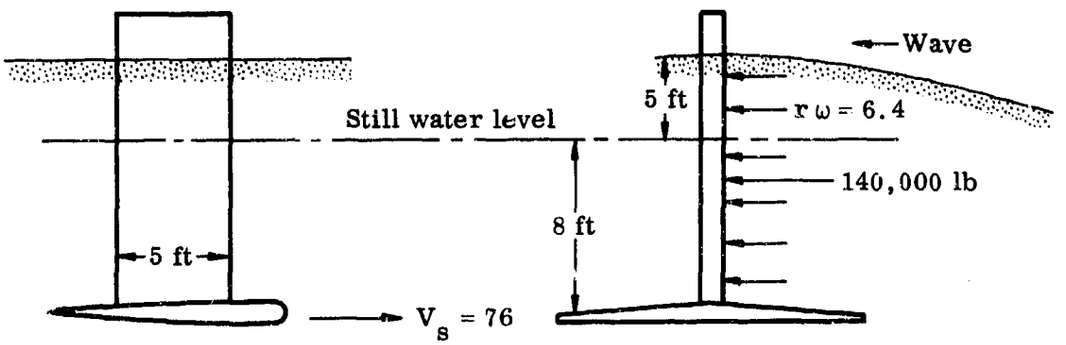

The occurrences of these loads within the wave spectrum are calculated in a manner similar to the foil load change curves. It is assumed that the boat spends an equal amount of time at each of the following headings:

$$\psi = 0°; 30°; 60°; 90°; 120°; 150°; \text{and } 180°.$$

Figure 4-30 represents the percentage occurrences of the strut side loads as functions of the strut design parameters (C_{L_α} and submerged area), design speed, and the wave distribution defined by Table 4-3. Using these generalized data and assuming a chord length of 5 ft with a lift curve slope of 4.3/rad for 45 and 100 kn, the load frequency spectrums of Fig. 4-31 were generated.

This analysis assumes the surface orbital velocity of the wave to be uniform over the entire depth of the submerged strut in spite of the fact that the orbital wave velocity diminishes as the inverse log of the submerged depth. This was

done since the load relief calculated by using the actual submerged orbital wave velocities for the reasonable design foil depth of 8 ft resulted in approximately a 15% reduction. Hence, the use of the uniform side load based upon the surface trochoidal velocity appears to be a reasonable conservatism in view of the statistical sea state derivation.

The spectrums in Fig. 4-31 correspond to the passage of the strut through the wave crest. A complete cycle of strut loading includes a reversal of the load when passing through the wave trough. These loads are smaller because of the reduced strut area involved by a factor ranging from 2.2 for 6-ft waves to 7 for 12-ft waves.

Turning the ship requires an additional steady side force on the struts. For fairly tight turns (0.3g) the load per strut is approximately (0.3/3) W = 63,000 lb. This is probably not additive in any substantial rough water since the roll control of the ship would be insufficient. It is assumed that some form of automatic control would be provided to prevent sharp turns at high speeds in rough water.

4.4 SPECIFIC COMPONENTS CRITERIA

The preceeding sections give the measure of the peak pressures and loads which will be experienced by the ship hull in dynamic encounters such as slamming and landing. In the application of these to the design of the actual structure there are some additional factors which must be considered with regard to the extent of the loaded area, the pressure distribution and the value of the peak pressure at the time of the maximum loads.

The peak pressure spectrums for the various impacts are given by Eq 5 using the normal velocity at initial contact. As soon as a significant area is loaded, the resulting force retards the normal velocity, and although the area increases, the pressure decreases. The maximum load occurs when the virtual water mass, M_w, equals 2/7 at the reduced ship mass, M_r (see Section 3.4). At this point the normal velocity equals the normal velocity at initial contact divided by $(1 + M_w/M_r) = 9/7$, and the peak pressure is the initial peak pressure divided by $(9/7)^2$.

The shape of the impact area at maximum load will depend upon the hull form and the water surface conditions. For simplicity and consistency with the load derivation (Section 3.4, Eq 10) a rectangular loaded area is assumed with a length-to-width ratio of 3. The width of the area, 2y, at the maximum load condition is given by:

$$\rho K \pi a y^3 = K (6\pi/8) (2y)^3 = M_w = (2/7) M_r$$

$$2y = \left[(8/21\,\pi K)\ M_r\right]^{1/3}$$

and the length of the impact area is 3 (2 y)

The distribution of the pressure across a section is primarily dependent upon the deadrise angle, as shown in Fig. 4-32 for constant velocity impact. (These curves from Ref. 4 are the source for the P average/P peak data which are shown in Fig. 3-12.) In addition to this pressure distribution (which is determined by the rate of expansion of the wetted area) there is a negative pressure due to the deceleration of the virtual water mass previously set in motion (the $a_x M_w$ term which is included in Eq 6).

The distribution of the inertial pressure is elliptical according to theoretical analysis at low deadrise angles, and this will be assumed to apply for all deadrises.

$$\text{(Pressure) (Area)} = \frac{\pi}{2}\left(P_{\text{inertial}_{\text{keel}}}\right) y\,(6\,y) = a_x M_w = a_x K\,6\,\pi y^3$$

$$P_{\text{inertial}_{\text{keel}}} = a_x\,2K\,y$$

The net pressure distribution for typical midship sections is shown in Fig. 4-33. Two examples are shown for a landing impact at Station 6: one for the initial design deadrise angle $\beta = 6^\circ$ and one for an increased deadrise $\beta = 17^\circ$. The conditions for the landing are the same as the Case 2 (cross wave at 45 knots) example used in Section 4.3.2:

β =	6°	17°
v_n (fps)	15.7	15.7
P_p/v_n^2 (psi)	178/144	26.5/144
$P_{p\ \text{initial}}$ (psi)	306	45.5
$n_{x_{max}}$ (g)	4	1.6
$K = 1 - \frac{2\tan\beta}{\pi}$	0.93	0.81
2 y (ft)	13.7	14.3
Length (ft)	41	43
$P_{\text{inertial}_{\text{keel}}}$ (psi)	11.4	4.4

β =	6°	17°
P_p at n_{max} (psi)	186	27.5
$P_{average}$ at n_{max} (psi)	39	15
$P_{average_{(net)}}$ (psi)	$39 - \frac{\pi}{4}(11.4) = 30$	$15 - \frac{\pi}{4}(4.4) = 11.5$

The net pressure distribution (constant velocity theory minus the inertial pressure) is to be used in the design of the ship structure. The transverse distribution of the load is not significant with respect to overall hull loading, but for plating, stringers, floors and bulkheads it is important to know the shape of the loading as well as the average value. As indicated in the general curves, Fig. 4-32 and the specific example, Fig. 4-33, the lower the deadrise the more extreme the variation in pressure on the bottom at any instant. In the low region the deadrise is 30° or more and the pressure is not far from uniform. In the initial design the midship and after sections have deadrise of 6° or less, and the pressure distribution is such that one-half the loading is concentrated in the outer 15% of the wetted area. Even for the higher deadrise (17°) of a revised hull form the pressure at the outer edge is 4 to 5 times the net pressure at the keel.

It should be noted that the peak pressure at the edge of the impact wetted area is directly related to the increase in width of the impact area and a component of the ship forward speed. Except for the bow regions the contribution of the planing pressure from the ship forward speed is usually quite small. Therefore, a reasonably estimate of the increase in width of the pressure area may be made directly from the value of the peak pressure

$$P_p = \frac{\rho}{2}(dy/dt)^2$$

$$(dy/dt) = \sqrt{P_p} \qquad (P_p \text{ in psf})$$

Thus, the peak pressure point for the example of $\beta = 6°$ ($P_p = 144 \times 186 = 26,800$) is moving outward on the hull bottom at 164 fps.

4.4.1 Hull Bottom Plating, Stringers and Bulkheads

The application of the computed loadings to the particular components of the structural design can not be given in the form of exact criteria except in a general way. The water loads applied to the hull skin as pressures are reacted by the stresses within the plating and stringers, which are in turn supported by floors and bulkheads to be distributed throughout the hull to the final reaction of the inertial forces of the ship mass. However, in consideration of the type of pressure distributions applied to the hull, it is possible to establish some guide lines for the conventional static structural analysis of plating, stringers and bulkheads.

The mechanism of the support of normal pressures by relatively flat plating is such that excessive permanent set of the plating occurs long before actual rupture of the plating. Actual breaks in bottom plating when they do occur are generally the result of fatigue cracking brought on by repeated loadings. The two general criteria for the bottom plating are given as an allowable permanent set of the plating (usually given as % of the span between stringers) and life expectancy required for typical operational experience.

The peak pressures given on a cumulative occurrence basis (as, for example, in Fig. 4-20) provide the basic information required for application of both criteria. However, reference to the typical instantaneous pressure distribution, Fig. 4-33, shows that the peak pressures on the cumulative occurrence curves must be modified for application to the plating design. First, the pressure must be averaged over the stringer spacing (particularly for low deadrise).

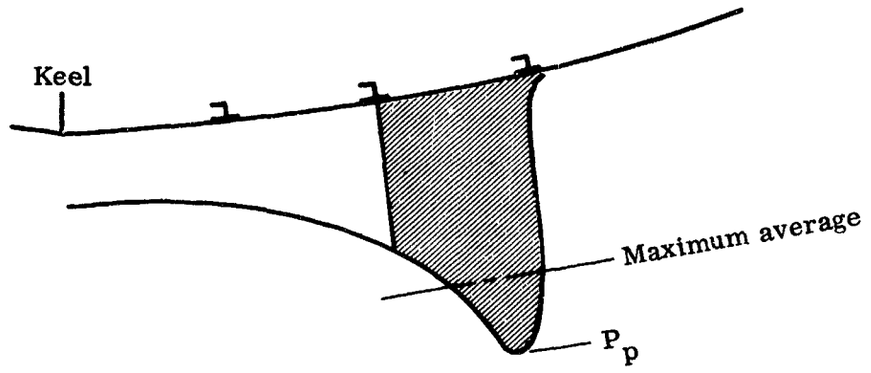

Secondly, for plating some distance from the keel, the peak pressure itself will be lower due to the progression of the impact (as in Fig. 4-33 the peak pressure 7 ft from the keel is $(7/9)^2$ of the peak pressure at the initial contact at the keel).

The stringers are loaded by the plating, and similar modifications to the pressures apply. Generally, the pressure for the stringers design is less than for the plating, since the bays on both sides of a stringer must be loaded for maximum loading.

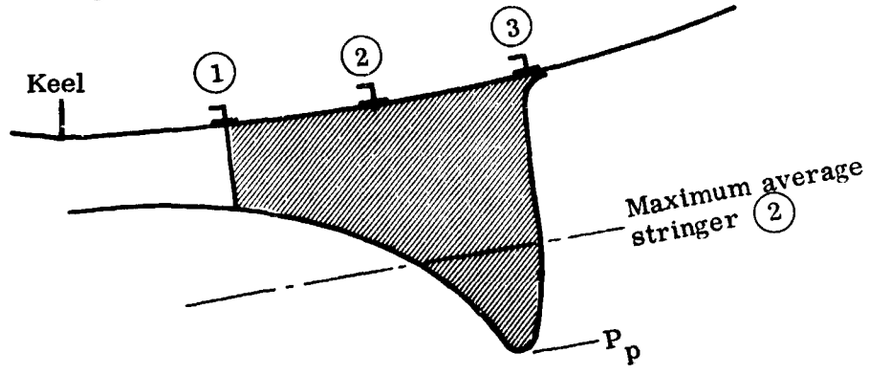

As progressively larger areas are wetted, the stringers build up the loads on floor frames and bulkheads. The value of peak and average pressures at the time of maximum total impact load may be determined as shown at the beginning of this Section (illustrated in Fig. 4-33). The arrangement of the hull structure may be such that some other lesser total load would be critical for structural design. In that case intermediate values of the pressures must be estimated between the initial values at the keel and the values at peak impact.

4.4.2 Deck Structure

The forward weather deck may experience substantial waterloads from waves, Section 4.2.5, but much of the deck is relatively lightly loaded. Thus, additional criteria were developed to ensure the stiffness of the deck as well as its strength.

The stiffness of the immediate underfoot deck structure was considered from a psychological as well as a structural point of view. Unlike the usual concept that a structure which is strong enough is stiff enough, the deck structure must be of such rigidity that personnel traversing it will sense that it is rugged, substantial, more than just adequate. For the various types of deck structure, the criteria for stiffness are:

(1) Plate stiffness

The parameter $\frac{Et^3}{b^3}$ should be greater than 20

where

E = modulus of elasticity, psi

t = plate thickness, in.

b = stringer spacing, in.

(2) Stringer stiffness

The parameter $\frac{EI}{L^3}$ should be greater than 45, but need not be greater than 70

where

E = modulus of elasticity, psi

I = section moment of inertia of the stringer, in.^{4}

L = longitudinal spacing of transverse supports, in.

These criteria were concluded by experimentation with actual fabricated panels of plate-stringer design. Two 34 x 60 inch aluminum alloy panels were constructed, one with 0.072-inch plating and stringers at 8-inch spacing, the other with 0.080-inch plating and stringers at 6-inch spacing. The stringers on each panel were 1-3/4-inch deep I-sections attached to the plating with two rows of spotwelds.

The experiment was conducted by placing the panels on various arrangements of simple transverse supports and determining, by the consensus of personnel traversing the panels, which configuration and support spacing provided a satisfactory "feel" of strength and rigidity considering individually the plating stiffness between stringers and the stringer stiffness between supports.

The plating stiffness of the panel with the wider spacing between stringers was considered inadequate. The plating stiffness of the panel with the narrower spacing between stringers was considered to be adequate. Since plating stiffness is directly proportional to the modulus of elasticity of the material and the cube of the thickness and indirectly proportional to the cube of the short span dimension, the parameter $\frac{Et^3}{b^3}$ can be used to describe the acceptable range of stiffness. This is shown in Fig. 4-34.

The effect of stringer spacing on the average deck weight using constant stiffness and strength as a basis is also shown in Fig. 4-34. The variation in weight shows a slight advantage for a design using light plating and closely spaced stringers.

The desired stringer stiffness is determined by considering a man's full weight to be concentrated at the midspan of one central span of a beam continuous over many equally spaced supports. To use the fabricated experimental panels for determining stringer stiffness, it was necessary to employ the simple beam equivalent, i.e., the simple beam whose distance between supports would result in the same deflection as a continuous beam over many supports but loaded in one central bay. The simple beam span equivalent is approximately eight-tenths of the continuous beam span. The consensus of personnel traversing the panels, with panel support provided at various spacings, was that simple spans greater than 34 inches felt too flexible and that spans less than 28 inches were more than adequate. Converting these simple beam spans to the equivalent continuous beam spans and using the parameter $\frac{EI}{L^3}$ to represent stiffness, it was concluded that for satisfactory stiffness the value of the parameter should be greater than 45 but that it need not be greater than 70. The recommended value is $\frac{EI}{L^3} = 60$.

For internal decks additional loading criteria should be included in the decking design for flooded conditions. This loading will depend upon details of the hull design layout, but it is generally estimated that allowance for a 10-ft head (640 psf) will be sufficient.

4.5 PRACTICAL CRITERIA FROM RELATED SEAPLANE EXPERIENCE

The takeoff and landing operation of a seaplane is in many respects similar to that of the hydrofoil ship. The hull is involved in substantial impacts, but must be constructed with minimum structural weight. The detailed specification of these impact loads and corresponding development of efficient structure for the seaplane was the subject of many years of study. Unfortunately, the design and production of new seaplanes came essentially to a halt just as it appeared that the various methods could be reconciled to form a unified set of design criteria substantiated by test. Although such a goal is not yet attained, a review of some of the major steps in seaplane hull structural design can provide a practical link between the experience of an existing operational system (seaplanes) and proposed criteria for a new system which is not yet operational (hydrofoil ships).

4.5.1 Landing Loads Specifications

The military specification for the determination of water loads for seaplanes at the time of last major designs was MIL-A-8629. This provided two basic formulas for the determination of pressures and overall loads:

$$P = f_1 K_1 V_s^2/\tan \beta$$

$$F = K_2 K_3 \left[W/(1 + x^2/k^2)\right]^{2/3} V_s^2/\tan^{2/3} \beta$$

Where

f_1 and K_2 are factors for relative position on the hull

K_1 and K_3 are factors for type of operation (sheltered of rough water) and the pressure area being considered (keel, chine or average across bottom)

V_s = landing speed

$W/(1 + x^2/k^2)\, g$ = reduced mass at impact point

β = deadrise angle

A formula is also given for the time for the impact load to reach its maximum value (to be used as a basis for dynamic analysis of the structure).

While these formulas provided a simple guide to the determination of applied pressures and loads, it was recognized that the empirical factors involved (f_1, K_1, K_2 and K_3) were based upon a fairly narrow range of seaplane designs. Particularly, it was noted that the formulas were based upon experience from designs with deadrise angles between 20° and 30° and previous seaplane hulls of moderate length-to-beam ratio. Thus, the specifications allowed the designer freedom to use rational methods for determination of the pressures and loads. Consideration was also given to the results of dynamic model tests in simulated wave conditions to modify the K_3 operational loads factor for advanced hull designs.

In recent years there has been a trend to specify a spectrum of landing approach conditions to be treated by a rational analysis to develop the corresponding design pressure and loading spectrums. This approach is given in MIL-A-8864 and MIL-A-8866 seaplane waterloads specifications but is not yet represented by an operating design example.

4.5.2 P5M Design

The P5M seaplane is an excellent example of a design which bridges the gap between rule-of-thumb design and the analytical approach to loading and design criteria. At the time of its design development the analysis of seaplane impact phenomena had yielded the basic formulas of MIL-A-8629. The deadrise of the hull was similar to previous designs, but the hull form was substantially changed by the extension of the afterbody. It had been shown in dynamic model tests that such an extension had a favorable effect on rough water behavior which resulted in substantially reduced impact loads. Thus, the loads determined by the MIL spec were reduced by 15% on the basis of these tests.

The structural design of the P5M followed previous seaplane experience. The applied pressures and loads were treated as steady state loadings, and the structure was designed to have sufficient strength or stiffness as required by a static design.

Two circumstances of the P5M development and operational history have provided valuable information for the correlation of design criteria and service experience. As a part of the development program, one ship was instrumented for the measurement of pressures and accelerations and flight tested in measured rough water conditions. A fairly large number of the production aircraft were in service with operating squadrons in a number of bases of varied sea conditions. The service life in these operations was sufficiently active to build up records of several thousand takeoff and landing cycles on many of the craft. The result was a scattering of plating failures and the detection of incipient fatigue cracks during regular overhaul and inspection periods.

4.5.2.1 Rough Water Demonstration Tests

The complete analysis of the P5M rough water tests is given in Ref. 14. Several of the plots are reproduced in this report to illustrate particular results.

The positive accelerations registered at the center of gravity for all landings and takeoffs are plotted in Fig. 4-35. The test data are shown in two sets, one is the relative distribution of the maximum value per landing or takeoff and the other includes all of the measurable impacts in each takeoff and landing. The two sets are essentially the same at the high load end of the spectrum, but the ratio of the number of occurrences at low load levels is quite high. It will be noted that the loading increases fairly regularly with the decrease in occurrence level (on log scale), as might be expected from a random sampling of landing conditions. However, there are not enough test data to fully define the curve. The one maximum acceleration of 4.8 g actually measured within the 52 landings might well correspond to an order of magnitude lower occurrence rate. An increase in the number of tests would be expected to fill in the distribution curve at least out to the maximum measured acceleration. An increase in the severity of the test conditions, higher waves and speed, could be expected to extend the distribution to higher loads.

The calculated maximum acceleration of the P5M according to the specification MIL-A-8629 was 6 g. This is higher than the maximum experienced during the test and would require the distribution to be extended in a straight line to an occurrence level below 0.0001. Considering the whole fleet of seaplanes, there have been well over 100,000 landings. However, the extent of rough water encounters is not known. The few cases of damage or loss to P5M hulls due to water impacts have generally been caused by some unusual circumstance not consistent with design loads requirements.

The cumulative frequency per takeoff and landing of pressures on the hull is shown in Fig. 4-36. Each diagram represents a particular pressure gage on the hull bottom. They are arranged in Fig. 4-36 in their relative location--keel at the top, chine at the bottom, step at the right and bow towards the left. In each block the design pressure according to specification MIL-A-8629 is indicated by the appropriate $|_p$ mark.

It is immediately apparent that the measured pressures regularly exceed the design values over most of the region. The trend of the pressure with decrease in occurrence level is fairly consistent among the various locations and indicates that even higher values might be expected in the normal life of a seaplane (where several thousand landings might be expected). A variation of pressure with the occurrence level is given in the later specification MIL-A-8866. This distribution is approximated by the slope of the dashed lines through occurrence level = 1 point on several of the diagrams in Fig. 4-36. While the later specification is qualitatively an improvement over the older one-point design, it appears that pressure increases faster with decrease in occurrence level than given by MIL-A-8866.

In spite of the relatively high frequency of occurrence of measured pressures higher than the design value there was little evidence of strain in the bottom plating during these tests. Part of the explanation for this may be in the detail review of a particular landing impact shown in Figs. 4-37 through 4-39. The particular instance is shown in overall context in Fig. 4-37. Of a series of impacts during a typical landing the maximum was No. 3 (about 4.4 sec after the first contact of the landing run). The value of the measured acceleration was the maximum of the whole test program, 4.8g. By noting the time of initiation of the pressure rise at each gage location, it was possible to deduce the shape and rate of growth of the wetted area as shown in the lower portion of Fig. 4-37. From these data it was then possible to compute the instantaneous pressure distribution at a given section for several time values as shown in Fig. 4-38. In this particular case the design plating pressure, the measured peak and the calculated peak are within good agreement up to the chine flare region. It will be noted that the high pressure area is traveling outboard at about 80 fps, which means that a particular plating area (6 in. between stringers) is loaded at peak pressure for less than 1/100 sec. Higher measured pressures in other cases would be moving even faster, and the duration of load would be correspondingly less.

The integration of the computed pressures over the bottom for the time intervals of the impact is compared with the measured acceleration in Fig. 4-39. Also shown is the maximum acceleration computed by the simplified theory, Eq 10b, using the measured peak pressure of 50 psi.

4.5.2.2 Hull Plating Fatigue Life

As a result of the detection of fatigue failures and incipient cracks in the hull bottom plating of P5M after several years of operations, a study was made of the life expectancy of the remaining ships. The results of this study were published, Ref. 15, and have been used as a guide to special inspection during overhaul periods.

Basically the results of this study showed the need for consideration of the loading distribution-occurrence spectrum. While the bottom plating and its supporting structure may withstand a transient load higher than the static design limit, each loading exacts its toll from the life of the structure.

The probability of damage to a typical bottom area was determined by applying Miner's Cumulative Damage Theory to the rough water flight test pressure distribution (Fig. 4-36) and combining with the statistical material fatigue properties. This established the no-failure probability plotted at a severity factor of 1.0 in Fig. 4-40.

The aircraft was operated in service in conditions which on the average were much less severe than the rough water test conditions. However, no statistical records were kept of the operating conditions. The severity factor in Fig. 4-40 is intended to represent the ratio of plating pressure in other operating conditions

to the distribution obtained in rough water tests. The full set of curves in Fig. 4-40 was determined by recomputing the cumulative damage ratios for several assumed severity factors. From statistical analysis of the two failures, as compared with the survival of the other P5M a/c in similar operating squadrons, it was determined that their probability of no-failure was quite high for the number of landings involved. The plotted points in Fig. 4-40 corresponding to the two service failures indicate that the average operational severity was between 0.6 and 0.7 of the rough water flight tests.

The results of operational experience on the P5M confirm the method of application of Miner's Cumulative Damage Theory to seaplane hull bottom loadings. On the basis of the loading spectrums for hydrofoil craft developed in Sections 4.2 and 4.3 the structural design can therefore include the consideration of operational life for the anticipated service conditions.

4.5.3 M-270 and P6M Seaplanes

4.5.3.1 High Impact Pressures at Low Deadrise Angles

The hull sections for the research seaplane, M-270, and the P6M were substantially different from normal design in that an attempt was made to approach an ideal "constant force" impact. This was to be achieved by using a rounded section near the keel as shown in the following sketch. Since little was known of the actual performance of such a design feature, a special drop test program was conducted on a full scale section of the M-270. These tests are reported fully in Ref. 3.

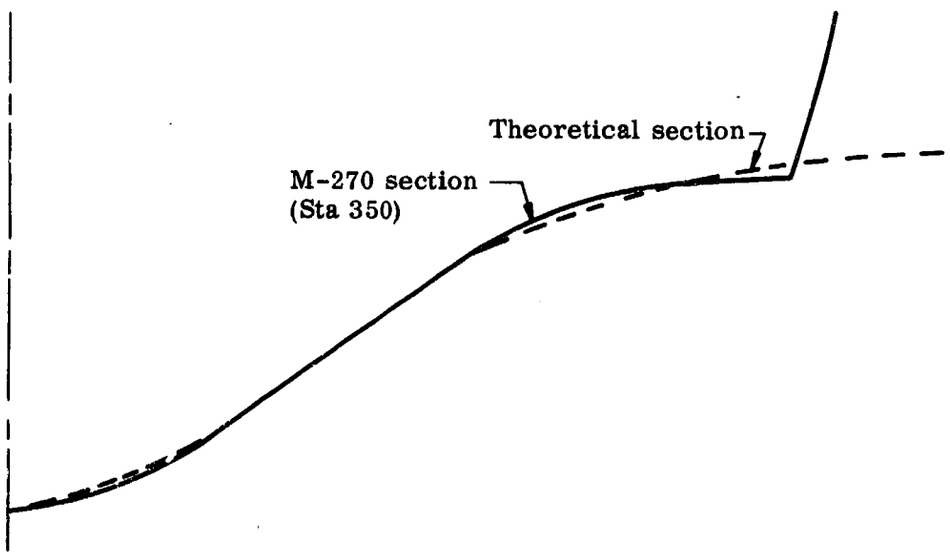

The results of the drop test of the rounded bottom section have a direct application to the impacts of relatively flat deadrise surfaces since the rounded bottom at initial contact is practically at 0 deadrise. Figure 4-41 shows a summary of pressure coefficients measured on the M-270 as compared with theory and some NACA tests on a circular section. Two curves are shown for the drop test data: one using the conventional recording of the pressure transducer outputs on 100 cps galvanometer units, the other with special high frequency response elements in the recording circuits (approximately 1000 cps). These very clearly indicate the sharp-peaked, transient nature of the pressure wave on the low deadrise surface, as shown in Fig. 4-33 and discussed in Section 4.4. However, even with the high frequency response, the theoretical peak pressure was not confirmed by measurement.

The significance of this very high pressure wave on the structure was not directly established in the drop tests, but tests were continued to the stage of visible damage or permanent set of the plating or back-up structure for several skin gages. From comparison of the typical static permanent set curves, Fig. 3-16, with the conditions of test that caused damage, an indirect measure of the effective pressure is obtained.

Plating	t/b	Pressure 1% Set	v_n	$P_{1\%}/v_n^2$
0.156	0.035	200	>40	0.125
0.081	0.018	155	35	0.127
0.064	0.0142	110	25	0.176

From these data it would appear that the theoretical average pressure at the time the first bay is fully wetted is in fair agreement with the inferred pressure on the basis of permanent set damage. Although this might be taken as a simple basis for design in the low deadrise areas of hulls, it must be kept in view that the wetted area was relatively narrow (less than 6 in. from the keel). For a constant deadrise bottom of greater extent the impact area would cover several stringer bays, and the outboard bay would be more heavily loaded.

The theoretical dynamic peak pressures estimated for the P6M hull design were averaged over the appropriate stringer spacings to obtain equivalent static design pressures. The structure was designed for limited permanent set under the derived equivalent static bottom pressures. In the limited wave conditions of the flight test programs, it is probable that maximum design pressures were not experienced by the bottom plating except near the step region. However, the lack of any visible signs of strain during the flight tests in waves up to 3 ft at speeds greater than 120 kn was taken as sufficient proof of the general adequacy of the bottom plating and stringer design.

4.5.3.2 Computation of Hull Loads

It is recognized that the method of computing the impact load for given hull form and water contact conditions, as given in Section 3.4 is a very simple representation of a complex problem. Two factors were considered particularly questionable: The use of lumped geometric hull form at a particular station and the neglect of hull bending response.

In the analysis of both the M-270 (Ref. 16) and P6M hull loadings, automatic computational methods were utilized which allowed the loads to be computed by a strip analysis of the hull loading and took into account the particular hull form, wave shape and vehicle structural response. These methods provided very detailed information on the shape of the wetted area as it varied with progress of the impact in assumed landing attitudes. However, the maximum impact loads were very close to those computed by the simple formulas using the lumped hull geometry at the station of load centroid, except for the effects of the vehicle flexibility. The P6M was relatively flexible due to a large structural cutout in the central portion of the hull, and loads were generally reduced by inclusion of the hull structural response in the computational program. The effect was much lower in the stiffer M-270 design, and it is anticipated that hydrofoil ships would generally be less flexible. Thus, although the hydrofoil ships might be affected by dynamic responses within the structure, it does not appear likely that the magnitude of the applied water loads would be affected by the hull bending flexibility.

4.6 ILLUSTRATIONS

Previous page was blank, therefore not filmed.

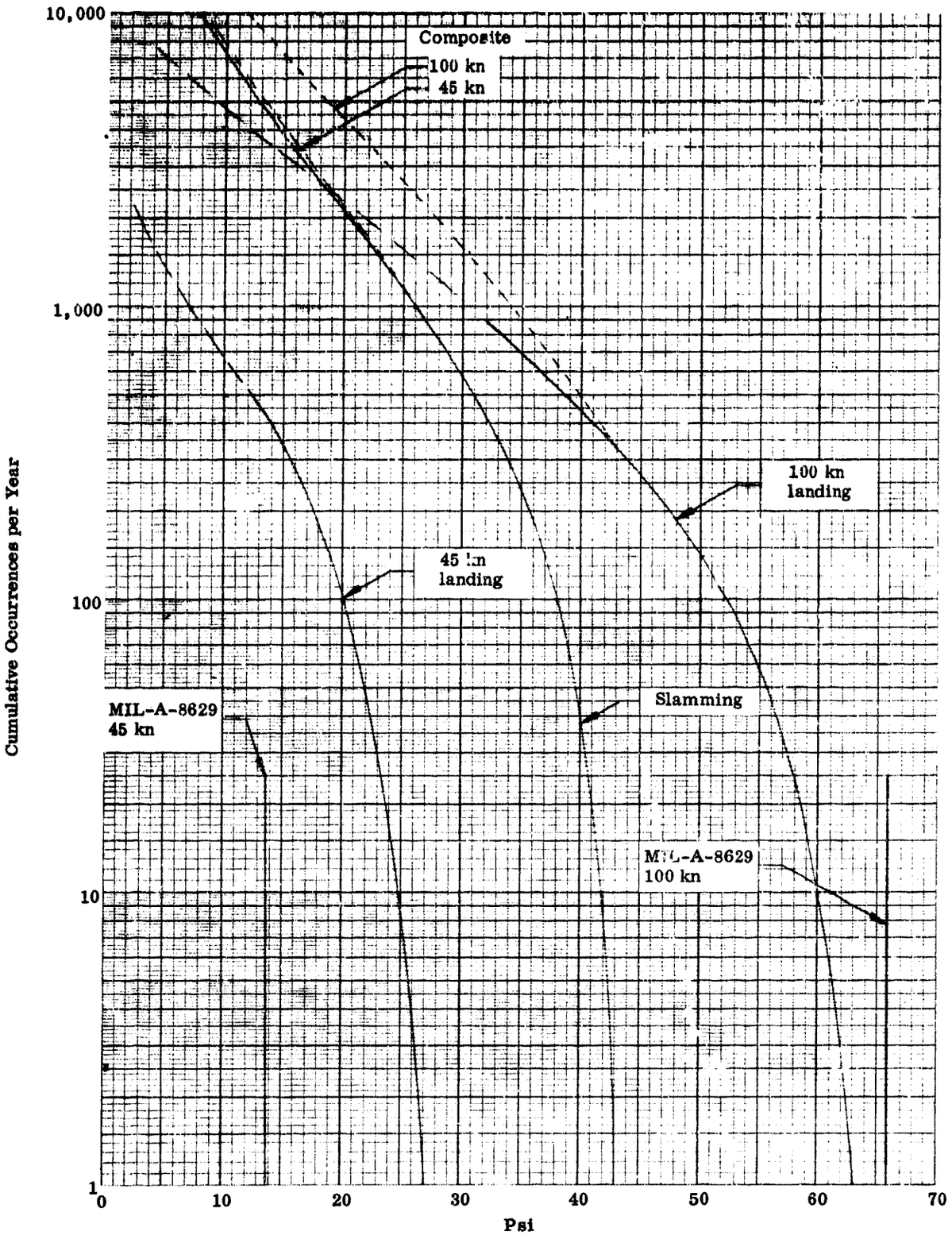

Fig. 4-1. Composite Pressure at Station 2

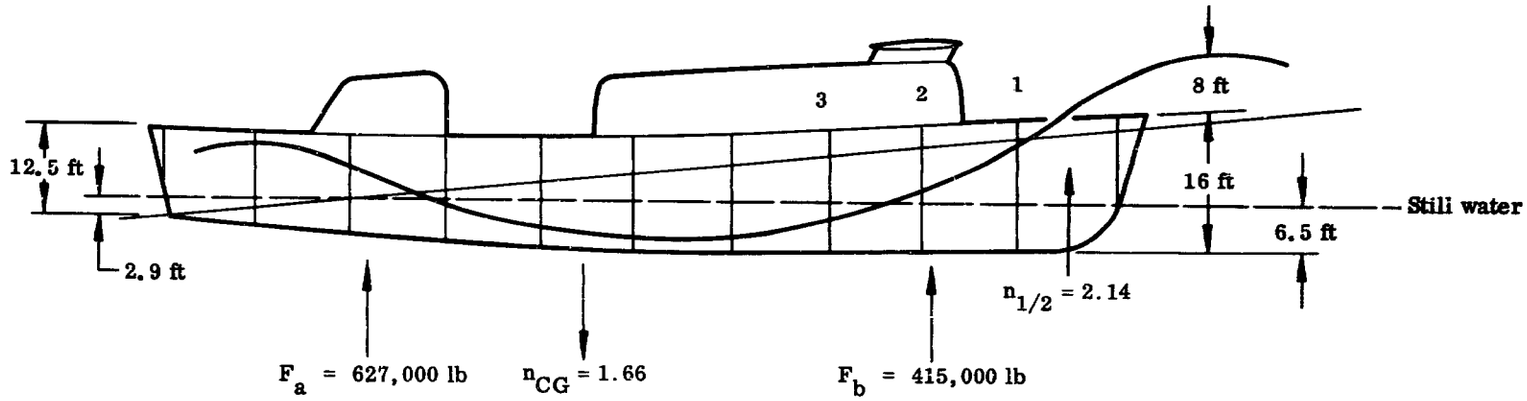

Fig. 4-2. Typical Ship Plunging Attitude

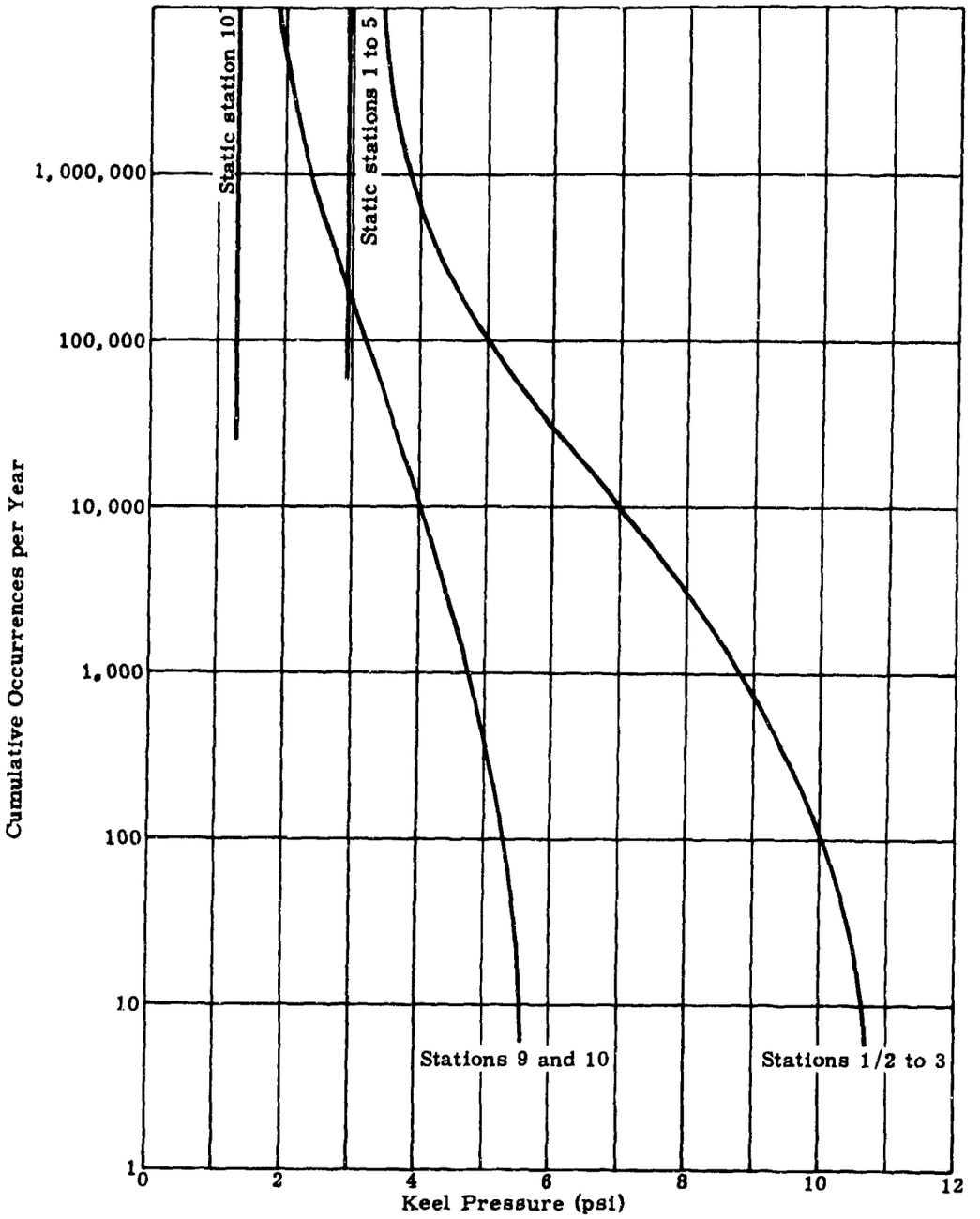

Fig. 4-3. Occurrences of Keel Pressures Due to Buoyant Forces

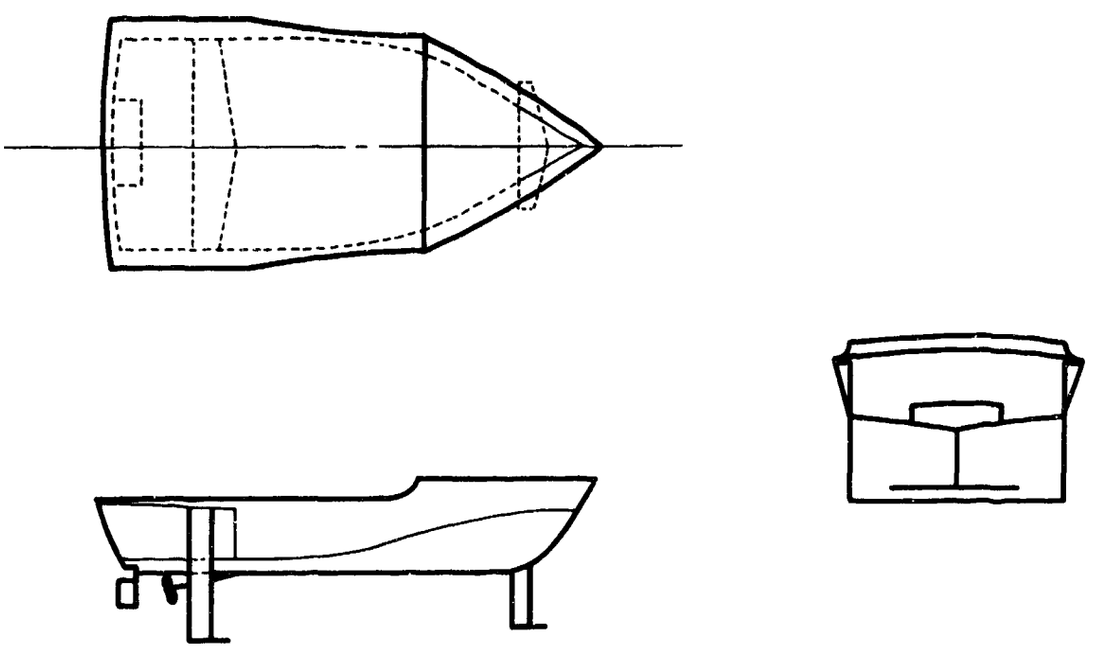

Fig. 4-4. Lenght-to-Beam Ratio 2--Hydrofoil Model

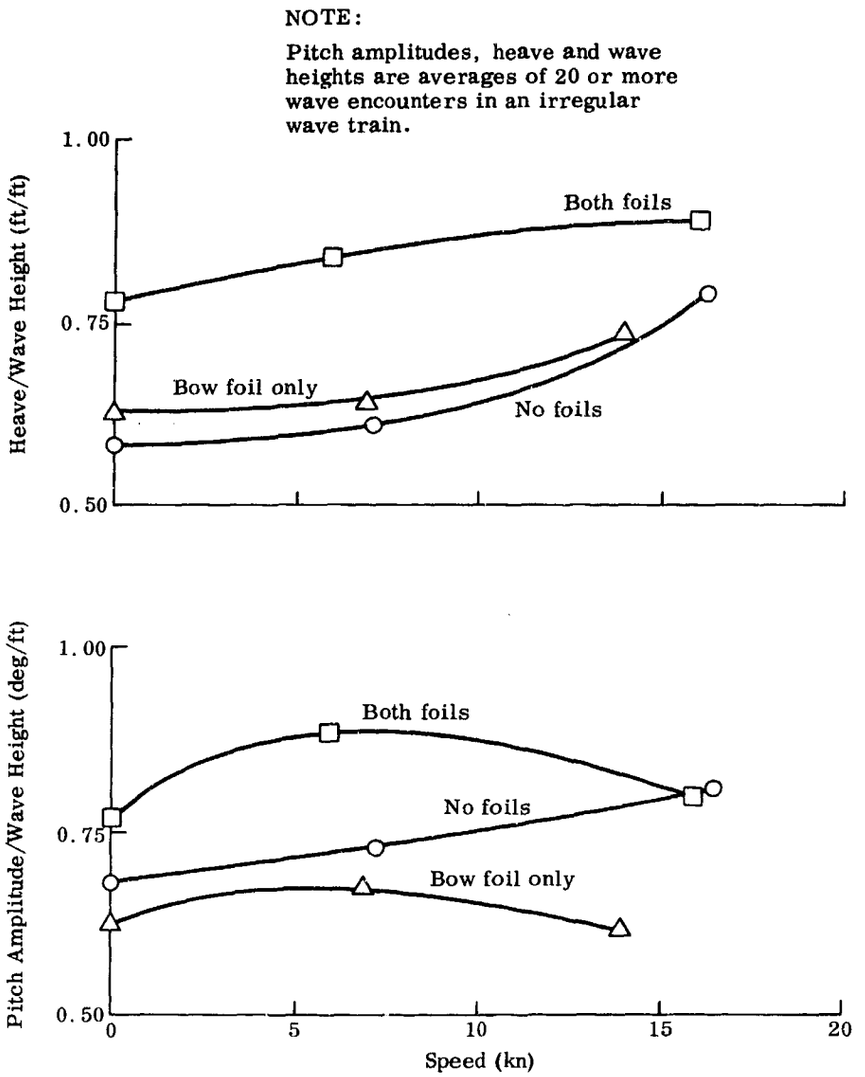

Fig. 4-5. Effect of Foil Damping on Heave and Pitch for PC(H)-Type Craft

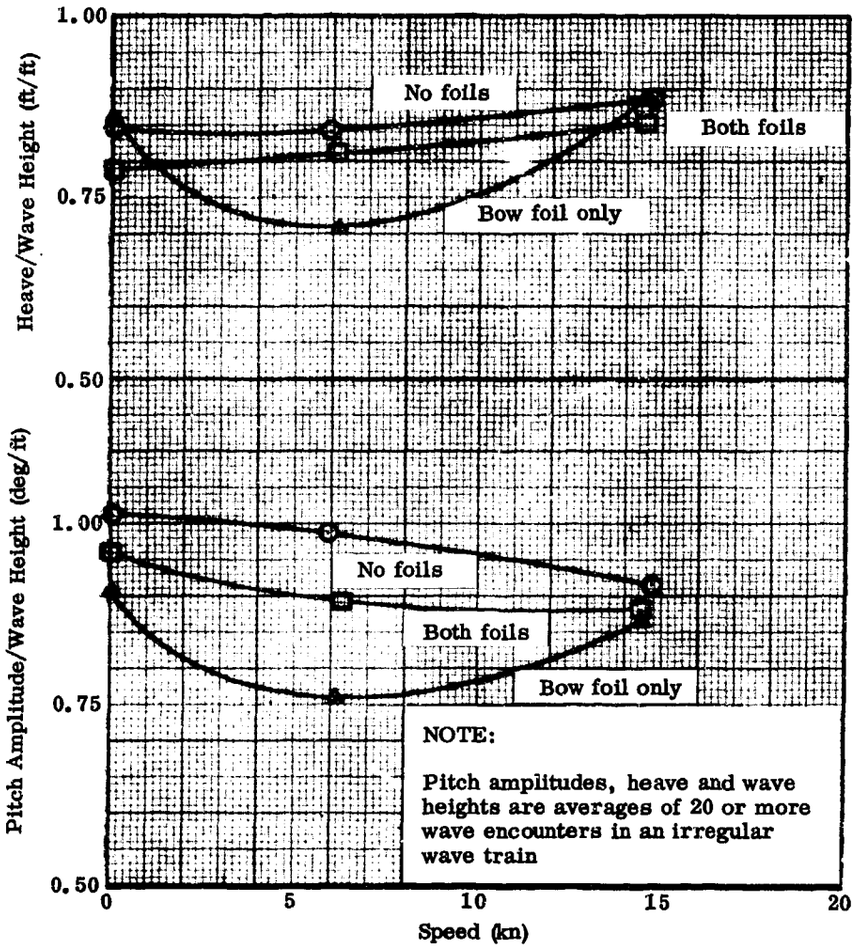

Fig. 4-6. Effect of Foil Damping on Heave and Pitch for L/B ≈ 2 Hull

Wave length to height ratio
Wave length ≈ ship length

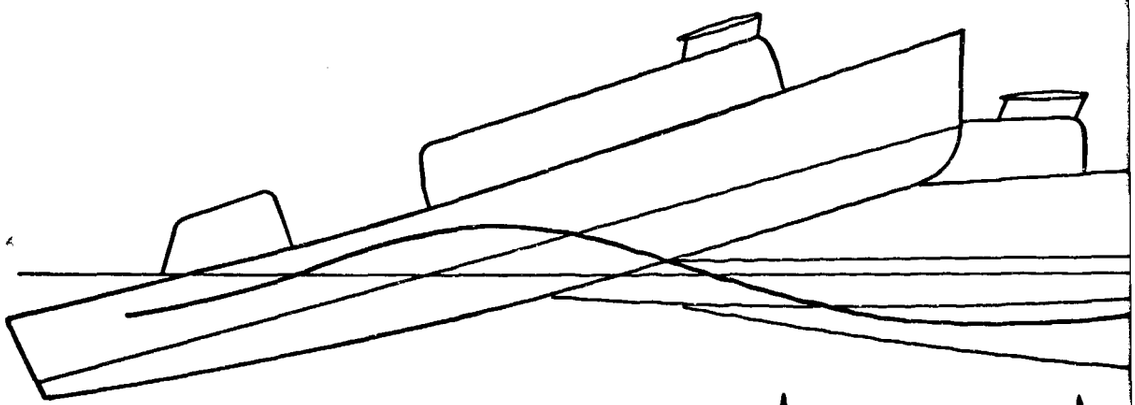

Maximum bow--upward pitch angle
Maximum angular acceleration down
Zero angular velocity
Heave ≈ zero

Pitching--bow down
Zero angular acceleration
Maximum angular velocity
Maximum upward heave
Vertical Velocity ≈ zero

Maximum bow--down p
Maximum angular acce
Zero angular velocity
Heave ≈ zero

ength to height ratio = 10
ength ≈ ship length

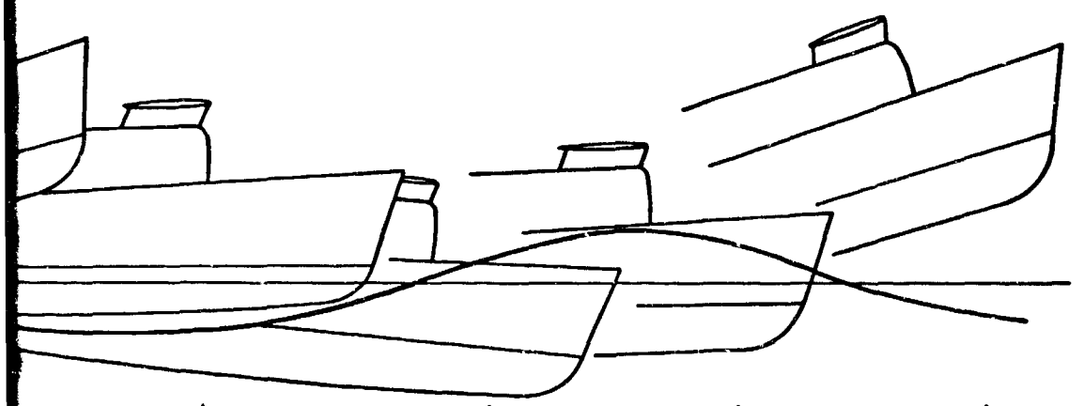

g--bow down
ngular acceleration
m angular velocity down
m upward heave
l Velocity ≈ zero

ximum bow--down pitch angle
ximum angular acceleration upward
o angular velocity
ve ≈ zero

Maximum bow--
upward pitch angle

Pitching bow upward
Zero angular acceleration
Maximum angular velocity upward
Maximum downward heave

Fig. 4-7. Positions of Angular Acceleration and Angular Velocity

2

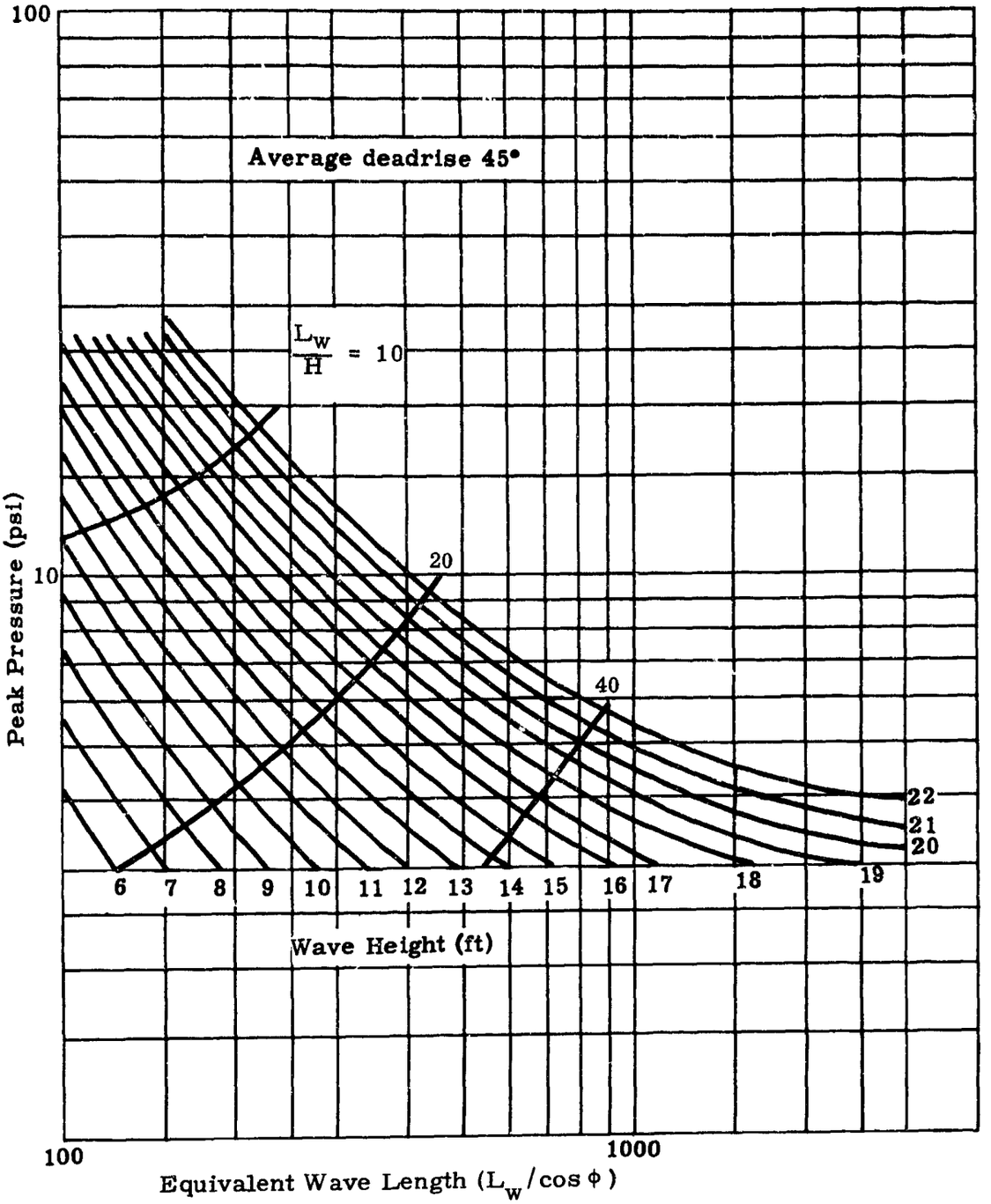

Fig. 4-8. Peak Pressure as a Function of Wave Length for Various Wave Heights--Station 1

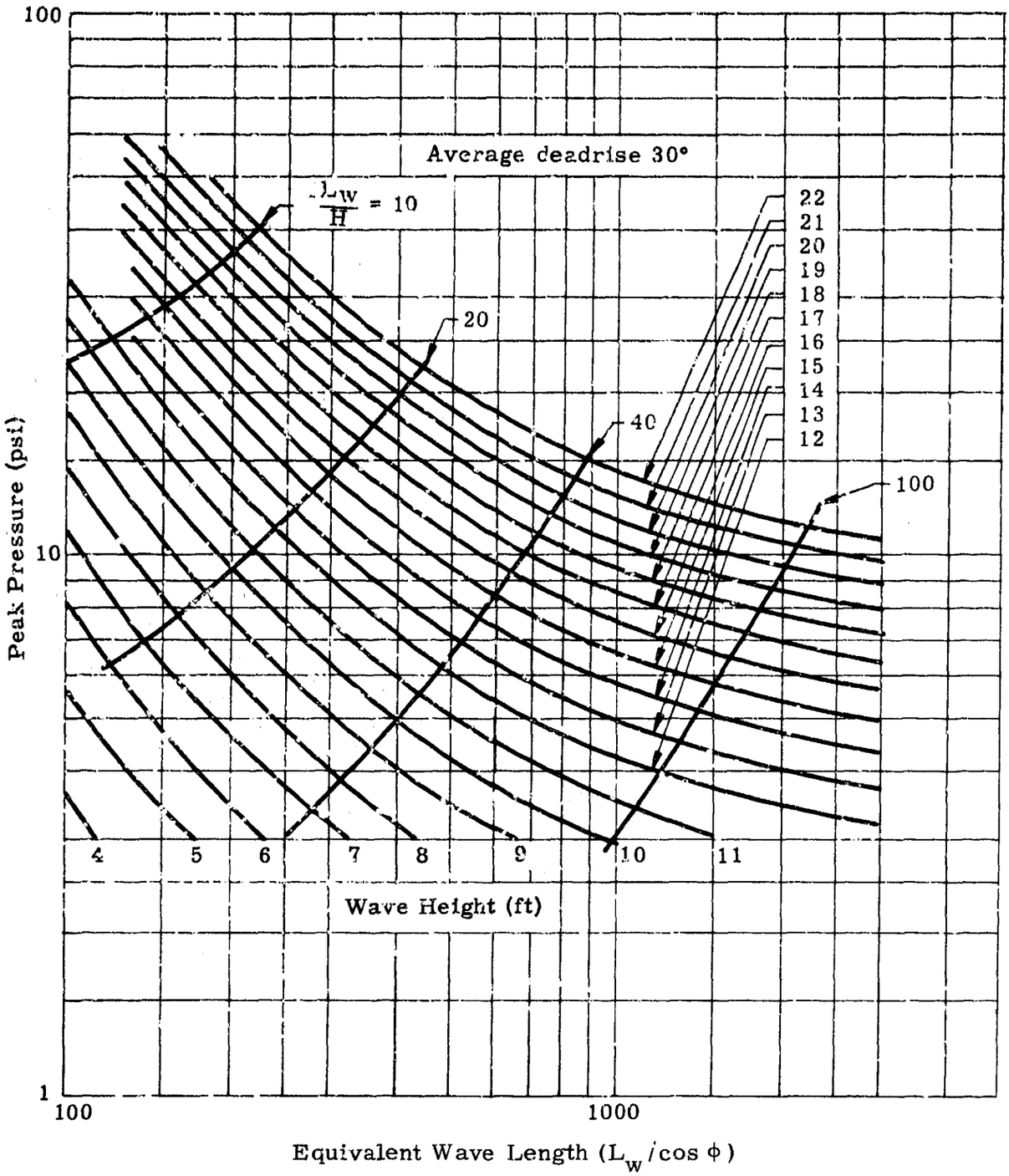

Fig. 4-9. Peak Pressure as a Function of Wave Length for Various Wave Heights--Station 2

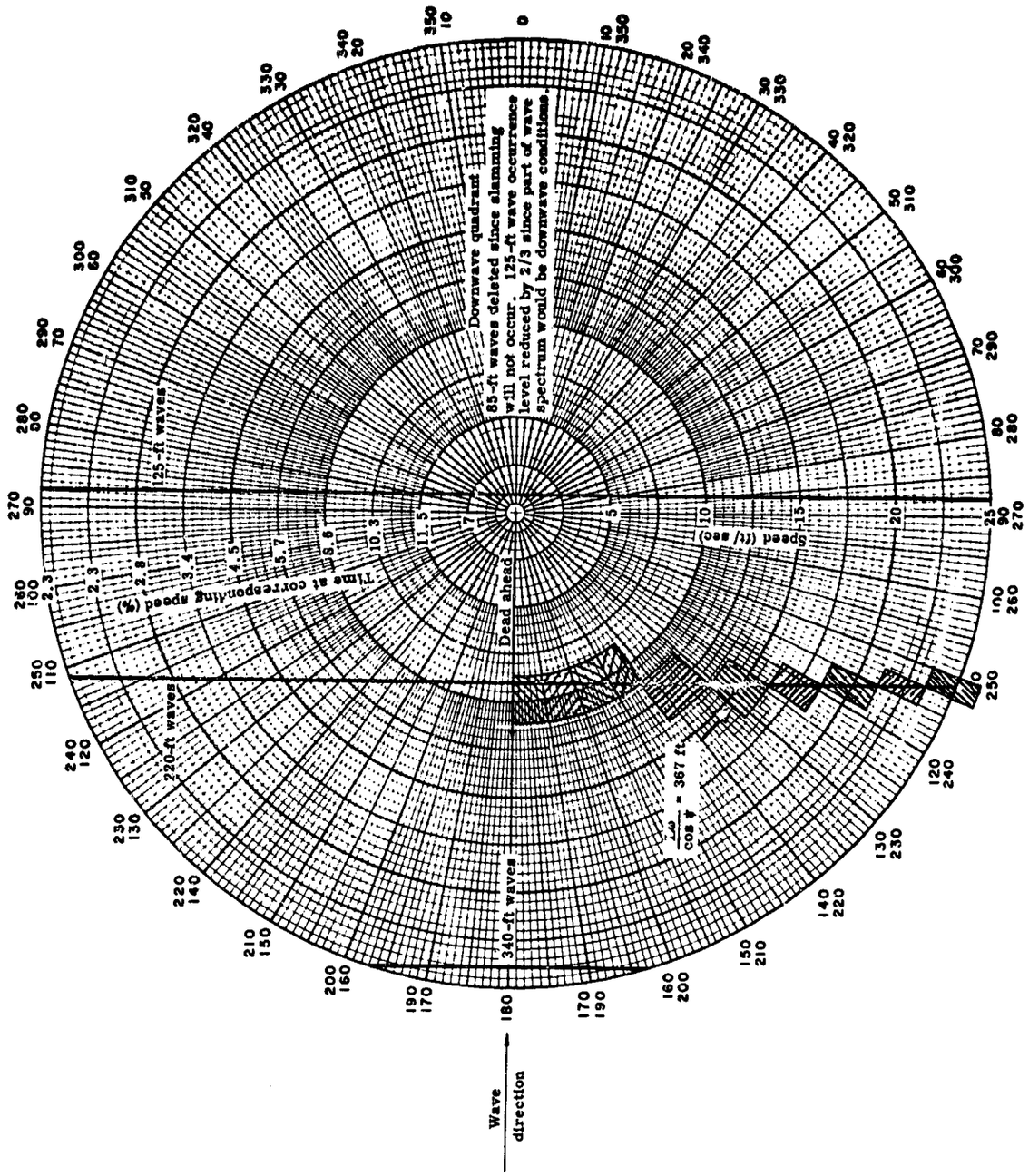

Fig. 4-10. Speed-Time-Heading, Polar

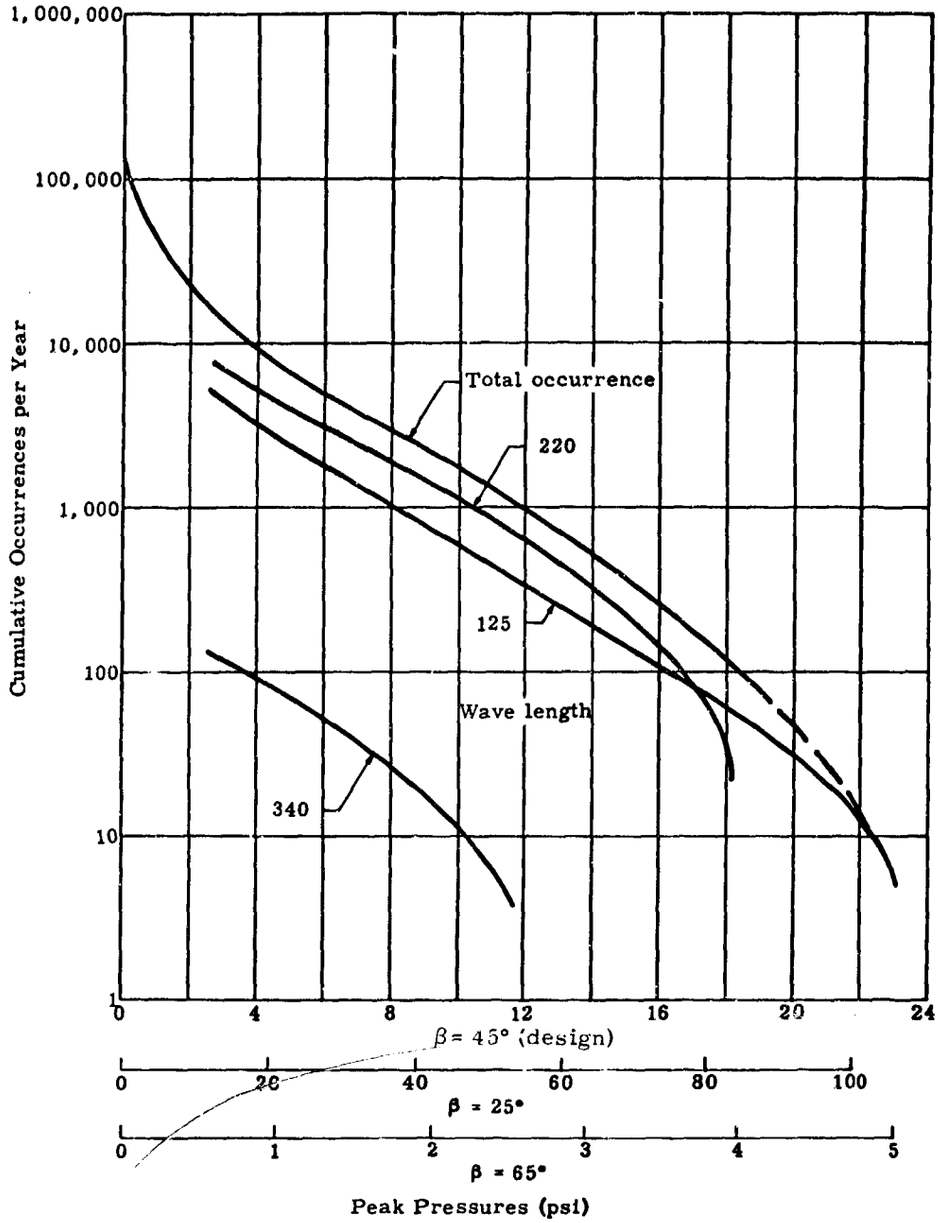

Fig. 4-11. Occurrence of Peak Pressures at Station 1 Due to Slamming

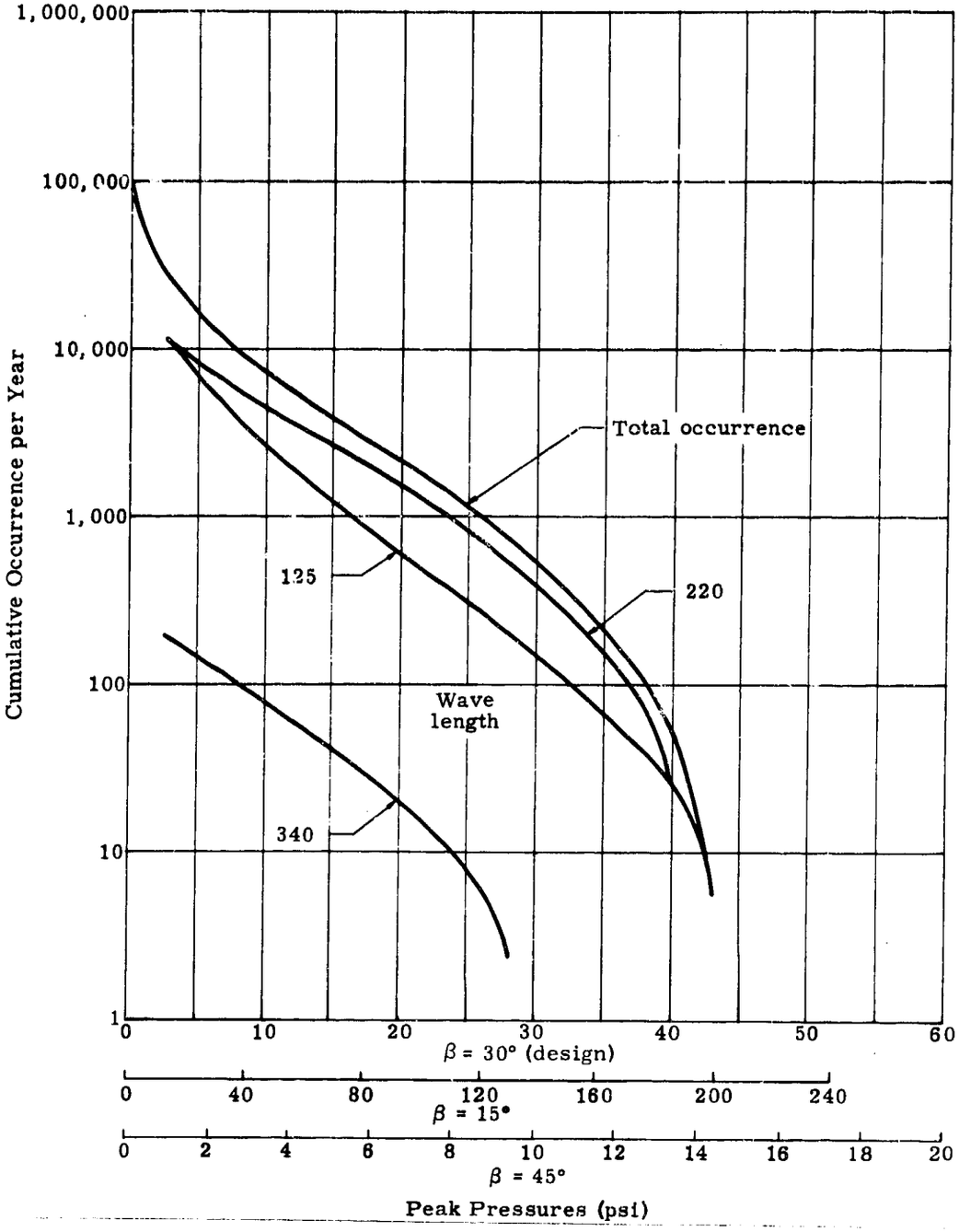

Fig. 4-12. Occurrence of Peak Pressures at Station 2 Due to Slamming

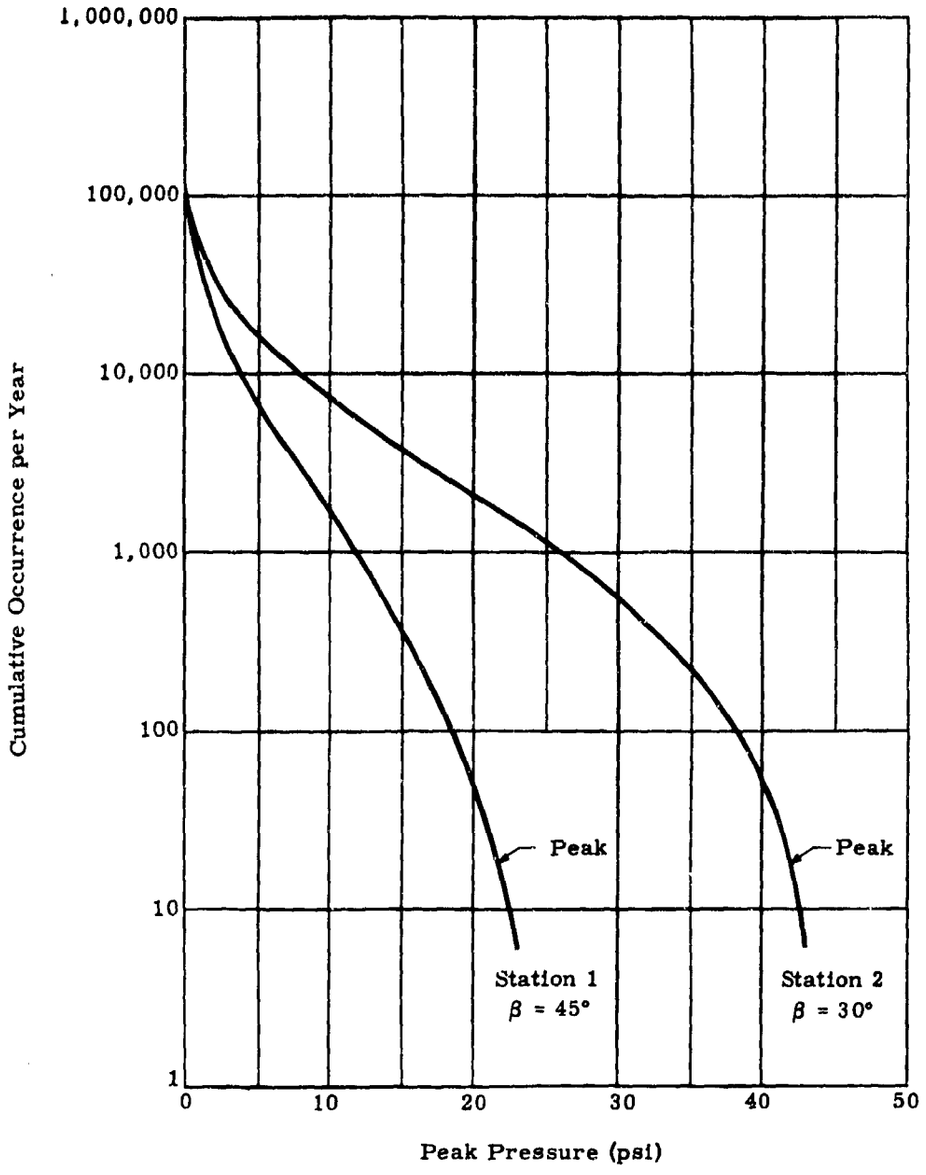

Fig. 4-13. Comparison of Pressures and Occurrences at Stations 1 and 2

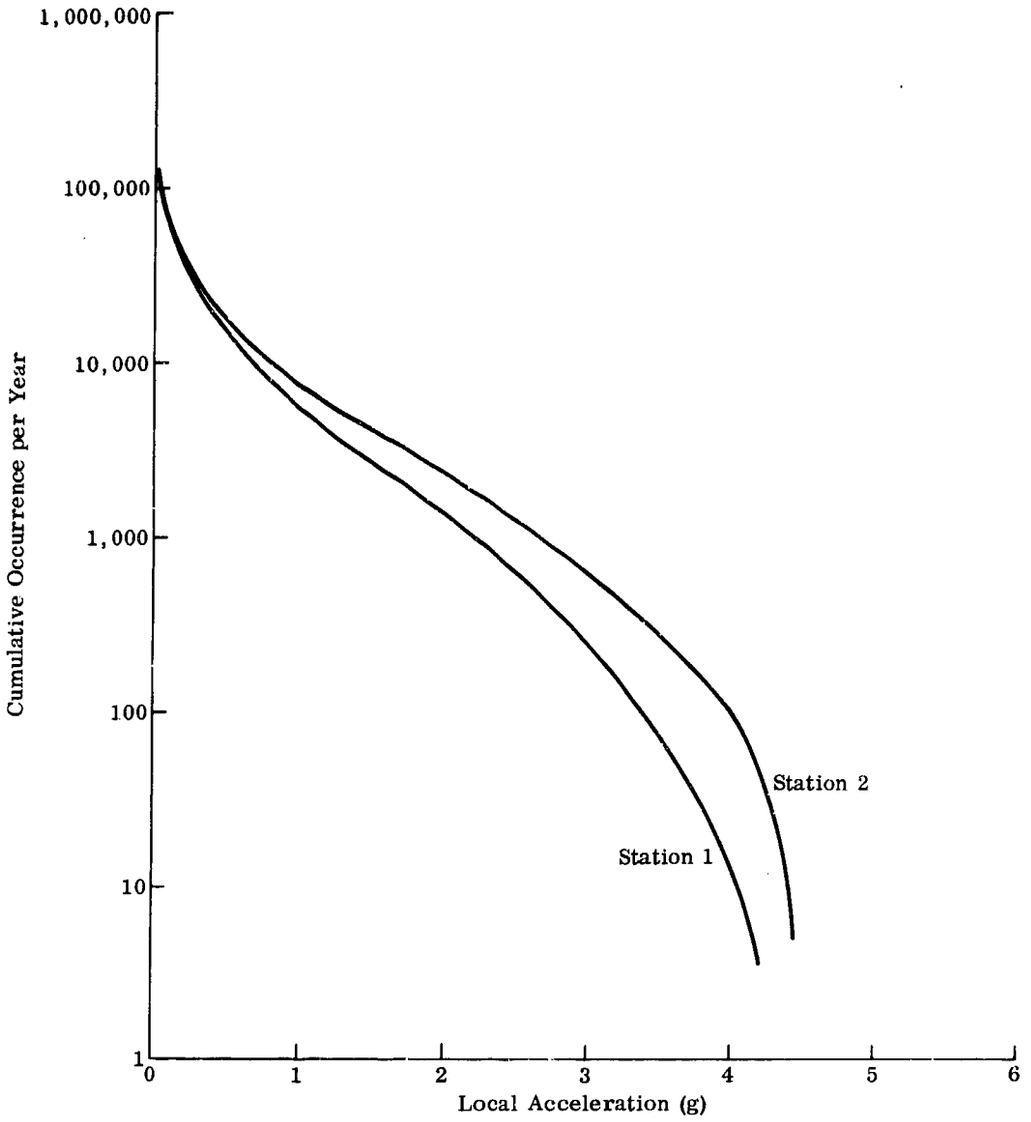

Fig. 4-14. Comparison of Local Acceleration in g Units for Stations 1 and 2 Due to Slamming Pressures

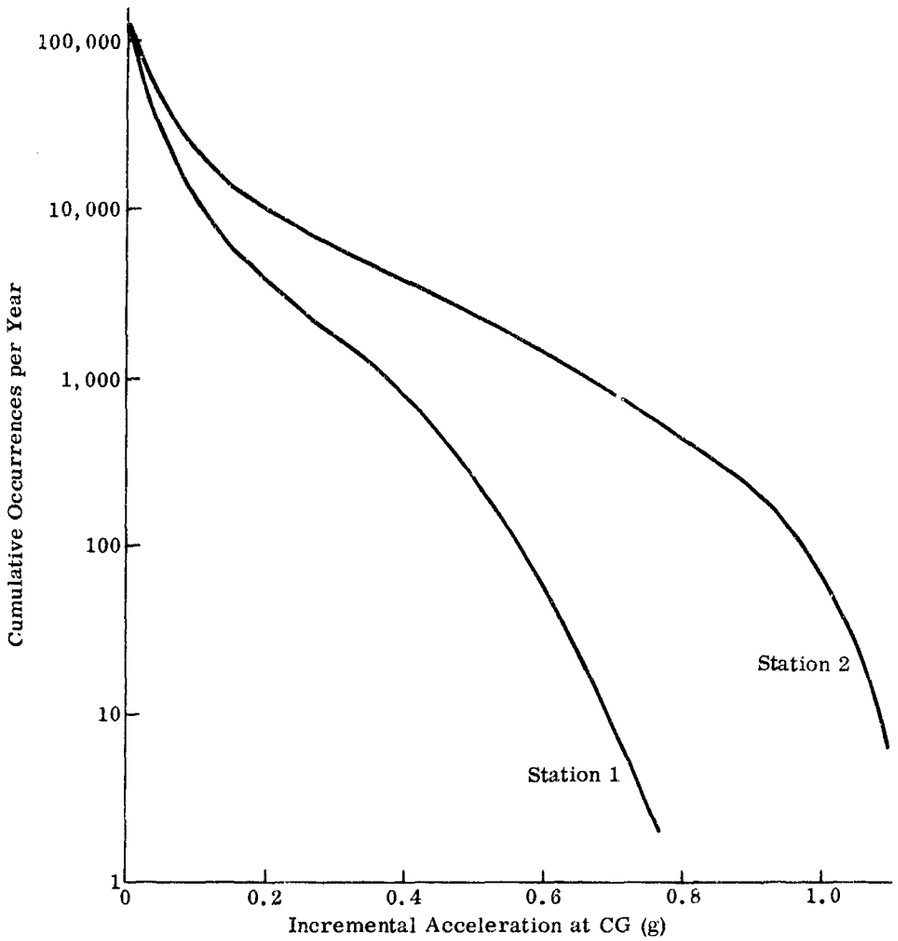

Fig. 4-15. Comparison of Acceleration at CG Due to Local Impacts at Stations 1 and 2

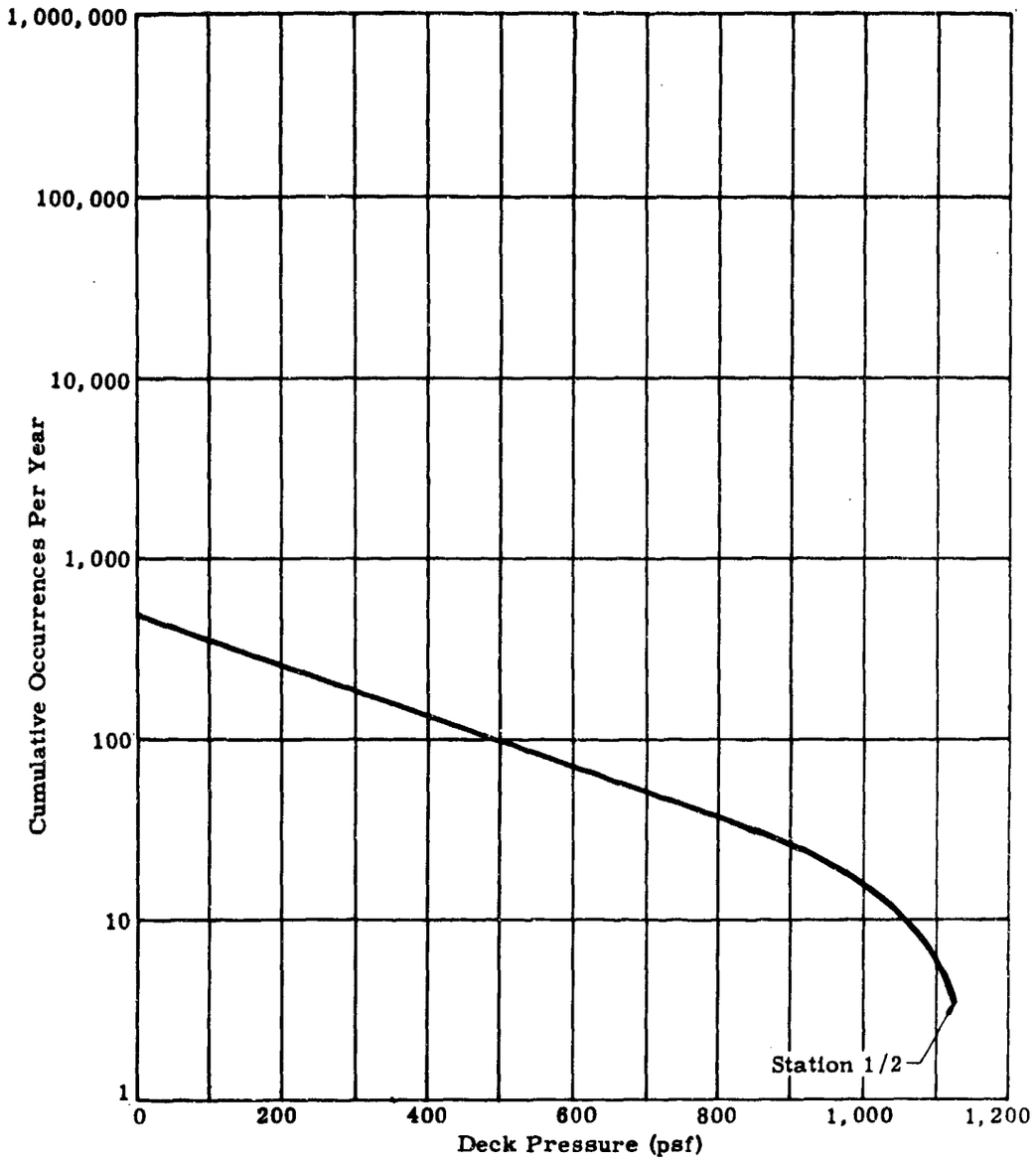

Fig. 4-16. Deck Pressures

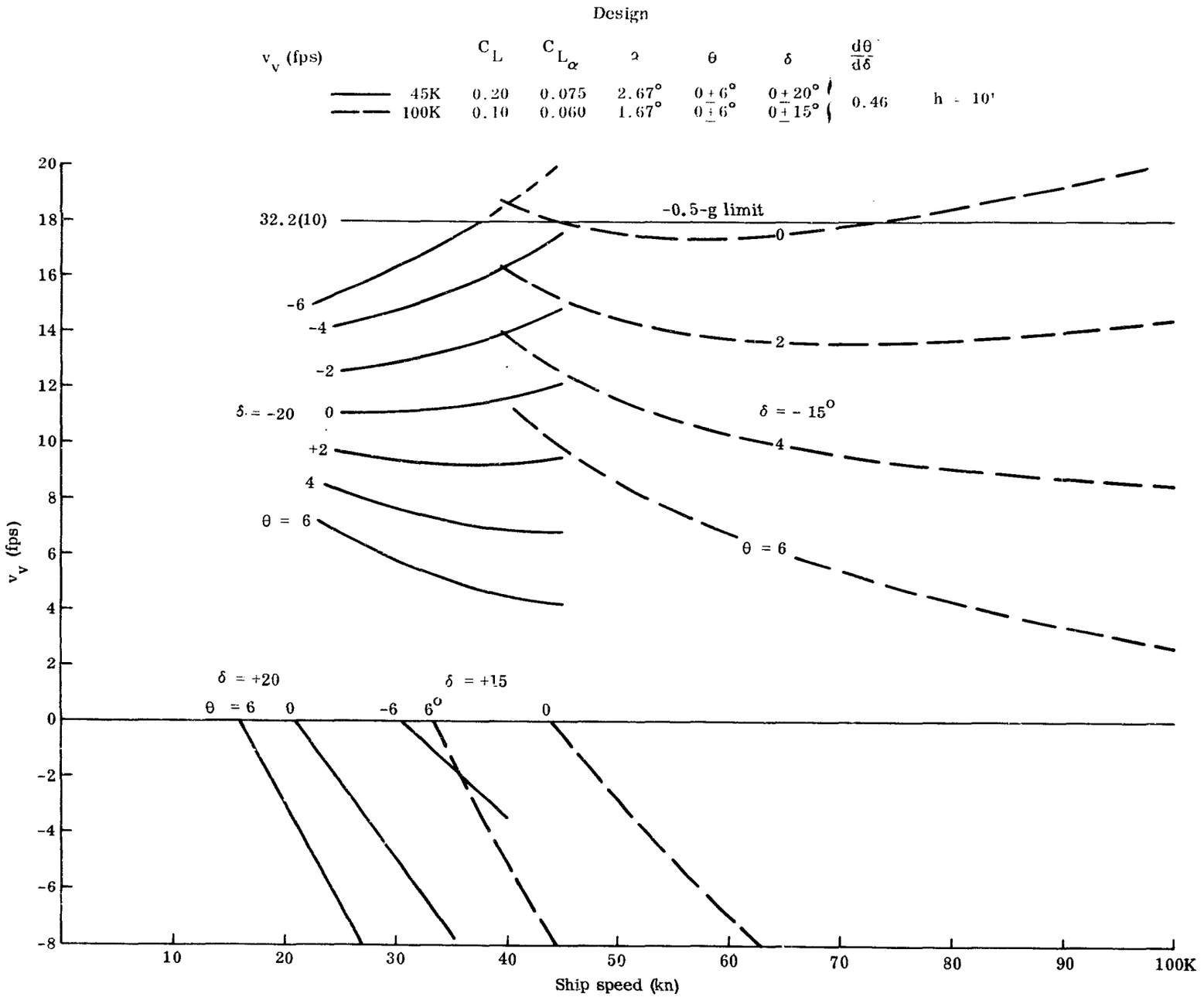

Fig. 4-17. Vertical Velocity at Landing

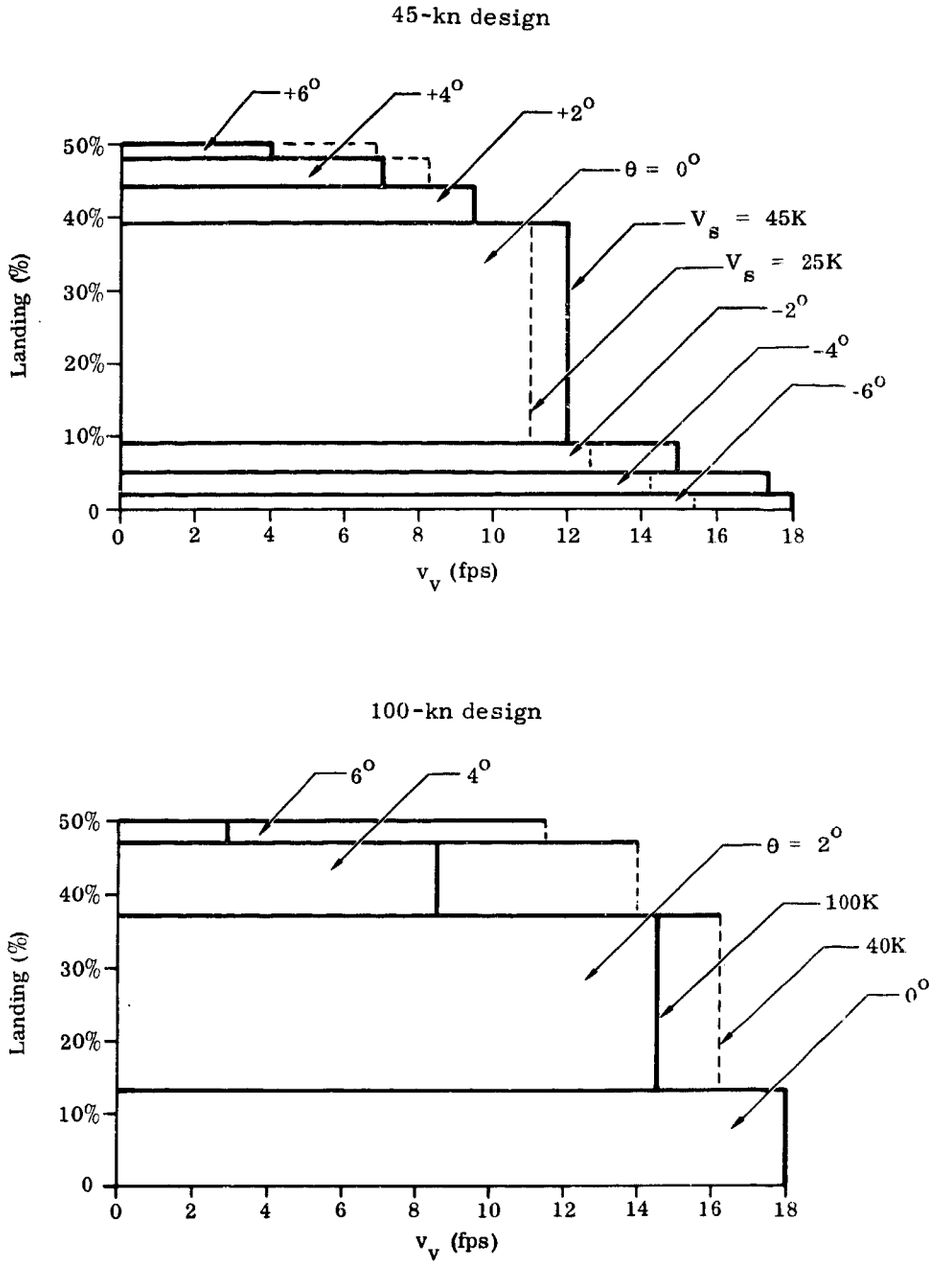

Fig. 4-18. Altitude and Vertical Velocity Distribution Assumed for Landing

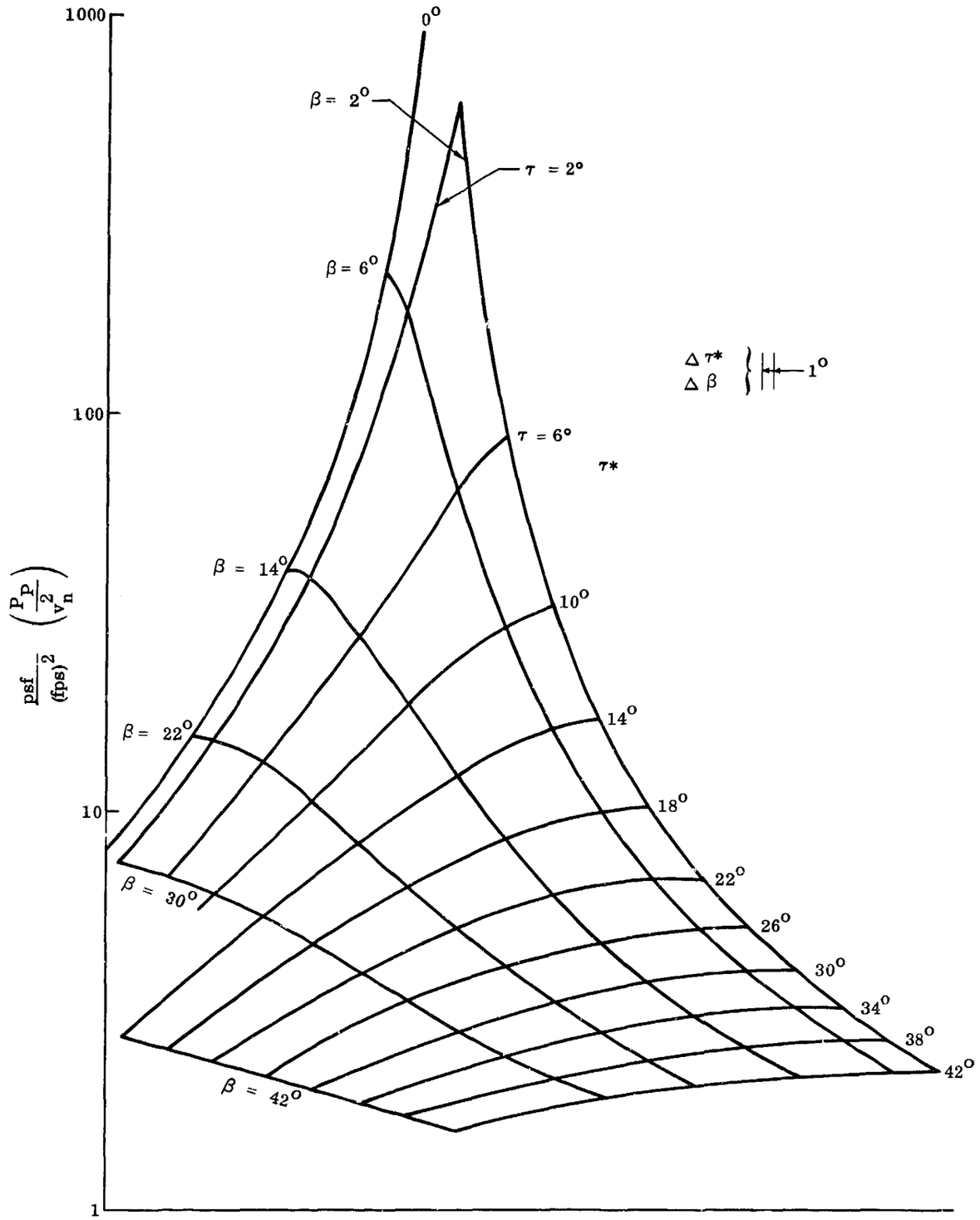

Fig. 4-19. Peak Pressure Coefficient for Combinations of Deadrise and Trim Angle

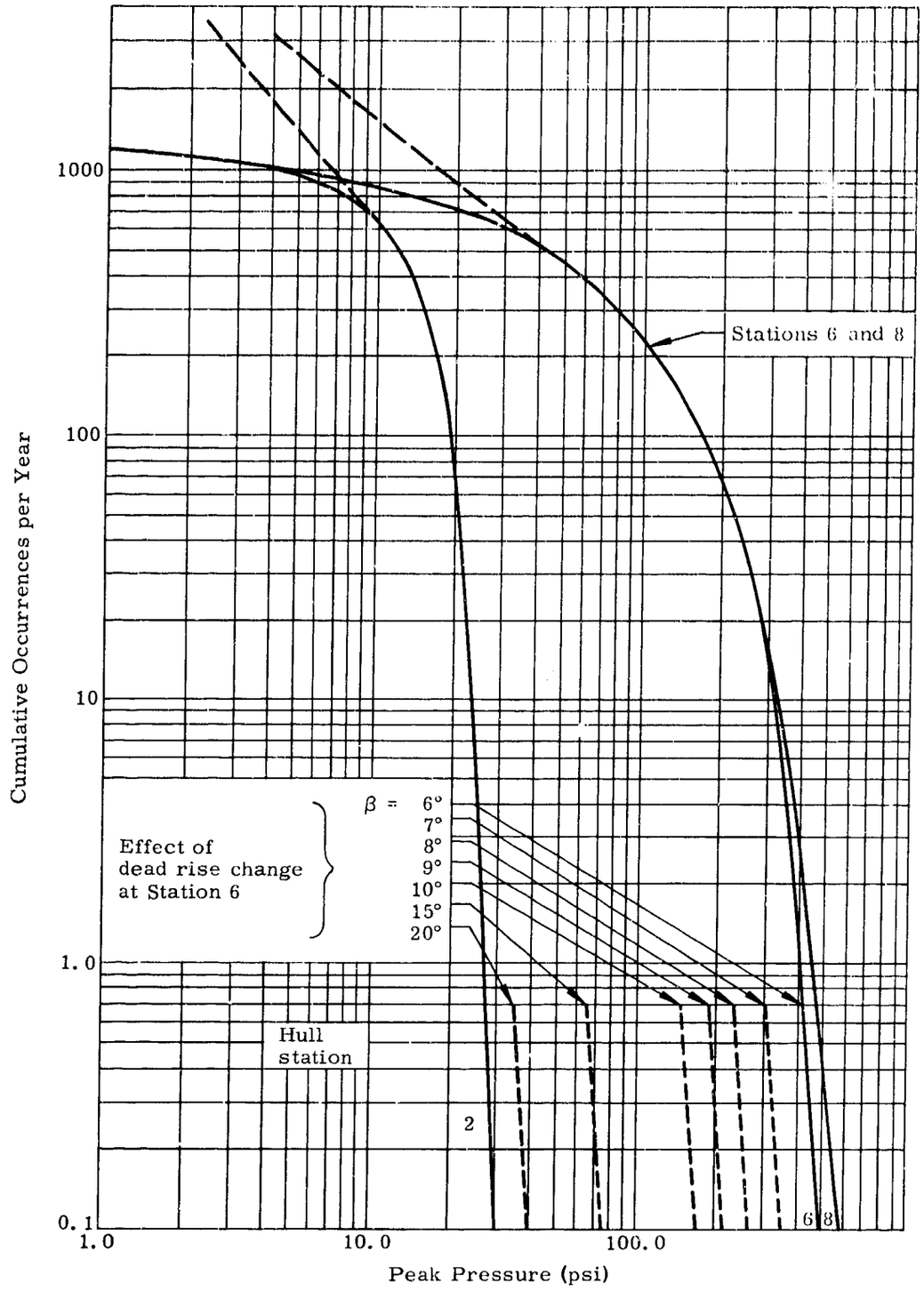

Fig. 4-20. Normal Landing Pressures--45-kn Ship

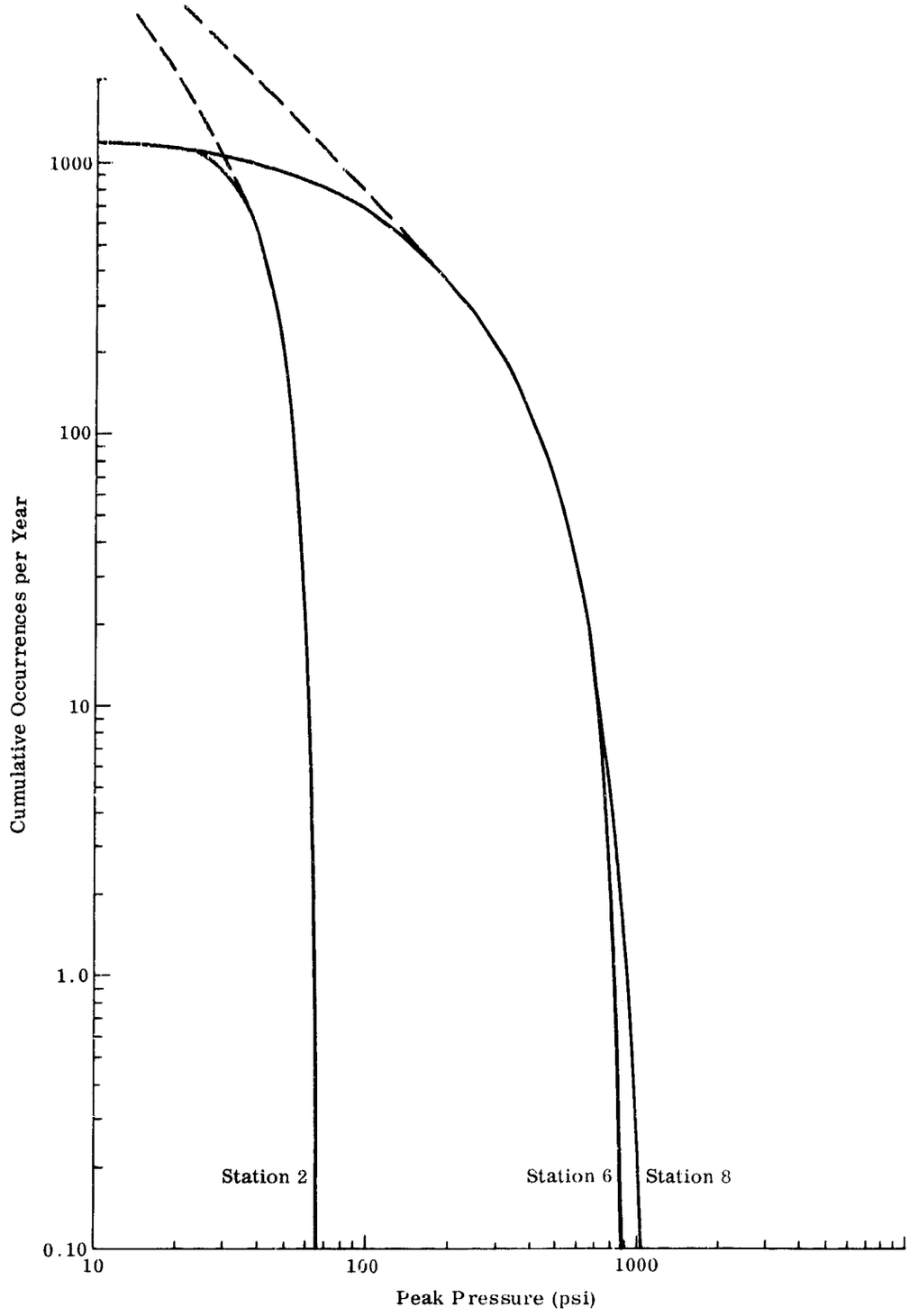

Fig. 4-21. Normal Landing Pressures--100-kn Ship

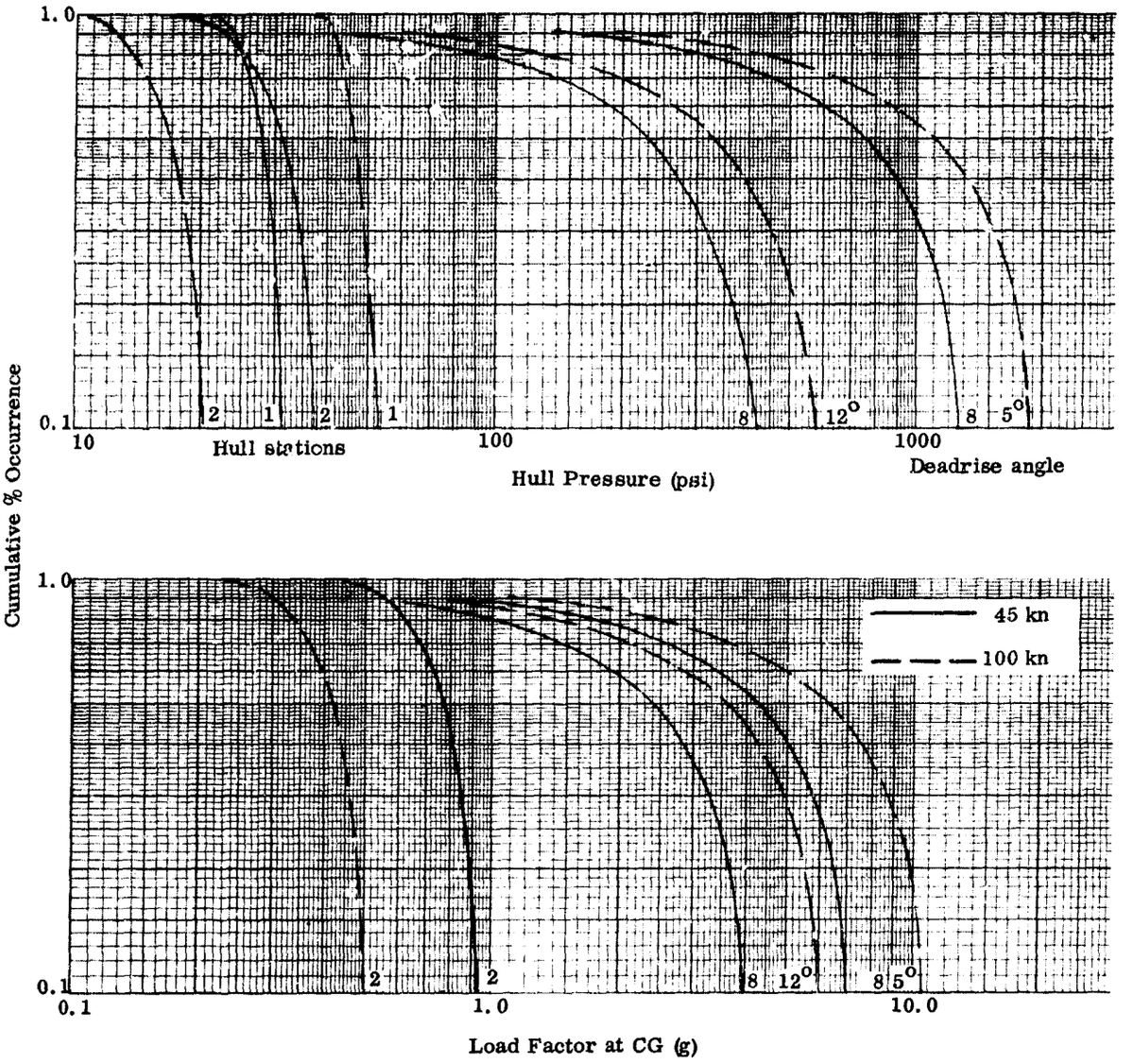

Fig. 4-22. Pressures and Acceleration Due to Crash Landings (foil loss)

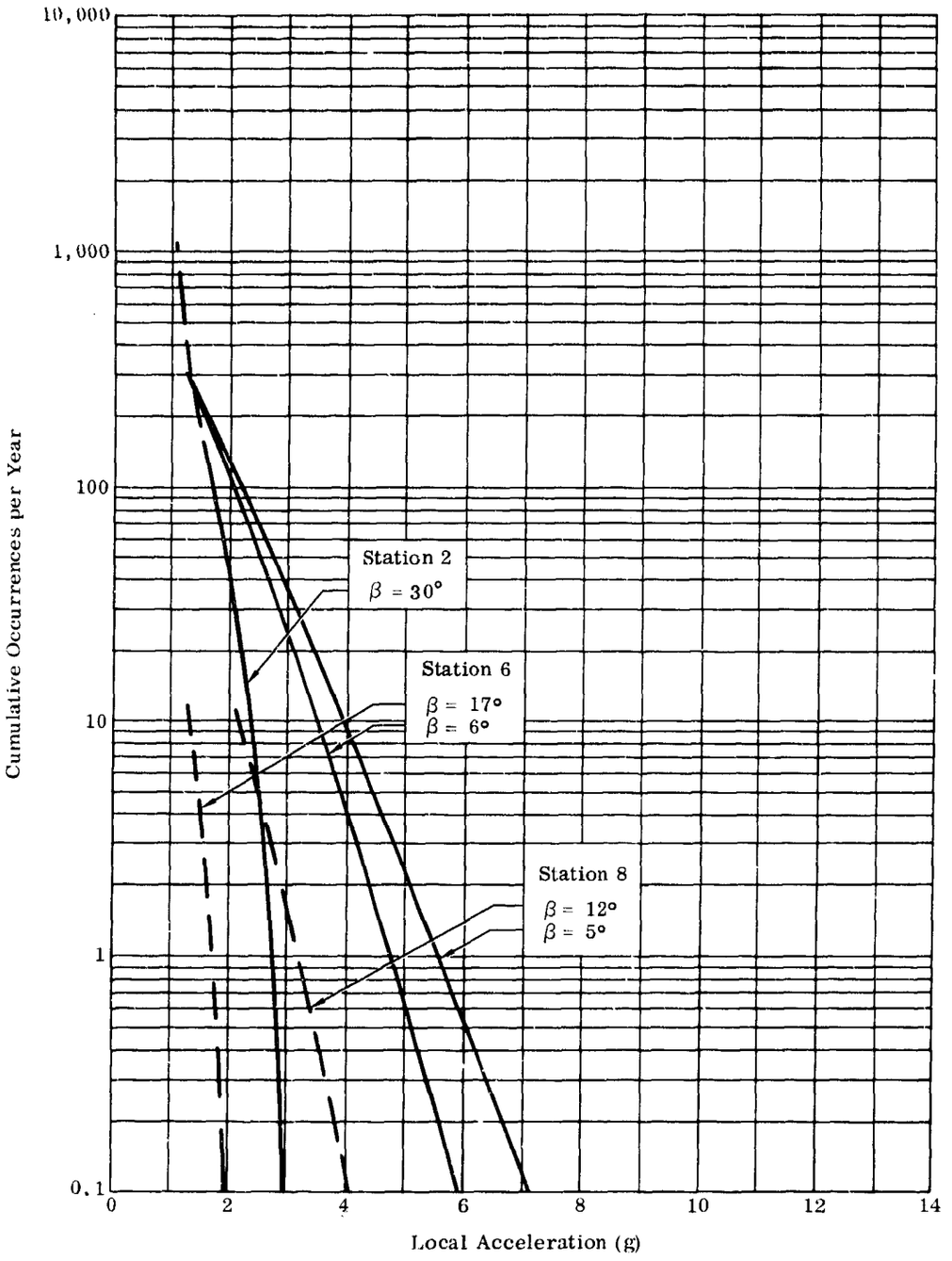

Fig. 4-23. Local Acceleration Due to Landing--45-Knot Ship

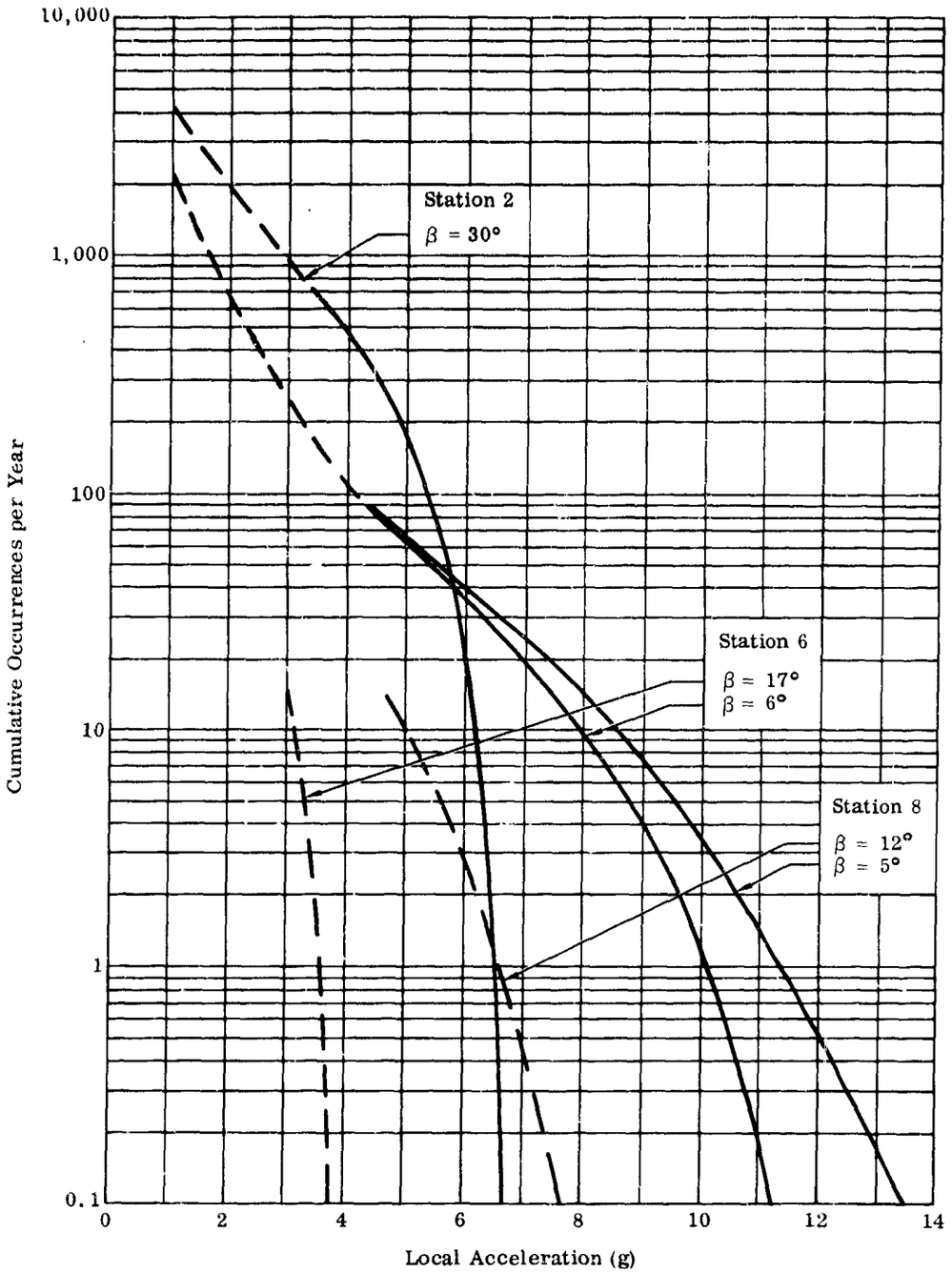

Fig. 4-24. Local Acceleration Due to Landing--100-kn Ship

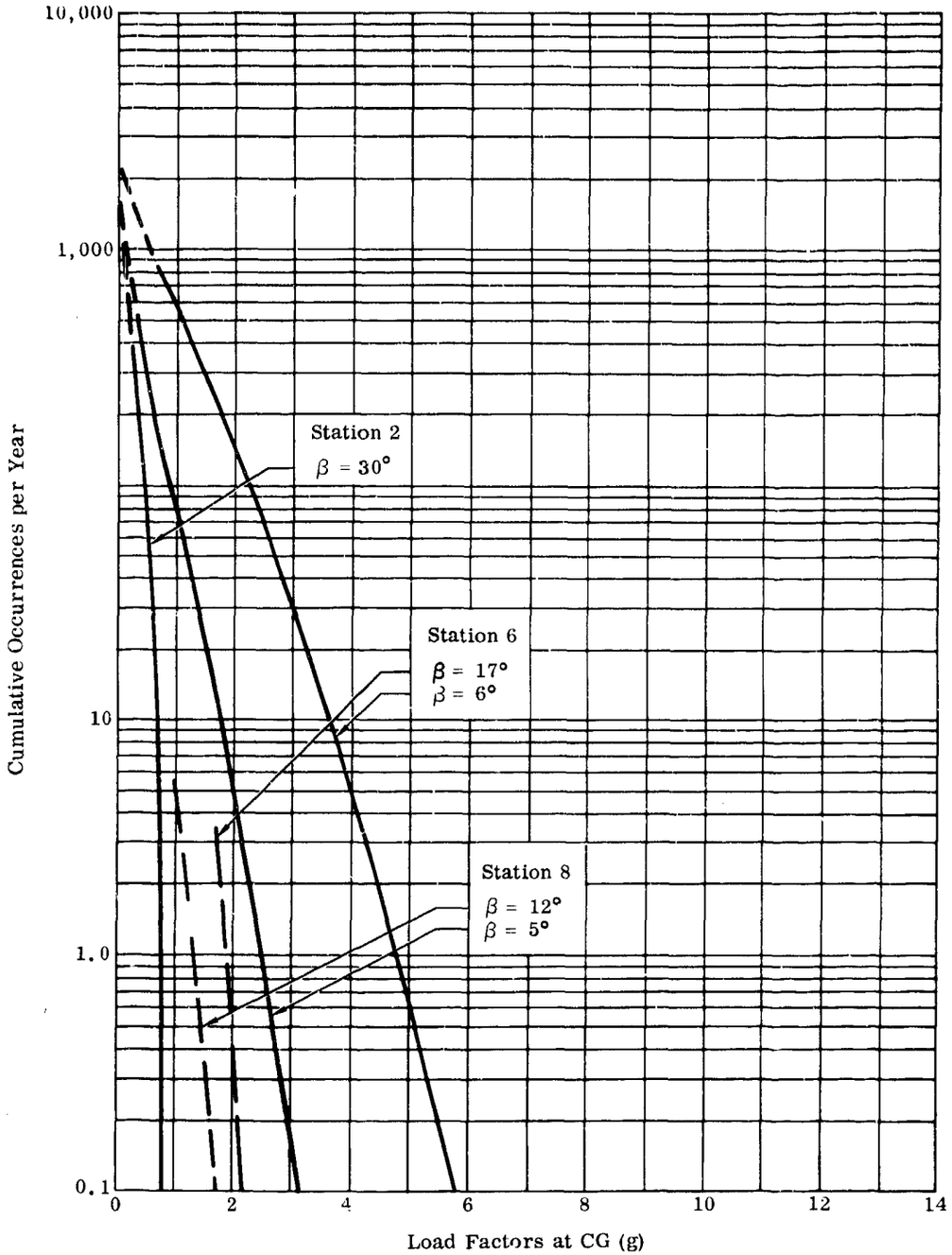

Fig. 4-25. Load Factors at CG Due to Impact at the Stations Shown--45- kn Ship

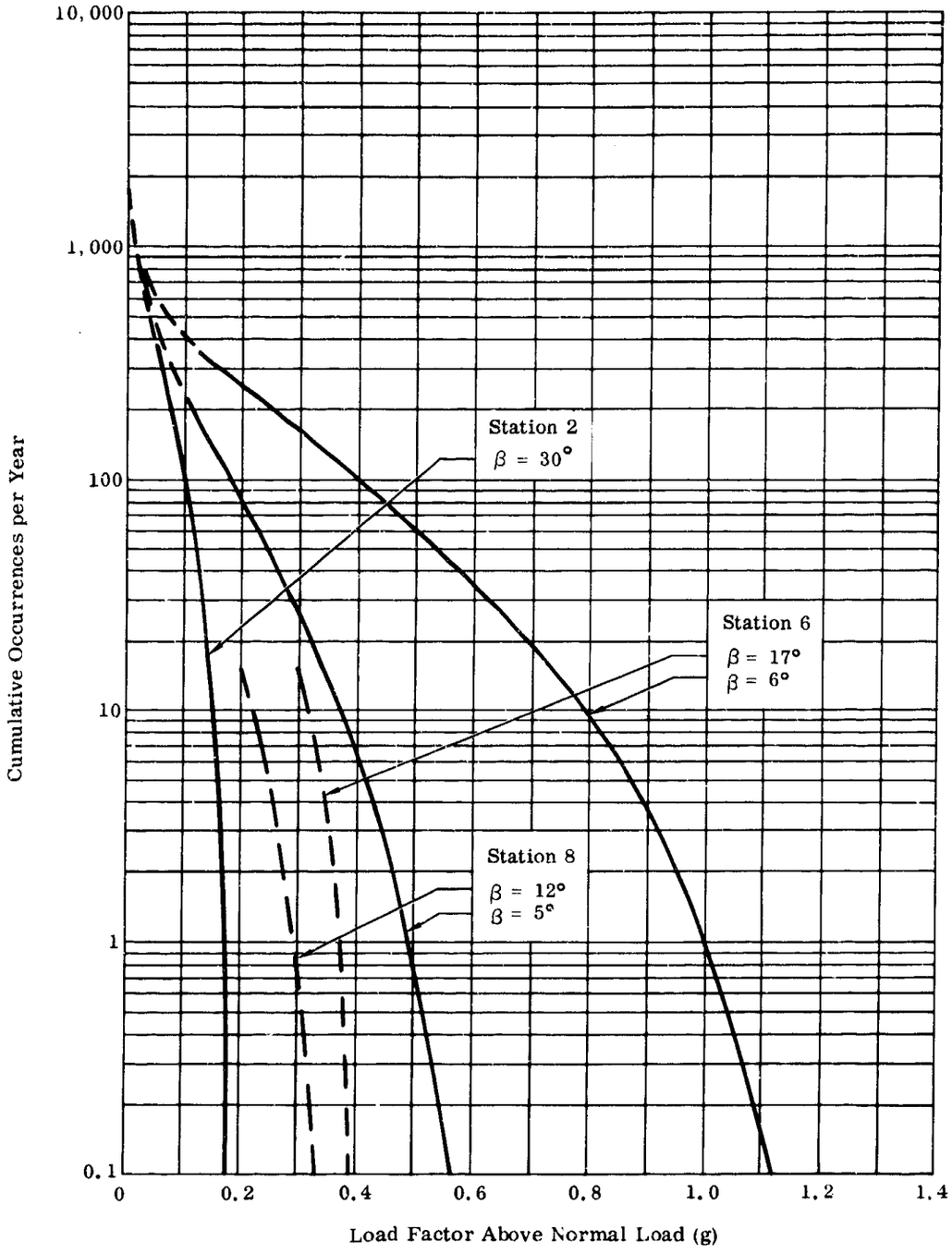

Fig. 4-26. Load Factor at CG Due to Impact Applied at the Stations Shown--100-kn Boat

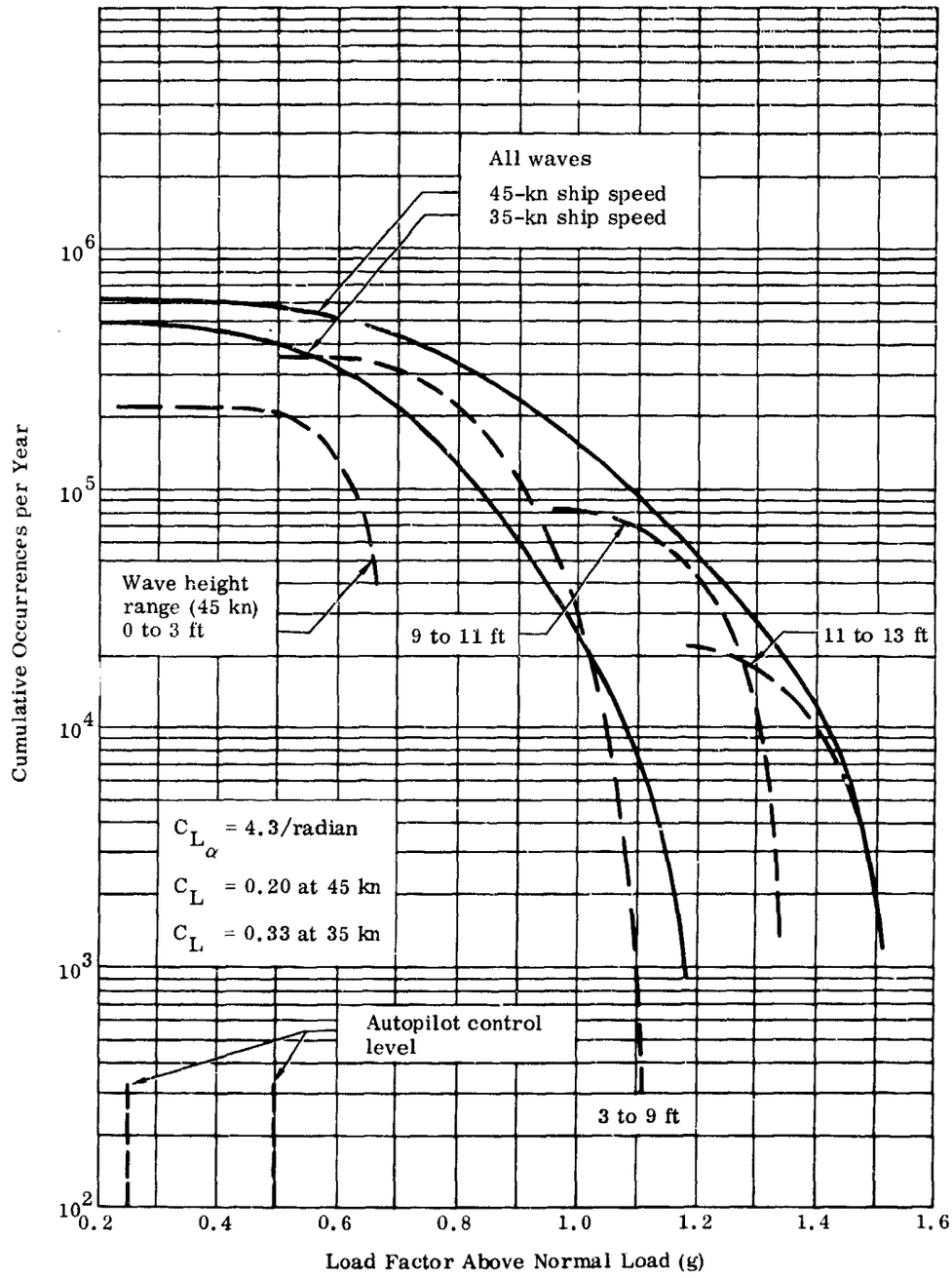

Fig. 4-27. Fixed Foil Response to Waves

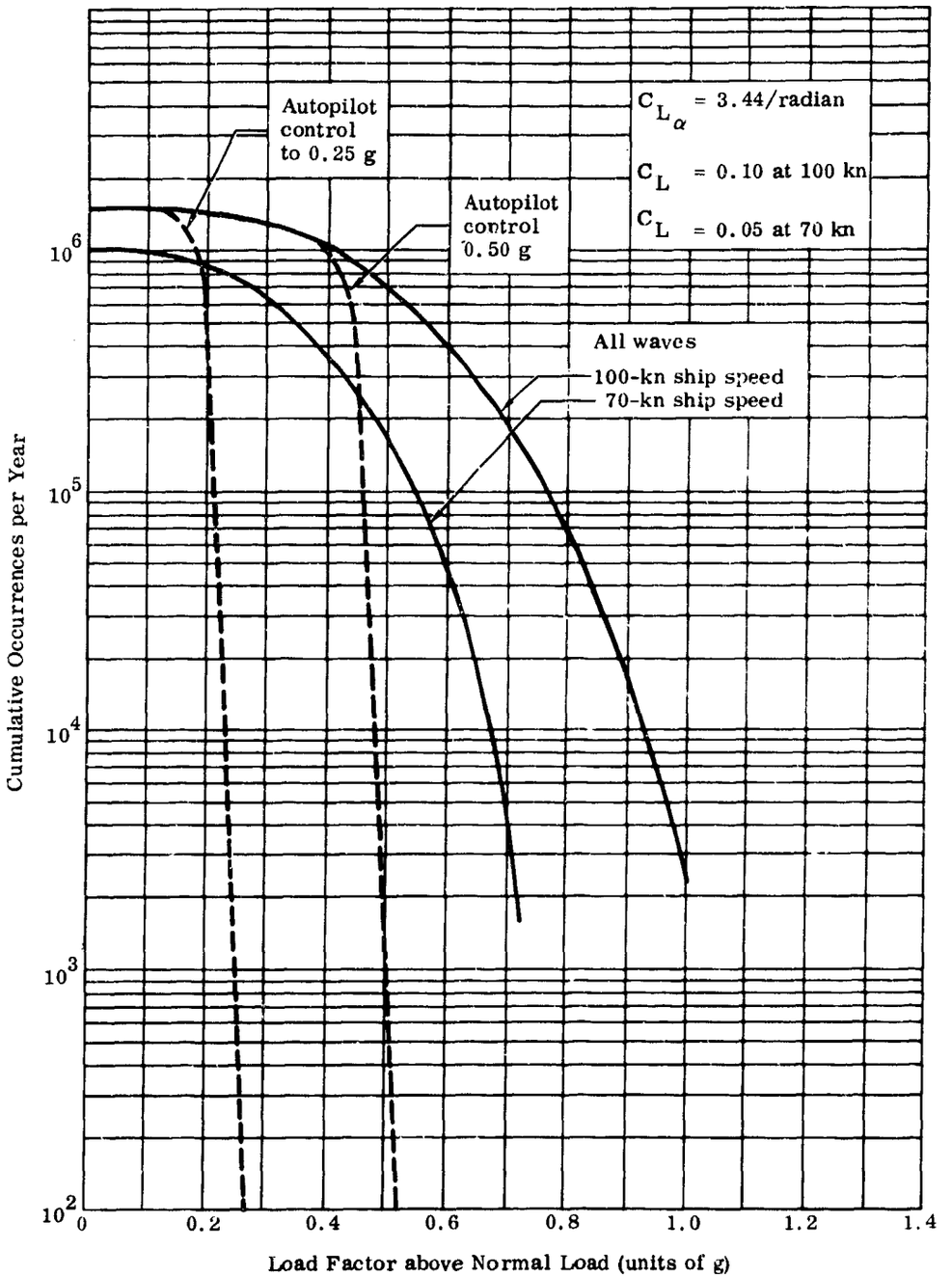

Fig. 4-28. Fixed Foil Response to Waves

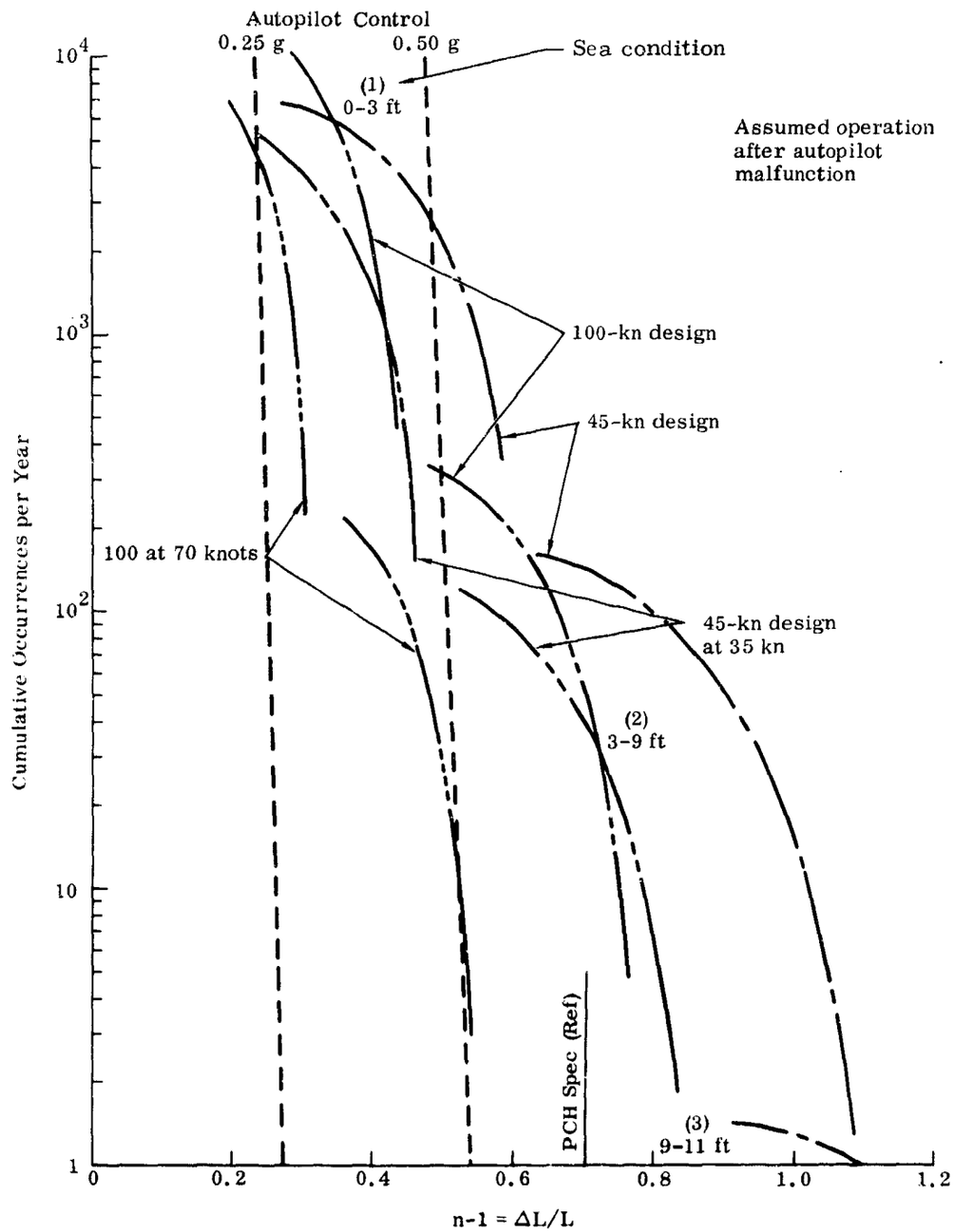

Fig. 4-29. Foilborne Load Factors

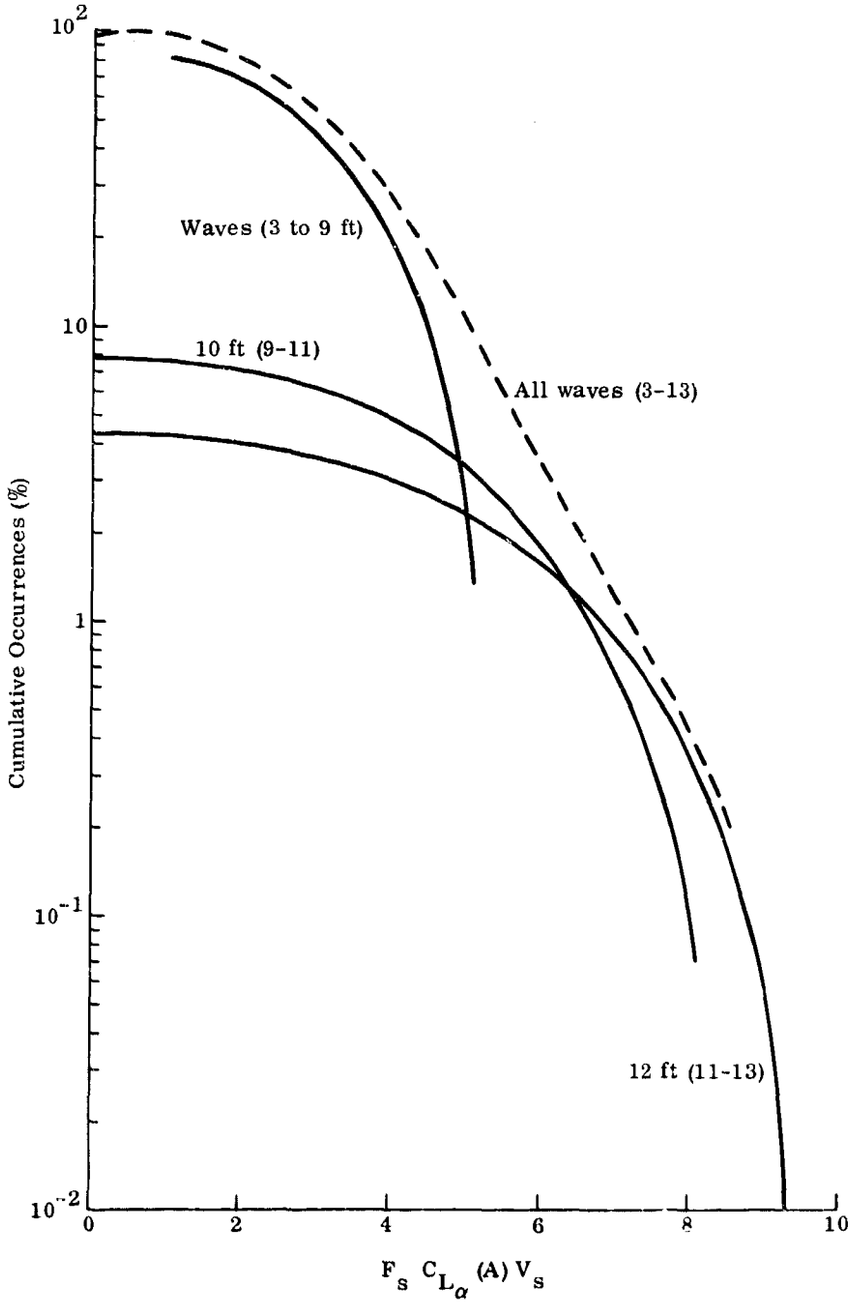

Fig. 4-30. Strut Loading Spectrum Due to Waves

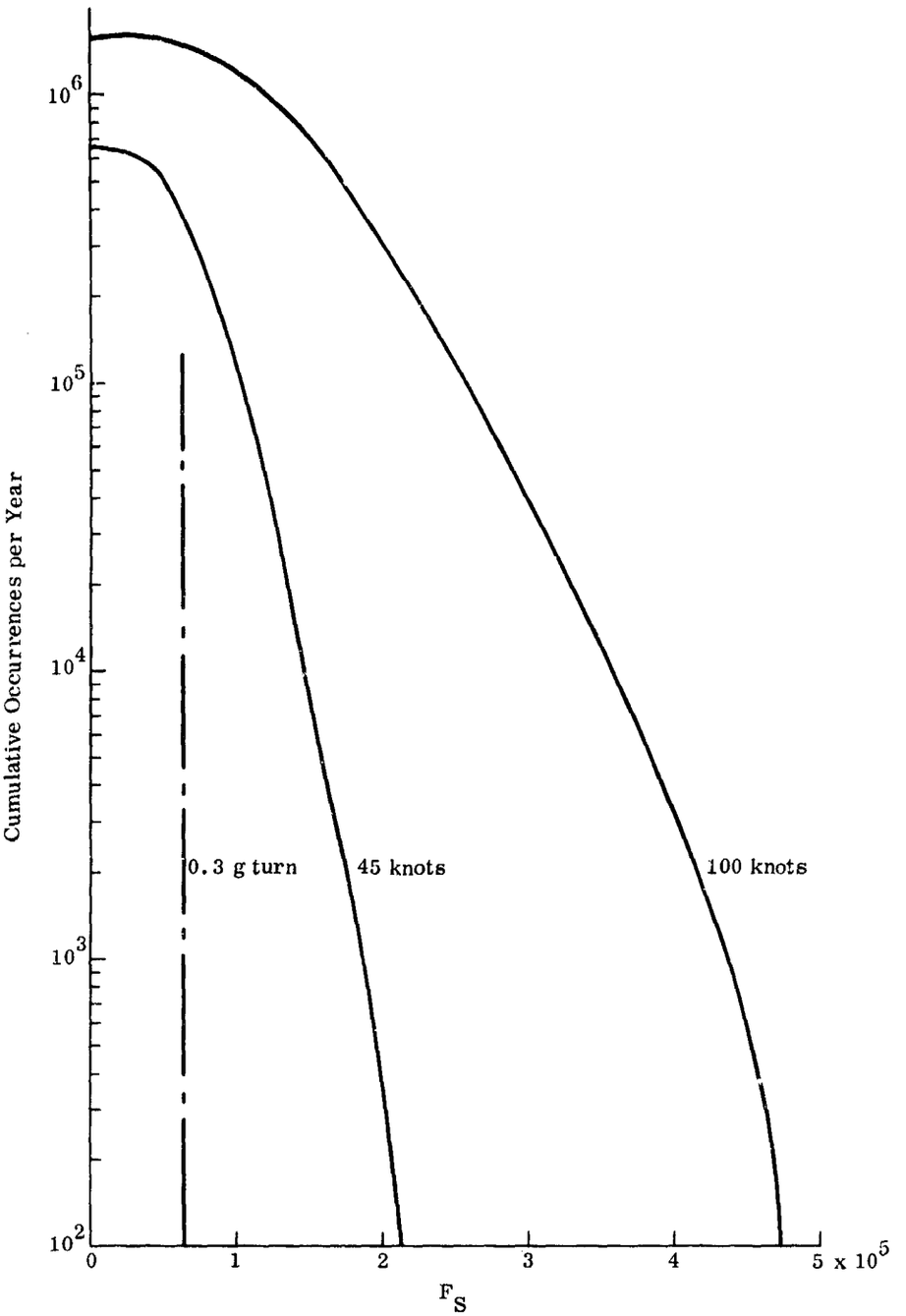

Fig. 4-31. Strut Side Loading

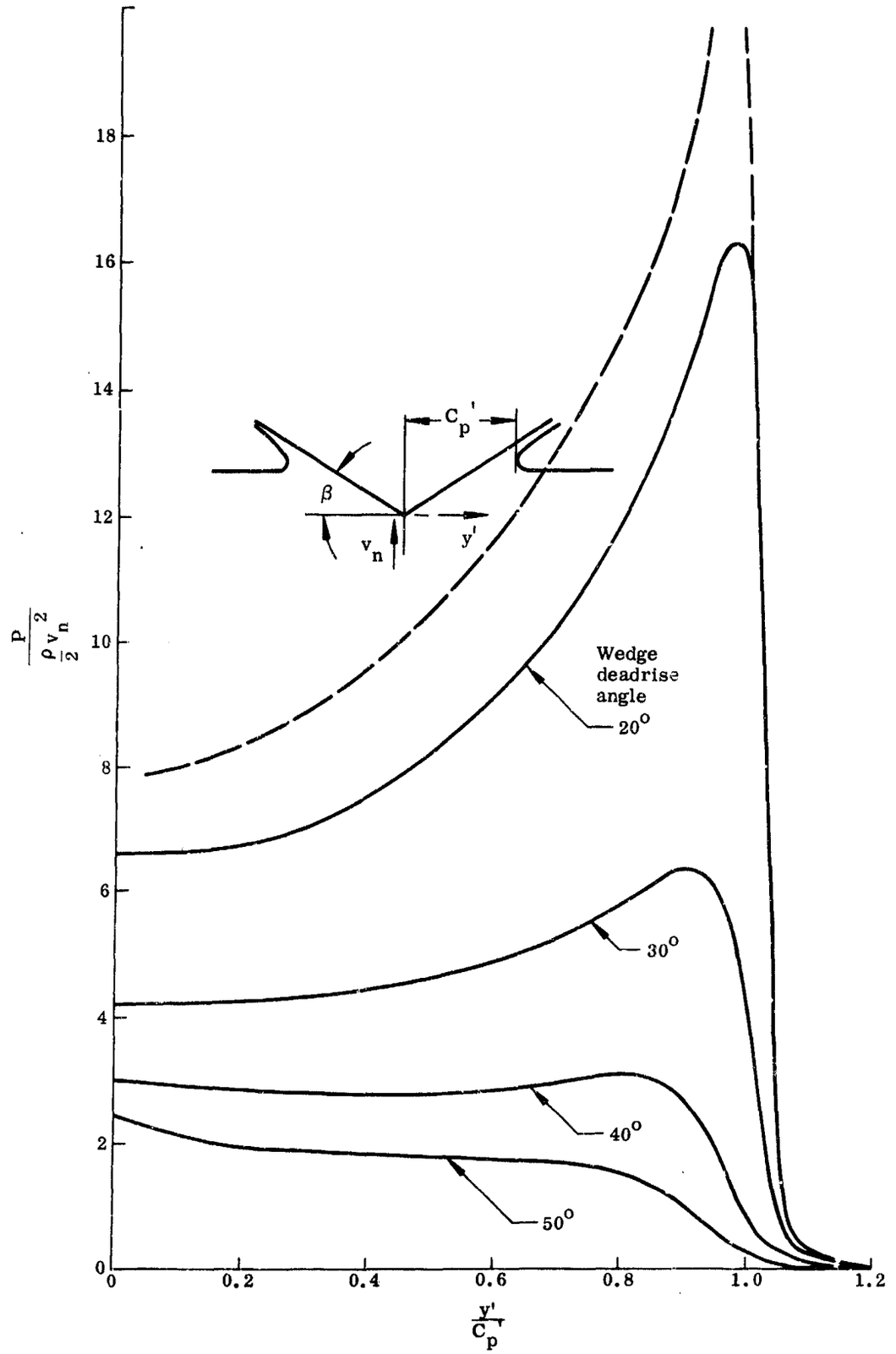

Fig. 4-32. Pressure Distribution Over Immersing Wedge (curves reproduced from Ref. 4)

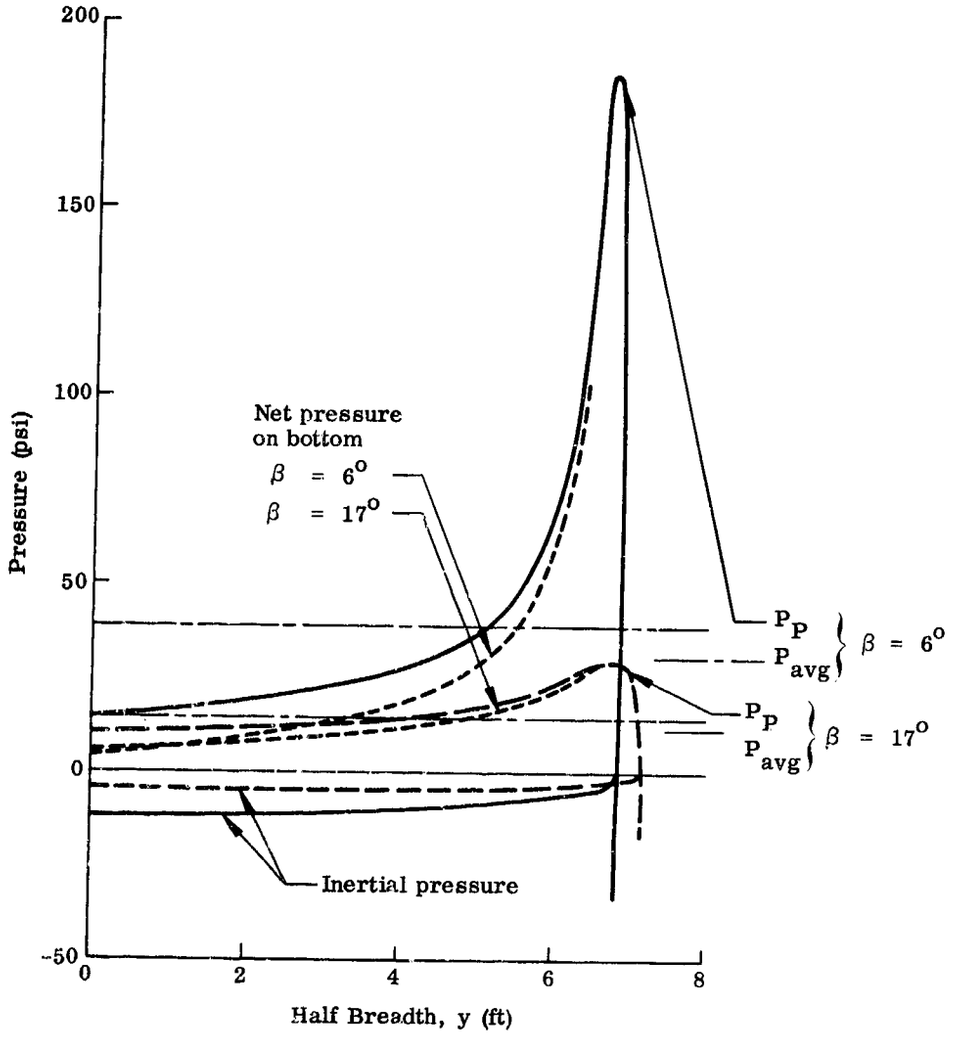

Fig. 4-33. Landing Pressure Distribution (example, Station 6)

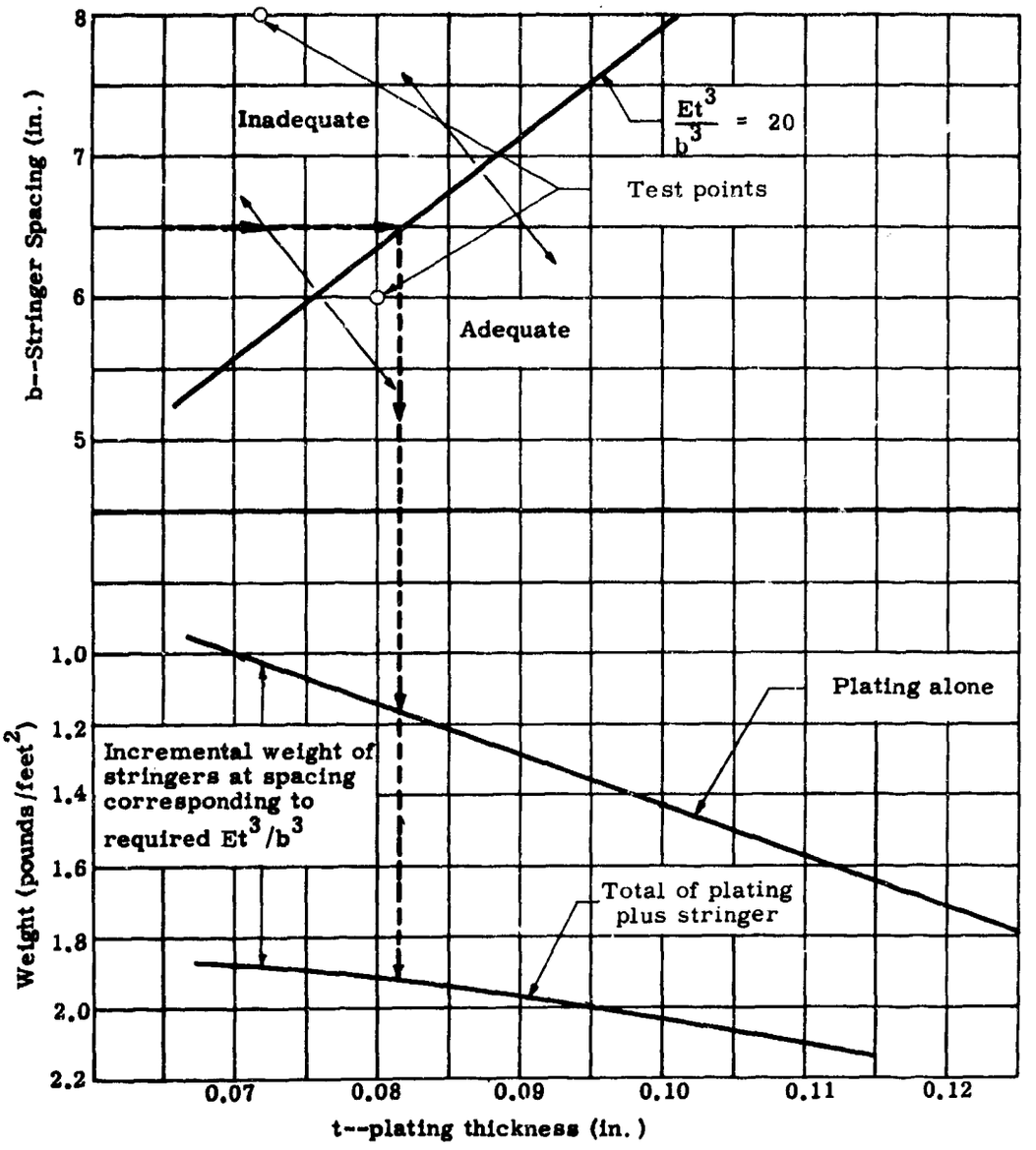

Fig. 4-34. Deck Plating Stiffness Criteria

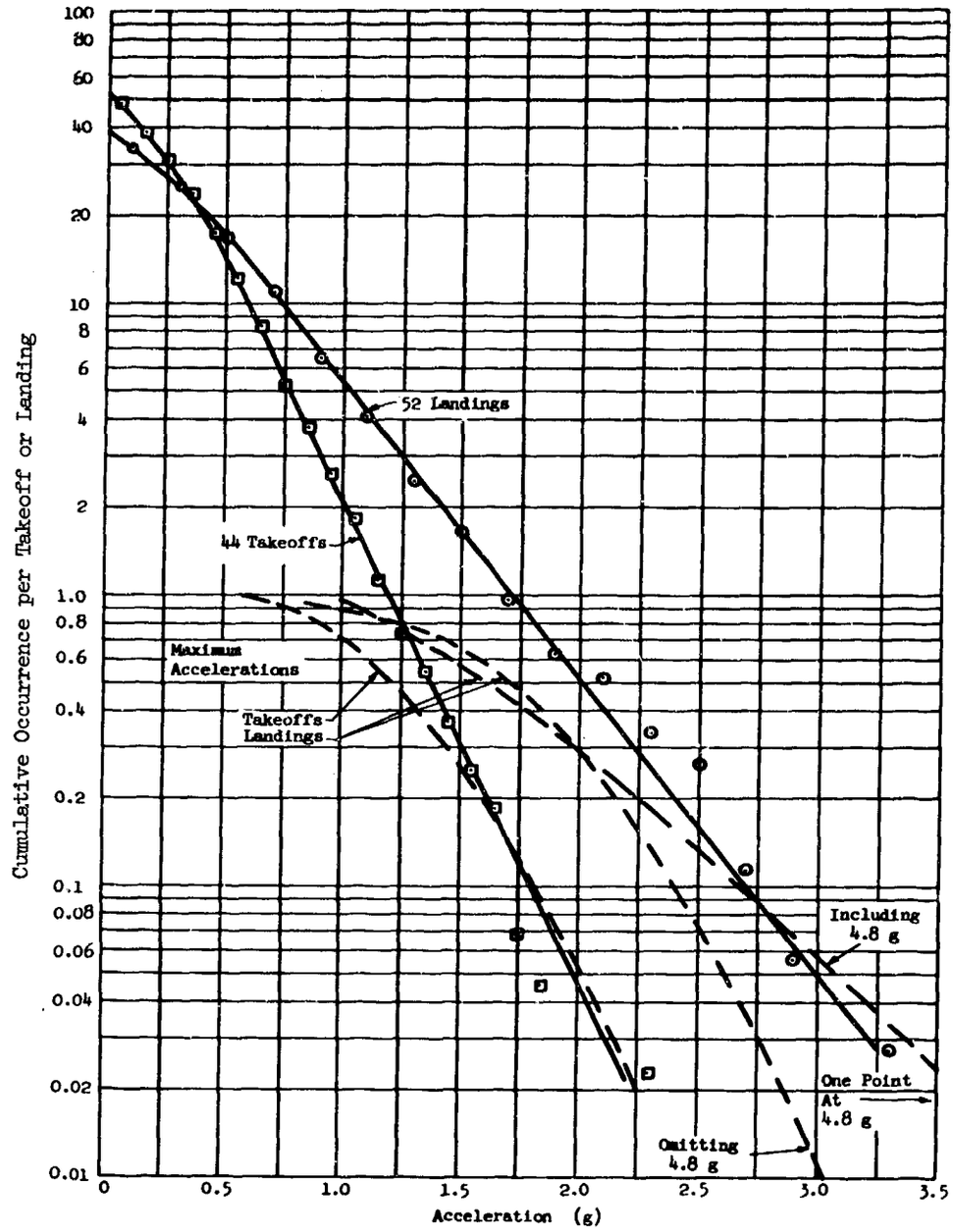

Fig. 4-35. Accelerations of All Magnitudes at CG
(a) Upward

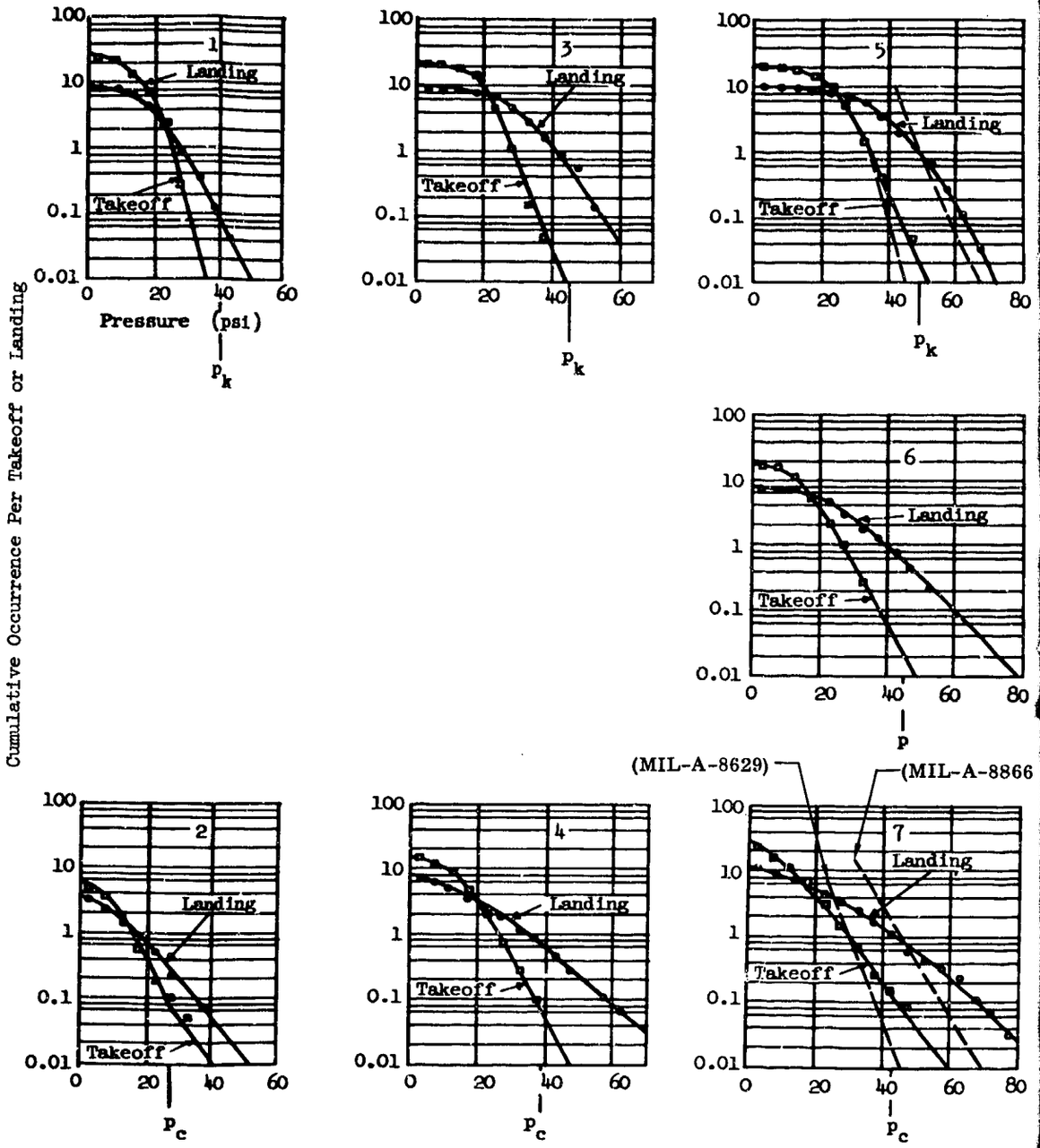
Cumulative Occurrence Per Takeoff or Landing
100
10
1
0.1
0.01
0
20
40
60
80
Pressure (psi)
1
Landing
Takeoff
p_k
3
5
6
p
(MIL-A-8629)
(MIL-A-8866
2
4
7
p_c

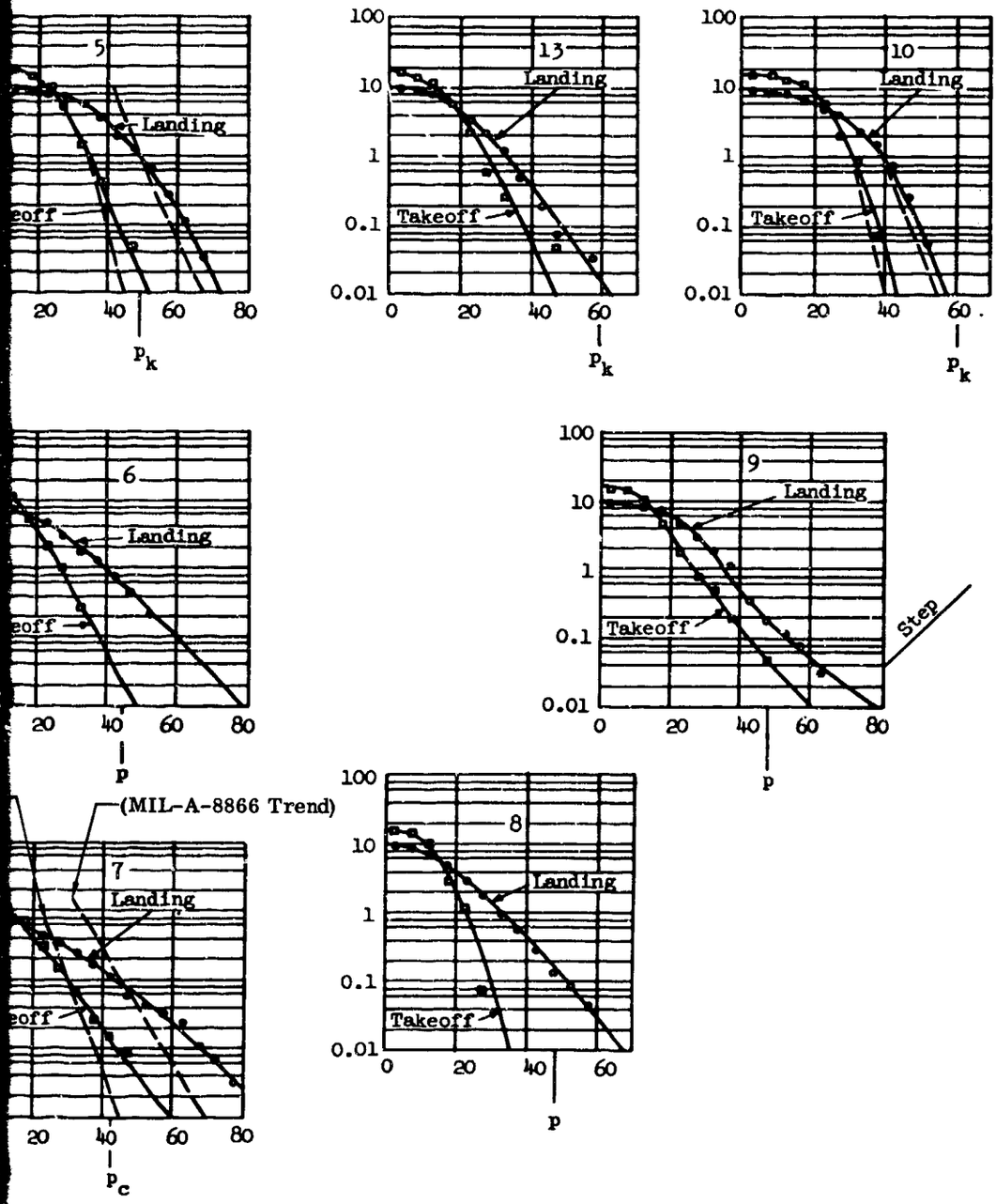

Fig. 4-36. Pressures of All Magnitudes on Forebody

2

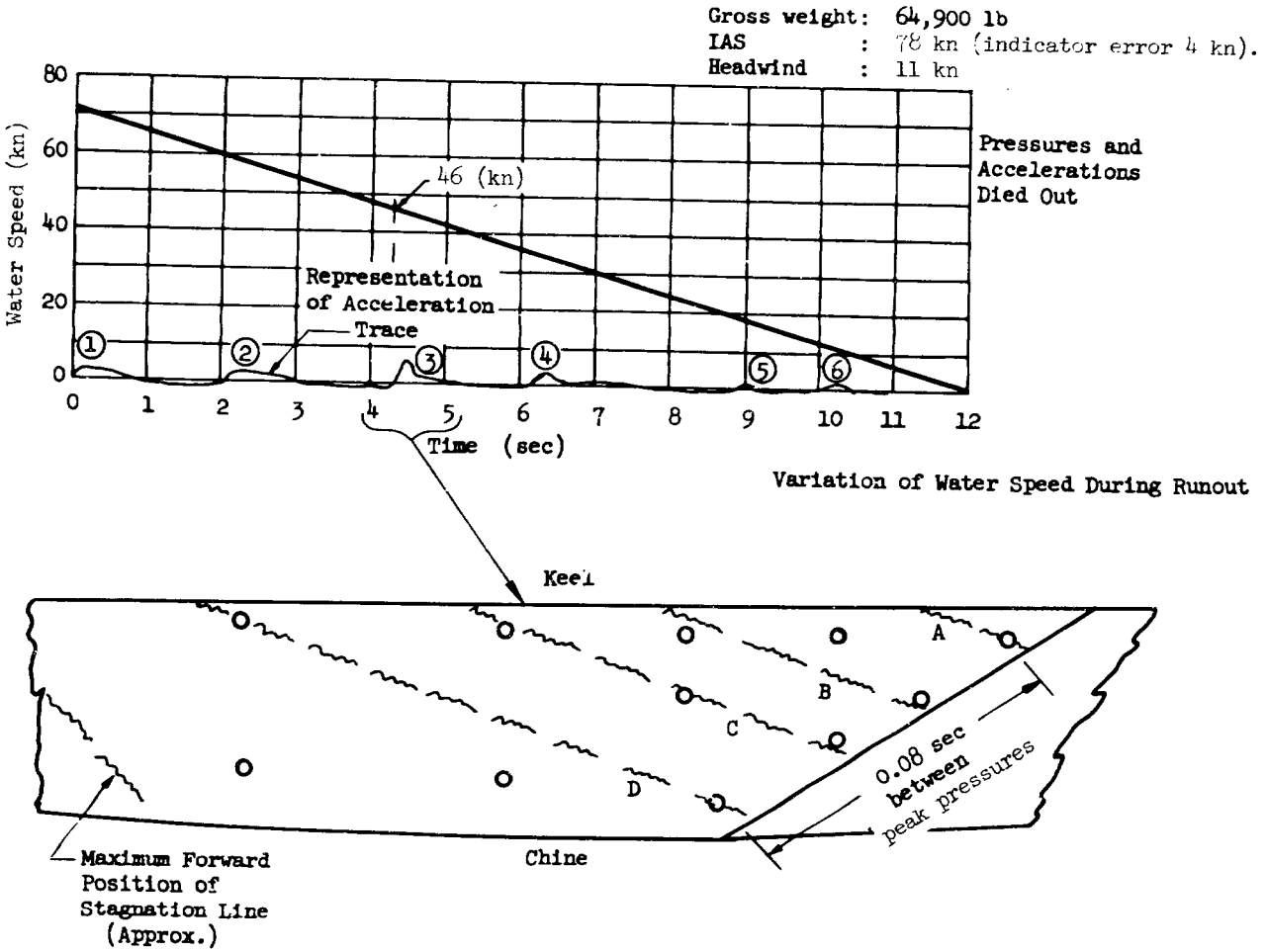

Fig. 4-37. Launching Conditions of the Example

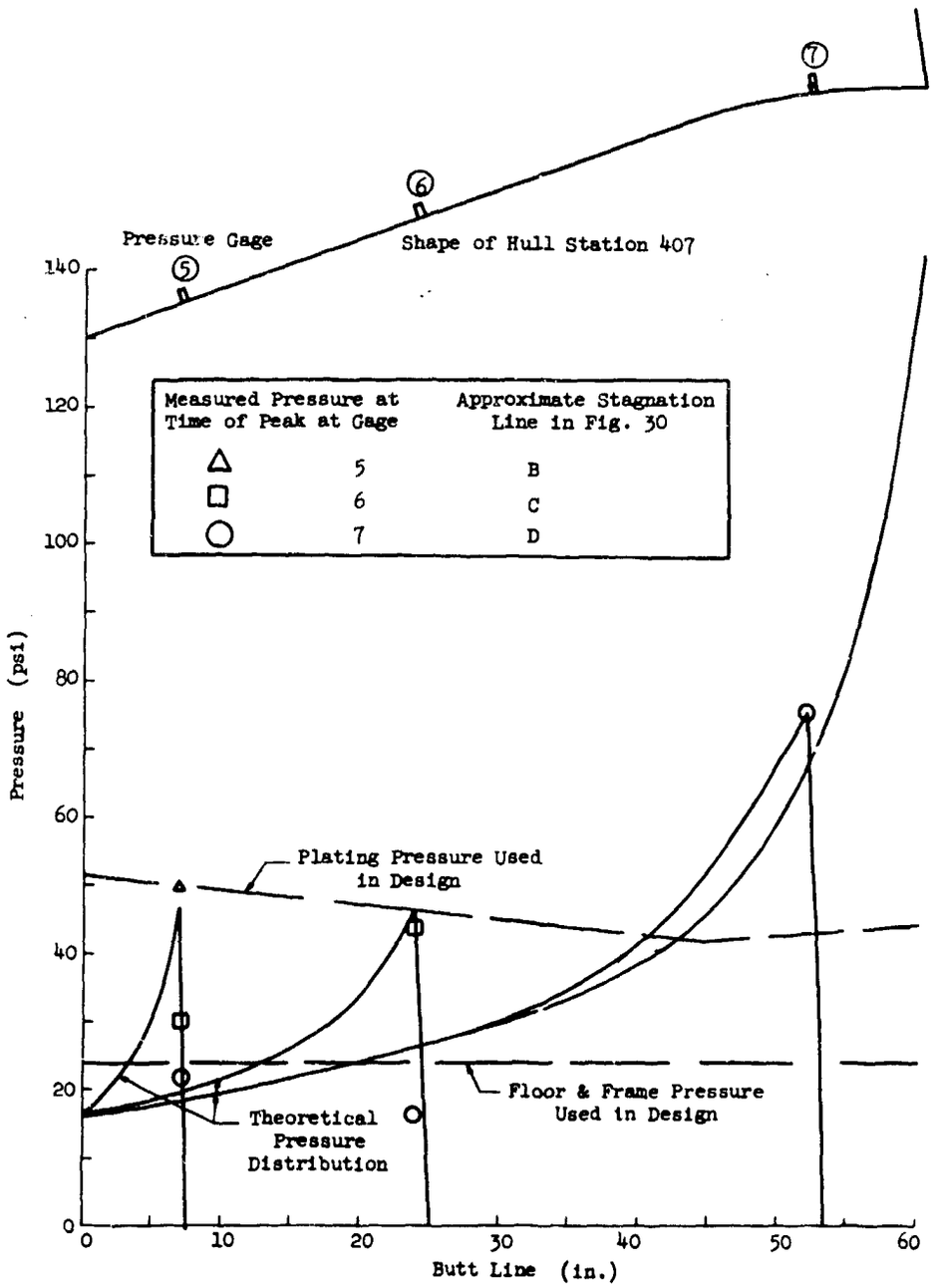

Fig. 4-38. Transverse Pressure Distributions

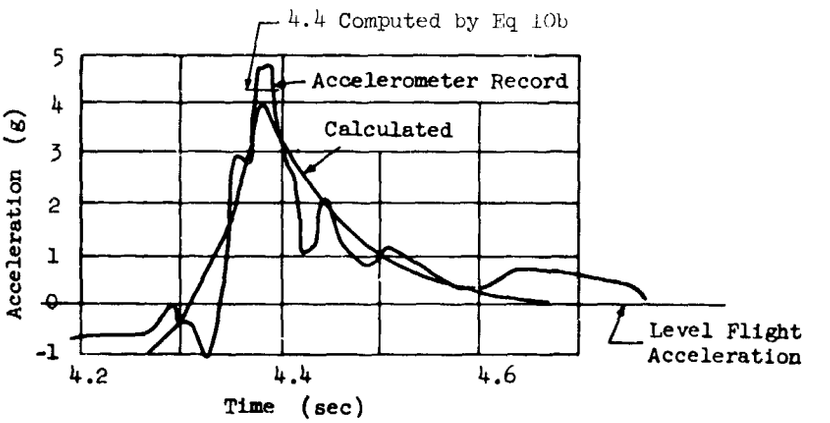

Fig. 4-39. Center of Gravity Acceleration: Landing 4, 3rd Contact

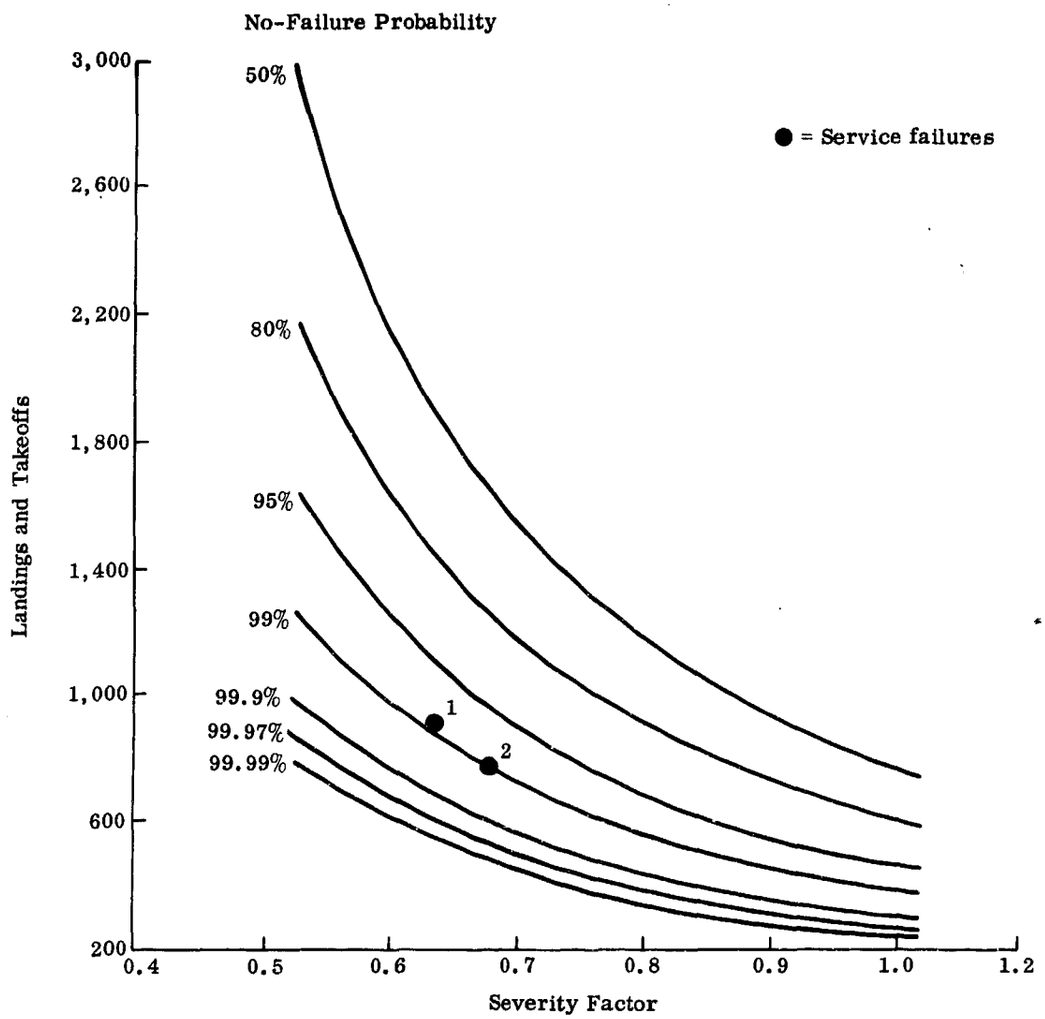

Fig. 4-40. No-Failure Probability (0.080 hull bottom plating)

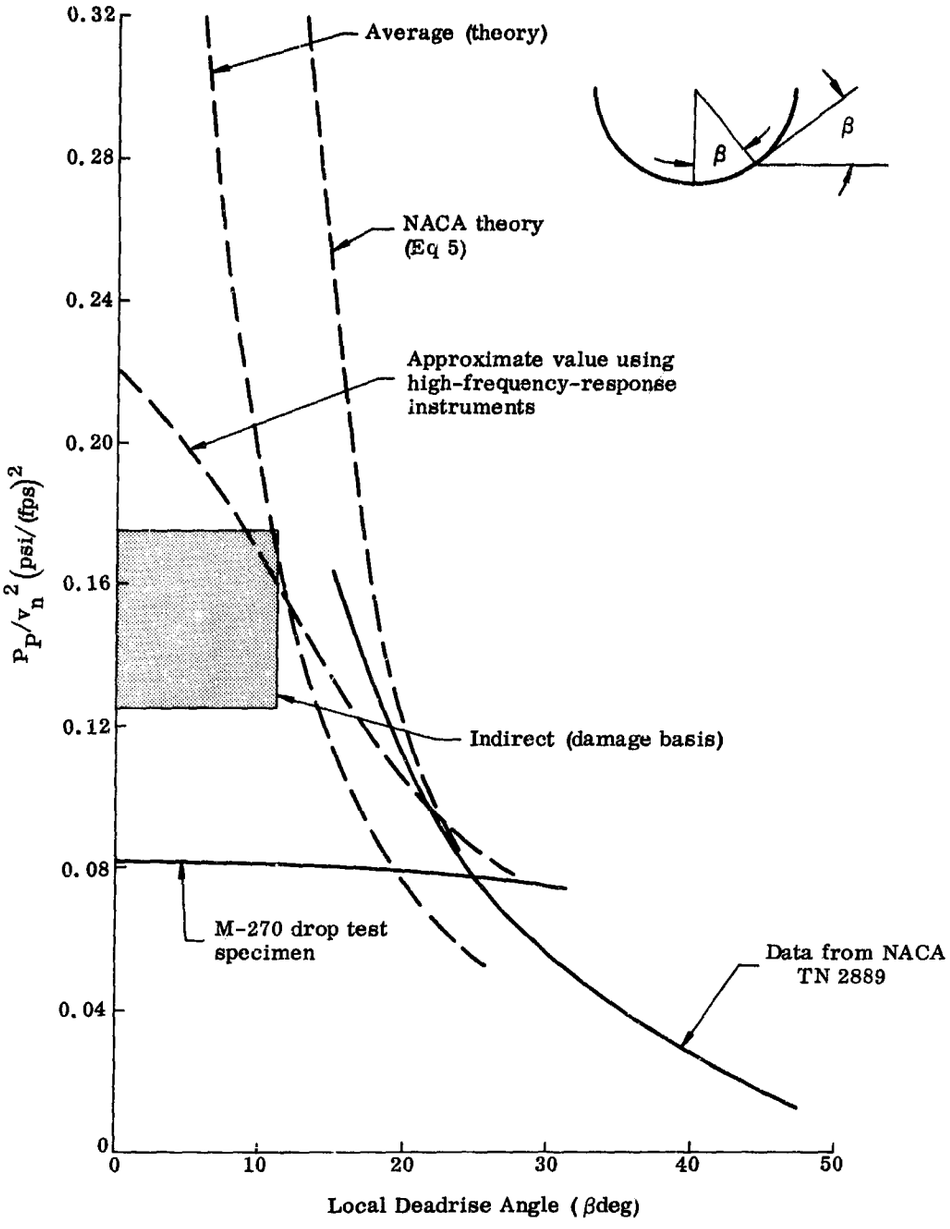

Fig. 4-41. Peak Pressure Coefficient for Impacts of Rounded Section

5.0 DESIGN PROCEDURES, SIZING CHARTS AND EXAMPLE PROBLEMS

5.1 SUMMARY

The significance of the design criteria to the structural design of a hydrofoil ship is illustrated by a number of examples. The general procedures used are a combination of typical ship and flying boat hull structural design methods.

The overall strength of the hull girder is investigated for hullborne, foilborne and landing conditions. Bending moments (longitudinal) are determined for a typical design deadweight loading. Typical longitudinal stresses at the keel and deck for an assumed midship section are used to show the relative importance of fatigue in the design of the hull girder.

The required local strength of the hull bottom plating and stringers is determined by landing pressures. Design charts based on seaplane hull experience are used as a basis for estimation of permanent set and fatigue life of the plating.

A large portion of the hull structure is made up of decking and sides which are relatively lightly loaded (compared with the hull bottom). A number of design charts are presented for decking, stringers and supporting structure combinations which provide stiffness and strength to meet the design criteria. Several types of structure are considered, and an example of a value analysis for selection of optimum design is given.

Although the complexities of the complete foil-strut structural design are beyond the scope of this report, design charts for section properties of typical thin walled sections are presented.

5.2 HULL GIRDER ANALYSIS

5.2.1 Summary

The maximum hull bending moments for all conditions of operation are summarized in Fig. 5-1. Each condition of loading is shown separately as the cumulative occurrence versus bending moment. A total cumulative plot of all types of occurrences could be constructed, but is not, since the various loadings have differing mean stress levels.

As expected, the landing conditions generate the maximum moments and highest stress levels for the initial design deadrise. Even with increased deadrise, moments due to the landing loads are still the greatest of all conditions. However, it will be noted that the most severe slamming impact in combination with a wave far aft on the hull gives relatively large moments also.

The normal foilborne and hullborne conditions in rough water give moderate hull bending moments, but the number of cycles of the loading is so high that fatigue becomes a major factor in the adequancy of the hull bending structure.

In order to make numerical comparisons of stress levels and fatigue damage for the various hull bending conditions, a typical midship section has been assumed. The deck and bottom scantlings were estimated to be consistent with local loading criteria. The deck is of 6061 aluminum alloy consistent with integral extrusions and minimum welding on assembly while the hull bottom is assumed to be 5456 aluminum alloy. The midship section moduli are:

$\frac{I}{c}$ for the deck $1.025 \times 10^6 / 81 = 1.265 \times 10^4$ in.^{3} $= 1.05 \times 10^3$ ft-in.^{2}

$\frac{I}{c}$ for the keel $1.025 \times 10^6 / 98 = 1.045 \times 10^4$ in.^{3} $= 0.87 \times 10^3$ ft-in.^{2}

The section shown in Fig. 5-2 is for the hull modified to a higher deadrise angle (17^o at Station 6, 12^o at Station 8). It is assumed that the structural bending modulus would not change with moderate changes in the hull deadrise.

For this selected section the fatigue damage analysis (primarily for the normal hullborne hogging and sagging conditions) shows a life expectancy of slightly more than one year. To increase this by a factor of 10 would require a reduction in the stress amplitude of approximately 25%. This coul. be accomplished by an increase in the structural section modulus and/or redesign for more uniform weight distribution.

5.2.2 Normal Hullborne Hogging and Sagging--Static Strength

In normal shipbuilding practice the design of the hull girder is based upon two assumed static buoyancy conditions. In one condition the vessel is balanced at its midportion upon a critical wave (hogging), and in the other the vessel is supported on waves at the bow and stern (sagging). The wave form usually chosen for these criteria is a hypothetical 20:1 trochoidal wave of length approximately equal to the length of the vessel.

In this study a broader treatment more representative of the actual sea environment is used to explore a fuller range of wave conditions. The study shows the determination of the limiting (critical) static condition and the spectrum of loadings to be used in determining fatigue damage.

The study begins with the North Atlantic wave data of Fig. 3-9 which was developed from the data of Figs. 3-4 and 3-6 to present cumulative wave data for all wave lengths in the range from (85 + 125)/2 = 105 ft to (125 + 220)/2 = 172 ft approximately. All waves in this range are assumed lumped at an average wave length, L_w, of 125 ft. Since this average length is approximately equal to the length (130 ft) of the study vessel, the response of the vessel to these critical ranges of data will produce the most severe static loading conditions and most damaging fatigue spectrum.

The 280-ton example ship design has a hull form similar to PC(H) as shown in Fig. 3-1. In the investigation which follows, the study vessel's weight is assumed to be the same for all design conditions and is distributed as shown in Fig. 5-3. All weight enclosed within the hull, i.e., the hull structure, fuel, furnishings, machinery etc., is assumed as distributed loads and included under the "Distributed Weight Curve." Foil weights are treated as concentrated loads.

The effect upon hull bending is examined for variations in the wave length-to-height ratio to establish the trend and the critical value. Figures 5-3, 5-4 and 5-5 present loading, shear and bending moment diagrams for smooth water, standard trochoidal waves of length-to-height ratio equal to 10:1 and 20:1 and a hypothetical "notch" wave of sufficient depth to utilize the total sectional buoyancy at each section, thus concentrating the buoyancy force over the shortest possible length and producing the maximum possible bending moment. From these figures the maximum values of bending moment at the midship section can be plotted as in Fig. 5-6 to show the variation of the bending moment with the L_w/H ratio. The extreme value at the top of the plot is still water; the extreme values at the bottom would approach the value for the hypothetical notch wave. (Note that the current formula for design length-to-height ratio, $1.1\sqrt{L}$--gives a value of approximately 12.5 for the sample ship.)

Figure 5-7 shows the cumulative occurrence of the moments produced by waves 125 ft in length (the approximate length of the study vessel). The frequency values of Fig. 5-7 are 54% of those of Fig. 3-9 and the bending moments are from Fig. 5-6. It is seen that even at the minimum L_w/H value, (6), a considerable number (approximately 500) of hogging and sagging loadings can be expected per year. Considering all waves higher than 2 ft to be encountered during the hullborne time (54% of the yearly values) the probability of encountering the most severe waves while operating is equal to $\frac{500}{(23.21\text{x}10^5)} = 0.00215$

where $(23.21\text{x}10^5)$ is determined as follows:

Figure	L_w	Waves >2 ft Total Cumulative Yearly	(0.54)x Cumulative Value
3-8	85 ft	$1.4\text{x}10^6$	$7.55\text{x}10^5$
3-9	125 ft	$2.0\text{x}10^6$	$10.80\text{x}10^5$
3-10	220 ft	$0.7\text{x}10^6$	$3.78\text{x}10^5$
3-11	340 ft	$0.2\text{x}10^6$	$1.08\text{x}10^5$
	Totals =	$4.3\text{x}10^6$	$23.21\text{x}10^5$

Thus, the probability of experiencing a near maximum load is 1 time out of each 4650 wave encounters. This frequency of occurrence is quite high, and as shown in Figs. 5-6 and 5-7, the midship girder bending moment for the minimum L_w/H value (6) approaches that of the arbitrary hypothetical notch wave, the maximum anticipated value for static analysis of the hogging and sagging conditions.

Thus, if in the analysis procedure a hypothetical notched wave is used for quick approximation, the structural sizing would be made using a yield factor of safety of 1. However, if it is preferred to use a 10:1 trochoidal wave, a yield factor of safety of 5.1/3 = 1.7 should be used for hogging and 9.2/6.2 = 1.5 should be used for sagging. (Refer to Fig. 5-7 for values.) If a 20:1 trochoidal wave is chosen for analysis, the yield factor of safety should be 5.1/2 = 2.6 for hogging and 9.2/3.7 = 2.5 for sagging. In each case the ultimate factor of safety should be 1.5 x yield load factor.

Thus, the following general recommendations can be made for vessels of the 130-ft class:

(1) If a hypothetical notch wave is used as a basis for static strength analysis of the hull girder, a yield factor of safety of 1.0 is recommended. The ultimate factor of safety should be 1.5.

(2) If a 10:1 trochoidal wave is used as a basis for analysis, a yield factor of safety of approximately 1.6 (rounded average of values determined above) should be used for both hogging and sagging. The ultimate factor of safety should be 1.5x1.6 = 2.4.

(3) If a 20:1 trochoidal wave is used as a basis for analysis, a yield factor of safety of approximately 2.5 (rounded average of values determined above) should be used for both hogging and sagging. The ultimate factor of safety should be 1.5x2.5 = 3.8.

On this basis the maximum static design stress for the normal hullborne sagging condition would be:

deck $9.2 \times 10^6 / 1.05 \times 10^3$ = 8,700 psi compression

keel $9.2 \times 10^6 / 0.87 \times 10^3$ = 10,500 psi tension

and for the hogging condition

deck $5.1 \times 10^6 / 1.05 \times 10^3$ = 4,800 psi tension

keel $5.1 \times 10^6 / 0.87 \times 10^3$ = 5,800 psi compression.

These stresses are well below the allowable yield strength of the structure. However, it is evident from the consideration of the large number of loading cycles involved that an assessment of the fatigue life should be made.

Figures 5-8 and 5-9 present the stress loading spectrum for the 280-ton study ship. Hogging and sagging is in reality only one type of loading because each (hog and sag) constitutes the passage of a single wave and consequently is one cycle. The deck is in tension at hogging and in compression at sagging. For the study ship the compression stress in the deck is almost twice the value of the tension stress and thus the mean stress is negative. In the keel and hull

TABLE 5-1

Fatigue Damage Study of Deck at Midship Section
Under Hogging and Sagging Loads

$\sum$ n/year	n/year	Fuel	Stress		a/u	m/u	N	n/N
			Maximum	Minimum				
Fig. 5-8		%	Reference	Fig. 5-8	①	②	Fig. 3-22	
5×10^3	3.5	100	3080	-6530	0.11	-0.04	∞	0
to	$\times 10^4$	50	4460	-5150	0.11	-0.01	10^7	0.004
4×10^4		25	5110	-4440	0.11	0.01	2×10^5	0.175
4×10^4		100	2480	-4980	0.09	-0.03	∞	0
to	6.0	50	3600	-3930	0.09	0.00	10^8	0
10^5	$\times 10^4$	25	4110	-3380	0.09	0.01	10^7	0.006
10^5		100	2000	-3780	0.07	-0.02	∞	0
to	3.0	50	2900	-2980	0.07	0	∞	0
4×10^5	$\times 10^5$	25	3320	-2570	0.07	0.01	∞	0
4×10^5		100	1450	-2580	0.05	-0.01	∞	0
to	6.0	50	2100	-2040	0.05	0	∞	0
10^6	$\times 10^5$	25	2410	-1750	0.05	0	∞	0

① $a/u = \frac{(\text{maximum} - \text{minimum})}{2u}$; ② $\frac{m}{u} = \frac{(\text{maximum} + \text{minimum})}{2u}$; u = 42,000 psi (6061)

$\sum$ n/N for 100% fuel = 0, therefore life = ∞

$\sum$ n/N for 50% fuel = 0.004, therefore life = $\frac{1}{0.004}$ = 250 years

$\sum$ n/N for 25% fuel = 0.181, therefore life = $\frac{1}{0.181}$ = 5.5 years.

TABLE 5-2

Fatigue Damage Study of Keel at Midship Section
Under Hogging and Sagging Loads

$\sum$ n/year	n/year	Fuel	Stress		a/u	m/u	N	n/N
			Maximum	Minimum				
Fig. 5-9		%	Reference	Fig. 5-9	①	②	Fig. 3-22	
5×10^3	3.5	100	7830	-3750	0.13	0.04	8×10^4	0.437
to	$\times 10^4$	50	6180	-5440	0.13	0.01	2×10^5	0.175
4×10^4		25	5320	-6220	0.13	-0.01	10^6	0.035
4×10^4	6.0	100	6080	-3080	0.10	0.03	1.7×10^5	0.353
to	$\times 10^4$	50	4800	-4460	0.10	0	10^5	0.060
10^5		25	4130	-5110	0.10	-0.01	10^7	0.006
10^5	3.0	100	4680	-2450	0.08	0.02	10^8	0.003
to	$\times 10^5$	50	3700	-3550	0.08	0	∞	0
4×10^5		25	3180	-4060	0.08	-0.01	∞	0
4×10^5	6.0	100	3200	-1750	0.05	0.02	∞	0
to	$\times 10^5$	50	2050	-2540	0.05	0	∞	0
10^6		25	2180	-2900	0.05	-0.01	∞	0

① $\frac{a}{u} = \frac{(\text{maximum}-\text{minimum})}{2u}$, ② $m/u = \frac{(\text{maximum}+\text{minimum})}{2u}$, $u = 46,000$ psi (5456)

$\sum$ n/N for 100% fuel = 0.793, therefore life = $\frac{1}{0.793}$ = 1.3 years

$\sum$ n/N for 50% fuel = 0.235, therefore life = $\frac{1}{0.235}$ = 4.2 years

$\sum$ n/N for 25% fuel = 0.041, therefore life = $\frac{1}{0.041}$ = 24 years

bottom the stress values are reversed and there exists a positive or tension mean. This situation exists on the study ship primarily because of the weight distribution used in determining the overall shears and bending moments. For the study ship a very large weight fraction, 1/3, was assumed for fuel. This fuel was concentrated midships which resulted in high midship bending moments during sagging and low midship bending moments during hogging. For ships with other arrangements and weight distributions this situation could easily be the reverse. To show the effect of variation in weight distributions, the damage study for the deck shown in Table 5-1 and for the keel shown in Table 5-2 is presented for full fuel, half fuel, and one-quarter fuel.

Examination of Table 5-1 indicates that if the ship were operated for its full life at full or half fuel weight, fatigue failure in the deck would be unlikely. The effect of a weight distribution which would result in a zero or positive mean while the amplitude remains constant is clearly indicated as a marked reduction in fatigue life. It can further be seen from the table and also from Fig. 3-22 that if (1) the mean stress level is held near zero, and (2) the stress amplitude held below values equivalent to approximately 8% of the ultimate breaking strength of the material, the probability of having a fatigue free structure is greatly improved.

Examination of Table 5-2 shows that fatigue damage in the keel area is critical but is lessened as the fuel weight is decreased. Likewise for a ship with weight more evenly distributed the amount of fatigue damage would be lessened.

Thus, we conclude that for ships of the 280-ton class which are constructed of aluminum and intended for extensive hullborne operation, it is important in the design stage to consider fatigue as a problem. The distribution of weight to effect a near zero mean stress level will be beneficial in increasing fatigue life.

5.2.3 Foilborne Flight

The overall hull loads during foilborne flight are limited by autopilot settings consistent with what may be considered a comfort level for the crew. Figures 4-27 and 4-28 in this report show load spectrums for 0.25 g and 0.50 g autopilot setting for 45-kn and 100-kn ships. Also shown are load factors for fixed foil responses, which assume autopilot or control malfunction. The values shown are for specific values of C_L and C_{L_D} which give optimum lift-to-drag ratios for subcavitating foils at 45 kn and for supercavitating foils at 100 kn. The cumulative occurrence rate for the loading under assumed malfunction/operational conditions is shown in Fig. 4-29.

Figure 5-10 presents shear and bending moment diagrams for the 280-ton study ship for 1 g flight. Maximum bending moments for 0.25 g and 0.50 g autopilot settings for 45-kn and 100-kn ships are presented in Fig. 5-11. In this figure, the foils are located at 24 ft aft of Station 0 for the forward foil and 94 ft aft for the rear foil which distributes the hull weight 30% to the forward foil and 70%.

to the rear foil. Assuming this same percentage load distribution, the bending moments (1 g flight) for a forward foil location at Station 12 and at Station 0 are as follows:

Forward foil at Station 24 Rear foil at Station 94	BM = 2.9×10^6 (Ref. Fig. 5-10)
Forward foil at Station 12 Rear foil at Station 99	BM = $(4.9)10^6$ ft-lb (limit) @ Sta 62
Forward foil at Station 0 Rear foil at Station 104	BM = $(6.9)10^6$ ft-lb (limit) @ Sta 62

For foilborne flight, the study ship is considered to be operating under full autopilot control in such a manner that at each wave encounter one full cycle of loading is experienced by the overall ship. For this study two autopilot settings are investigated, $\pm$ 0.25 g and $\pm$ 0.5 g.

Figure 5-11 presents the midship bending moment spectrums for the two autopilot settings during 1 g flight at 45 kn and at 100 kn. For the fatigue damage study for this operation several simplifying assumptions are made to minimize the determinations without grossly affecting the results.

(1) The minimum and maximum stress are assumed constant and equal to the values at the 10^5 cycle level.

(2) The number of cycles cumulated per year will be 6×10^5 for the 45-kn boat and 1.6×10^6 for the 100-kn design.

(3) The stresses at the keel of the midship section will be determined by

$$\sigma = \frac{Mc}{I}$$ where $I = 1.025 \times 10^6$ in.^{4} and c = 98 in. (Ref. Fig. 5-2).

Only keel stresses are examined since the deck stresses are compression and therefore not critical in fatigue. u = 46,000 psi, the ultimate strength of the 5456 aluminum alloy hull bottom plating and stringer.

1. 45-kn ship (1 $\pm$ 0.25) g

At 10^5 level $M_{min} = 2.29 \times 10^6$ ft-lb

$$\sigma_{min} = \frac{2.29 \times 10^6 \times 12 \times 98}{1.025 \times 10^6} = 2620 \text{ psi}$$

$$M_{max} = 3.52 \times 10^6 \text{ ft-lb}$$

$$\sigma_{max} = 3.52 \times 1145 = 4030 \text{ psi}$$

$$\frac{a}{u} = \frac{4030 - 2620}{2 \times 46,000} = 0.015 \quad \frac{m}{u} = \frac{4030 + 2620}{2 \times 46,000} = 0.072$$

(See Table 5-1 for symbols.)

From Fig. 3-22 N = ∞; $\therefore$ life = ∞

2. 45-kn ship (1 ± 0.5) g

At 10^5 level $M_{min} = 1.62 \times 10^6$ ft-lb

$$\sigma_{min} = 1.62 \times 1145 = 1850 \text{ psi}$$

$$M_{max} = 4.18 \times 10^6 \text{ ft-lb}$$

$$\sigma_{max} = 4.18 \times 1145 = 4780 \text{ psi}$$

$$\frac{a}{u} = \frac{4780 - 1850}{2 \times 46,000} = 0.032 \quad \frac{m}{u} = \frac{4780 + 1850}{2 \times 46,000} = 0.072$$

From Fig. 3-22 N = ∞; $\therefore$ life = ∞

3. 100-kn ship (1 ± 0.25) g

Values are the same as for 45-kn ship.

Therefore, N = ∞ and life = ∞.

4. 100-kn ship (1 ± 0.5) g

Values are the same as for 100-kn ship. Therefore, N = ∞ and life = ∞.

From the above investigation it is concluded that under foilborne flight the fatigue damage to be expected is negligible even with an autopilot setting of ±0.5 g. Should severe dynamic conditions exist and remain undetected for a long period of time at very high speeds some damage could occur.

5.2.4 Hull Bending Due to Impact

Substantial impacts on the hull can occur in hullborne operation (bow slamming) and in landing from the foilborne flight condition. These impact loads may be combined with foil lift or buoyant forces and are reacted by inertial forces of the ship's deadweight. The resulting bending moments within the hull will depend upon both the magnitude and location of the applied forces and in some cases the distribution of the applied load.

A parametric form of the hull bending moment for concentrated applied loads is shown in Fig. 5-12. A 1 g loading at various stations determines the angular acceleration:

$$\dot{\omega} = 32.2 \text{ (x cg)}/k^2$$

The inertial reaction of the ship deadweight to the 1 g loading plus the resulting angular acceleration yields the bending moments from which the parameter lines of hull station are constructed. Moments corresponding to applied loads greater or less than the gross weight are obtained by direct ratio. For example, 1 g loading applied at the location of the front foil causes a hull moment, $M = 7.1 \times 10^6$ ft-lb (Fig. 5-12); front foil lift equal to 30% weight gives a bending moment maximum between Station 60 and 70 $M = 0.3 \times 7.1 \times 10^6 = 2.13 \times 10^6$ and for 70% weight on rear foil the bending moment at Station 60 is $M = 0.7 \times 1.1 \times 10^6 = 0.77 \times 10^6$. The total bending moment for the 1 g foilborne condition is thus a maximum close to Station 60 with a value of $M = (2.13 + 0.77)\ 10^6 = 2.9 \times 10^6$ (which is the value obtained for the specific calculation shown in Fig. 5-10).

This general bending moment chart (Fig. 5-12) may be used for various combinations of loadings where the loading itself is actually concentrated or does not extend into the region of maximum moment. Bow and stern landings, slamming, slamming with aft buoyancy and foilborne conditions generate sagging moments which peak near midship and thus fit the requirements for application of the bending moment chart on the example design.

Midship landing impacts (Station 6) cause hogging of the hull, and the loaded area is generally across the region of maximum moment. For example the typical loading analyzed at the beginning of section 4.4 shows a maximum acceleration for an impact at Station 6 of 1.6 g (for $\beta = 17°$). For this impact as a concentrated load the maximum hogging moment from Fig. 5-12 would be $M = 1.6 \times 6.3 \times 10^6 = 10 \times 10^6$. However, as indicated in the earlier section (4.4), the load is actually spread over 43 feet (for the assumed rectangular loading). The effect upon the bending is shown in Fig. 5-13 where the peak moment for a 1.7 g impact is calculated to be 5.4×10^6. (It is interesting to note that, if the water loading is assumed triangular rather than rectangular,

the maximum bending moment is substantially unchanged.) The maximum bending moment for other load factors applied at the same station (Station 6) is obtained by direct ratio to the 5.4×10^6 ft-lb reaction to the 1.7 g load $\frac{5.4}{1.7} = 3.18 \times 10^6$ ft-lb/g.

For the 1.6 g example in Section 4.4 the actual moment would be $1.6 \times 3.18 = 5.08 \times 10^6$ ft-lb slightly more than 1/2 of the moment for a concentrated load at Station 6.

The cumulative occurrences for bending moments for impacts at Station 6 are obtained directly from the load factor distribution in Figs. 4-25 and 4-26 and are plotted in Fig. 5-1 for the 45- and 100-kn designs for both initial and modified deadrise angles.

The cumulative occurrences for maximum hull bending moments for the sagging conditions may be constructed from a combination of the load factor occurrences in Section 4 and the parametric moment curves (Fig. 5-12).

Bow landing impacts are represented by the loads applied at Station 2. It is assumed that the main foil is still lifting its normal share of the weight (70%). Thus, the maximum hull bending is made up of the impact load factor (Figs. 4-25 and 4-26) x 6.4×10^6 ft-lb/g plus $(0.7 \times 0.8 = 0.56) \times 10^6$ ft-lb.

Stern landing impacts are represented by the loads applied at Station 8. In this case it is assumed that the bow foil is still lifting its normal share of the weight (30%). Thus, the maximum hull bending is the impact load factor (Figs. 4-25, 4-26, and 4-22) x 3.7×10^6 lb/g plus $(0.3 \times 7.1 = 2.1) \times 10^6$ ft-lb.

Bow slamming is represented by impacts at Stations 1 and 2. It can be noted from the data for the impact load in Fig. 4-15 and the induced moments, Fig. 5-12, that the loads are sufficiently higher at Station 2 to yield practically the same hull bending moments. Thus, it is assumed for analysis that all the bow slamming is at Station 2. The hull bending moment for the impact only is (from Fig. 5-12) load factor x 6.45×10^6 ft-lb. It is considered likely that a substantial buoyant force may be acting at the same time on the after portion of the hull. Thus, two distributions of moments for slamming load occurrences are shown in Fig. 5-1, one for the slamming impact only and one for slamming plus a buoyant force equal to the weight centered at Station 8. The maximum bending moments are: load factor (Fig. 4-15) for slam at Station 2 x 6.45×10^6 ft-lb plus 3.7×10^6 ft-lb for 1 g buoyance at Station 8.

The moments due to crash landings from sudden loss of a foil are included in the summary distributions in the occurrence level range from 1 and 0.1. This is a completely arbitrary assumption so that the extreme conditions can be shown in the same plot.

Scales for deck and keel stresses corresponding to the hull bending moments are included on Fig. 5-1. These apply to the assumed section modulus for the midship section shown in Fig. 5-2.. It can be seen that the static stresses do not exceed the yield strength within the extent of the cumulative occurrence of once in ten years (0.1). However, the major improvement in the stress level with the revised deadrise is evident. In fact, with the modified deadrise, the crash landings due to loss of the main foils do not cause overall bending stresses beyond the yield strength even for the 100-kn design.

From the overlay of the moments versus cumulative occurrence it appears that slamming in combination with aft buoyancy is a condition of possible significant fatigue damage. This is assessed in Table 5-3 assuming that a complete cycle is the normal hullborne hogging bending followed by a slam.

TABLE 5-3

Fatigue Damage Study for Keel at Midship Section Under Slamming

$\sum$n/year	n/year	σ max	σ min	a/u	m/u	N	n/N
Fig. 5-1							
10 to 100	90	12,000	-4500	0.18	0.08	1.5×10^4	6×10^{-3}
100 to 1000	900	10,300	-4000	0.155	0.07	3×10^4	30×10^{-3}

$\sum n/N = 0.036$

This value represents less than a 5% increase in the damage assessment for the hullborne bending, Table 5-2.

5.3 HULL BOTTOM PLATING AND STRINGERS

5.3.1 Summary

The hull bottom pressures determined from the rational analysis of slamming and landing conditions for the hydrofoil ship and the practical experience from years of seaplane design and operation have been presented in Section 4. Their application in the design of the hull bottom structure is shown by several examples in the bow and midship sections of the example hydrofoil ship design.

Two main criteria are used for the design--permanent set of plating allowable between stringers and fatigue life expectancy under the cumulative occurrence distributions of the applied pressures. In the bow sections the fatigue life is the controlling factor due to the large combined number of loadings from slamming and normal landing. At other areas on the hull bottom the cumulative distribution of pressure occurrences is substantially lower, and yield strength (permanent set criteria) is of primary importance.

The results from the sample analyses were based upon the assumption that the materials and overall structural responses to repeated loadings would be similar to seaplane hull structures. This may be a conservative assumption for the lower yield strength, welded structure of the hydrofoil ship.

5.3.2 Plating Design

The plating design pressures are determined from the peak pressure distributions given in Figs. 4-1, 4-20 and 4-21 according to the general criteria and practical experience presented in Sections 4.4 and 4.5. Examples of the application of the design method are given for two hull locations: bow (Station 2) and midship (Station 6). The midship section is considered at the initial design deadrise, $\beta = 6°$, and also for a modified hull form of increased deadrise, $\beta = 17°$.

Two basic structural criteria are used:

(1) Static strength--allowable permanent deformation.

(2) Fatigue life.

For the sake of the hydrodynamic performance and appearance of the hull form the plating is designed to an allowable permanent set between stringers (rather than to a rupture strength criterion). The deformation characteristics for several typical plating-stringer combinations are given in Figs. 3-16 and 3-17. From comparable seaplane experience and the general form of the cumulative occurrence curves for the pressures, the set criterion is selected to be:

> Permanent set less than 1/2% of the span between stringers for a pressure level corresponding to one occurrence per year.

The fatigue life expectancy for the plating at various pressure levels is given in Figs. 3-20 and 3-21.

5.3.2.1 Plating, Station 2

For the 30° deadrise section at Station 2 the average pressure over one bay of plating is approximately 90% of the peak pressure (see Fig. 4-32). From Fig. 4-1 the permanent set design pressure is:

	45-kn design (slamming)	100-kn design (landing)
$P_D = 0.9\ P_P$	0.9 (43) = 39 psi	0.9 (63) = 57 psi

for 7075-T6 plating on Z stringers (upper graph Fig. 3-16)

t/b	0.0104	0.0127
b = 7.5 in.	t = 0.080	t = 0.100

t/b	0.0095	0.0115
t = 0.156 in.	b = 16.5 (13)	b = 13.5 (11)

(1) With the 7075 plating, Z stringer arrangement, any convenient plating thickness may be used that meets the thickness/span ratio required.

(2) The integral extrusion will be limited to some practical minimum gage for the extrusion process (0.156 estimated) and the stringer spacing is determined. Actually the curves of Fig. 3-17 are for an extrusion which has a thickened section at the stringer such that the effective plating span is only 2/3 of the nominal b. The span values in parentheses are the values for an arbitrary extrusion where the thickened plate at the stringer extends only 2 in. (b) = 2/3 (b + 2).

The fatigue life of the plating at Station 2 is developed in Table 5-4 for the 100-kn design with 7075-T6 plating. Two plating thicknesses are investigated for a 7.5-in. stringer spacing, t = 0.100 (as required for the permanent set criteria) and t = 0.156. The relatively short life (3 years) expected of the thinner plating indicates that for the bow loading conditions the fatigue characteristics will outweigh the permanent set requirements.

Specific test curves for the extruded plating fatigue life are not available for a like comparison on the 5456-H111 bottom. However, since the 5456 aluminum alloys have a much lower yield strength than 7075-T6, it is inferred that a greater fatigue life would result from the 5456 alloys when designed to the same permanent set criteria.

5.3.2.2 Plating, Station 6

Both original and modified deadrise sections at Station 6 fall in the low deadrise category, which requires considerable modification to the peak pressure values for use in design. The method of application of the approach described in Sections 4.4 and 4.5 will be shown for both forms (β = 6° and 17°) for the cumulative occurrences of pressures for the 45-kn design, given in Fig. 4-20.

The maximum design pressure for the plating will occur in the outermost bay of wetted area. The value of this pressure in terms of the peak pressure, P_D/P_P, is plotted in Fig. 5-14 for the two deadrise angles. (At these low values, $\beta < 20°$, the expanding plate pressure theory, Ref. 5, is used.) It will be noted that the average pressure in the outermost bay increases quite rapidly

TABLE 5-4

Fatigue Damage--Hull Plating at Station 2 (100-kn design)

7075-T6 Plating t/b = 0.0133 (and 0.0208)

Design Pressure P_D	P_P (P_D/0.9)	Occurrence Cumulative (Fig. 4-1)	n/Year	Cycles to Failure, N (Fig. 3-20)	Partial Damage (n/N)	$\sum$n/N
		20,000				
10	11		14,000	220,000 (1,000,000)	0.064 (0.014)	0.064 (0.014)
		6,000				
20	22		3,800	40,000 (250,000)	0.095 (0.015)	0.159 (0.029)
		2,200				
30	33		1,600	17,000 (65,000)	0.094 (0.025)	0.253 (0.054)
		600				
40	44		460	9,000 (30,000)	0.051 (0.015)	0.304 (0.069)
		140				
50	55		115	6,000 (20,000)	0.019 (0.006)	0.323 (0.075)
		25				
55	61		25	3,000 (15,000)	0.008 (0.002)	0.331 (0.077)
		0				

Relative mean life = $1/\sum$n/N = 3 years t/b = 0.0133
(13 years t/b = 0.0208)

with increase in the width of the impact area (number of bays). However, a contrary trend is brought about by the reduction in the normal velocity due to the progress of the impact. As noted in Section 4.4 the velocity at maximum impact load is 7/9 of the initial contact velocity, and the wetted half-width for the typical impact is 7 ft. A typical effect of the velocity change can be superimposed on the P_D/P_P curves in Fig. 5-14 for an assumed stringer spacing.

For 8.5-in. stringer spacing the 7-ft half-width corresponds to 10 bays. The variation in peak pressure from initial contact at the keel to width of maximum impact load is estimated to be as shown in Fig. 5-14. The net plating design pressure including the estimated deceleration is determined by multiplying the values at constant velocity times the velocity reduction factor. Thus, although the initial rise in plating design pressure is quite rapid, the vehicle deceleration due to the impact causes a decrease in pressure for large wetted areas. Under the estimated impact conditions and assumed stringer spacing the maximum plating pressure load occurs on the fifth or sixth plating panel from the keel.

From Figs. 5-14 and 4-20 the permanent set design pressure at one occurrence per year is:

	6°	17°
$P_D = K_D P_P$	0.35 (405) = 142	0.70 (50) = 35

for 7075-T6 plating, Z stringers (upper graph Fig. 3-16)

t/b	0.025	0.0096
b = 8.5 in.	t = 0.213	t = 0.082

for 5456-H111 integral extrusion (upper graph Fig. 3-17)

t/b	0.0245	0.0085
b = 8.5 in.	t = 0.208	t = 0.072

The fatigue life of the plating at Station 6 is developed in Table 5-5 for the 45-kn design with 7075-T6 plating on the low deadrise hull, $\beta = 6^\circ$. The relatively long mean life, 30 yr, indicates the importance of the difference in the occurrence levels between the bow station and the midship area. Since only the landing impacts give significant pressures at Station 6, the total occurrence levels are lower than for the bow station (which experiences slamming pressures as well as normal landing). In addition, the low deadrise section is more critical to the attitude of the ship at contact so that the slope of the occurrence curves is greater for the midship section.

Although only the one case is shown in Table 5-5, review of the occurrence curves in Figs. 4-20 and 4-21 and the fatigue life characteristics, Fig. 3-20,

shows that the other design conditions (β = 17° and 100-kn design speed) will not be more critical for the repeated loading conditions. Thus, for most of the hull bottom of the example ship the plating will be determined by the permanent set criteria.

TABLE 5-5

Fatigue Damage--Hull Plating at Station 6 (45-kn design)

7075-T6 Plating t/b = 0.025 (β = 6°)

Design Pressure P_D	P_P (P_D/K_D)	Occurrence Cumulative (Fig. 4-20)	n/Year	Cycles to Failure, N (Fig. 3-20)	Partial Damage (n/N)	$\sum$ n/N
		500				
50	143		400	45,000	0.009	0.009
		100				
75	214		160	15,000	0.011	0.020
		40				
100	285		30	5,000	0.006	0.026
		10				
125	357		10		<0.006	<0.032

Relative mean life = $1/\sum n/N$ = 30 years

5.3.3 Stringer Design

The results of the plating design analysis indicate that the bow section may be critical for fatigue. Thus, a typical stringer design will be considered in the Station 2 area for the 100-kn design. Although the design pressure over the stringer will actually be less than for the plating, at β = 30° the difference is not large, and for this example the same design pressure will be used as for the plating, 57 psi. The stringer spacing is assumed to be 12 in., corresponding to 0.156 in plating of 5456-H111.

The tentative stringer section can be determined in Fig. 5-15 for a selected span between floor frames or bulkheads. The design chart (Fig. 5-15) is constructed for a wide range of pressures, stringer spacing, span, material allowable yield stress and stringer height. It may be used for design where the

stringer and plating are either separate or made integral, but the particular stringer section used is intended to represent typical proportions for integral extruded plating-stringer combinations. For other effective sections the crippling limit might be different, and the curves of Quadrant III would have to be suitably adjusted.

For the example, a 3-ft span between stringer support is assumed. Enter Quadrant I at the given design pressure, 57 psi, proceed across to the stringer spacing, 12 in., and then down to the line for span, L = 3 ft. These combinations determine the moment (for average continuous loading and fixity conditions $M = w L^2/10$). In Quadrant II the moment is combined with the allowable bending stress to determine the required section modulus. Proceed down into Quadrant III to a selected stringer height, across to Quadrant IV to the conversion lines for height and down to the span lines to determine the stringer weight per foot of length and total stringer weight per bay. Because of the rapid change of bending allowable for b/t values > 10 it will usually be found that the stringer of the assumed proportions will have minimum weight close to b/t = 10. In the example case this is a stringer 5 in. high with a nominal thickness of 0.24 in. (Note that the adjustment for reduced bending allowables due to flange crippling is done in Quadrant III rather than II. The geometric section modulus of the stringer is reduced by the ratio of the critical crippling stress to the nominal stringer allowable stress.)

The analysis of the fatigue life of the stringer design is given in Table 5-6. The characteristics of 7075-T6 aluminum alloy design reference structure, Fig. 3-22, will be used, although this may be too conservative for the 5456 alloy construction assumed for the hull bottom. The relatively short life determined in Table 5-6 is an indication that fatigue may be the most significant criterion for the bow section stringers as well as for the plating. However, it must be noted that the general fatigue life chart, Fig. 3-22, applies to composite riveted structures with the normal manufacturing tolerances and thus includes large margins as compared to the plating fatigue design charts. Thus, a substantial improvement in the estimated mean life of the stringers might result when fatigue design data for a typical hydrofoil ship with welded and/or extruded integral structure become available.

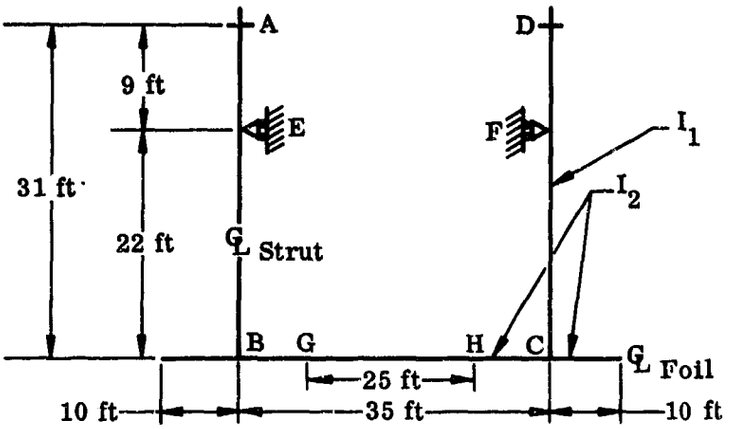

Specific Foil and Strut Configuration

TABLE 5-6

Fatigue Damage--Stringers at Station 2 (100-kn design)

5456-H3111 Integral Plating and Stringer (design pressure 57 psi, σ = 25,000 psi)

R = 0 (u = ultimate tensile strength = 46,000 psi)

Design Pressure P_D	n/Year (Table 5-4)	Stress, σ $\frac{(25{,}000\ P_D)}{57}$	a/2u	Cycles to Failure, N (Fig. 3-22)	Partial Damage n/N	Σn/N
10	14,000	4,400	0.048		0	0
20	3,800	8,800	0.096	80,000	0.048	0.048
30	1,600	13,200	0.144	25,000	0.064	0.112
40	460	17,600	0.191	6,000	0.077	0.189
50	115	22,000	0.24	2,600	0.045	0.234
55	25	24,000	0.26	1,800	0.014	0.248

Relative mean life $= \frac{1}{\sum n/N} = 4$ years

5.4 FOIL AND STRUTS

5.4.1 Bending Moments in Typical Foil-Strut Configurations

A series of two-legged rectangular bents that simulate a general foil and strut configuration have been investigated for several types of loadings and end fixity. In view of the large number of variables entering into the general expressions, it is apparent that a direct comparison and evaluation of the various configurations could not be readily made. For this reason, an appraisal of the study vehicle was made for the specific foil and strut configuration shown below.

TABLE 5-7

Bending Moment Summary Specific Configurations

Moment / w	$n = I_2/I_1$	1	2	3	4	5	6	7	8
		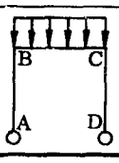	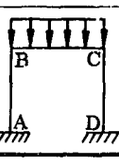	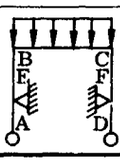	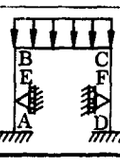	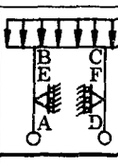	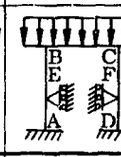	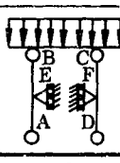	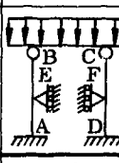
M_A, M_D	0.75	0	38	0	16	0	18	0	0
	1.00	0	35	0	15	0	7	0	0
	1.25	0	33	0	14	0	7	0	0
M_E, M_F	0.75	21	16	29	62	15	32	0	0
	1.00	19	15	27	58	14	30	0	0
	1.25	17	14	25	55	13	28	0	0
M_{BA}, M_{CD}	0.75	71	77	81	82	41	42	0	0
	1.00	64	71	76	76	39	40	0	0
	1.25	59	66	72	72	37	37	0	0
M_{BC}, M_{CB}	0.75	71	77	81	82	90	57	50	50
	1.00	64	71	76	76	88	54	50	50
	1.25	59	66	72	72	86	52	50	50
$M_{L/2}$	0.75	82	77	73	72	62	62	103	103
	1.00	89	83	77	77	64	64	103	103
	1.25	94	88	82	81	67	67	103	103

Moment / w	$n = I_2/I_1$	9	10	1	2	3 (5)	4 (6)	7	8
		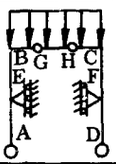	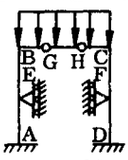	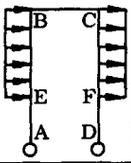	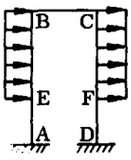	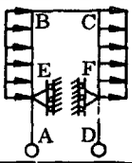	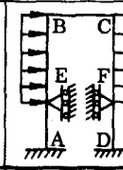	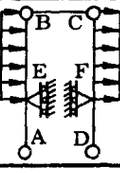	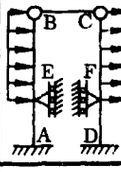
M_A, M_D	0.75	0	14	0	553	0	85	0	77
	1.00	0	15	0	560	0	83	0	77
	1.25	0	15	0	563	0	80	0	77
M_E, M_F	0.75	28	29	198	224	191	171	242	286
	1.00	28	29	198	238	183	165	242	286
	1.25	28	29	198	246	175	161	242	286
M_{BA}, M_{CD}	0.75	77	77	440	112	51	72	0	0
	1.00	77	77	440	120	58	78	0	0
	1.25	77	77	440	125	62	81	0	0
M_{BC}, M_{CB}	0.75	77	77	440	112	51	72	0	0
	1.00	77	77	440	120	58	78	0	0
	1.25	77	77	440	125	62	81	0	0
$M_{L/2}$	0.75	77	77	0	0	0	0	0	0
	1.00	77	77	0	0	0	0	0	0
	1.25	77	77	0	0	0	0	0	0

Bending moments for selected points in the specific configuration are calculated in terms of the loading for several foil to strut stiffness ratios. The effect of end fixity at points A and D is included.

The bending moments for all types of bents studied are summarized in Table 5-7 and apply only to the specific configuration. The following conclusions are drawn from Table 5-7.

(1) Under side or asymmetrical loading, the bending moment at the midspan of the foil is zero.

(2) The maximum bending moments on the foil occur in the vertical loading conditions.

(3) The maximum bending moments on the strut occur in the asymmetrical loading conditions.

(4) For vertical loadings on the foil only, the optimum configuration, depending on the degree of fixity at points A and D, is configuration 5 or 6.

(5) For side or asymmetrical loading on the struts, the optimum configurations, depending on the degree of fixity at points A and D, are 3, 4, 5 and 6.

(6) The optimum overall foil and strut specific configuration is 5 or 6. Note that the optimum configuration selected is based on a comparison of the bending moments only and that deflections have not been considered. Configuration 6 would have the least deflection.

5.4.2 Foil Section Properties

Section moduli were calculated by an automatic machine program for a series of symmetrical and cambered NACA airfoils as a function of foil shell thickness with varying chord lengths. On the basis of these section moduli, design charts for determining the allowable bending moment for various airfoil sections, with chord length, shell thickness and material as variables, are established and presented in Figs. 3-15 and 5-16.

The allowable bending buckling stress of Fig. 3-15 is determined as follows:

(1) The limiting buckling stress for low values of b/t is assumed equal to the yield stress of the material.

(2) For large values of b/t, the bending buckling stress is determined from the general buckling equation for flat rectangular plates:

$$\sigma_{cr} = KE\left(\frac{t}{b}\right)^2$$

where

σ_{cr} = initial elastic buckling stress

K = buckling coefficient for flat plates in compression with all sides simply supported, $K = 3.62 \times 0.75^{*} = 2.72$

E = modulus of elasticity of the material

t = plate or shell thickness

b = unsupported plate width.

*Design manual for high-strength steels, p. 41, USS.

(3) For intermediate values of b/t, a straight line variation between steps (1) and (2) is used along with the recommended intercept values of the Alcoa Structural Handbook and that of the United States Steel Design Manual for high strength steels.

The use of these figures is explained as follows:

(1) Assume an airfoil section, chord length, shell thickness, material and unsupported panel width.

(2) Enter Fig. 3-15 with a calculated value of b/t and proceed vertically to the material selected. The allowable bending buckling stress is read to the left.

(3) Enter Fig. 5-16 with the assumed chord length and proceed vertically upward to the airfoil section, then horizontally to the left to the assumed shell thickness. Proceed vertically downward to the bending stress established in step (2) and then horizontally to the right. Read the allowable bending moment.

An example problem illustrating the use of these figures is as follows.

Determine the allowable bending moment for an NACA 16-206 airfoil section that has a 10-foot chord, 0.5-inch shell thickness, 25% chord movable surface, shear webs located at 25%, 50% and 75% of full chord,and is fabricated from T-1 steel material.

(1) Calculate, $b/t = \frac{0.25(10)12}{0.5} = 60.$

(2) Enter Fig. 3-15 with a b/t = 60 and proceed vertically upward to T-1 steel material, then horizontally to the left and read $\sigma_{cr} = 22,000$ psi

(3) Enter Fig. 5-16 with a chord length of 10 feet and proceed vertically upward to the NACA 16-206 curve, then horizontally to the left to the shell thickness of 0.5 inch. Proceed vertically downward to a stress of 22,000 psi and horizontally to the right. Read the allowable bending moment of 35,000 ft-lb.

From Fig. 3-15, the following observations are noted:

(1) The shell buckling stress is very sensitive to small changes in b/t values.

(2) At b/t values greater than 60, no advantage can be realized from the use of high strength steels.

(3) For b/t values between 20 and 60, high strength steels are the more efficient structural materials and for b/t values less than 20, a titanium alloy is more efficient than the high strength steels.

(4) Multiple-span type of construction is required to obtain a high shell buckling stress, i.e., low values of b/t.

We conclude that the foil and strut structure shall basically consist of multiple-spar type of construction that is fabricated by fusion welding of either USS T-1 type high strength steel or 13V-11Cr-3Al titanium material.

5.5 DECK STRUCTURE

5.5.1 Summary

The occurrences of high design pressures on the decking are relatively low and confined to the bow areas. Thus, fatigue life will not be a significant problem, and much of the deck may be designed by stiffness criteria rather than by the water loadings.

An arbitrary loading of 975 psf was used to examine the relative merits of various decking structural systems including both the local decking and the deck supporting structure. Most of the decking is determined by the stiffness criteria, while the deck framing support is determined by the assumed loading.

Optimum frame spacing for the deck support lies between 3 and 5 ft in terms of total weight of deck plus framing, and the variation between 3 and 5 is rather small. A value analysis example for a number of the possible deck structures including both weight and cost factors indicates that the integral plating is the best choice for decking.

5.5.2 Decking Design

Two basic criteria are given for the decking structural design. The requirement for stiffness from the psychological point of view is given in Section 4.4.2. The distribution of pressure loads from waves on the deck is given in Section 4.2.5.

Since the total occurrences of wave loadings on the deck are below 1000, fatigue damage to the structure will not be significant.

For convenience in comparing the various examples, one value of the deck pressure loading (975 psf) will be used throughout this section.

The actual bending moment stresses in the decking are a result of the beam action of the deck loading upon the panels acting as continuous beams over many supports. Although the deck loading is not actually a constant loading and can thereby produce various combinations of loaded and unloaded bays, the maximum beam bending moment will not often be greater than a value somewhat less than that of a simply loaded beam. For this study the maximum bending moment is taken equal to $WL^2/10$, where

W = the running load

L = the span (transverse frame spacing).

This maximum value of moment is assumed to be plus or minus and applies either over the beam supports or anywhere within the beam span. In this study

of decking design, the overall decking tension or compression stresses due to overall hogging or sagging conditions on the vehicle have been neglected. In performing an actual detail design, overall stresses greater than 2000 psi (±) would be considered.

The allowable bending stress for the decking is derived from the data presented in Fig. 3-13. In this figure, the local flange crippling stress is presented as a function of the b/t of the individual flanges. The method of determining the composite crippling allowable stress, σ_{max}, is indicated.

5.5.2.1 Plate-Stringer Design

I-section type stringers have been selected because they are generally the lightest and most stable open-type sections for such applications. The upper flange of the I-section provides symmetrical support to the plating while the lower flange has good lateral stiffness and provides ample space for attaching the stringer to support members such as transverse or longitudinal frames. The actual size and dimensions of the I-section stringers and the integrally stiffened plating used in this design are influenced by structural requirements and certain manufacturing and assembly methods:

(1) The present minimum thickness recommended by the aluminum industry for integrally stiffened extruded plating is 0.080 in.

(2) The installation methods for attaching the lower flange of any I-section stiffener to a transverse support frame by mechanical attachments require a tool clearance of at least 1-3/4 in.

(3) Structural requirements demand certain minimum edge distances on members through which mechanical attachments are made. In this design, 1/4-in. diameter fasteners are assumed for attaching the stringers to the support structure. The proper flange width to satisfy this requirement is 1 in.

Thus, a stringer of minimum dimensions would be as follows:

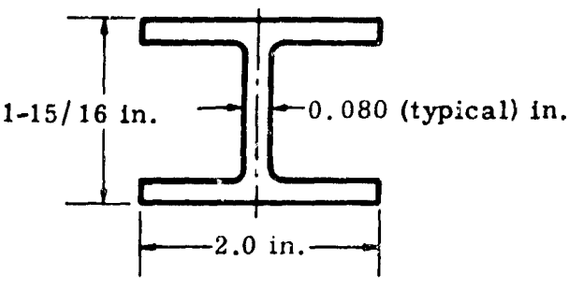

The selection of the optimum plate-stringer design for deck structure can be accomplished only by considering the many variable factors associated with both the deck structure itself and the support or framing structure. Since all factors have not yet been evaluated, this phase of the study has been limited to the production of data which can be used to show how deck weight varies with various combinations of plating and stringers. Figure 5-17 has been constructed and is described below.

5.5.2.1.1 Explanation of Fig. 5-17

1. In Quadrant A both strength and stiffness requirements are shown. The strength lines (dotted curves) were calculated, assuming the stringers at 6-inch spacing and the material to be working at 19,000 psi allowable bending stress under a deck loading of 975 psf. Values of the moment of inertia required are shown for various stringer depths and frame spacings. The formula $\frac{wL^2}{10F_{cy}}$ was used,

   where

   w = running load, lb/in.

   L = frame spacing, in.

   F_{cy} = compression yield--allowable bending stress.

2. The stiffness criterion was used to calculate the moments of inertia required for stringer stiffness. The band of acceptable stiffness is shown along with the recommended value of $EI/L^3 = 60$.

3. Also in Quadrant A is a set of radiating lines to be used for determining the moments of inertia required for other combinations of loadings, stringer spacing and allowable stress.

4. In Quadrant B, the curves reflect the relationship between the moment of inertia and flange thickness for various depths of I-section with the central web thickness held constant at 0.080 in. A correction factor may need to be applied to account for the reduction in flange strength below the compression yield strength due to local crippling where the flange thicknesses are small.

5. Curves in Quadrant C show the relationship between stringer depth, flange thickness and stringer weight per foot.

6. The weights of various plating and stringer combinations can be read in Quadrant D for both integrally stiffened and plate-stringer types of design. The weights are given in terms of deck unit weight. The stringer spacing is related to the plating thickness by the stiffness requirements, Fig. 4-34.

5.5.2.1.2 An Example on the Use of Fig. 5-17

To determine an optimum deck plating design for 6061-T6 material for a frame spacing of 55 in. and a uniform loading of 2100 psf using a stringer depth of 2-1/2 in., proceed as follows:

Step 1

Enter Quadrant A at a frame spacing of 55 in. and proceed vertically to the recommended stiffness factor curve of $EI/L^3 = 60$. To the left is indicated the moment of inertia required for stiffness, I = 1.

Step 2

Re-enter Quadrant A at the 55-in. frame spacing and proceed vertically to the strength curve for a 2-1/2-in. deep stringer.

Step 3

Proceed horizontally to the basic load line and then vertically to the load line corresponding to the material, loading and stringer spacing, b; $A = \frac{2100}{35,000} \times b$. For b = 6.3 in., A = 0.38, and the plating gage is 0.80 corresponding to the stiffness criteria of Fig. 4-34. The strength and stiffness requirements for inertia are the same. Other stringer spacing and plating combinations will require different inertia (e.g., b = 8 in., t = 0.1; A = 0.48 and I = 1.25). To the left is then indicated the moment of inertia required for strength.

Step 4

Using the higher of the values of required moment of inertia determined in Step 1 and Step 3, proceed horizontally into Quadrant B and then to Quadrant C and Quadrant D, determining the weight per square foot of the preferred deck plating configuration.

5.5.2.2 Sandwich Construction Design

Sandwich-type structure is composed of two faces of high density material which can support tension, compression, and bending loads, and a core of low density material which can support the shear load. These parts are bonded together under controlled heat and pressure to form the sandwich panel.

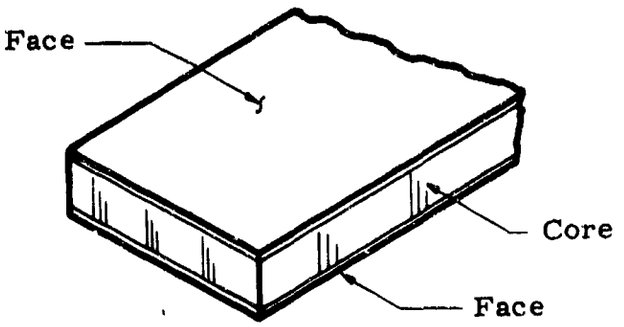

The materials selected for this design are divided into face materials and core materials.

The face materials are aluminum alloys of various strengths.

	F_{cy} (psi)
7075-T6 Alclad	62,000
2024-T4 Alclad	37,000
6061-T6	35,000

The cores which are of different types of materials and densities are shown in Table 5-8.

TABLE 5-8

Material	Density (lb/ft^3)	Ultimate Shear Strength (psi)
Balsa wood--end grain	10	150
Lockfoam	10	320
Lockfoam	12	420

TABLE 5-8 (continued)

	Cell Size (in.)	Foil Thickness (in.)	Density (lb/ft^3)	Ultimate Shear Strength (psi)
5052 aluminum foil	3/16	0.001	3.1	197
	3/16	0.0015	4.4	322
	3/16	0.002	5.7	431
	1/4	0.003	6.0	471
	1/4	0.004	7.9	620

The allowable tension and compression strengths of the faces are equivalent to the tension yield and compression yield strengths of the face material because in sandwich construction the face plates are completely stabilized by the sandwich core. To determine a practical method of analyzing sandwich-type decking, numerous combinations of panel size and end conditions were investigated. It was determined that when the length-to-width ratio of the panel was greater than 3, beam theory analysis would suffice for structural design purposes. It was assumed that both the longitudinal and the transverse splices would be so designed as to make the panels effectively continuous-type beams.

The maximum shear in the panel is equal to 1/2 wL and will occur at the transverse frames. The maximum bending moment is assumed equal to $wL^2/10$ where

w = running load, lb/inch

L = frame spacing, in.

From a history of tests and field service reports on sandwich panel applications in military and commercial aircraft, the following dimensions are recommended as practical minimums for deck-type structure:

(1) Panel thickness = 1 in.

(2) Face thickness = 0.060 in.

(3) Foil thickness = 0.001 in.

Considering the foregoing limitations and assumptions with regard to materials, allowables, and methods of analysis, the charts of Figs. 5-18 and 5-19 have been prepared for the selection of sandwich-type decking for variations in transverse frame spacing, face gage, core and cell size and deck loading. A detailed description of these charts follows.

5.5.2.2.1 Explanation of Fig. 5-18

Figure 5-18 is used to determine the panel thickness needed to meet bending stiffness and bending strength requirements assuming a particular combination of face thickness, frame spacing, deck loading and ultimate allowable bending stress.

1. In Quadrant A_1, the stiffness requirements are shown. The stiffness lines were calculated using the recommended stiffness value, $EI/L^3 = 60$. The value of $EI/L^3 = 60$ was developed for typical plate-stringer type of deck design. For sandwich-type decking, it has been assumed that the moment of inertia of a strip of decking 12 in. in width is the approximate equivalent of the plate-stringer combination used to establish the value if $EI/L^3 = 60$. Hence, the value of I for the sandwich panel is

$$I = (2\ t_f)\left(\frac{t_d}{2}\right)^2 (x)$$

$$= 6\ t_f\ t_d^2 \text{ for } (x) = 12 \text{ in.}$$

where

t_f = face thickness

and

t_d = centroidal height between faces.

In addition to the values of panel thickness, the weight in psf is shown for the assumed face thicknesses.

2. In Quadrant A_2, the strength requirements are shown. The strength lines were calculated using the compression yield strength of 6061-T6 aluminum alloy (35,000 psi) as the allowable stress and a deck loading of 975 psf. Values of panel thickness required are shown for various face thicknesses and frame spacings. The formula used was

$$t_d = \frac{wL^2}{10\ t_f\ F_{cy}}$$

where

w = running load, lb/in.

L = frame spacing, in.

F_{cy} = compression yield, psi

t_f = face thickness of the panel, in.

t_d = centroidal height between faces, in.

3. Quadrant B contains a set of radiating lines which may be used to determine panel thicknesses for loadings other than 975 psf using an allowable bending stress of 35,000 psi.

4. Quadrant C presents a set of radiating lines which may be used to determine panel thicknesses for allowable bending stresses other than 35,000 psi.

5.5.2.2.2 Explanation of Fig. 5-19

Figure 5-21 is used to determine the core thickness required to support the beam shear in the core for various types and densities of core materials. The weight in psf of deck area is also given for the type and density of core thus determined.

1. Section A contains a set of radiating lines which may be used to determine the maximum beam shear for various deck loadings using the formula,

$$S_{max} = \frac{1}{2} wL$$

where

S_{max} = maximum shear (lb)

w = running load (lb/in.)

L = frame spacing (in.)

The shear thus determined is termed uncorrected because in applying it to the core material, a reduction is necessary to account for the shear carried by the faces. This is true only in the case of aluminum foil-type core.

The shear strength of aluminum foil core is influenced by both the core and face thicknesses. There is no simple method available for computing core shear strength with these two variable factors considered. Therefore, the factor of K_1 (curve A) and K_2 (curve B) was determined through a series of tests, and the formula

$$S_c = \frac{S_u}{K_1 K_2}$$

was derived where

S_u = uncorrected shear (Fig. 5-21)

S_c = corrected shear

K_1 = correction factor for the influence of face thickness on core shear strength

K_2 = correction factor for the influence of core thickness on core shear strength.

The shear value thus determined for aluminum foil is then used in Section B.

2. Section B presents a set of radiating lines of different densities and materials from which the core thickness can be determined using corrected shear values. The ultimate allowable shear stress used for determining these lines is shown in Table 5-8.

3. Section C presents core weights in psf of deck area for various types of core material.

5.5.2.2.3 Example of the Use of Figs. 5-18 and 5-19

It is desired to determine, for a loading of 975 psf, the panel thickness and weight of a sandwich-type deck using a frame spacing of 5 ft. Use the recommended minimum face thickness of 0.060 in. and 6061-T6 material.

Step 1

Enter Quadrant A_1 of Fig. 5-18 at a frame spacing of 5 ft and proceed vertically to a face thickness of 0.060 in. To the left is indicated a panel thickness of 1.83 in., which is that required for proper stiffness.

Step 2

Enter Quadrant A_2 at a frame spacing of 5 ft and proceed vertically to a face thickness of 0.060 in. To the left is indicated a panel thickness of 1.22 in., which is that required for strength.

Step 3

Enter Section A of Fig. 5-19 at a frame spacing of 5 ft and proceed vertically to the deck loading of 975 psf. To the left is the uncorrected shear, 208 lb/in.

Step 4

Enter curve B of Fig. 5-19 at a core thickness of 1.71 in., which is determined by subtracting twice the face thickness from the larger of the two panel thicknesses obtained in Steps 1 and 2. The value of the correction factor, K_2, is read as 0.73.

Step 5

Enter curve A at a face thickness of 0.060 in. To the left is read 1.16, the value of the correction factor, K_1.

Step 6

Determine the corrected shear value using the equation $S_c = S_u/K_1 K_2$. The correct shear is

$$\frac{208}{(1.16)(0.73)} = 245 \text{ lb/in.}$$

Step 7

Enter Section B of Fig. 5-19 at the corrected shear of 245 lb/in. and proceed vertically to 3.1 lb/ft^3 density line. To the left is indicated the core thickness (1.25 in.) required for shear strength.

Step 8

Compare the core thickness values determined in Step 4 and Step 7. Enter Section C with the larger value, 1.71, and proceed horizontally to the 3.1 lb/ft^3 column. The indicated weight in psf of deck area for the core alone is 0.443.

Step 9

Add the weight of the core, 0.443 psf, to the weight of the faces, 1.73 psf (see upper end of curves in Quadrants A_1 or A_2 of Fig. 5-18) to determine the basic weight of the sandwich decking, 2.173 psf.

NOTE:

To the basic weight of the sandwich panel must be added the weight of edge members and filler block for attachment of the panels to the support structure and for attaching fittings, equipment, etc. This additional weight will vary from 20% to 40% of the basic panel weight. Thus, the total weight per square foot of the sandwich decking is 2.173 x 1.30 = 2.82 psf.

5.5.2.3 Plate Corrugation Design

The plate corrugation design has been selected for study because of the ease of manufacture, assembly and installation. Also, a wide variety of corrugation can be readily formed, by braking, from standard sheet materials. The actual size and dimensions of the trapezoidal corrugation used are influenced by structural requirements and certain manufacturing and assembly methods.

To provide the maximum panel stiffness under loads, the trapezoidal corrugation is required to have a minimum width of flat and a minimum taper to the sides.

1. The proper width of flat depends upon the clearance required for the head of the attaching mechanical fasteners. In this design 3/16 in. diameter fasteners are assumed for attaching the corrugation to the support structure. Thus, 13/32 in. is the minimum flat to satisfy this requirement.

2. The minimum slope of the side is 15° and is required by manufacturing for forming.

The installation of the corrugated panels to the support structure by a blind mechanical fastener requires a minimum clearance of one inch between the corrugation valley and plating.

The material selected for this design is a medium strength aluminum alloy, 6061-T6 bare sheet, which has excellent forming and good mechanical properties.

In the plate and corrugation type of construction, the plate is stabilized from buckling by the corrugation. The allowable plate buckling stress σ_{max}, determined from the data presented in Fig. 3-13, is presented as a function of the b/t of the plating (both edges supported)

where

b = the pitch of the corrugation (in.)

t = the plate thickness (in.)

The allowable buckling stress for the valleys of the corrugation is equal to the compression yield, F_{cy}, of the material because, for the thicknesses being studied, the b/t values of the corrugation flats are less than 28

where

b = the width of the flat (in.)

t = the thickness of the corrugation (in.)

The b/t value of 28 is the maximum that a flat plate in compression, with the unloaded edges supported, can have and work to compression yield F_{cy}. Therefore, the allowable bending stress, F_b, for the flat plate and corrugation is assumed equal to σ_{max}. The beam theory analysis is used for structural design purposes since, as in the case of sandwich panels, the length-to-width ratio of the corrugated panels is greater than three. It is assumed that both the longitudinal and transverse splices would be so designed as to make the panels effectively continuous beams. Therefore, for this design, as well as for the designs previously studied, the maximum bending moment is assumed equal to $w L^2/10$

where

w = the running load (lb/in.)

L = frame spacing (in.)

From a study of tests and field service reports on various types of deck construction on military and commercial aircraft, it is recommended that a practical minimum plating thickness for plate and corrugation-type deck structure is 0.063 in.

Considering the foregoing limitations and assumptions, with regard to materials, allowables and methods of analysis, the charts of Fig. 5-20 have been prepared for the selection of plate and corrugation-type decking for variations in transverse frame spacing, plate and corrugation thickness and deck loading. A detailed description of these charts follows.

5.5.2.3.1 Explanation of Fig. 5-20

1. In Quadrant A_1, the stiffness requirements are shown. The stiffness lines were calculated using the recommended stiffness values, $EI/L^3 = 60$,

   E = modulus of elasticity for aluminum (psi)

   I = moment of inertia ($in.^4$)

   L = frame spacing (in.)

   The value of $EI/L^3 = 60$ was developed for typical plate-stringer type of deck design. For plate and corrugation decking, it has been assumed that the moment of inertia of a strip of decking 12 inches in width is the approximate equivalent of the plate-stringer combination used to establish the value of $EI/L^3 = 60$.

2. In Quadrant A_2, the maximum bending moments are shown. The deck loading lines were calculated using the formula $M = wL^2/10$

where

M = the maximum bending moment per inch of width (in.-lb/in.)

w = the running load (lb/in.)

L = frame spacing (in.)

3. In Quadrant B, the strength requirements are shown. The strength lines were calculated for the minimum allowable bending moment the section will carry, in either direction, using the allowable bending stress, F_b, for 6061-T6 aluminum alloy, of either the plate or the corrugation valley with its respective section modulus. Values of corrugation depth required are shown for various skin and corrugation thicknesses and bending moments. The formula $M = F_b I/c$ was used for calculating the allowable bending moment

where

M = the minimum allowable bending moment per inch of width (in.-lb/in.)

F_b = the allowable bending stress (psi)

I = the moment of inertia per inch of width ($in.^4$ /in.)

c = the distance from the outer fibers to the neutral axis (in.)

4. Curves in Quadrant C show the relationship between corrugation depth, plate and corrugation thicknesses and deck weight in pounds per square foot.

5.5.2.3.2 Example of the Use of Fig. 5-20

It is desired to determine, for an ultimate deck loading of 975 psf, the corrugation depth and weight of the decking, using a frame spacing of 5 ft and the recommended minimum plate and corrugation thickness of 0.063 in. and 6061-T6 material.

Step 1

Enter Quadrant A_1 of Fig. 5-20 at a frame spacing of 5 ft and proceed vertically to the thickness of 0.063 in. To the left is indicated the depth of corrugation, 1.98 in., which is required for proper stiffness.

Step 2

Enter Quadrant A_2 at a frame spacing of 5 ft and proceed vertically to the deck loading of 975 psf. To the left is indicated the maximum bending moment per inch.

Step 3

Proceed horizontally into Quadrant B along the required bending moment line to the plate and corrugation thickness of 0.063 in. Vertically downward is indicated the depth of corrugation, 1.82 in., which is required for proper strength.

Step 4

Compare the corrugation depth values determined in Step 1 and Step 3. Enter Quadrant C with the larger value, 1.98 in., and proceed vertically downward to the plate and corrugation thickness of 0.063 in. To the right is indicated the weight, 2.82 psf, of deck area.

5.5.3 Main Deck Transverse Frames

5.5.3.1 Number of Supports

The average beam of the hull used in this study is approximately 30 ft. If transverse beams of this length were used to support the deck loading, they would be quite deep and heavy. To provide maximum clearance between decks and to reduce the overall frame weight, it is therefore necessary to determine an optimum number of intermediate supports.

The maximum bending moment of the transverse frame treated as a simple beam uniformly loaded over its entire unit span, S, is used as a basis of comparison. Maximum frame bending moments were then calculated for a uniformly loaded continuous beam. Both pinned and fixed ends were considered and the number of equally spaced rigid intermediate supports was varied. The continuous beam bending moments thus calculated were then ratioed to that of the simple beam.

The results, presented in Fig. 5-21, show that the frame bending moments decrease rapidly as the number of supports is increased to two and that they then level off with the end fixity effects becoming negligible. Hence, from Fig. 5-21, it can be concluded that two intermediate supports should be used with the transverse frames to provide for minimum frame weight and depth and that the frame end fixity has a negligible effect on the frame bending moments.

Optimum frame weight and spacing are dependent upon many considerations involving materials, loadings, strength and deflection criteria, and methods of stabilization.

The selection of the transverse frame material is based on a comparison of the mechanical strength properties of extruded aluminum alloys in the welded and nonwelded conditions. Of the various aluminum alloys available, 5456-0, 6061-T6, and 7075-T6 are selected for study for the following reasons:

(1) 5456-0 possesses the highest tensile yield strength of the easily weldable aluminum alloys.

(2) 6061-T6 is a heat-treated medium strength aluminum alloy that can be used in the welded or nonwelded condition.

(3) 7075-T6 is a high strength aluminum alloy that is recommended for nonwelded applications. This material has low corrosion resistance properties.

Using the conclusions derived from Fig. 5-21, a constant section transverse frame is then treated as a continuous beam of three spans (of equal length S/3 = L) supported by two rigid intermediate supports (all supports on the same level) considering the frame ends as both fixed- and pin-ended, and subjected to a uniformly distributed loading acting in each bay or any combination of bays. The maximum bending moment for the simply supported continuous beam occurs at the supports when one outer bay and the center bay are loaded simultaneously; $M = 0.117\ wL^2$ (limit). For the fixed-ended continuous beam, the maximum bending moment occurs at the frame ends when both outer bays are loaded simultaneously; $M = 0.112\ wL^2$ (limit). Note that the maximum bending moment is practically identical for the fixed- and pin-ended conditions.

The maximum bending deflection for the simply supported continuous beam is $0.0099\ wL^4/EI$ and occurs in the outer bay when both outer bays are loaded simultaneously. The maximum bending deflection for the continuous beam with fixed ends is $0.0061\ wL^4/EI$ and occurs in the center bay when that bay only is uniformly loaded. Shearing deflections have been neglected because for a uniformly loaded I-section frame with a span to depth ratio of 10, the shearing deflection is only 6% of the bending deflection.

In determining the transverse frame weight as a function of frame spacing, the following design criteria and data are used:

(1) With a main deck design pressure of 975 psf, the permissible frame deflection is set at 0.50 in. This deflection is estimated to provide sufficient inherent overall transverse hull stiffness and is also considered a maximum to which secondary structure, such as plumbing and other lines attached to the frame, may be deflected without damage.

(2) The frame structure shall withstand this deflection without buckling.

(3) The allowable bending stresses used are as follows:

5456-0, F_b = 19,000 psi--welded or nonwelded

6061-T6, F_b = 35,000 psi--nonwelded

7075-T6, F_b = 60,000 psi--nonwelded.

(4) The plating material of the deck is neglected in the deflection calculations.

(5) The deck camber is neglected in the deflection calculations.

(6) The maximum bending moments are $0.117\ wbL^2$.

where

L = 10 ft

w = 975 psf

b = transverse frame spacing (in.)

(7) The frames are aluminum I-sections or channel sections of constant cross section with $E = 10^7$ psi.

The results of this study are presented in graphical form in Figs. 5-22 and 5-23. Two methods of frame stabilization are considered: one provides tension straps at proper intervals to reduce the frame span and the other selects sections that are of sufficient inherent stiffness to be stable without straps.

The plots shown in Figs. 5-22 and 5-23 result from the use of American Standard sections. Optimizing each section would result in smoother plots. Numbers on the plots represent frame weight per square foot of deck area.

A summary of the calculations performed in comparing the two methods of frame stabilization is presented in Table 5-9. In this table, it is noted that the frame bending moments are critical for 5456-0 material and that deflections are critical for 6061-T6 and 7075-T6. Also, it should be noted that the resulting average stress levels for the inherently stable system are lower than those for the tension strap system. This indicates that heavier frame sections are required for the inherently stable system.

Calculations performed for the inherently stable system are in accordance with the procedures set forth in the Alcoa Structural Handbook.

TABLE 5-9

Frame Stabilization Comparison

Type of Stabilization System	Tension Strap			Inherently Stable		
I-Section Frame***						
Materials	5456-0	6061-T6	7075-T6	5456-0	6061-T6	7075-T6
Allowable bending stress	19,000	35,000	60,000	19,000	35,000	60,000
Stresses resulting from bending moments or deflection requirements	18,000*	18,000**	18,000**	12,000*	17,000**	17,000**
Channel Frame***						
Allowable bending stress	19,000	35,000	60,000	19,000	35,000	60,000
Stresses resulting from bending moments or deflection requirements	16,000*	20,000**	20,000**	12,000*	16,500**	16,500**

NOTES:

*Critical for bending moments
**Critical for deflection requirements
***American Standard sections listed in the Alcoa Structural Handbook
All values listed are psi.

The following conclusions are derived from Figs. 5-22 and 5-23 and Table 5-9.

(1) The frame tension strap stability system is generally lighter.

(2) Frame weight per square foot of deck area decreases for both I-sections and channel sections as frame spacing is increased.

(3) The established frame deflection criterion is the determining factor for the frame design using 6061-T6 and 7075-T6 materials. For lower strength materials such as 5456-0, the deck loading criteria is critical.

Not indicated in Figs. 5-22 and 5-23 or Summary Table 5-9 is the fact that frame depths increase with increased frame spacing, and that channel frames require slightly larger depths than I-section frames.

5.5.3.2 Frame Selection Diagrams

Diagrams for selecting transverse framing of 5456, 6061, and 7075 aluminum alloys are developed using strength, deflection and shear buckling criteria. Optimum frame spacing is selected on the basis of weight comparisons.

It was concluded previously that the transverse frames should have two intermediate supports. Continuing with this arrangement, the maximum beam bending moments, shears and deflections were calculated for the continuous beam-type frame having various combinations of bay loadings. Both simply supported and fixed end beams were considered with intermediate supports assumed rigid. The results are tabulated in Table 5-10 below.

TABLE 5-10

Beam Bending Moment, Shear and Deflection Coefficients and Formulas

	3 Single Bays-- Simple Beam	Continuous Beam-- 3 Equal Bays	
	Simply Supported	Simply Supported	Fixed
K_1 --moment	0.125	0.117	0.112
K_2 --deflection	0.0132	0.010	0.006
K_3 --shear	0.050	0.617	0.567

Maximum bending moment = $K_1 \, wL^2$

Maximum bending deflection = $K_2 \, wL^4/EI$

Maximum beam shear = $K_3 \, wL$

where

w = beam loading

L = beam bay length

E = modulus of elasticity

I = moment of inertia about bending axis

K_1, K_2, K_3 are constants of Table 5-10.

Beam bending moments due to a unit deflection of a support, for a three equal bay continuous beam, are shown in Table 5-11, considering both simply supported and fixed ends.

TABLE 5-11

Beam Bending Moments Due to a Unit Support Deflection
Continuous Beam with Three Equal Bays

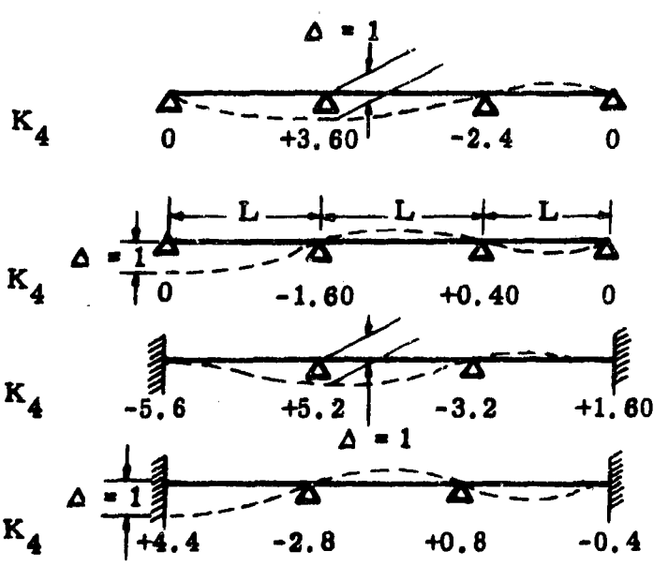

Positive moment is tension on bottom fibers

Bending moment = $K_4 EI\Delta/L^2$

where

K_4 is the constant in Table 5-11.

For continuous beam-type frames the maximum bending moment due to deck loading and support deflection is calculated as follows:

M_F = maximum frame bending moment

M_L = bending moment due to the deck loading

M_D = bending moment due to deflected support

w = beam loading

L = beam bay length

E = modulus of elasticity

I = moment of inertia about bending axis

b = frame spacing

p = deck load per unit area

Δ = support deflection

Subscripts:

F = frame

B = longitudinal beam.

The maximum bending moment occurs at the supports and is expressed as:

$$M_F = M_L \pm M_D$$

where

$$M_L = K_1 w_F L_F^2, \quad M_D = K_4 E_F I_F \Delta_B / L_F^2$$

$$M = K_1 w_F L_F^2 \pm K_4 E_F I_F \Delta_B / L_F^2.$$

Assuming that the longitudinal beam is uniformly loaded by the frames, and no interaction exists between the frame and longitudinal beam,

$$\Delta_B = K_2 w_B L_B^4 / E_B I_B.$$

Substituting

$$M_F = K_1 w_F L_F^2 \pm K_4 K_2 \left(\frac{E_F I_F}{E_B I_B}\right) w_B \left(\frac{L_B^4}{L_F^2}\right)$$

$$w_F = pb, \; w_B = L_F p, \; w_B = \frac{w_F L_F}{b}$$

$$M_F = K_1 w_F L_F^2 \pm K_4 K_2 \left(\frac{E_F I_F}{E_B I_B}\right) \left(\frac{L_B^4}{L_F}\right) \frac{w_F}{b}$$

or

$$M_F = w_F L_F^2 \left[K_1 \pm K_4 K_2 \left(\frac{E_F I_F}{E_B I_B}\right) \left(\frac{L_B}{L_F}\right) \frac{L_B}{b}\right]$$

$$M_F = C w_F L_F^2$$

A diagram for evaluating the parameters of the above equation is shown in Fig. 5-24. The moment coefficient, K_1, may be assumed equal to the average (0.115) of the two values given in Table 5-10 for a simply supported and fixed continuous 3 bay beam. $K_2 K_4$ is assumed for a simply supported continuous beam system as 0.010 x 3.60 and for a fixed continuous beam system as 0.006 x 5.2. As the values of $\frac{E_F I_F}{E_B I_B}$, $\frac{L_B}{L_F}$, and $\frac{L_B}{b}$ are increased the effective moment coefficient, C, is also increased. Thus, as the relative stiffness of the transverse frame is increased with respect to the longitudinal beam, the bending moment in the frame increases. Also, as the beam length of the longitudinal supports increases with respect to the transverse beam's span or the frame spacing, the coefficient is increased. It is also to be seen that, since the value of K_1 for a simple beam is 0.125, the limiting value of C should be 0.125. In other words, when C is determined to be a value greater than 0.125 for a continuous beam concept, it would be advantageous to use individual simple consecutive beams instead of a continuous three-span beam. Since the difference between K_1 as a simple beam and C as a continuous beam is small, it is concluded that individual simple consecutive beams will usually be the lightest construction. For this study, then, simple consecutive beams will be used. However, a value of 0.15 will be conservatively assumed for K_1 in order to take care of some nonuniformity of the loading, i.e., assuming the loading to be somewhat higher than average at the midspan. This value is used in Fig. 5-25.

The maximum frame deflection coefficients, K_2, are listed in Table 5-10 for various combinations of uniform bay loadings. The deflection criterion for this study was tentatively established as 0.5 in. for a 10-ft bay. In more general terms, this can be expressed as 0.0042 L. This value has been revised to 0.005 L for future phases of study to make deflection criterion more compatible with strength criteria.

The frame shear coefficients shown in Table 5-10 are the maximums for various combinations of uniform bay loadings. A value of 0.65 is assumed for this weight study to provide for an anticipated increase in shear loads due to support deflection. Frame webs are assumed to be nonbuckling under the imposed shear loads. The use of lightening holes has not been considered.

Figures 5-25, 5-26 and 5-27 show the variation of the transverse frame weight in pounds for:

(1) Square foot of main deck area.

(2) American Standard I-sections and channel sections.

(3) Newly developed I-sections, using the preceding criteria for strength deflection and shear buckling.

The use of these figures is illustrated by the following example.

It is required to find the weight per square foot of deck area of 6061-T6 American Standard I-section frames spaced at 4 ft and designed to an ultimate deck loading of 975 psf. The frames are 10 ft in span and are assumed to be simply supported.

Enter the upper right-hand quadrant of Fig. 5-25 at a frame spacing of 4 ft and proceed vertically to the 975-psf deck loading line. Proceed horizontally to the left to the 10-ft frame bay length and then vertically downward to read the design bending moment of approximately 60,000 ft-lb. Continue downward to an allowable bending stress of 35,000 psi for the 6061-T6 material. Proceed horizontally to the right to read the required section modulus of 20 in. cubed. Continue to the right and find the closest American Standard I-section for which the section modulus exceeds the required value of 20 in. cubed. As indicated on the figure, this section is a 10-in. deep by 8.76 lb/ft I-section having a section modulus of 24.7 in. cubed. Thus, to meet the strength requirements, a framing weight of 8.76/4 = 2.19 psf of deck area is required.

If, in the example above, the transverse frames were considered as continuous and as having parameters equivalent to those shown in the example in Fig. 5-24, then the maximum frame bending moment would be altered by the ratio of the moment coefficient indicated for this condition to that used in Fig. 5-25. The ratio would be 0.105/0.15 and the new design frame bending moment

would be $\frac{(0.105)(60,000)}{0.15}$ = 42,000 ft-lb. Entering Fig. 5-25 with this value and proceeding downward to an allowable bending stress of 35,000 psi, it is seen that a section modulus of 14.5 in. cubed is required and that an 8-in. deep by 6.4 lb/ft I-section would be required. In this case, a framing weight of 6.4 lb/ft = 1.60 psf of deck area would be needed to meet the strength requirements.

Figures 5-25 and 5-26 are used to check the hypothetical frame for the deflection criteria and shear buckling criteria. The example for the simple support case is illustrated. Thus, the selection of American Standard I-section members to meet the assumed requirements is shown in Table 5-12.

TABLE 5-12

American Standard I-Section Member

	I-Section	psf	Figure
Bending strength	10 in. x 8.7 lb/ft	2.19	5-25
Deflection	10 in. x 8.7 lb/ft	2.19	5-26
Shear buckling	6 in. x 4.3 lb/ft	1.18	5-27

An examination of the American Standard section shapes as utilized for deck support structure has indicated that excessively weighty sections are required where more efficient lighter sections would suffice. A new I-section, proposed as shown, is proportioned to be stable in bending at the yield strengths of 5456-0 and 6061-T6, and to be stable in shear at a stress of 19,800 psi which will suffice for 5456-0, 6061-T6 and 7075-T6 materials. See Fig. 5-25 for the allowable bending stress. In Figs. 5-25, 5-26 and 5-27, the dashed line represents the proposed new I-section properties for the respective design criteria.

The selection of new I-section members to meet the assumed requirements of the previously illustrated example is shown in Table 5-13.

TABLE 5-13

New I-Sections Members

	New I-Section	psf	Figure
Bending strength	14 in. x 6.4 lb/ft	1.6	5-25
Deflection	13 in. x 5.5 lb/ft	1.38	5-25
Shear buckling	9 in. x 2.64 lb/ft	0.66	5-27

Comparing the values of Tables 5-12 and 5-13, it is seen that the newly developed I-section is superior weightwise to the American Standard I-section in a proportion of 1.6 to 2.19, a 27% reduction.

5.5.3.3 Optimum Frame Spacing

The optimum frame spacing based upon the total weight of both decking and transverse framing is determined from Figs. 5-16, 5-17, 5-25, 5-26 and 5-27. The weight, determined as a function of frame spacing, bay lengths, material and type of frame and deck section, is shown in Figs. 5-28 through 5-32, inclusively. From these curves it is evident that, for the design criteria contained herein, the optimum frame spacing is approximately 4 ft, with only slight weight variations between 3 and 5 ft.

The following conclusions, based on the design criteria established herein, are drawn from this study:

(1) For deck structure, the optimum frame spacing is approximately 4 ft, with only a slight weight variation between 3 and 5 ft.

(2) The newly developed I-section is superior weightwise to the American Standard sections.

(3) The lightest practical deck structure consists of integrally stiffened 5456-0 or 6061-T6 decking and 6061-T6, 6066-T6 or 7075-T6 I-section transverse frames of the new design proposed in this study.

5.5.4 Longitudinal Deck Supports

In the main deck transverse frame optimization study, it was concluded that two intermediate supports should be used. To support each transverse frame individually with such supports would seriously interfere with a suitable platform deck arrangement. The addition of two longitudinal support beams will provide structural support for the frames, minimize the number of vertical supports and provide added hull longitudinal bending stiffness.

Since the longitudinal support structure is similar in design and loading to the transverse support structure, the results of the study of the transverse frames can be applied directly. Hence, it can be concluded that two intermediate supports should be used with each longitudinal beam to provide minimum beam weight and depth.

5.5.4.1 Stanchions

Allowable column stress curves are plotted in Fig. 5-33 for standard, round, extruded tube stanchions of 5456-0, 6061-T6 and 7075-T6 materials. The curves were determined by the method presented in the Alcoa Handbook.

From these curves, allowable column loads for the 5456-0 and 6061-T6 materials were established for 100-in. long pin-ended columns using standard tube wall thicknesses and outside diameters. The results are plotted in Fig. 5-34.

The plots for 6061-T6 are curved since the slenderness ratios for the chosen combinations of wall thicknesses and outside diameters fall, primarily, in the Euler range. For 5456-0, the plots are primarily straight lines.

Indicated on the plots are the weights of 100-in. stanchions for the various wall thicknesses and diameters chosen. It can be seen by inspection that the weight difference between the heaviest and lightest is not very great.

When considering the small number of stanchions that will be used in a ship of the size considered in this study, it is apparent that the stanchion diameter and wall thickness can be chosen for reasons other than column strength without seriously affecting the overall vehicle weight.

5.5.5 Value Analysis

A cost was determined for several possible structural configurations in the hull. These included different fabrication and installation methods, materials, standard commercial and special extrusions, etc. For the purposes of this analysis, only the material and manufacturing costs, including overhead, are considered. Other design factors such as weight, panel size, flatness, water leakage, reparability, handling and machining cost were evaluated separately.

Four different manufacturing methods were investigated. They were plate and stringer, integrally stiffened extrusion, machined plate and honeycomb panels. Figure 5-35 reflects the relative rating these four methods attained in evaluating each with the aforementioned design factors. These assigned number values are relative only to each other and have weighted values of 1 to 4 with number 1 being the best and number 4 the worst.

Using the decking and supporting structure as an illustration, the findings and conclusions on cost and weight derived from Table 5-14 can apply to many other areas of the hull such as plating, superstructure, bulkheads, frames, etc. This analysis is for 6061 and 5456 aluminum at three different frame spacings with the type of structure described in Figs. 5-36 through 5-41.

Table 5-14 shows the weight and corresponding "cost per pound" for the installations investigated. Caution should be exercised in any use of the "cost per pound" figure, especially in regard to any decision-making that concerns a design selection based on cost. The association of a low "cost per pound" value with an overall minimum cost is not necessarily true. For example, the bonded plate-stringer with standard channel support design has a $1.86 per pound cost against a $2.58 per pound cost for a bonded plate-stringer with special I-supports. However, their total costs are approximately the same. The reason for the

TABLE 5-14

Decking and Support--Relative Cost and Weight Study

Part	Type	2-1/2-ft spacing			3-3/4-ft spacing			5-ft spacing		
		Cost ($)	Weight (lb)	$/lb	Cost ($)	Weight (lb)	$/lb	Cost ($)	Weight (lb)	$/lb
1. Integral extrusion	Standard I (6061)	74,427	22,920	3.25	66,501	21,025	3.16	62,866	21,525	2.92
2. Integral extrusion	Standard [(6061)	73,326	21,280	3.45	66,404	21,225	3.13	62,281	20,500	3.04
3. Integral extrusion	Special I (6061)	73,886	17,460	4.23	66,962	15,870	4.35	62,927	16,360	3.85
	(5456)	71,300	20,075	3.55	66,900	18,600	3.60	61,000	18,980	3.21
4. Plate-stringer--riveted	Standard I (6061)	53,851	24,550	2.19	45,260	22,730	1.99	41,460	23,155	1.79
5. Plate-stringer--riveted	Standard [(6061)	53,270	22,910	2.32	45,921	22,930	2.00	40,875	22,130	1.85
6. Plate-stringer--riveted	Special I (6061)	52,010	19,090	2.72	46,739	17,575	2.66	40,531	17,990	2.25
	(5456)	51,250	21,500	2.38	46,100	20,075	2.30	38,900	20,400	1.91
7. Plate-stringer--spotwelded	Standard I (6061)	52,596	24,220	2.17	44,313	22,400	1.98	40,505	22,825	1.77
8. Plate-stringer--spotwelded	Standard [(6061)	51,185	22,580	2.27	44,216	22,800	1.96	39,900	21,800	1.83
9. Plate-stringer--spotwelded	Special I (6061)	52,045	18,760	2.77	46,774	17,245	2.71	40,566	17,660	2.30
	(5456)	51,300	20,800	2.46	46,000	19,700	2.33	39,750	20,075	1.98
10. Plate-stringer--bonded	Standard I (6061)	50,490	24,420	2.06	42,554	22,600	1.88	38,919	23,025	1.69
11. Plate-stringer--bonded	Standard [(6061)	48,579	22,780	2.13	42,457	22,860	1.86	38,314	22,000	1.74
12. Plate-stringer--bonded	Special I (6061)	49,939	18,960	2.63	45,015	17,445	2.58	38,980	17,860	2.18
	(5456)	49,200	21,500	2.29	44,400	20,075	2.21	38,350	20,400	1.88
13. Machine plate	Standard I (6061)	83,200	22,720	3.66	79,480	20,825	3.82	72,000	21,325	3.38
14. Machine plate	Standard [(6061)	86,000	21,080	4.08	78,100	21,025	3.71	71,000	20,300	3.50
15. Machine plate	Special I (6061)	84,900	17,260	4.92	77,560	15,670	4.95	70,000	16,160	4.33
	(5456)	83,900	19,700	4.26	76,300	18,250	4.18	69,000	18,600	3.63
16. Honeycomb	Standard I (6061)	79,500	29,478	2.70	70,168	27,795	2.52	67,605	29,183	2.32
17. Honeycomb	Standard [(6061)	79,000	27,838	2.84	71,207	27,995	2.54	68,700	28,158	2.44
18. Honeycomb	Special I (6061)	81,500	24,018	3.39	72,597	22,640	3.21	69,265	24,018	2.88

"cost per pound" difference is caused by the weight differential. Therefore, the total cost associated with corresponding total weight should be the parameter to consider.

Because Table 5-14 has 69 different combinations shown in a tabular form, it is difficult to derive any quick conclusions. Figure 5-42 is an attempt at clarification of some of these data by graphical representation and simplification by showing only one frame spacing of 6061 aluminum.

A significant point in Fig. 5-42 is the consistent cost of all the plate-stringer types ($45,000 average). However, the weight variance of these designs is 5500 lb, with a range from 17,500 to 23,000 lb.

The integral extrusion-type designs include $13,000 for die costs which is reimbursable in whole or part, depending upon the quantities involved. Therefore, subtracting this from the average cost of $67,000 makes it more compatible with the other designs whenever more than one craft is considered. This reduces the cost to $54,000 which puts it in the dollar class with the plate-stringer types but with the additional advantage of minimum weight.

The machine plate design does not appear to have any strong points as it is the most costly and has a negligible weight advantage. One of the disadvantages of the honeycomb design is that it is the heaviest.

The integral extrusion design with special I-section supports is recommended as a compromise because of the favorable weight and adequate strength with good structural design for hydrofoil operation at relatively low cost.

5.6 ILLUSTRATIONS

Previous page was blank, therefore not filmed.

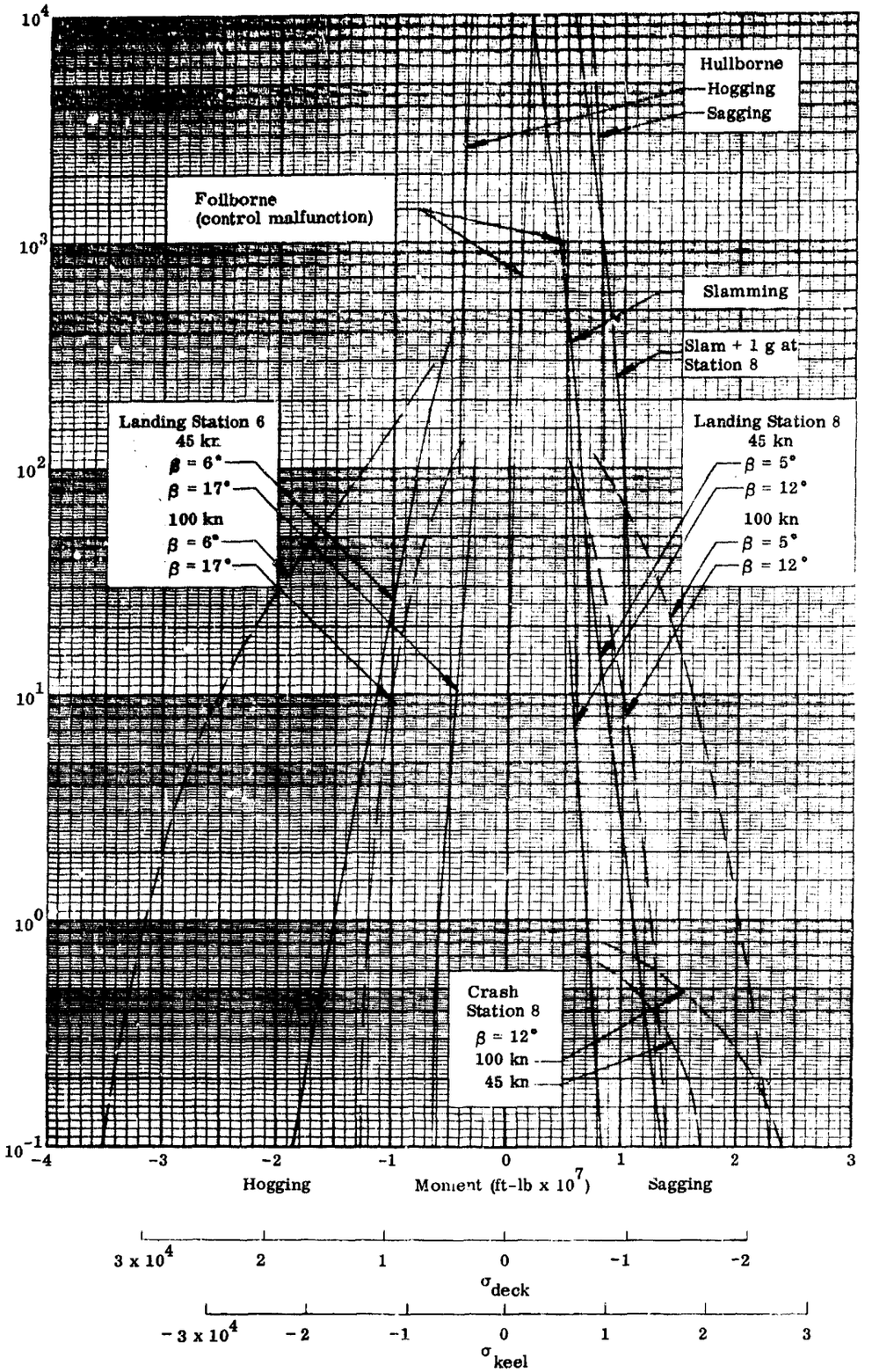

Fig. 5-1. Summary of Cumulative Occurrences of Hull Bending

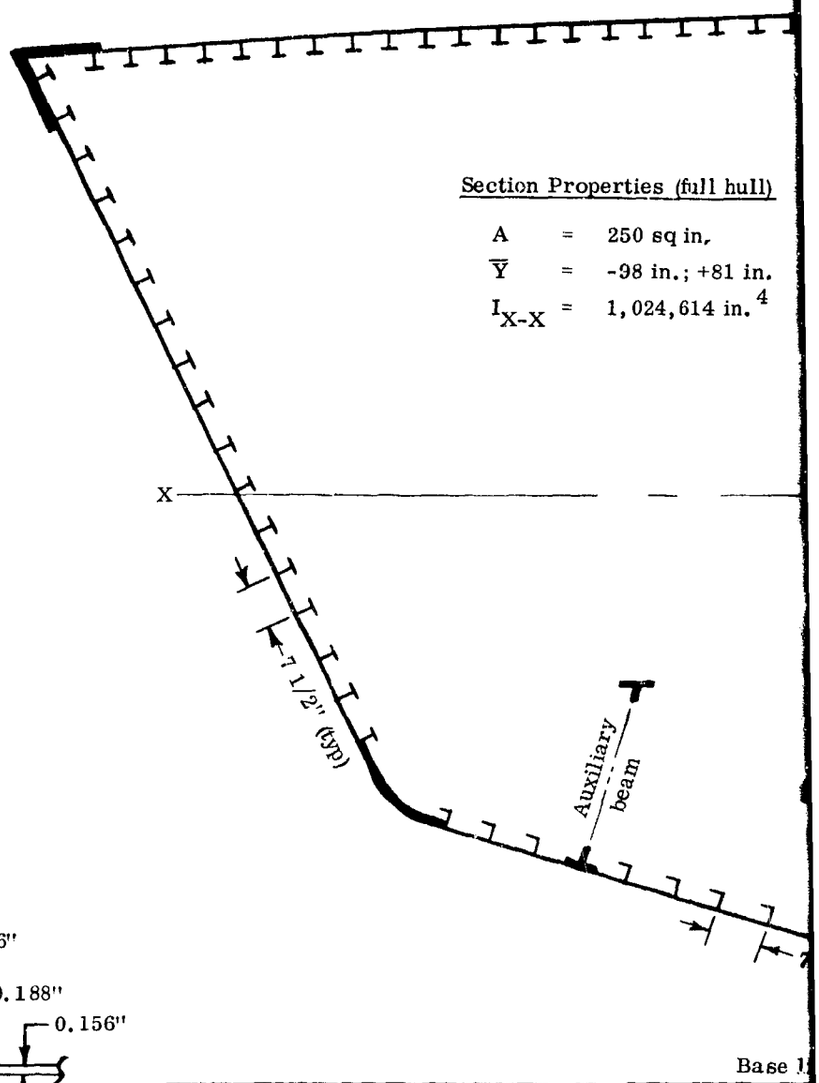

Stringer Sections

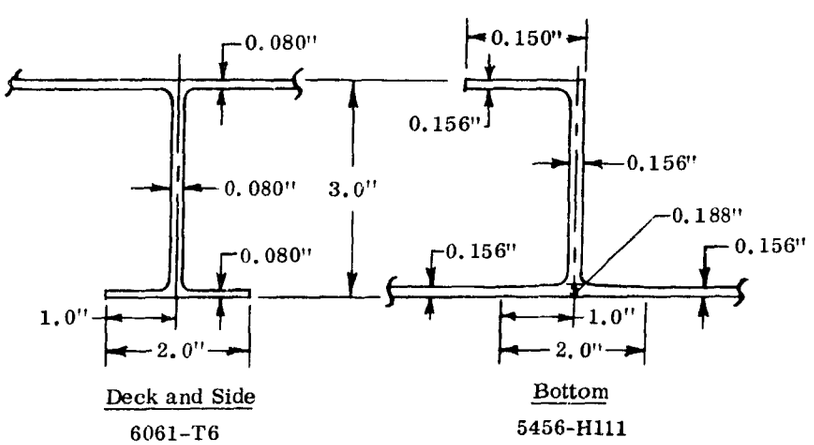

Deck and Side
6061-T6

Bottom
5456-H111

Fi

ER 13727
5-54

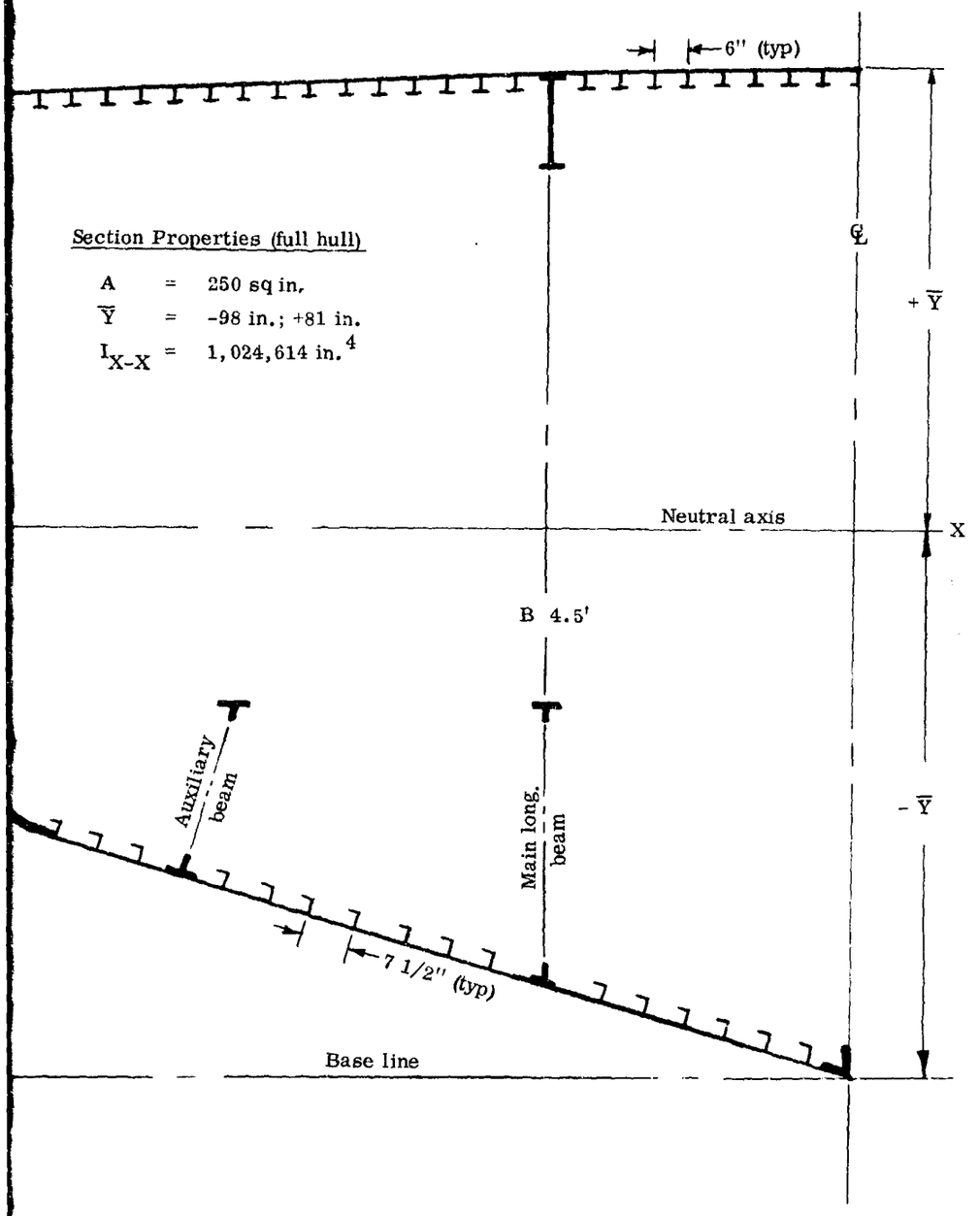

Fig. 5-2. Modified Hull Transverse Midship Section

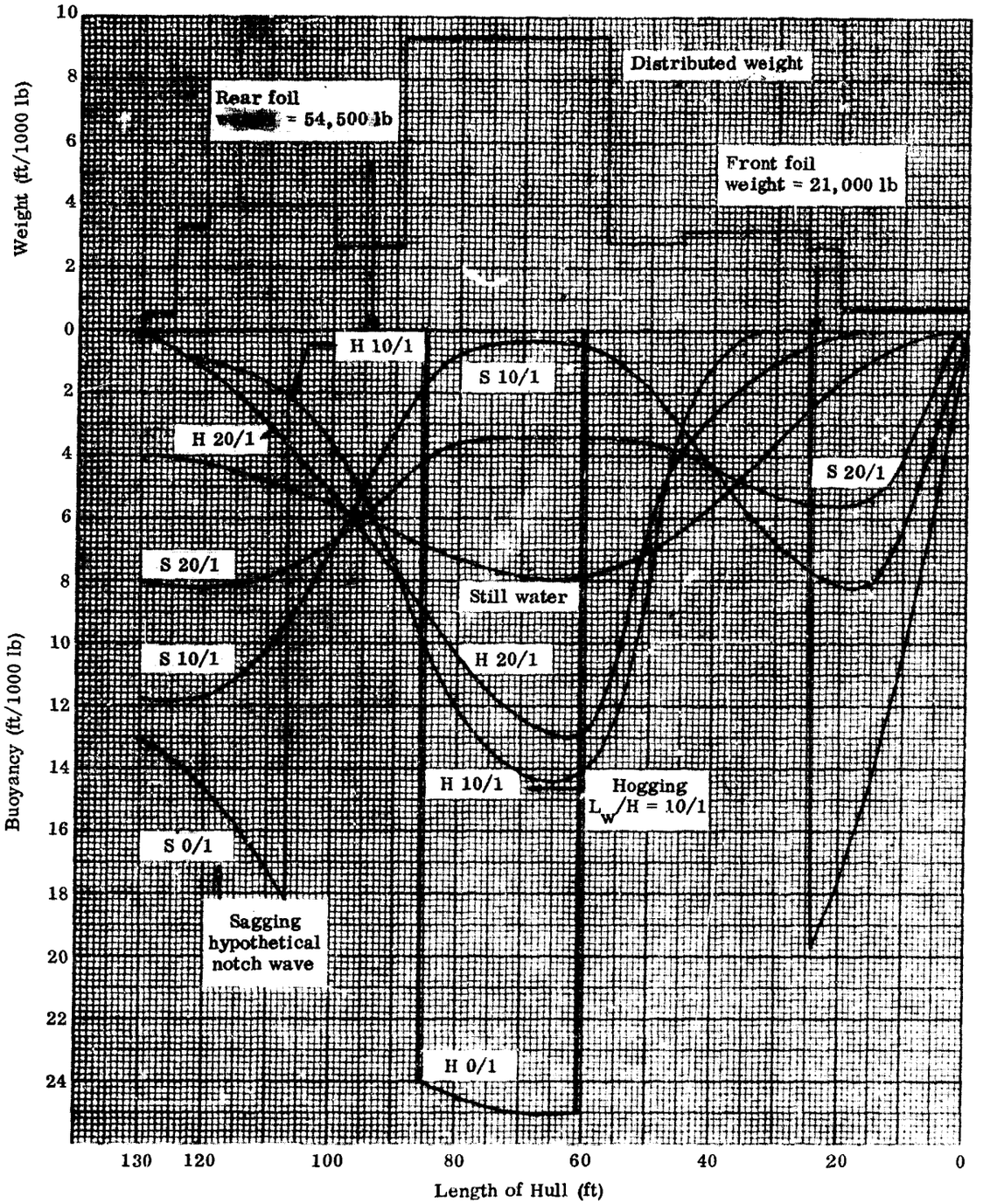

Fig. 5-3. Hull Deadweight and Loading, Hogging and Sagging

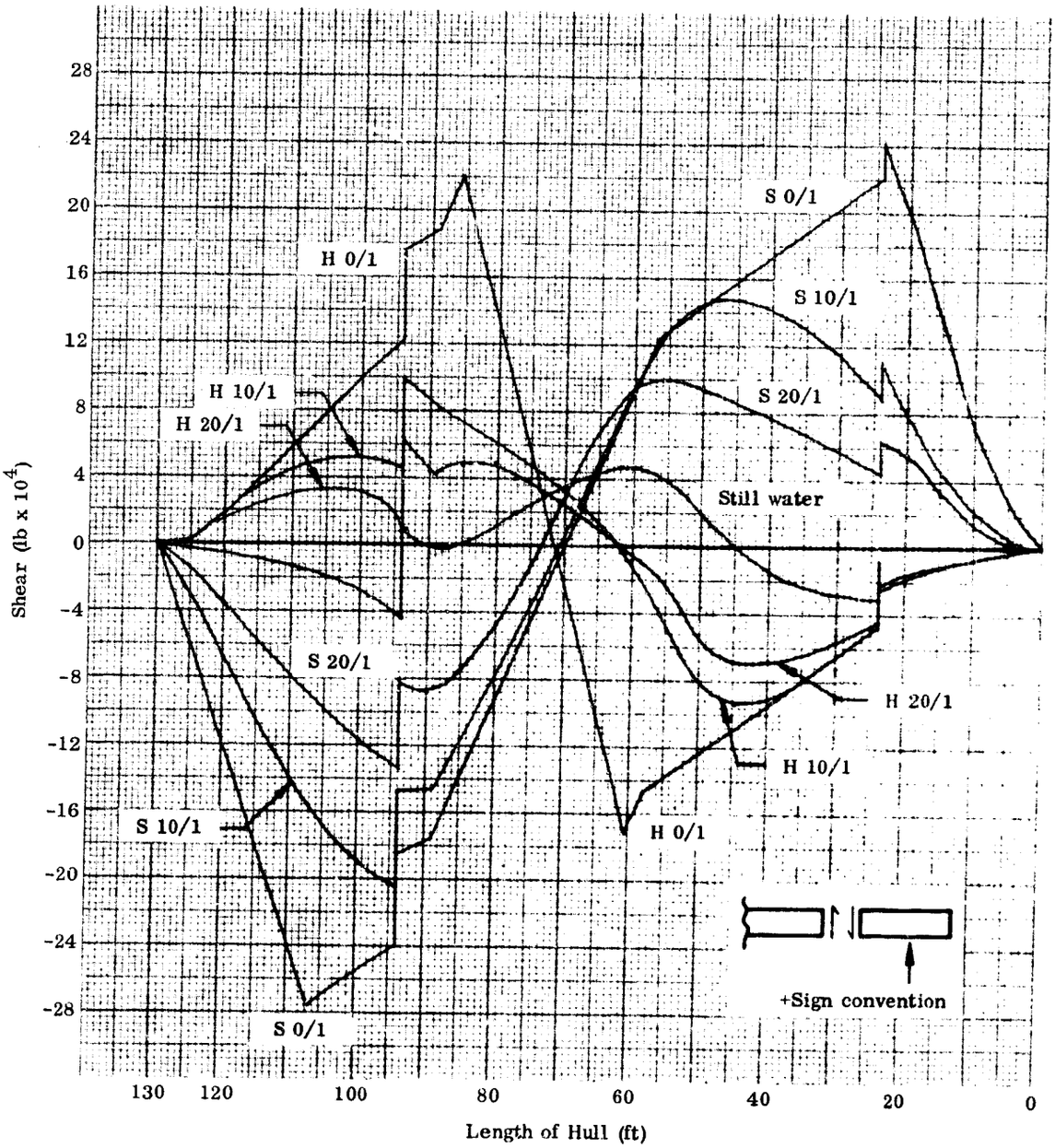

Fig. 5-4. Hull Shear, Hogging and Sagging

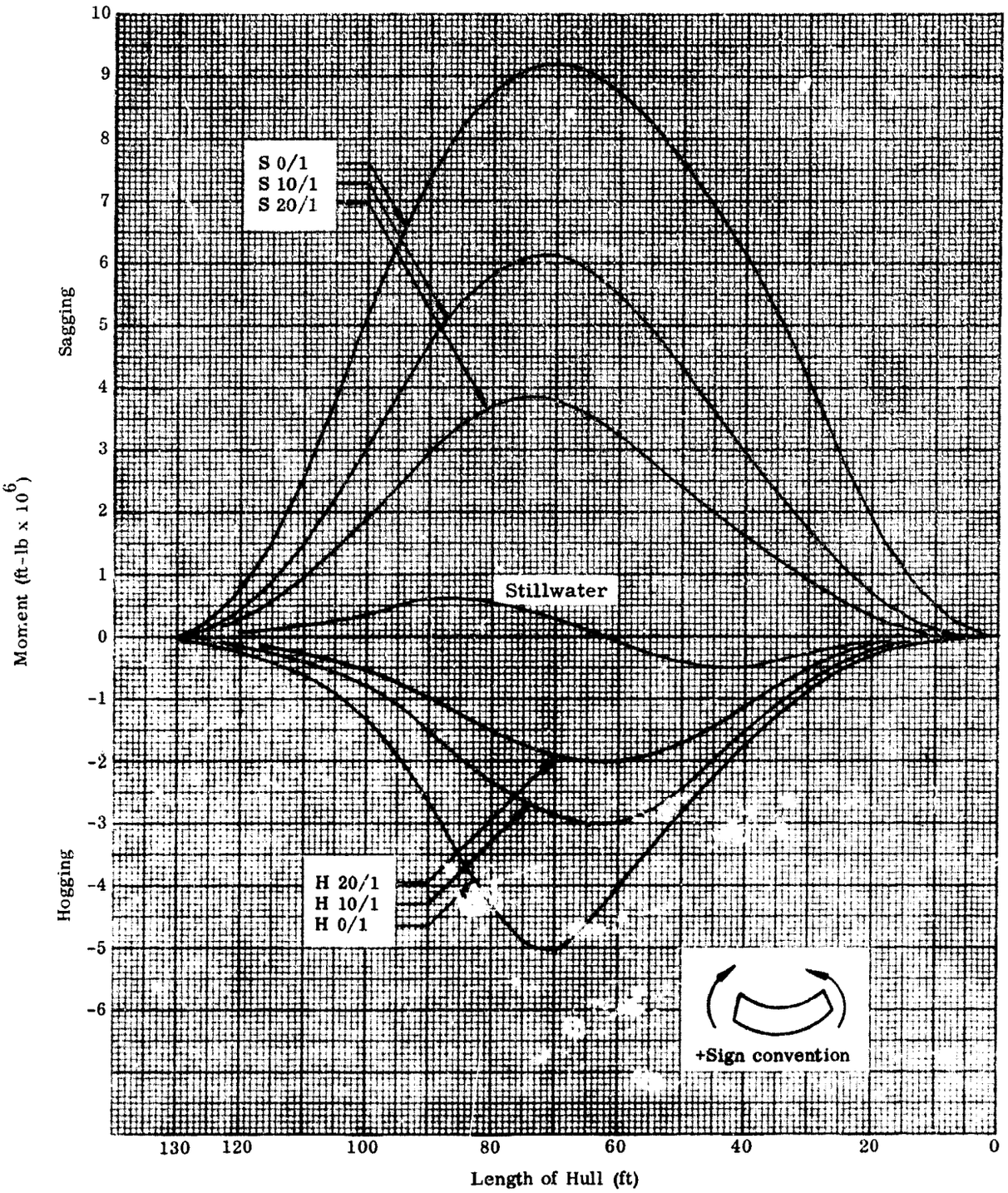

Fig. 5-5. Hull Bending Moments, Hogging and Sagging

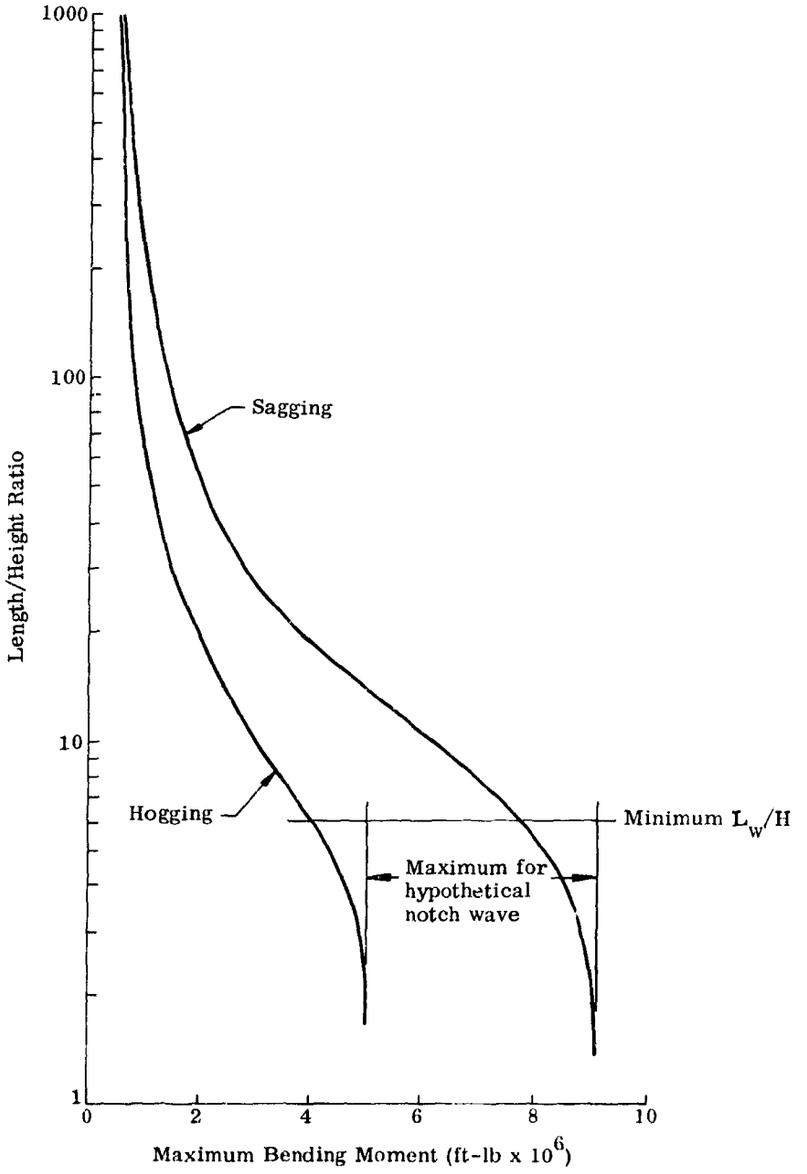

Fig. 5-6. Maximum Hull Bending Moments Versus Wave Length/Height Ratio

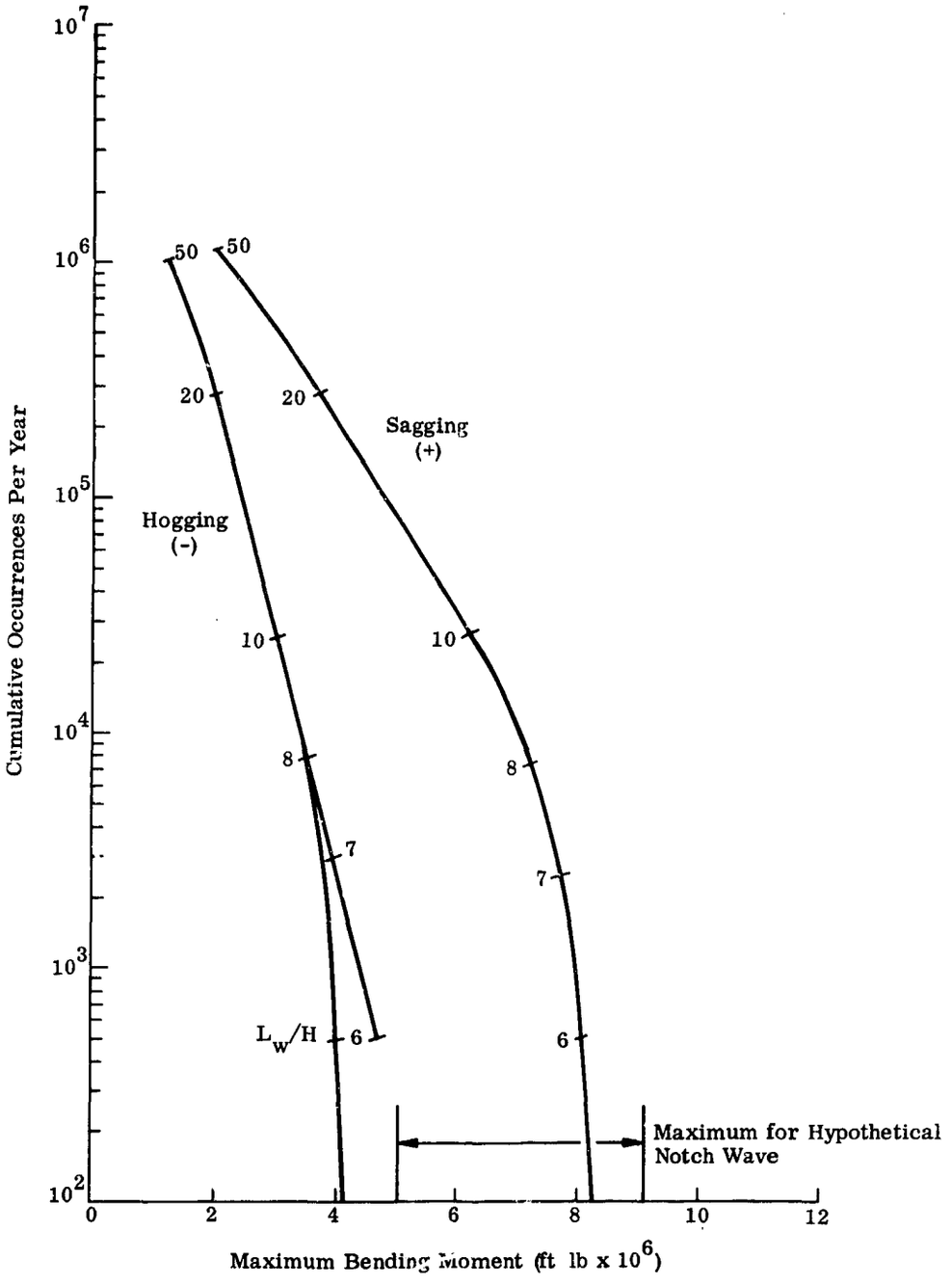

Fig. 5-7. Cumulative Bending Moment Occurrence for Hogging and Sagging

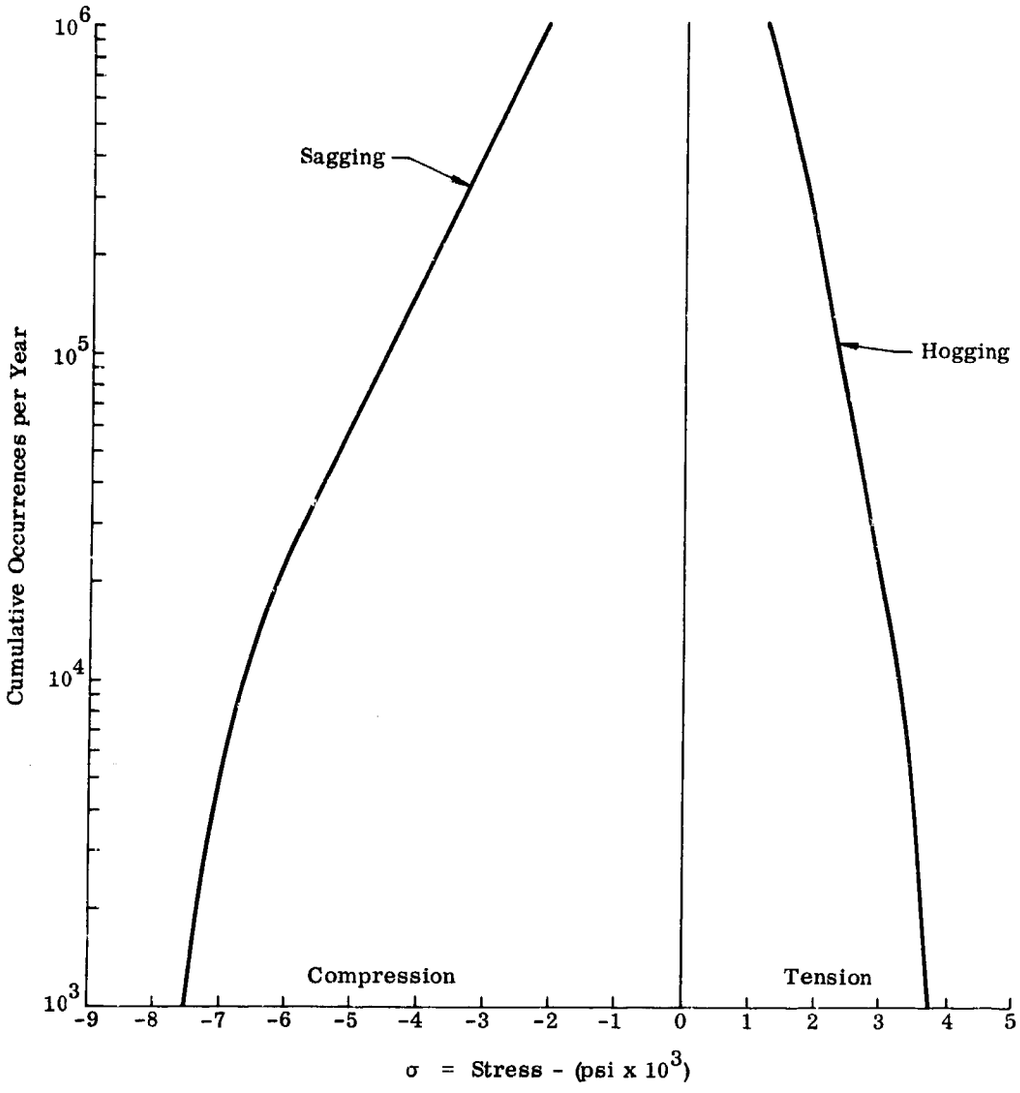

Fig. 5-8. Deck Stress Occurrence, Hogging and Sagging

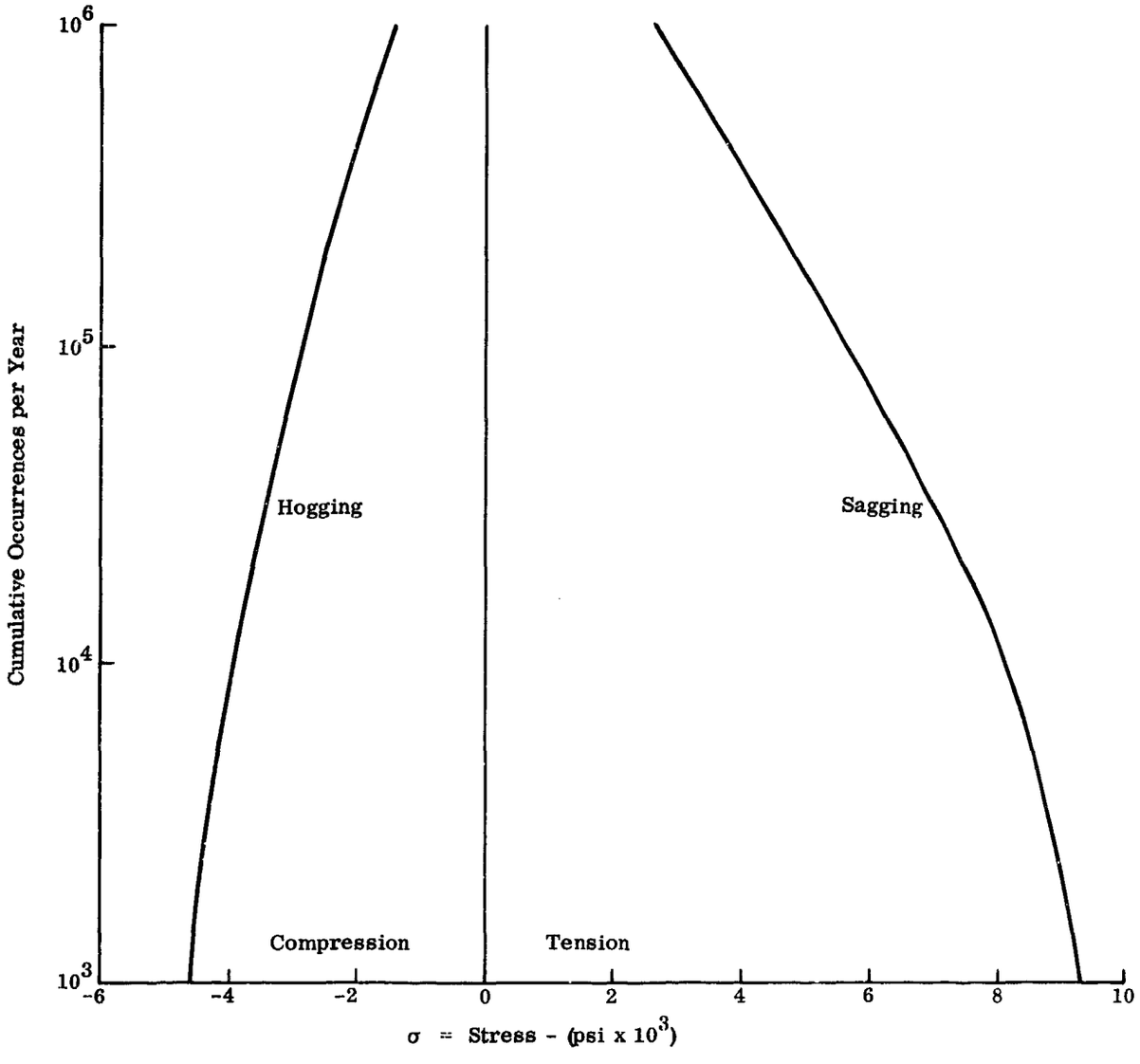

Fig. 5-9. Keel Stress Occurrence, Hogging and Sagging

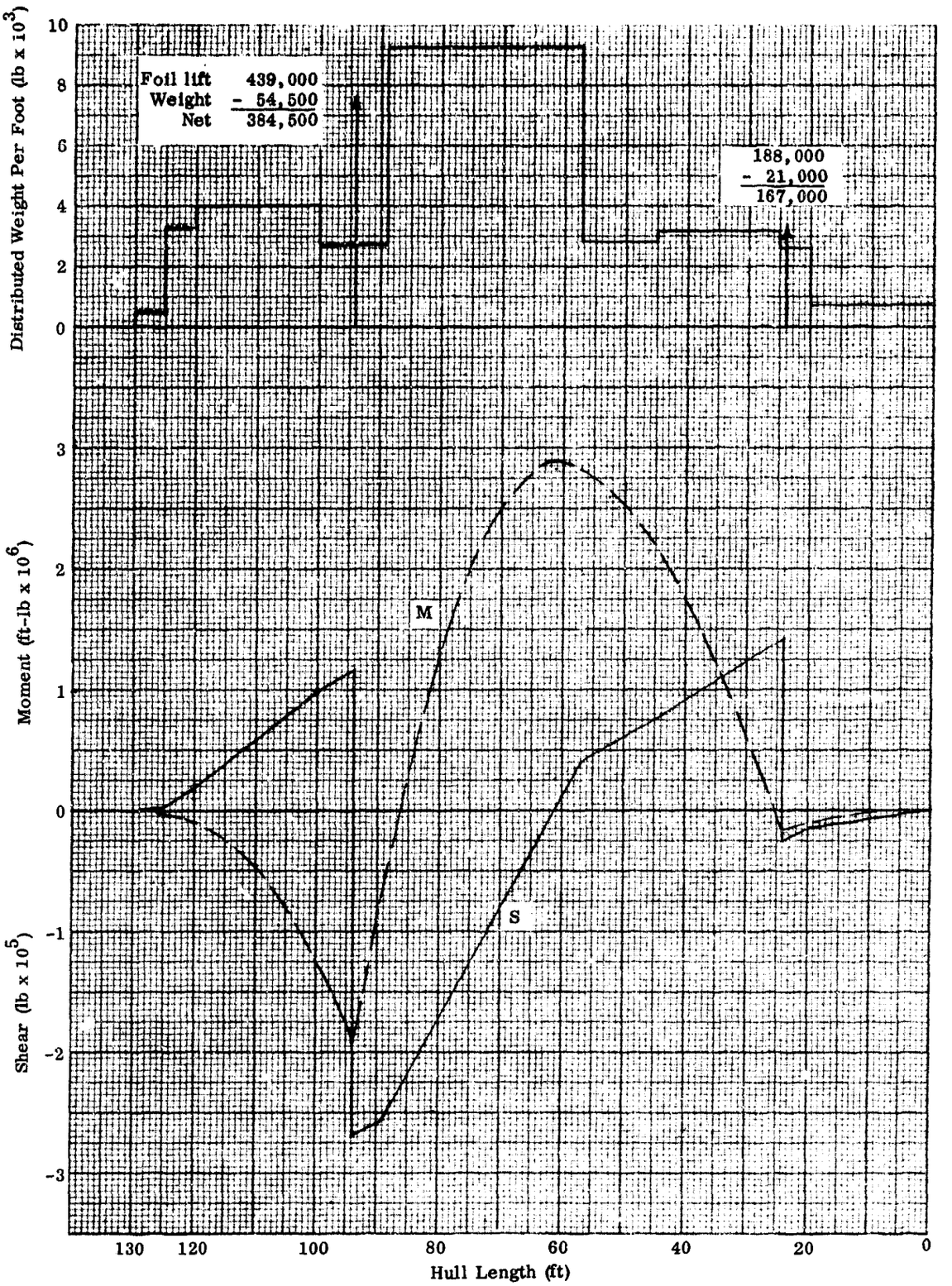

Fig. 5-10. Hull Loading, Shear and Bending Moments, Foilborne (1-g) Foilborne Hull

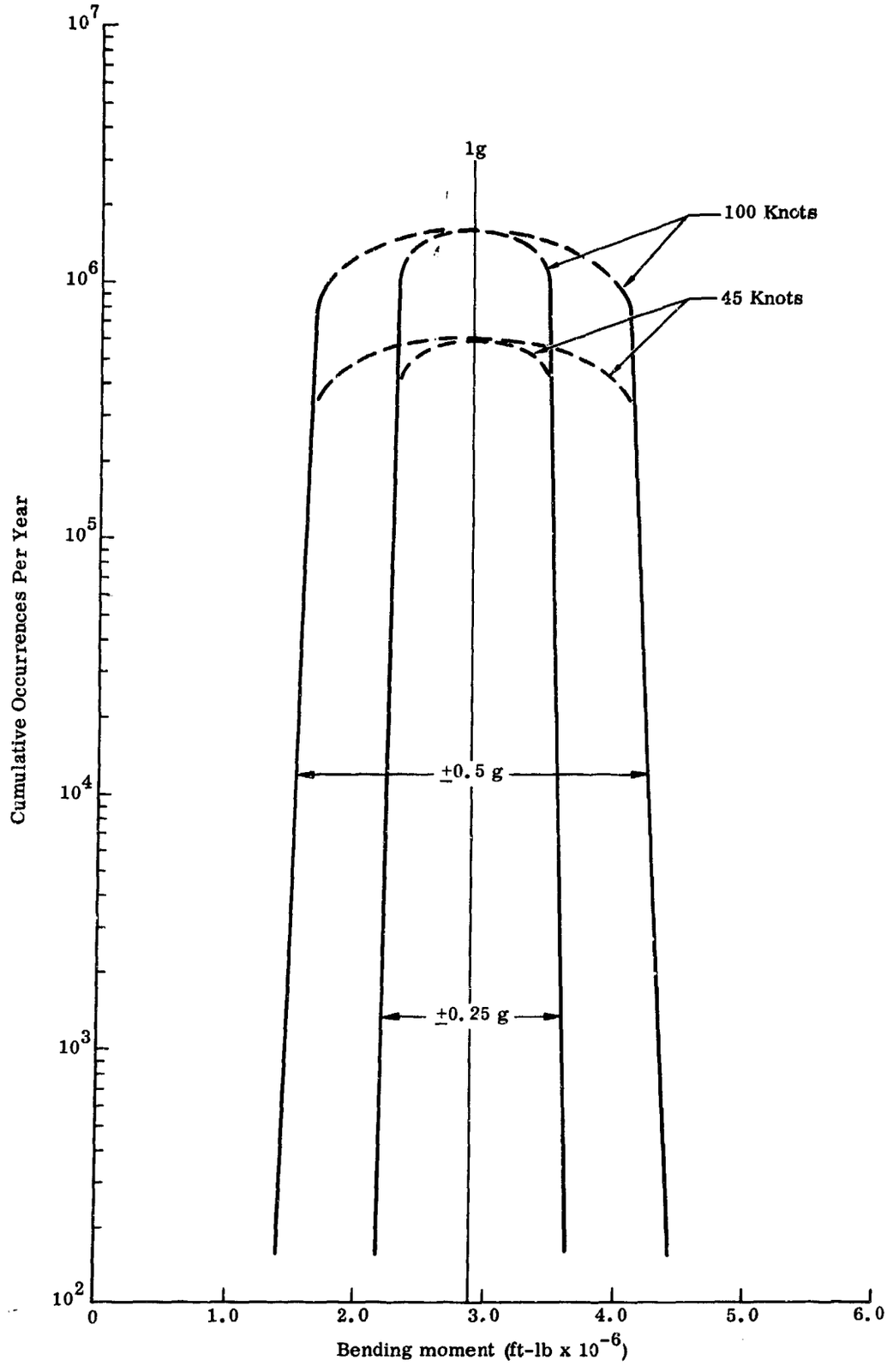

Fig. 5-11. Maximum Foilborne Hull Bending Moments for 0.25-g and 0.50-g Autopilot Control

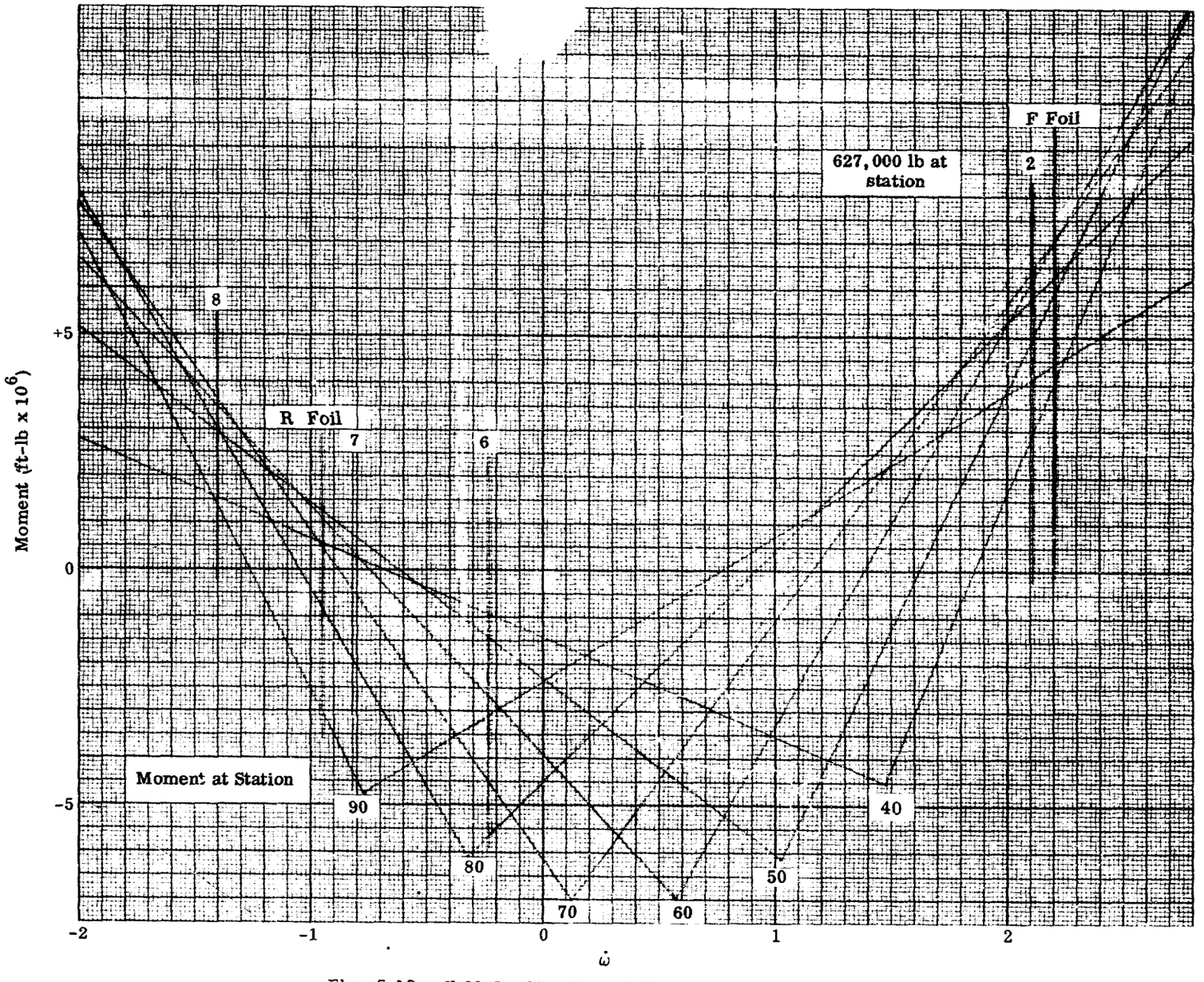

Fig. 5-12. Hull Bending Moment for Concentrated Load Applied at Any Location

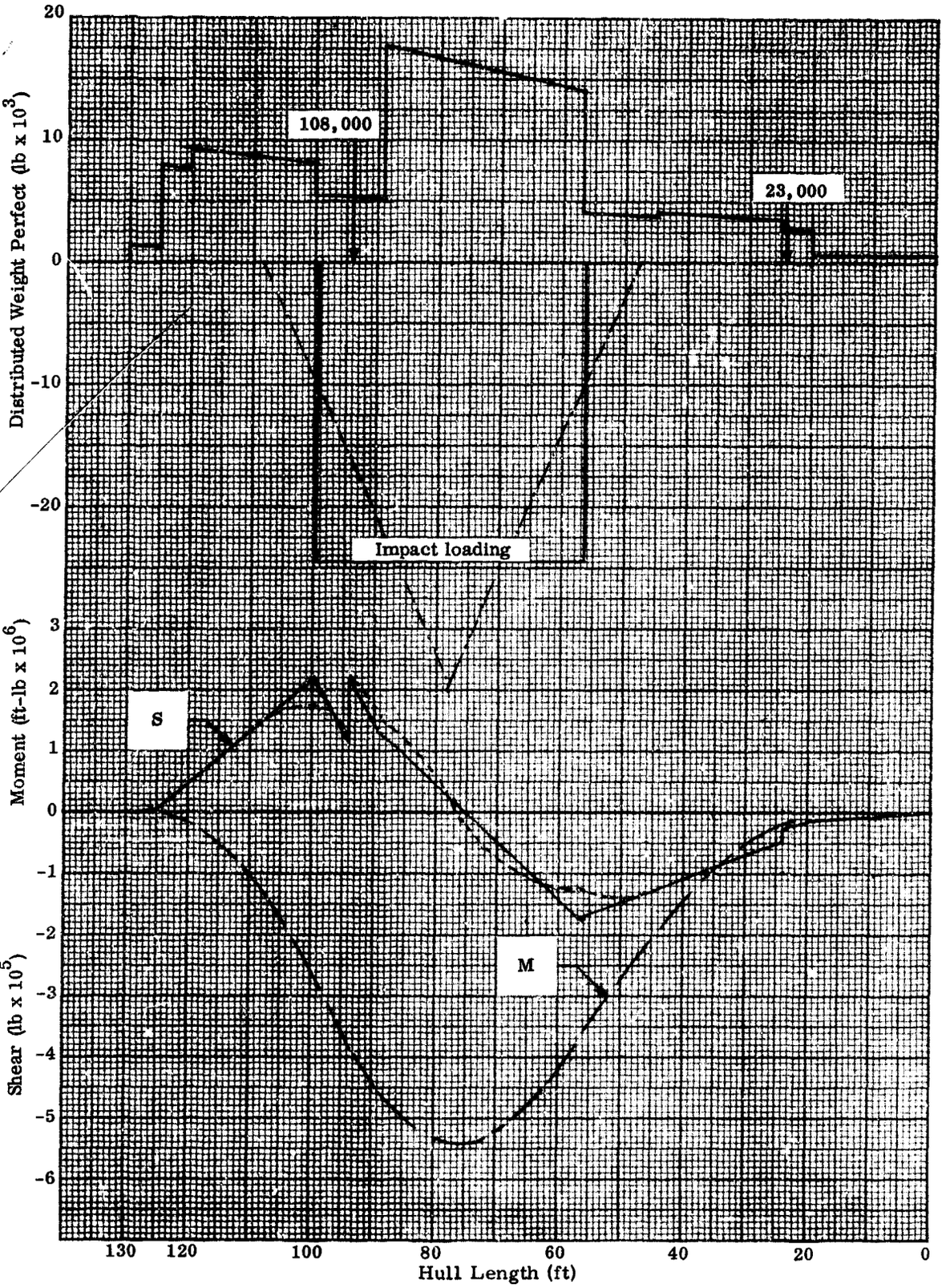

Fig. 5-13. Landing at Station 6 (45 kn)

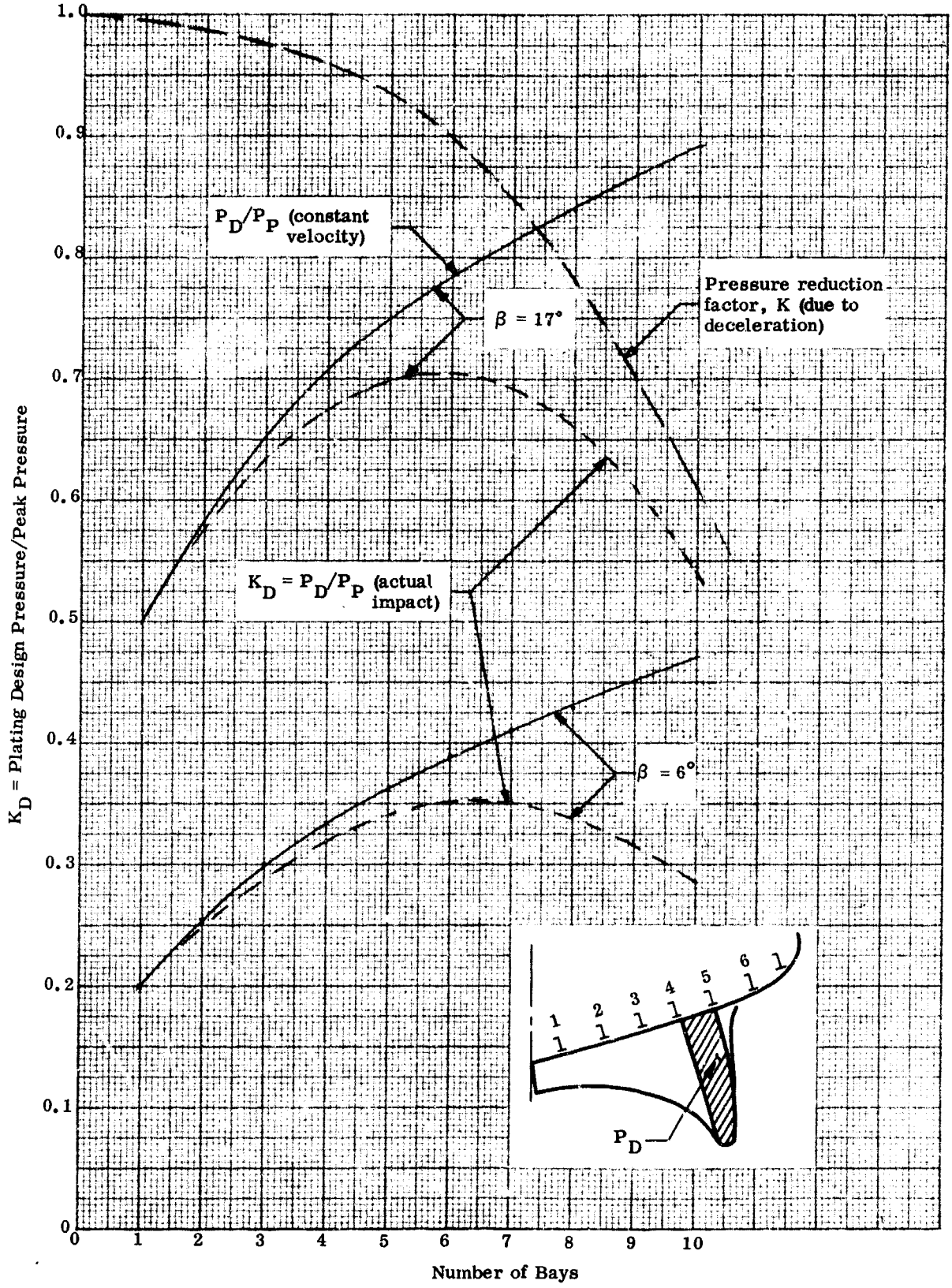

Fig. 5-14. Plating Design Pressure

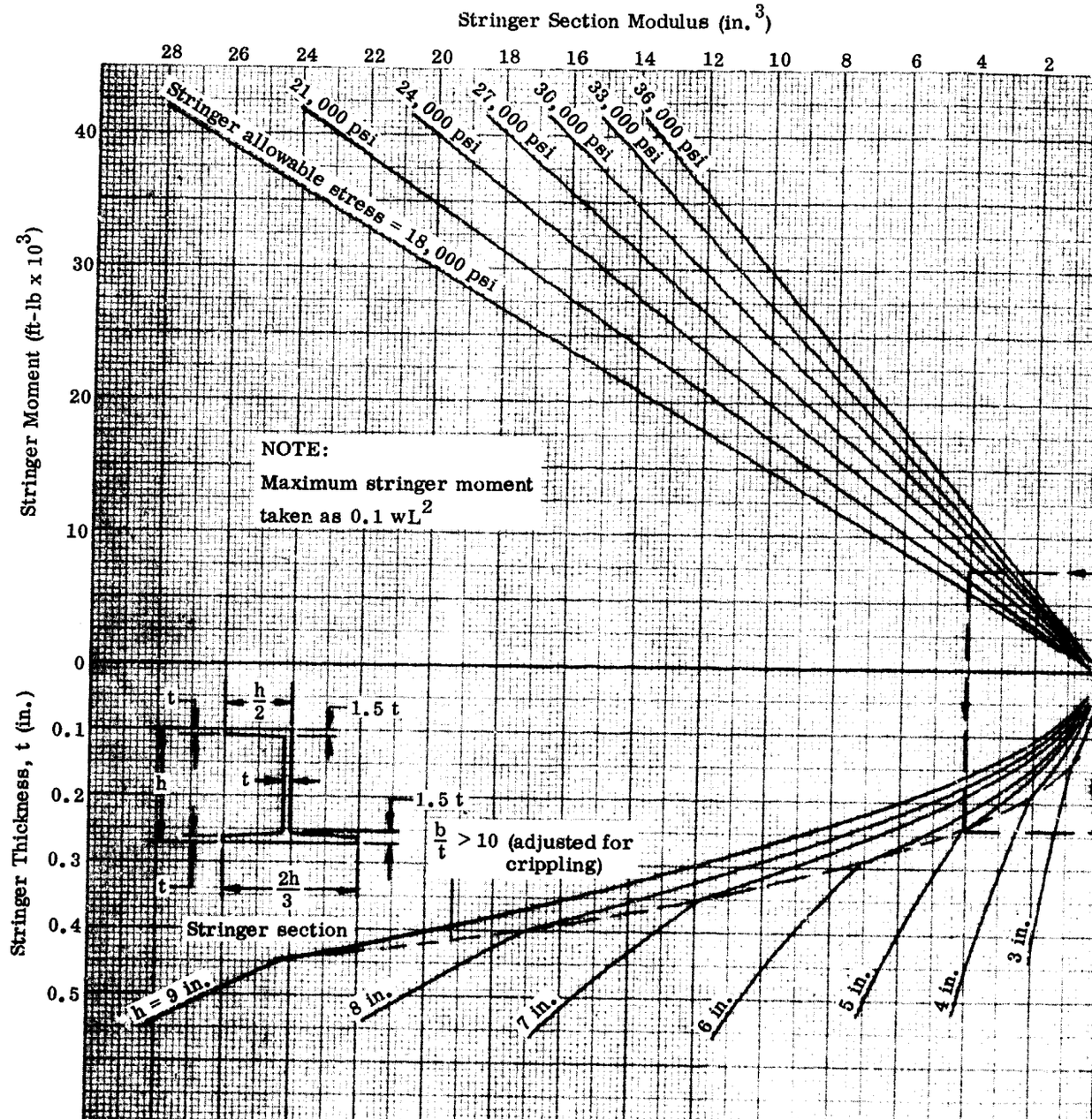
Stringer Section Modulus (in.^{3})
28
26
24
22
20
18
16
14
12
10
8
6
4
2
Stringer Moment (ft-lb x 10^3)
40
30
20
10
0
Stringer Thickness, t (in.)
0.1
0.2
0.3
0.4
0.5
Stringer allowable stress = 18,000 psi
21,000 psi
24,000 psi
27,000 psi
30,000 psi
33,000 psi
36,000 psi
NOTE:
Maximum stringer moment
taken as 0.1 wL^2
t
h/2
1.5 t
h
t
1.5 t
b/t > 10 (adjusted for
crippling)
t
2h/3
Stringer section
h = 9 in.
8 in.
7 in.
6 in.
5 in.
4 in.
3 in.

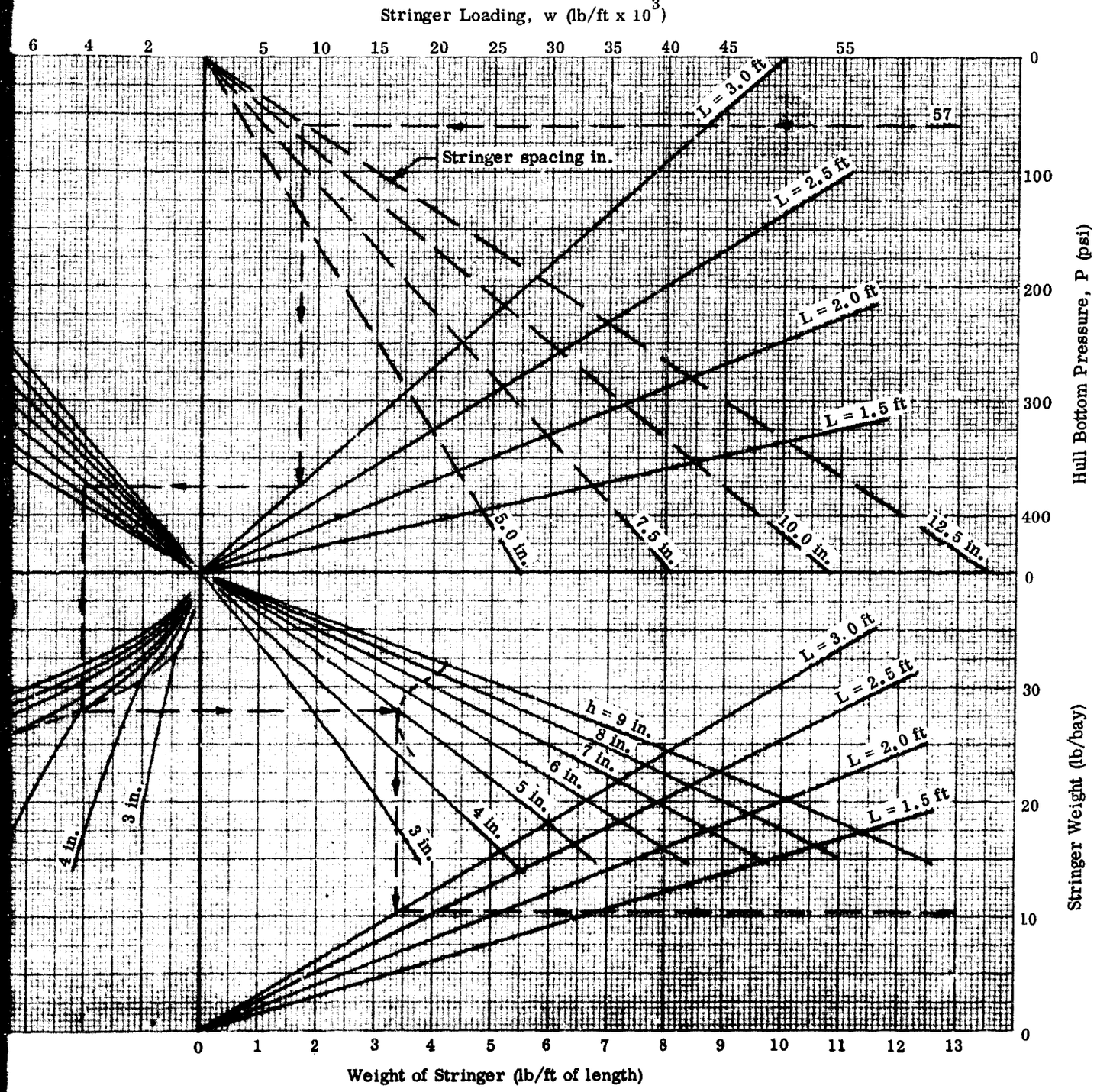

Fig. 5-15. Diagrams for Selecting Hull Bottom Stringers

2

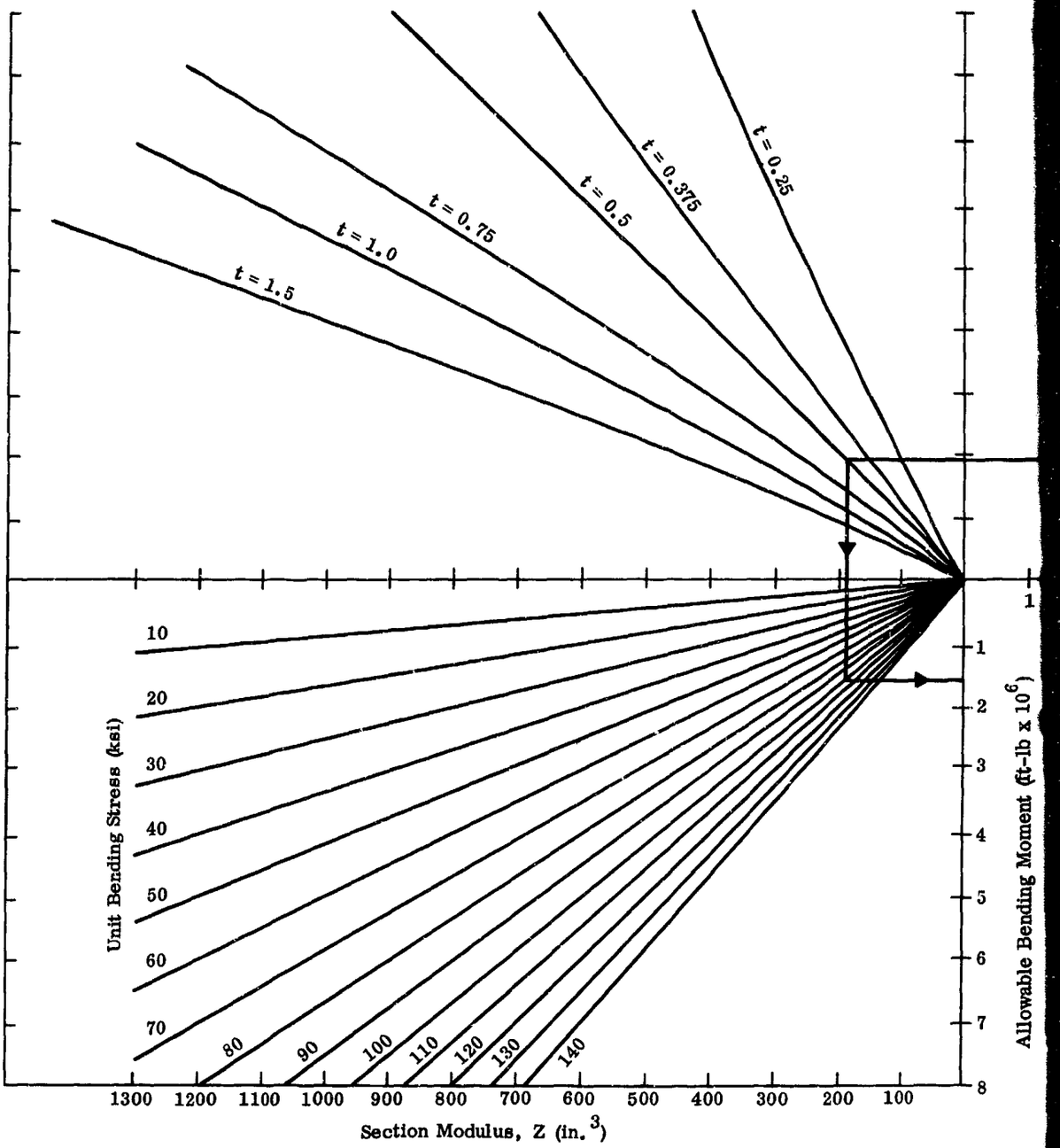
t = 0.25
t = 0.375
t = 0.5
t = 0.75
t = 1.0
t = 1.5
10
20
30
40
50
60
70
80
90
100
110
120
130
140
Unit Bending Stress (ksi)
1300 1200 1100 1000 900 800 700 600 500 400 300 200 100
Section Modulus, Z (in.^{3})
1
1
2
3
4
5
6
7
8
Allowable Bending Moment (ft-lb x 10^6)

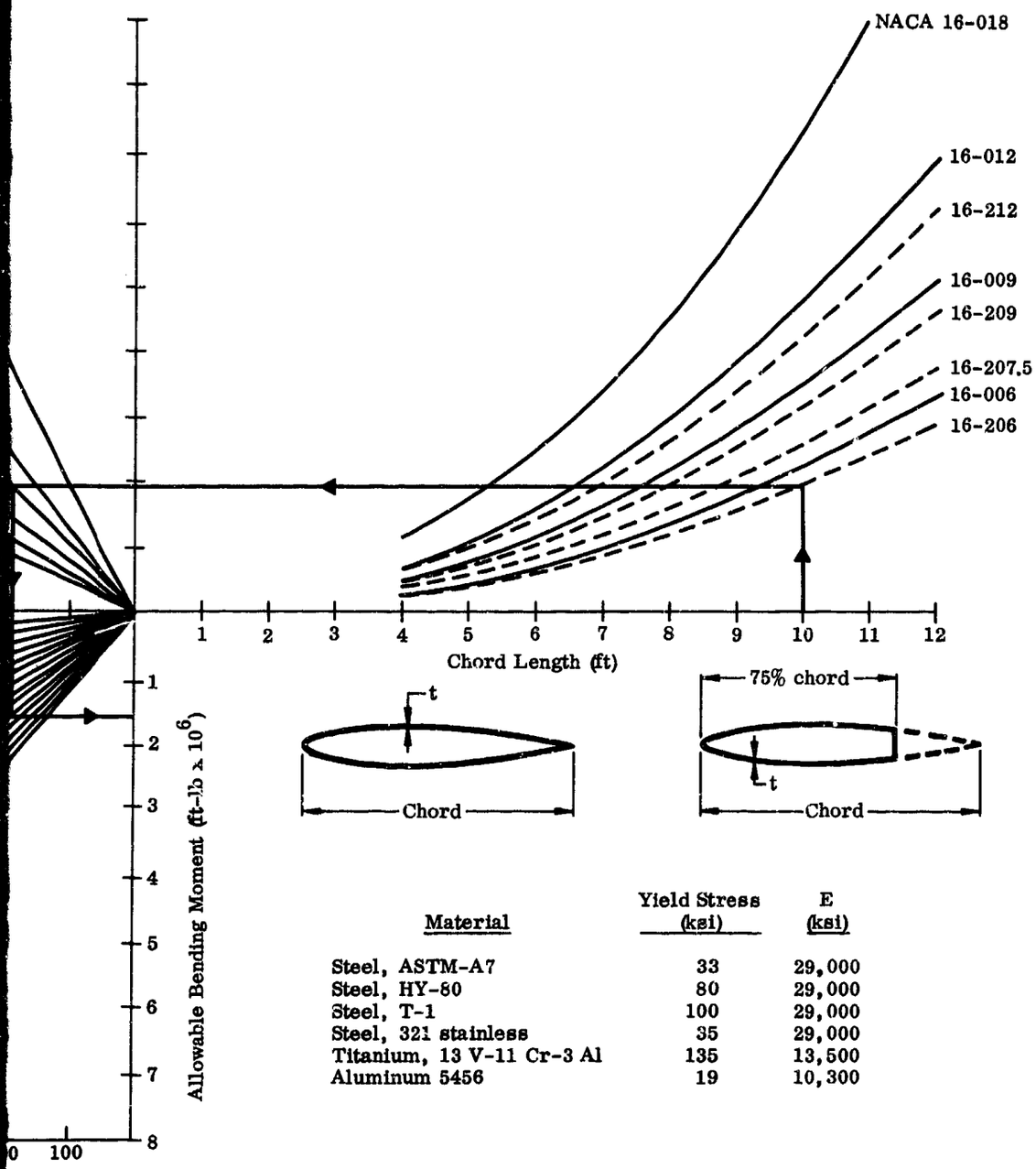

Material	Yield Stress (ksi)	E (ksi)
Steel, ASTM-A7	33	29,000
Steel, HY-80	80	29,000
Steel, T-1	100	29,000
Steel, 321 stainless	35	29,000
Titanium, 13 V-11 Cr-3 Al	135	13,500
Aluminum 5456	19	10,300

Fig. 5-16. Allowable Foil and Strut Bending Moment

2

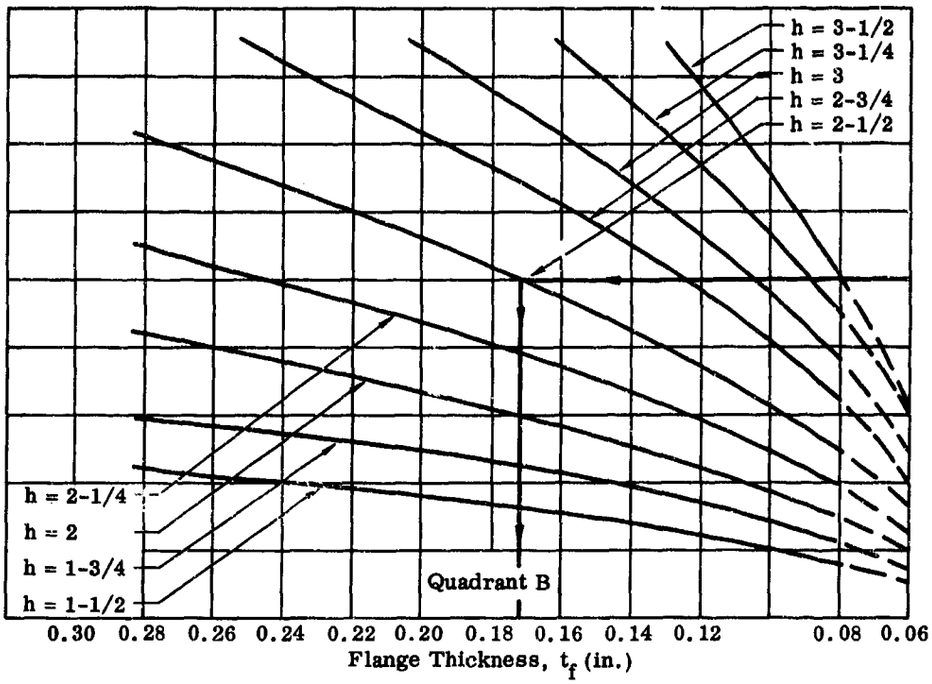
h = 3-1/2
h = 3-1/4
h = 3
h = 2-3/4
h = 2-1/2
h = 2-1/4
h = 2
h = 1-3/4
h = 1-1/2
Quadrant B
0.30 0.28 0.26 0.24 0.22 0.20 0.18 0.16 0.14 0.12 0.08 0.06
Flange Thickness, t_f (in.)

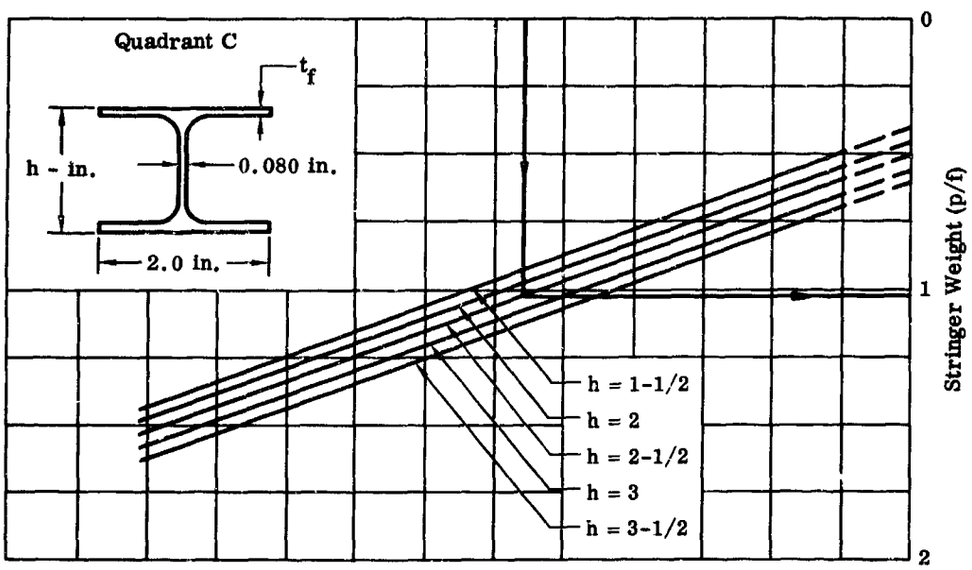
Quadrant C
t_f
h - in.
0.080 in.
2.0 in.
h = 1-1/2
h = 2
h = 2-1/2
h = 3
h = 3-1/2
0
1
2
Stringer Weight (p/f)

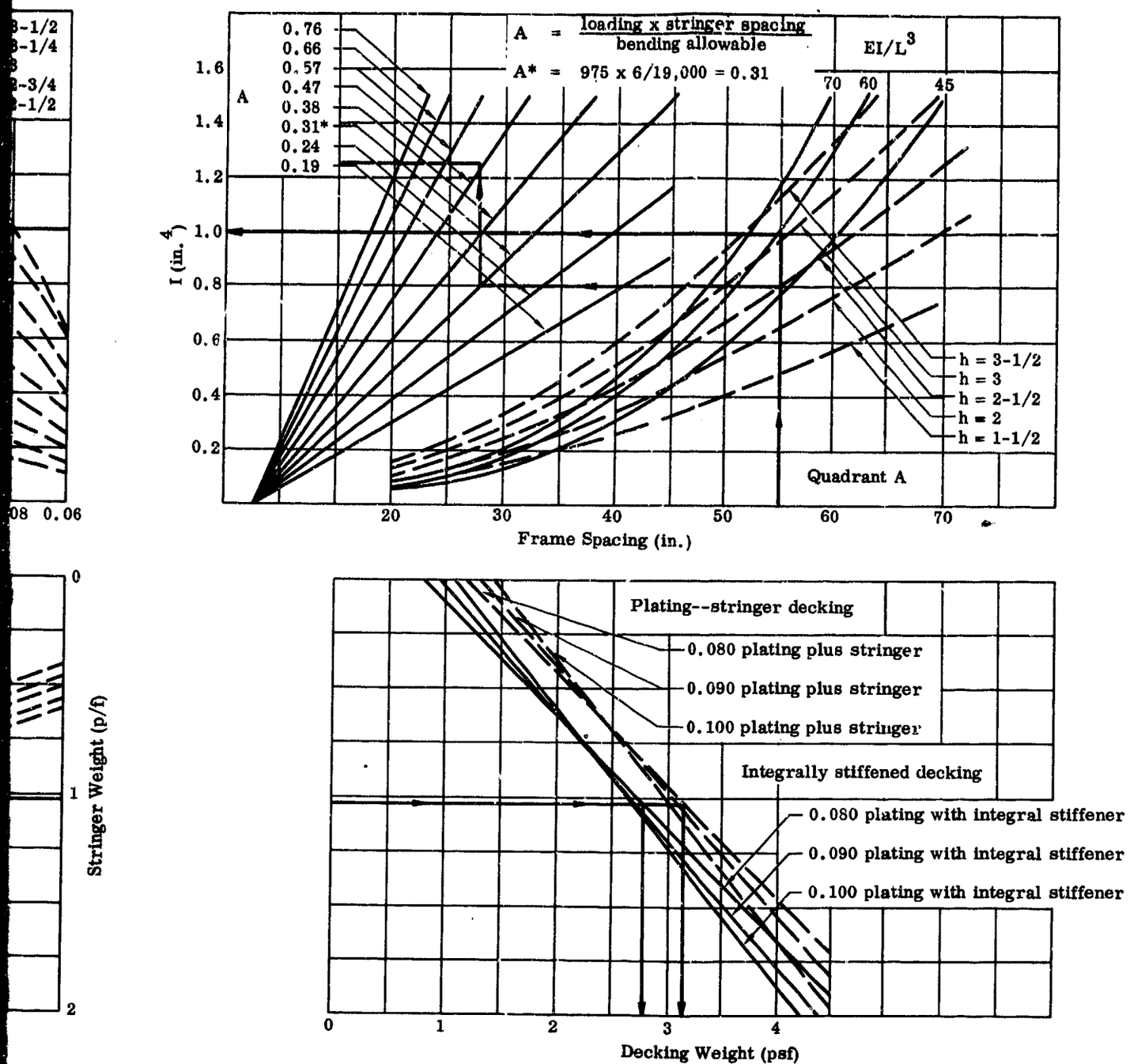

Fig. 5-17. Diagram for Selecting Plate--Stringer Decking

2

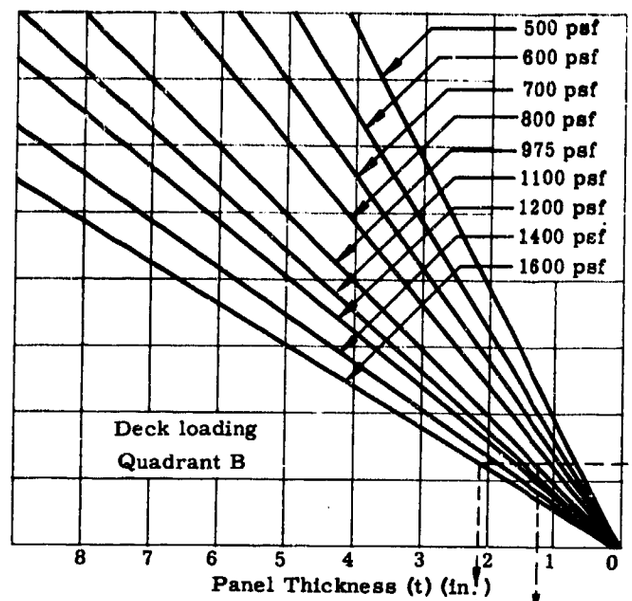
500 psf
600 psf
700 psf
800 psf
975 psf
1100 psf
1200 psf
1400 psf
1600 psf
Deck loading
Quadrant B
8 7 6 5 4 3 2 1 0
Panel Thickness (t) (in.)

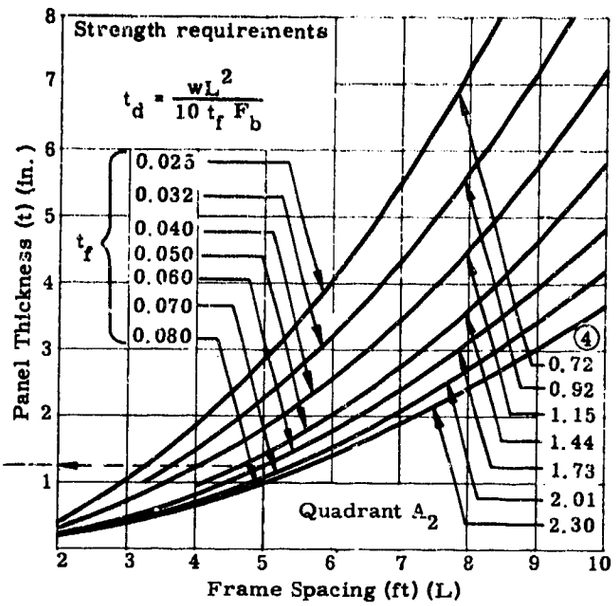
Strength requirements
$t_d = \frac{wL^2}{10\, t_f\, F_b}$
t_f
0.025
0.032
0.040
0.050
0.060
0.070
0.080
④
0.72
0.92
1.15
1.44
1.73
2.01
2.30
Quadrant A_2
Panel Thickness (t) (in.)
Frame Spacing (ft) (L)

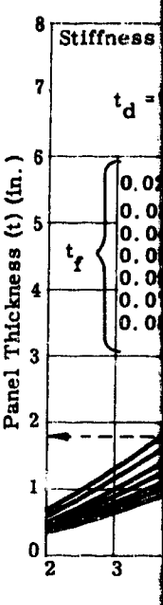
Stiffness
t_d =
t_f
Panel Thickness (t) (in.)

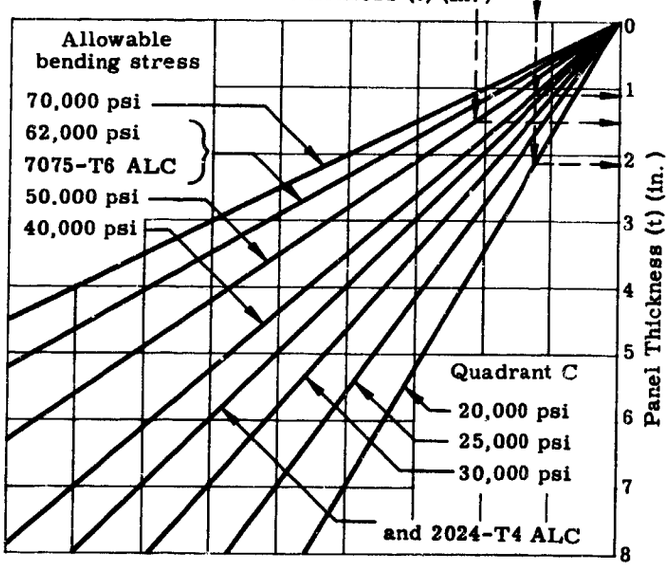
Allowable
bending stress
70,000 psi
62,000 psi
7075-T6 ALC
50,000 psi
40,000 psi
Quadrant C
20,000 psi
25,000 psi
30,000 psi
and 2024-T4 ALC
Panel Thickness (t) (in.)

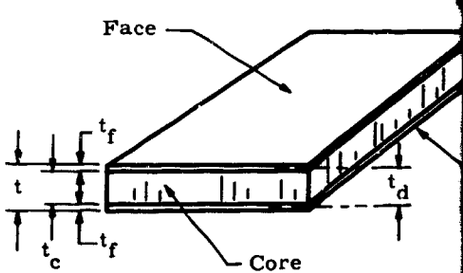
Face
t_f
t
t_c
t_f
t_d
Core

$t_d = t - t_f$

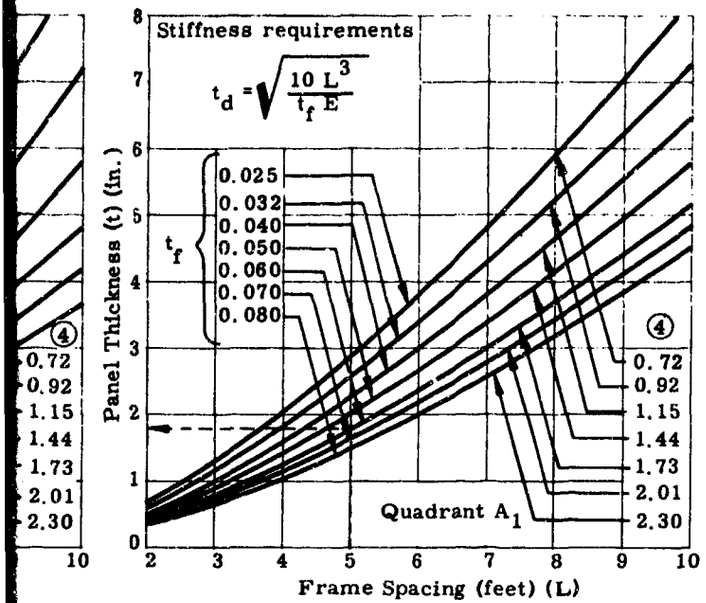

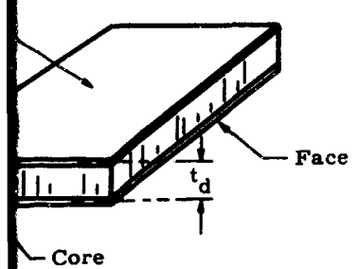

NOTES:

1. Curves in Quadrant A_2 are determined for a deck loading of 975 psf and an allowable stress, F_b of 35,000 psi. The bending moment used is $M = wL^2/10$.
2. Curves in Quadrant A_1 are determined from the stiffness criteria, $EI/L^3 = 60$. The moment of inertia used is that of an assumed equivalent panel width of 2 in.
3. Quadrants B and C are used to determine panel thicknesses for deck loadings and bending allowables other than those used in Quadrant A_2.

   Examples:

   (a) $L = 5$ ft, $t_f = 0.060$ in., $F_b = 35,000$ psi, and $w = 975$ psf.

   Therefore, from Quadrant A_2, $t = 1.22$ in.

   (b) $L = 5$ ft, $t_f = 0.060$ in., $F_b = 20,000$ psi and $w = 975$ psf.

   Therefore, from Quadrant C, $t = 2.05$ in.

   (c) $L = 5$ ft, $t_f = 0.060$ in., $F_b = 50,000$ psi and $w = 1600$ psf.

   Therefore, from Quadrant C, $t = 1.45$ in.

④ Values are weight of both faces of panel, psf.

Fig. 5-18. Diagram for Selecting Panel and Face Thickness of Sandwich-Type Decking

2

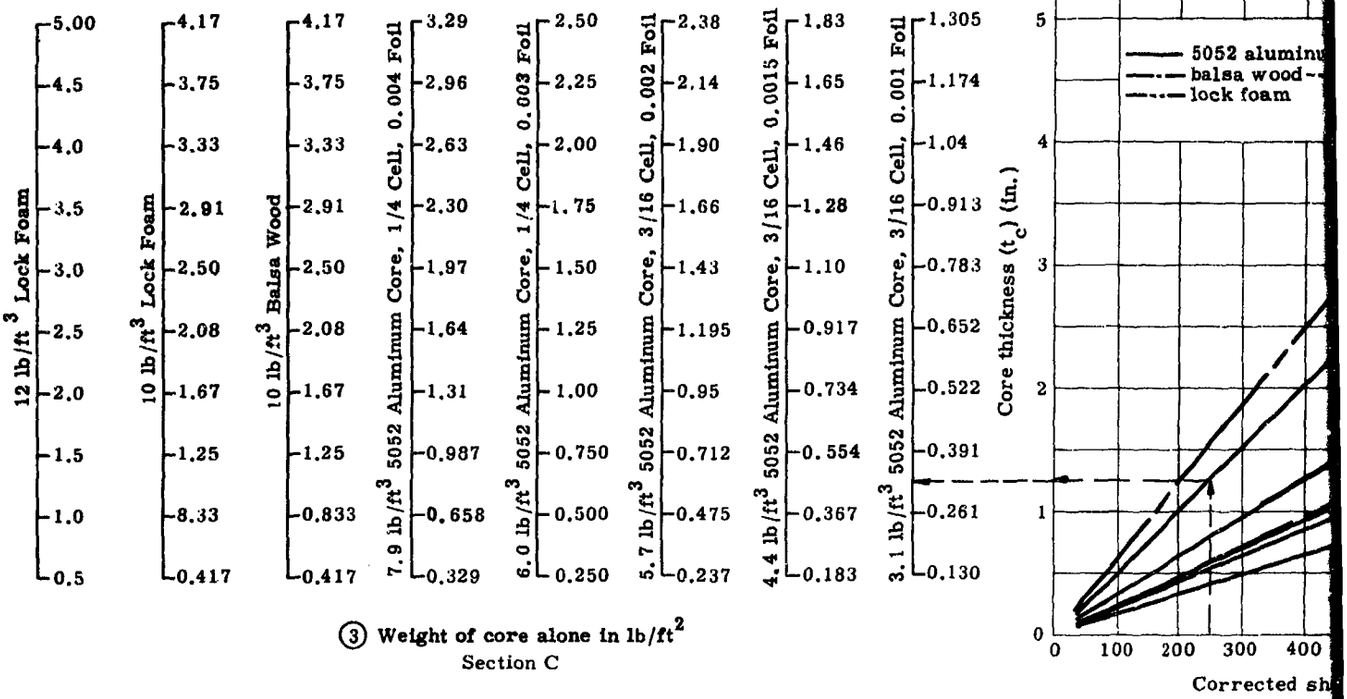

③ Weight of core alone in lb/ft²

Section C

Influence of face thickness on core shear strength

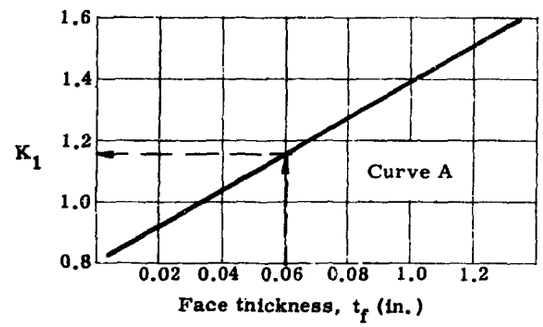

Influence of core thickness on core shear strength

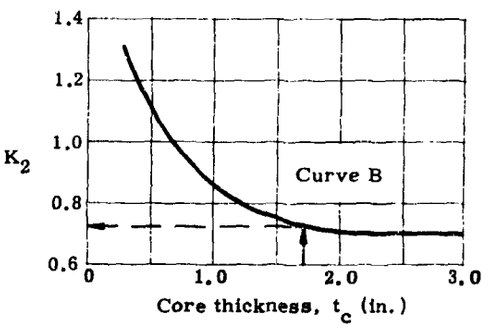

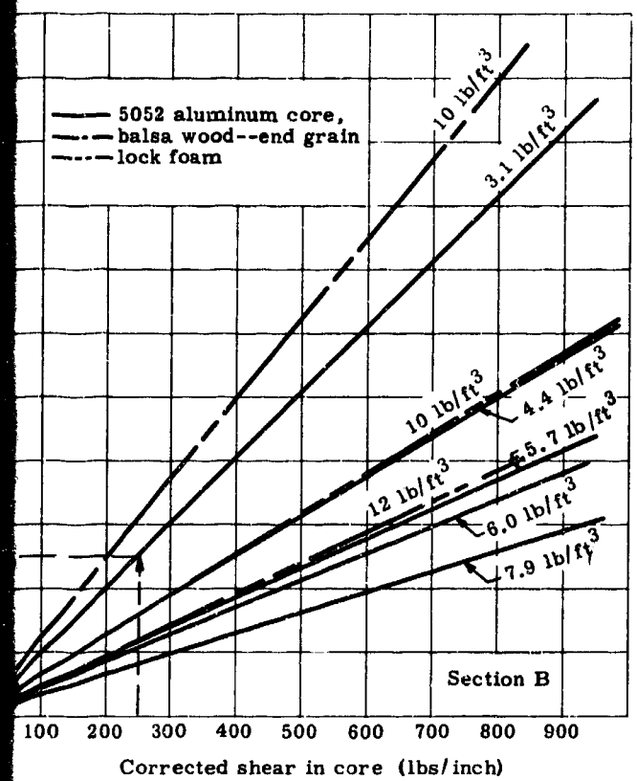

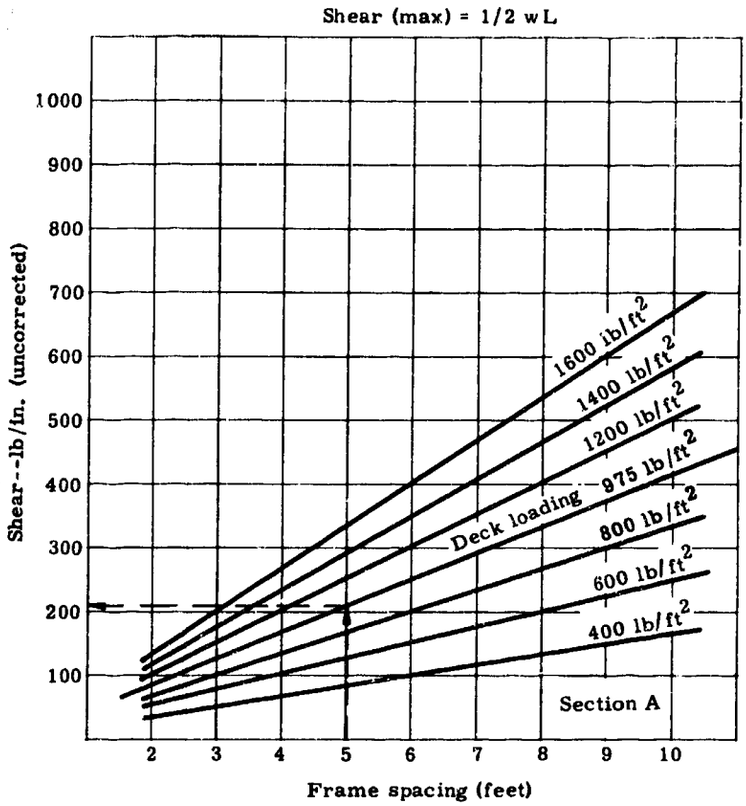

core shear strength

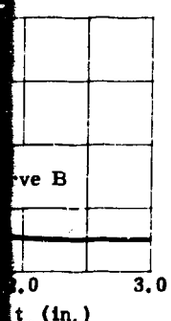

NOTES:

1. The correction factors, K_1 and K_2 are used in determining the corrected shear in aluminum foil core. No correction factor is needed for determining the correct shear for balsa wood or lock foam.
2. The corrected shear for aluminum foil core is determined as follows:
   $S_c = S_u/K_1 \times K_2$
   S_c = corrected shear
   S_u = uncorrected shear
3. Weight of core alone. The weight of core inserts necessary for attachments and splices must be included for total weight.

2

Fig. 5-19. Diagram for Selecting Core Material and Thickness of Sandwich-Type Decking

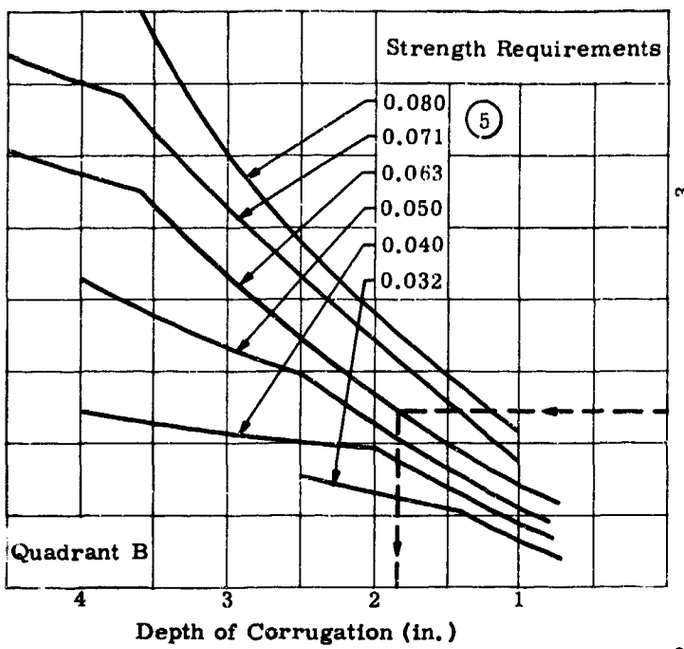
Strength Requirements
0.080
0.071
0.063
0.050
0.040
0.032
5
Quadrant B
4
3
2
1
Depth of Corrugation (in.)

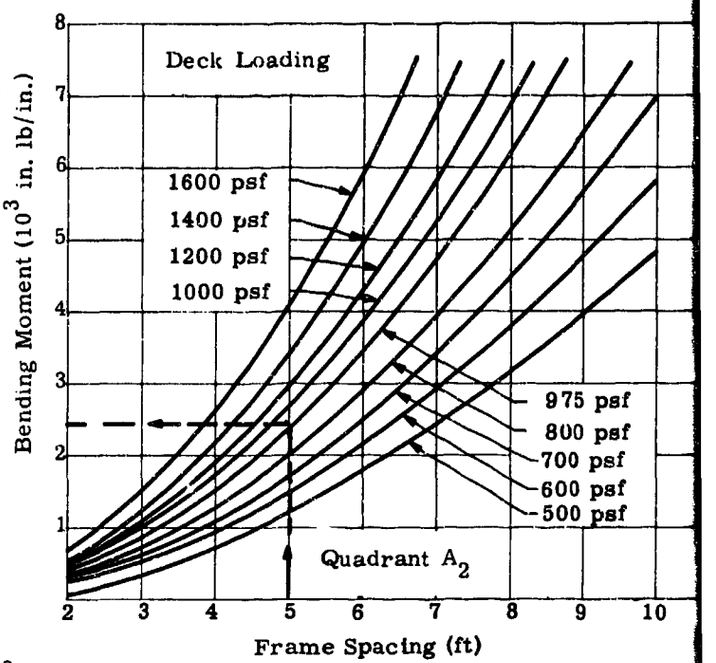
Deck Loading
1600 psf
1400 psf
1200 psf
1000 psf
975 psf
800 psf
700 psf
600 psf
500 psf
Quadrant A_2
Bending Moment (10^3 in. lb/in.)
Frame Spacing (ft)

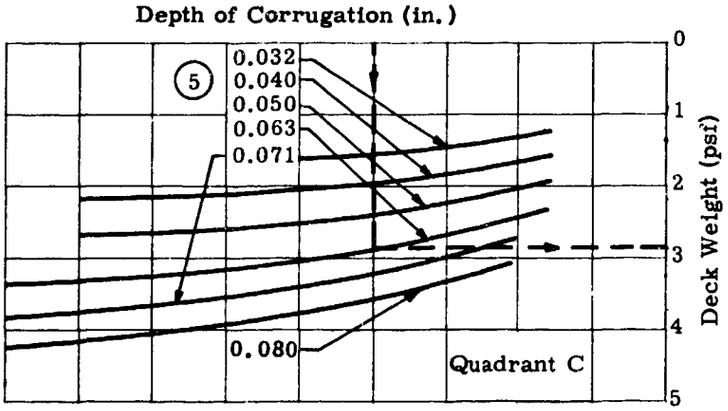
5
0.032
0.040
0.050
0.063
0.071
0.080
Quadrant C
Deck Weight (psf)

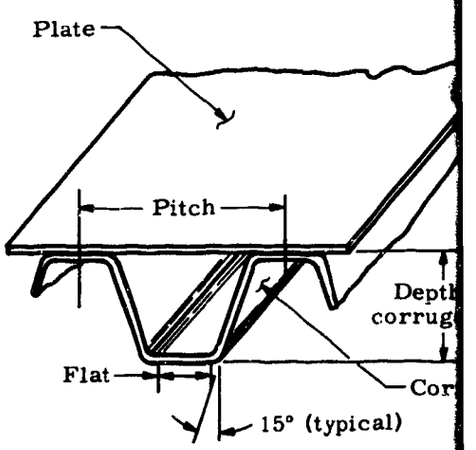
Plate
Pitch
Depth
corrug
Flat
Cor
15° (typical)

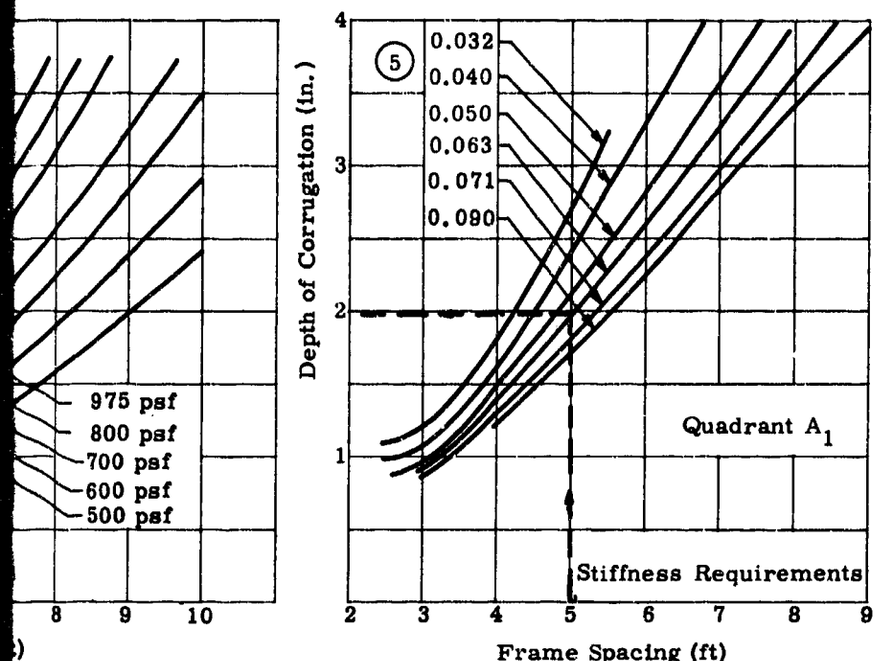

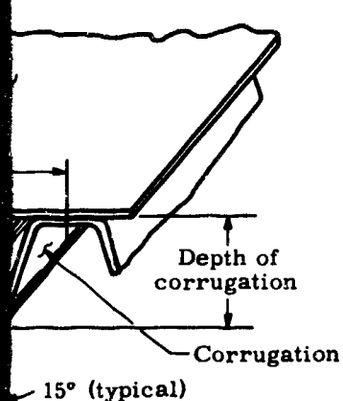

Notes:

1. Curves in Quadrant A_1 are determined from the stiffness criteria, $EI/L^3 = 60$. The moment of inertia used is that of an assumed equivalent section width of 12 in.
2. Curves in Quadrant A_2 are various deck loadings used to determine the bending moment, $M = wL^2/10$.
3. Curves in Quadrant B are used to determine the plate and corrugation and corrugation depth.
4. Curves in Quadrant C are used to determine the deck weight in psf
5. Values are thicknesses of both the plate and corrugation.
6. The dash lines (---) are for the example in the text.

Fig. 5-20. Diagram for Selecting Plate and Corrugated Decking Material--6061-T6 Bare Sheet Aluminum Alloy

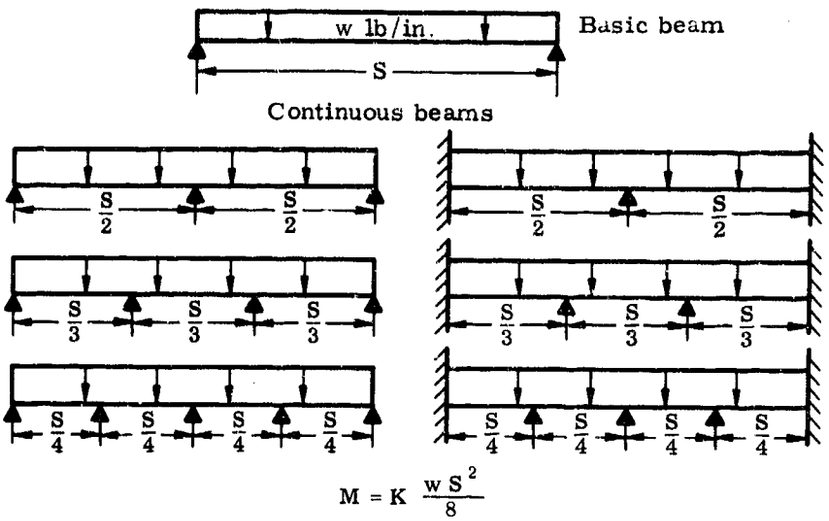

$$M = K \frac{w S^2}{8}$$

$$K = \frac{\text{maximum continuous beam bending moment}}{\text{maximum simply supported beam bending moment}}$$

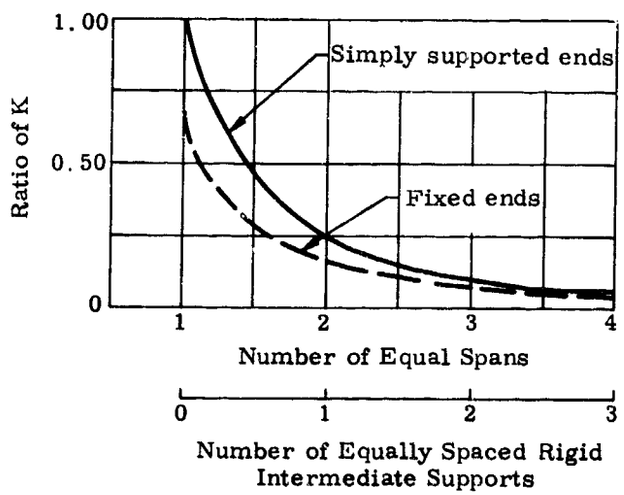

Fig. 5-21. Main Deck Transverse Frame Bending Moment Ratio Variation with Number of Intermediate Supports. Frame Uniformly Loaded over Constant Span S

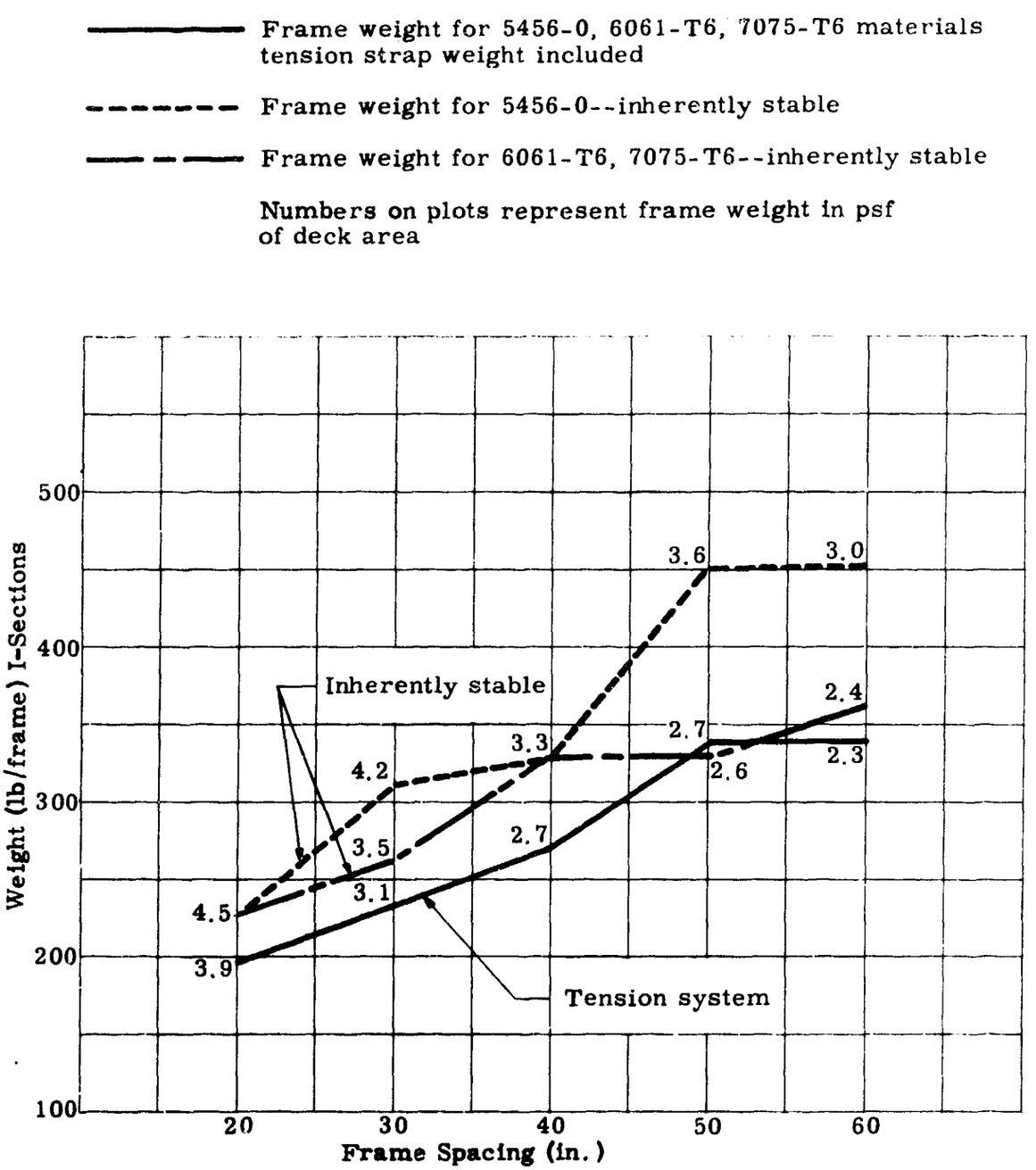

Fig. 5-22. Main Deck Transverse Frame Weight Variation with Frame Spacing--I-Sections

———— Frame weight for 5456-0--tension strap weight included

- - - - - - - Frame weight for 6061-T6, 7075-T6--tension strap weight included

——— — ——— Frame weight for 5456-0--inherently stable

— — — Frame weight for 6061-T6, 7075-T6--inherently stable

Numbers on plots represent frame weight in psf of deck area

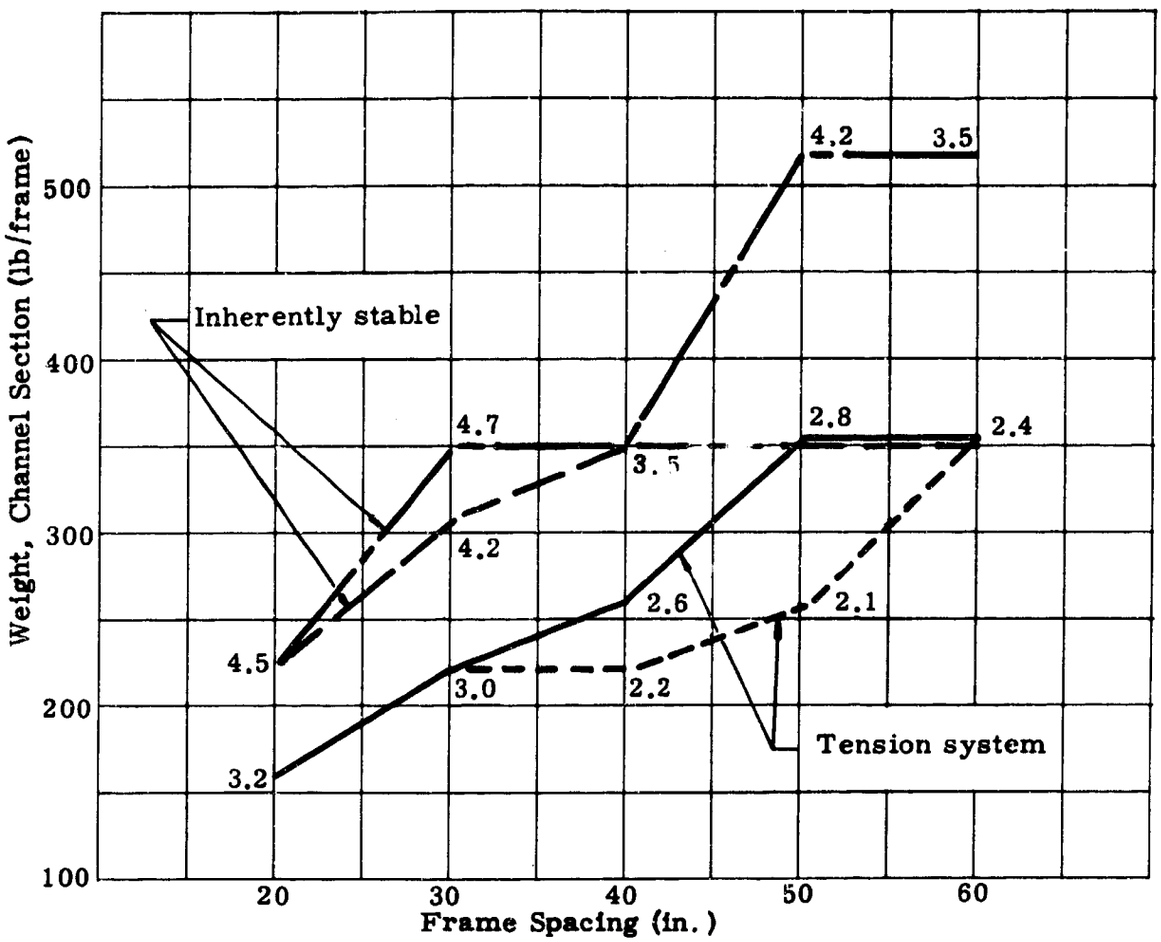

Fig. 5-23. Main Deck Transverse Frame Weight Variation with Frame Spacing--Channel Sections

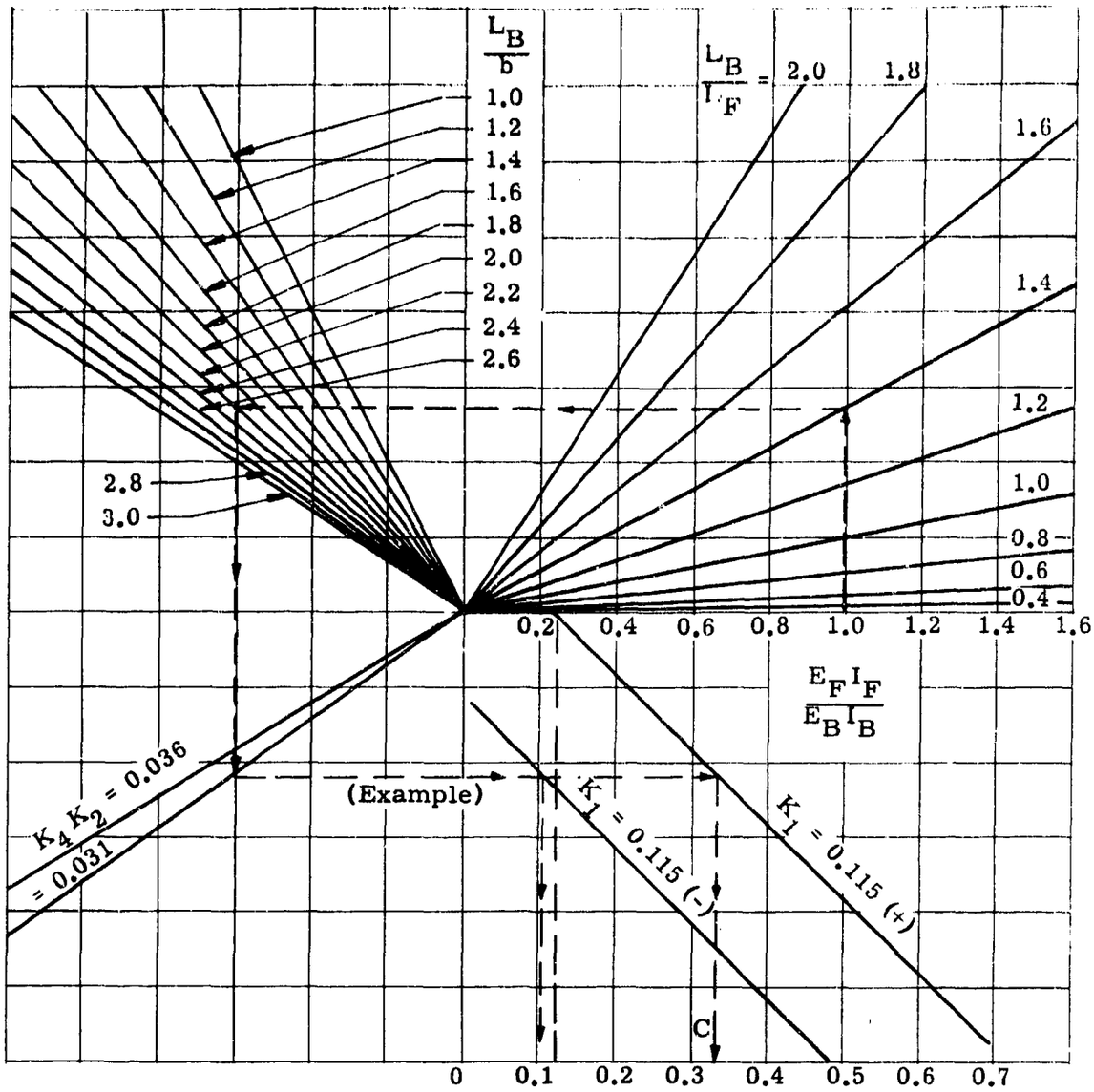

$$M_F = \left[K_1 \pm K_4 K_2 \left(\frac{E_F I_F}{E_B I_B}\right)\left(\frac{L_B}{L_F}\right)^3 \frac{L_B}{b}\right] w_F L_F^2$$

$$M_F = C w_F L_F^2$$

Fig. 5-24. Continuous Frame Bending Moments Due to Main Deck Load and a Deflected Support

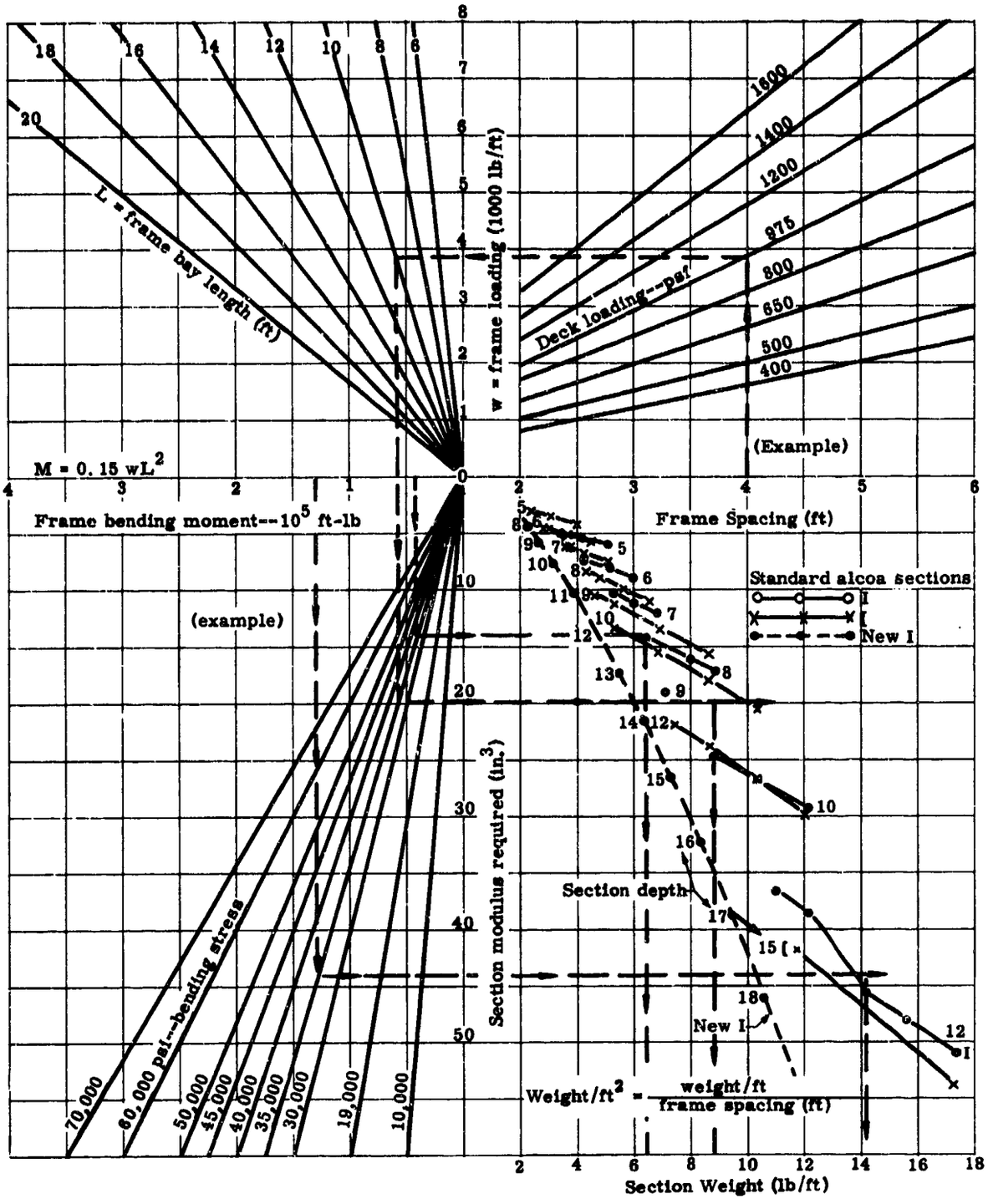

Allowable Crippling Stress due to Bending

	5456-0	6061-T6	7075-T6	6066-T6
Amer. Std. I-	19,000	35,000	70,000 psi	--
New I	19,000	35,000	45,500	45,000

Fig. 5-25. Transverse Frame Bending Strength Requirements

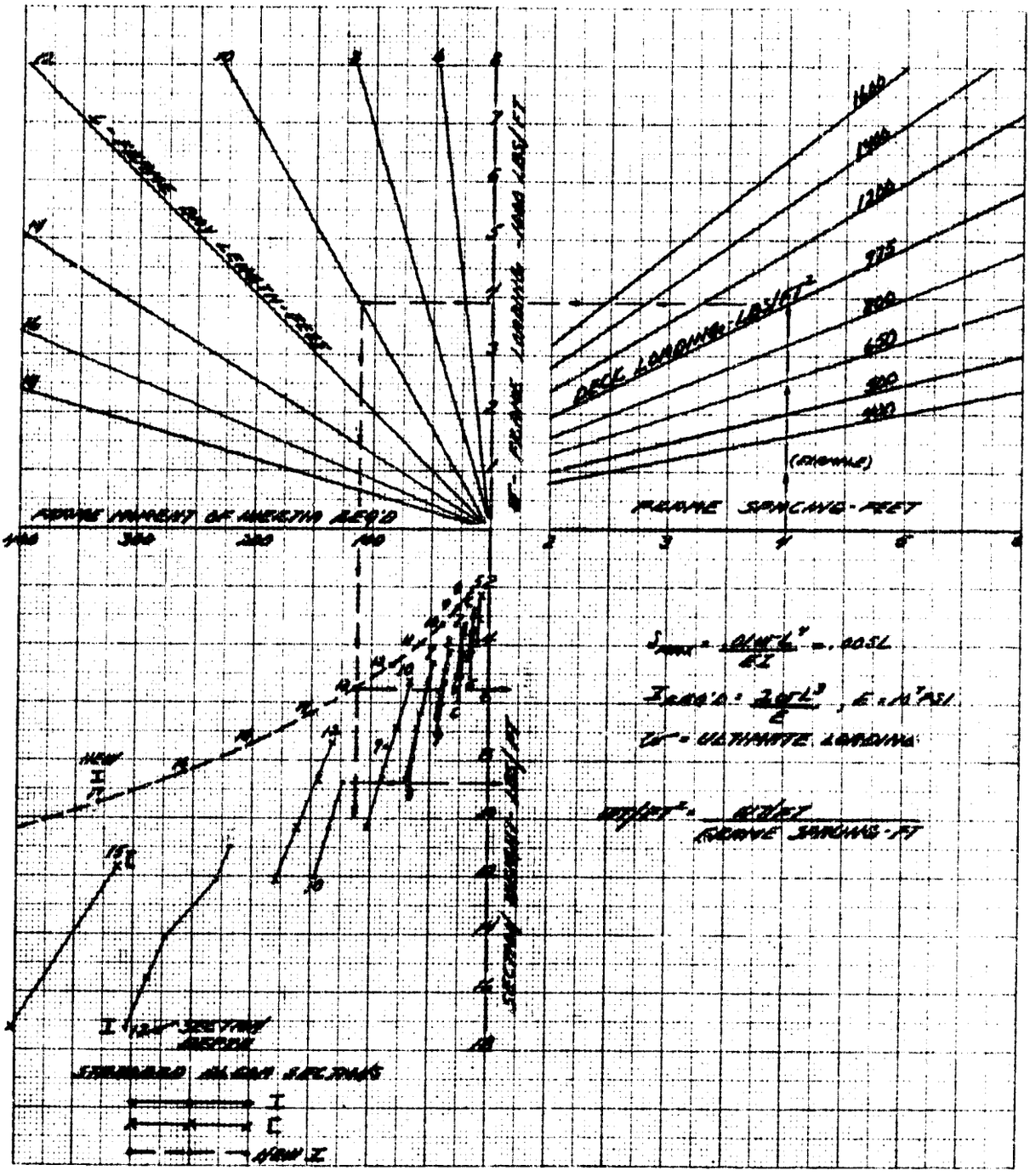

Fig. 5-26. Transverse Frame Deflection Requirements Maximum Deflection = 0.005L (ultimate)

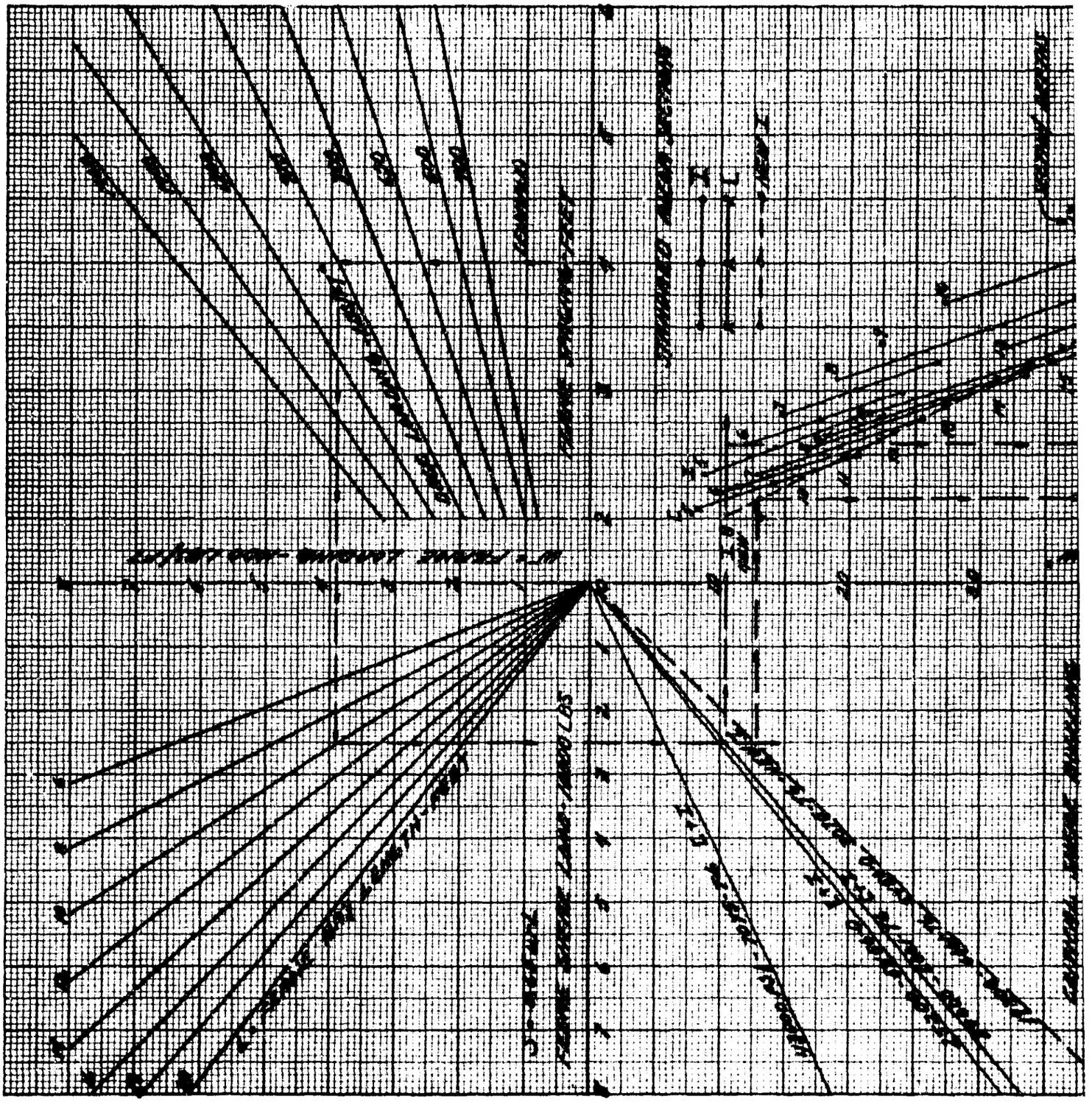

Fig

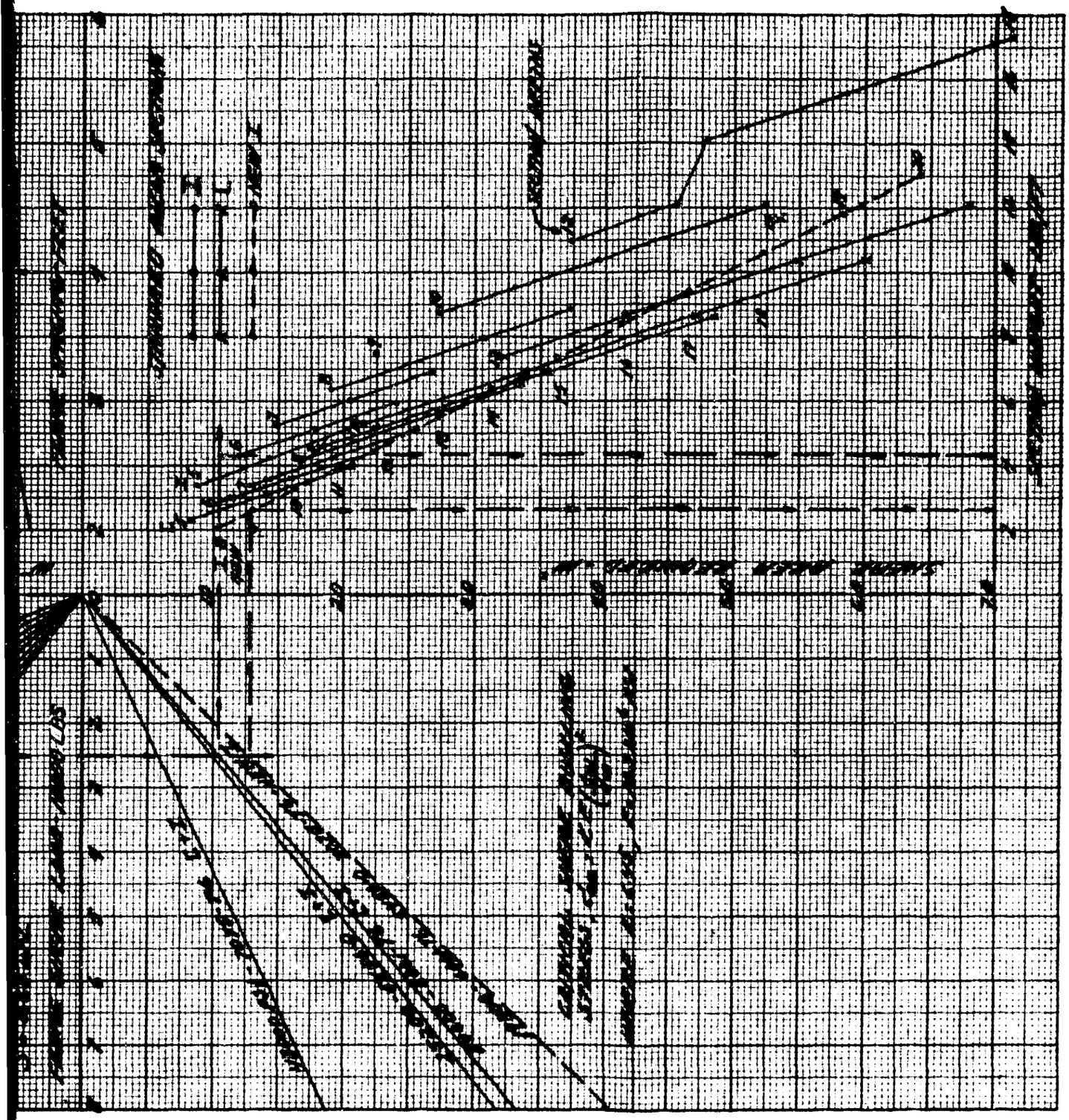

Fig. 5-27. Transverse Frame Shear Buckling Requirements

Deck loading = 975 psf
Frame material--5456-0
Deck material--5456-0 or 6061-T6
American standard frame sections
Frame sections assumed laterally stabilized

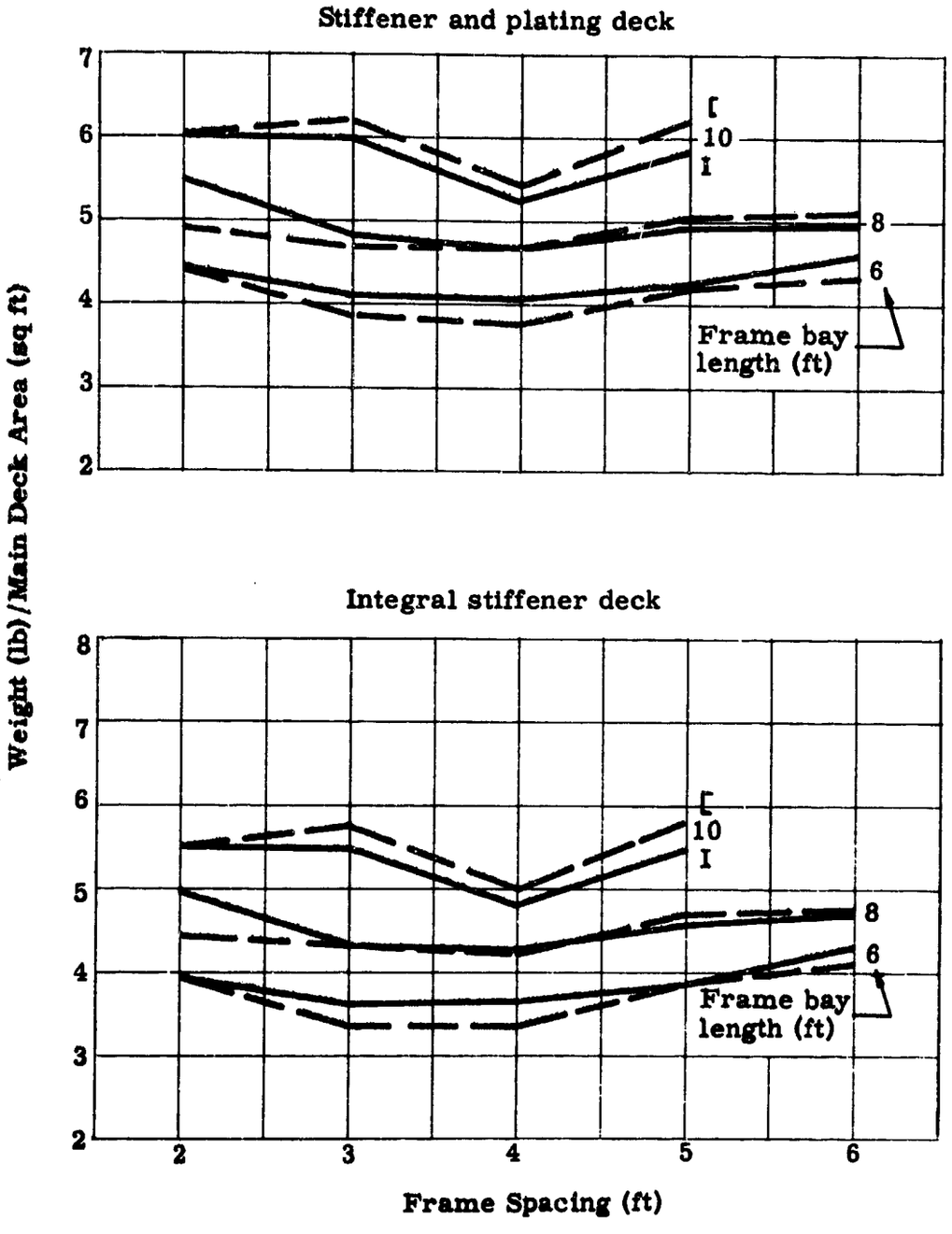

Fig. 5-28. Total Weight Variation of Transverse Frame and Main Deck with Transverse Frame Spacing

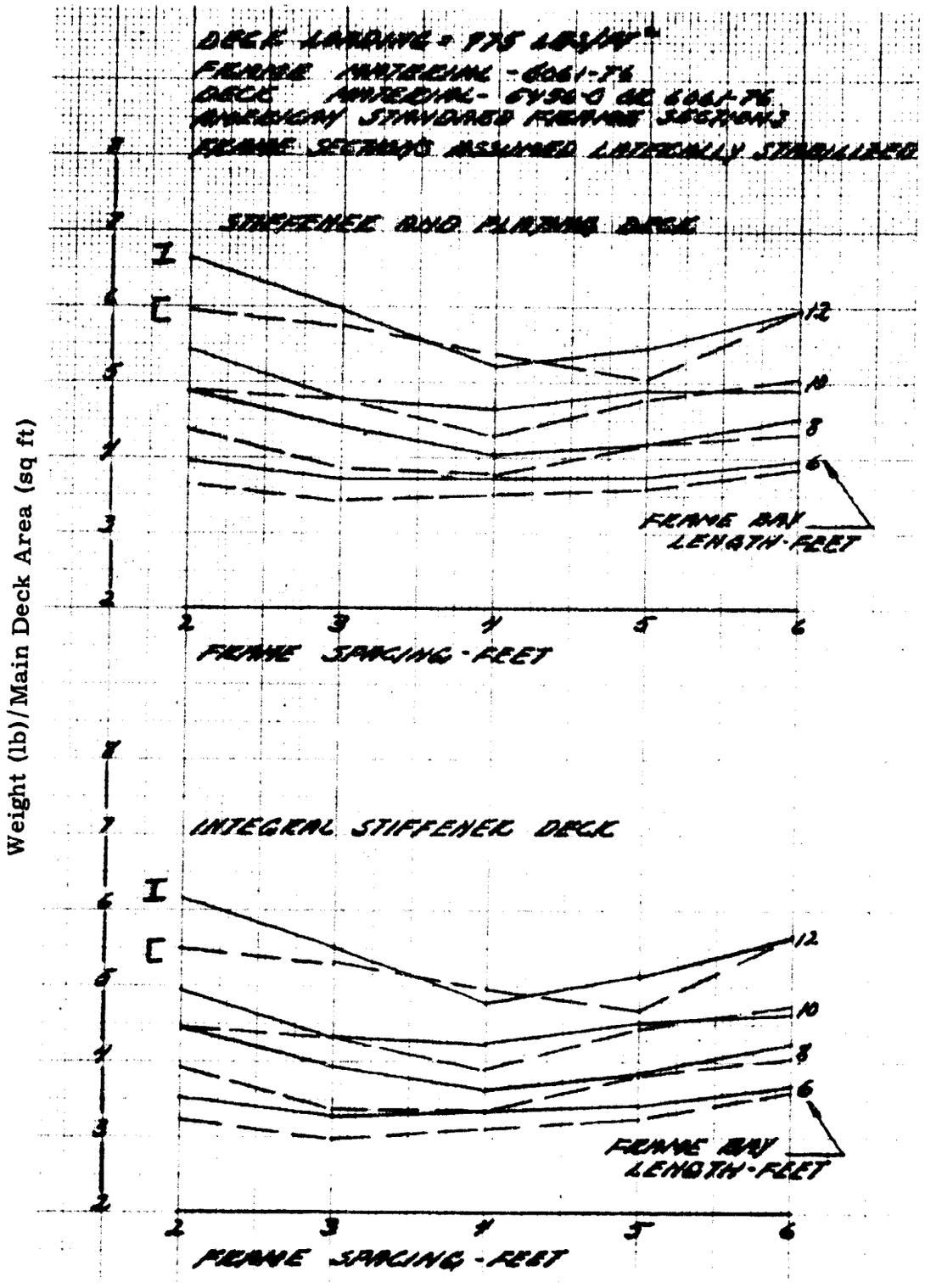

Fig. C - Fig. 5-29. Total Weight Variation of Transverse Frame and Main Deck with Transverse Frame Spacing with

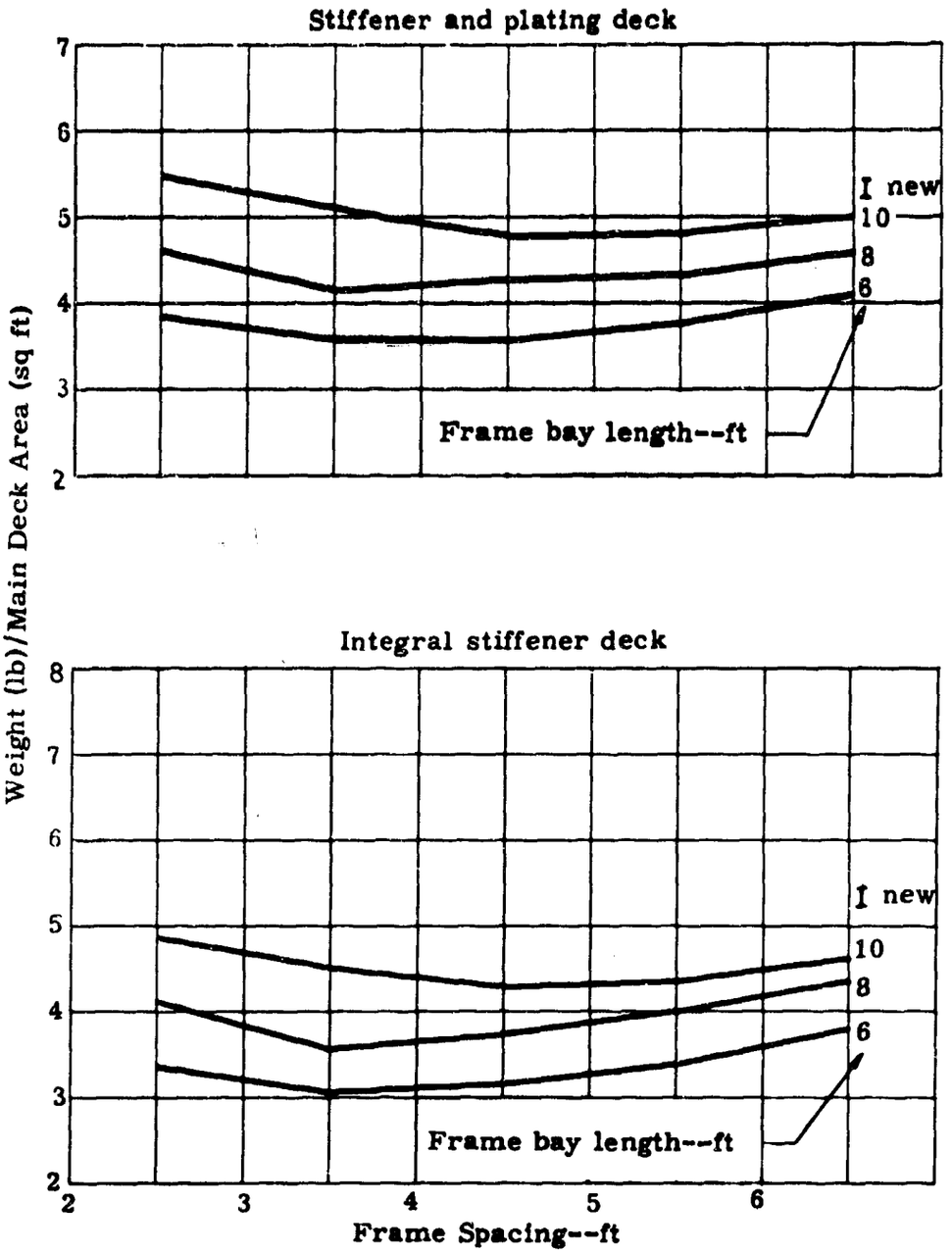

Fig. 5-30. Total Weight Variation of Transverse Frame and Main Deck with Transverse Frame Spacing

Deck loading--975 psf

Frame material--6061-T6

Deck material--5456-0 or 6061-T6

New I section--frame sections assumed laterally stabilized

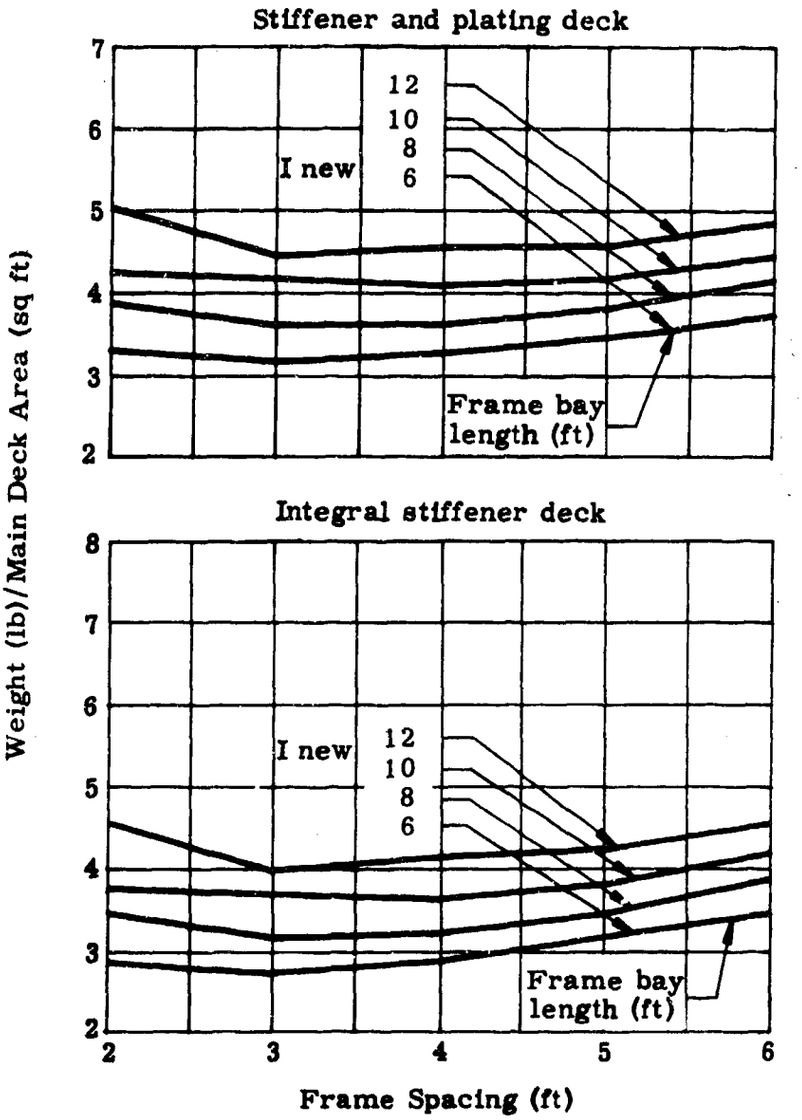

Fig. 5-31. Total Weight Variation of Transverse Frame and Main Deck with Transverse Frame Spacing

Deck loading = 975 psf
Frame material = 7075-T6
Deck material = 5456-0 or 6061-T6
New I-section
Frame sections assumed laterally stabilized

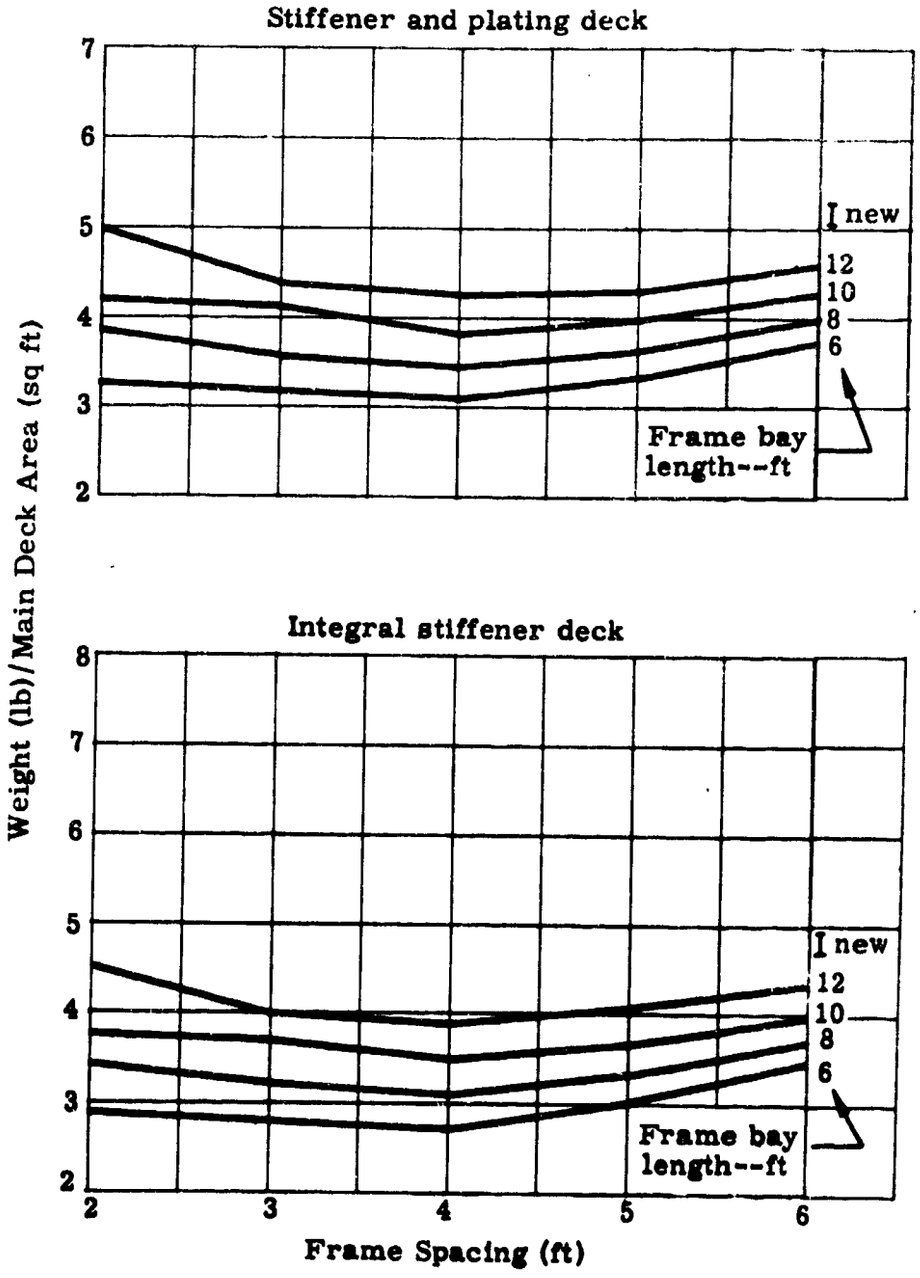

Fig. 5-32. Total Weight Variation of Transverse Frame and Main Deck with Transverse Frame Spacing

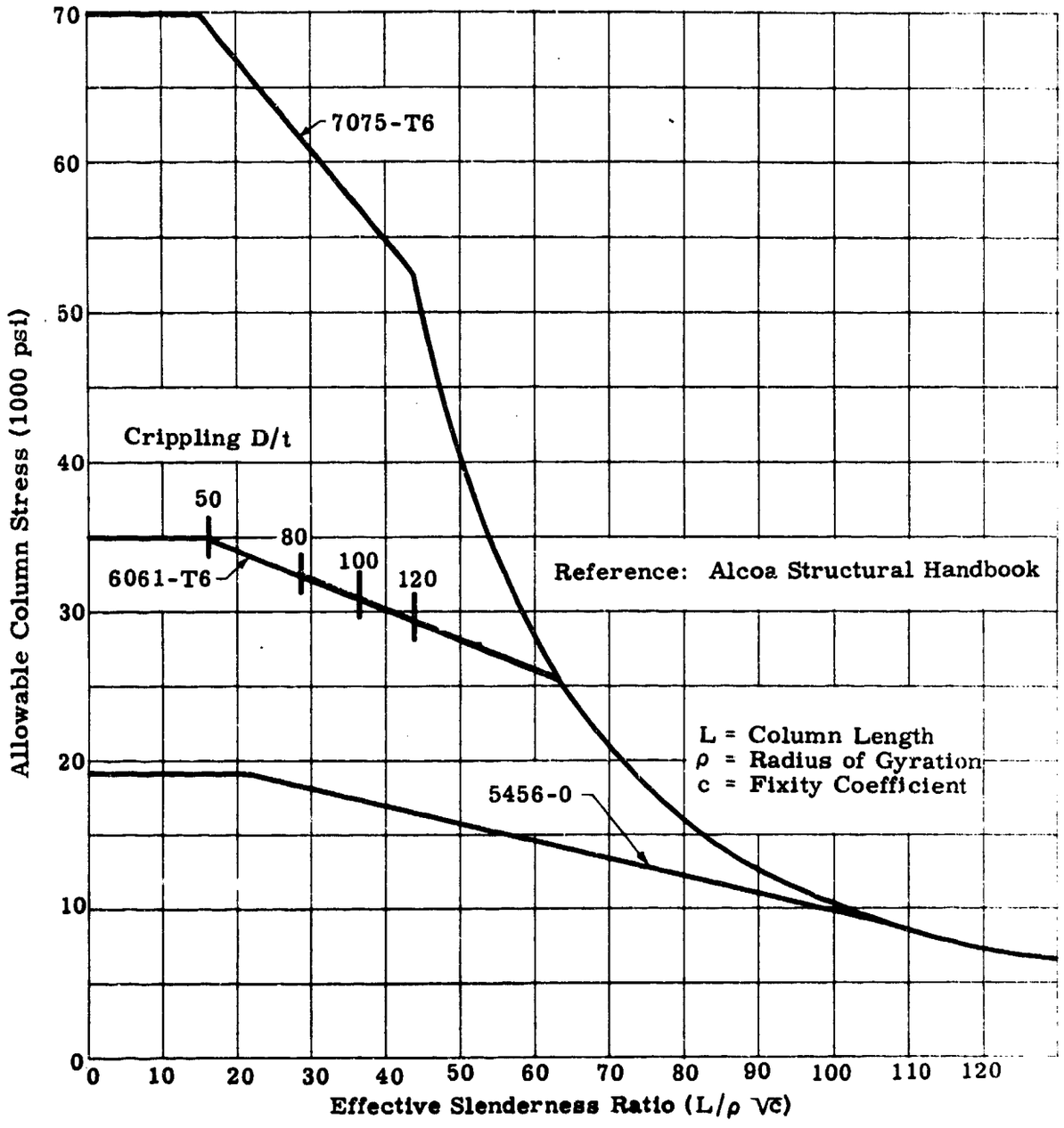

Fig. 5-33. Allowable Column Stress-Extruded Shapes

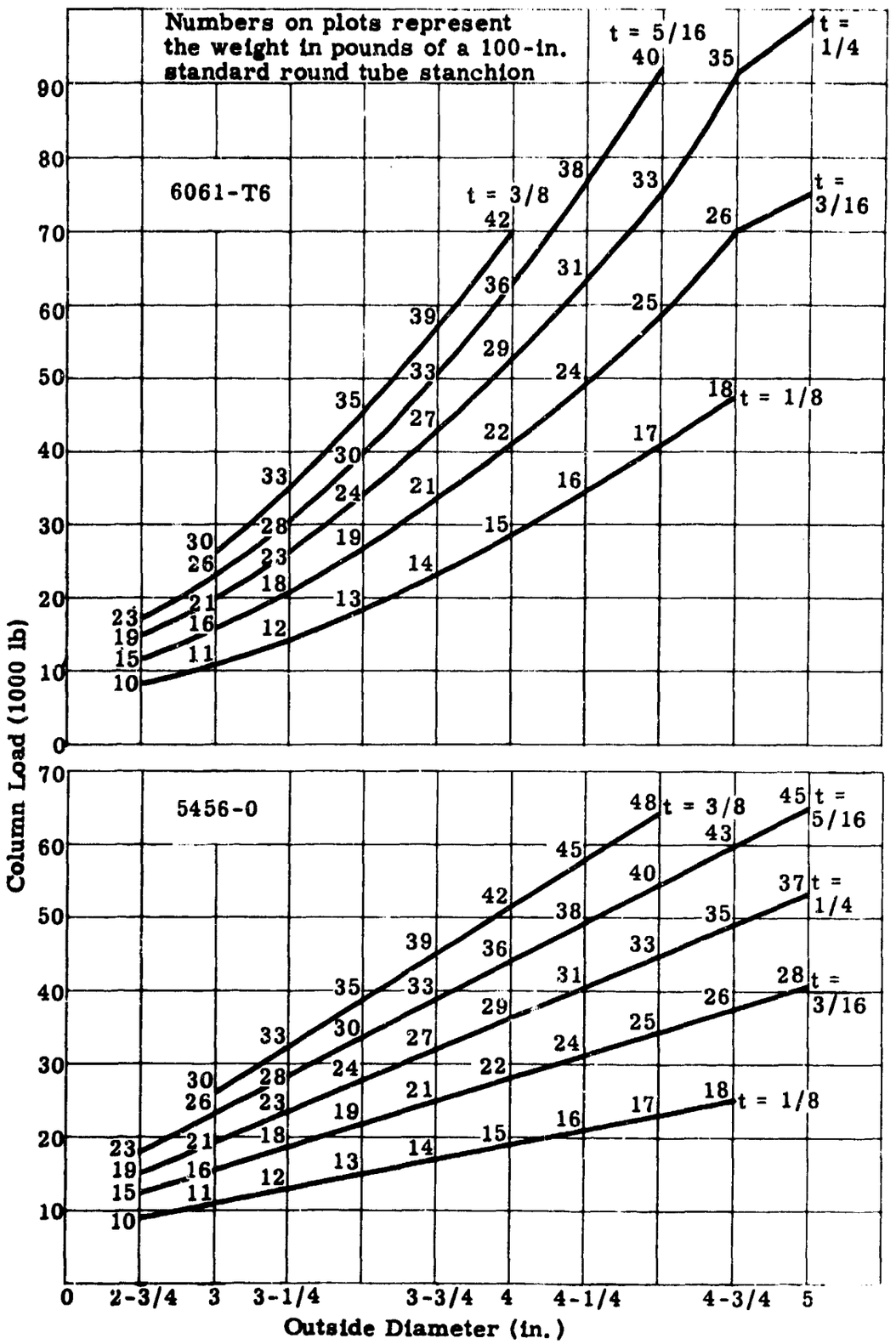

Fig. 5-34. Allowable Stanchion Round Tube Column Load-Pin-Fuded Column--100 in. Length

Design Factors	Plate and Stringer	Machined Plate	Honeycomb	Integral Extrusion
Handling problems	2	4	3	1
Water leakage susceptibility	1	1	2	1
Repairability	1	1	2	1
Machining costs	1	3	2	1
Flatness	3	1	2	4
Fabrication costs riveting, bonding, etc.	4	2	3	1

1 = Best

4 = Worst

Fig. 5-35. Relative Comparison of Manufacturing Methods

I Plating gage = 0.090 6061-T6
Stringer spacing 6.00 in.
Frame spacing 2.5 ft
Longitudinal beam 12 x 17.28 lb I-section
Weight 2.49 psf

II Plating gage = 0.090 6061-T6
Stringer spacing 6.00 in.
Frame spacing 3.75 ft
Longitudinal beam 12 in. x 17.28 lb I-section
Weight 2.63 psf

III Plating = 0.090 6061-T6
Stringer spacing 6.00 in.
Frame spacing 5.00
Longitudinal beam 12 in. x 17.28 lb I-section
Weight 2.87 psf

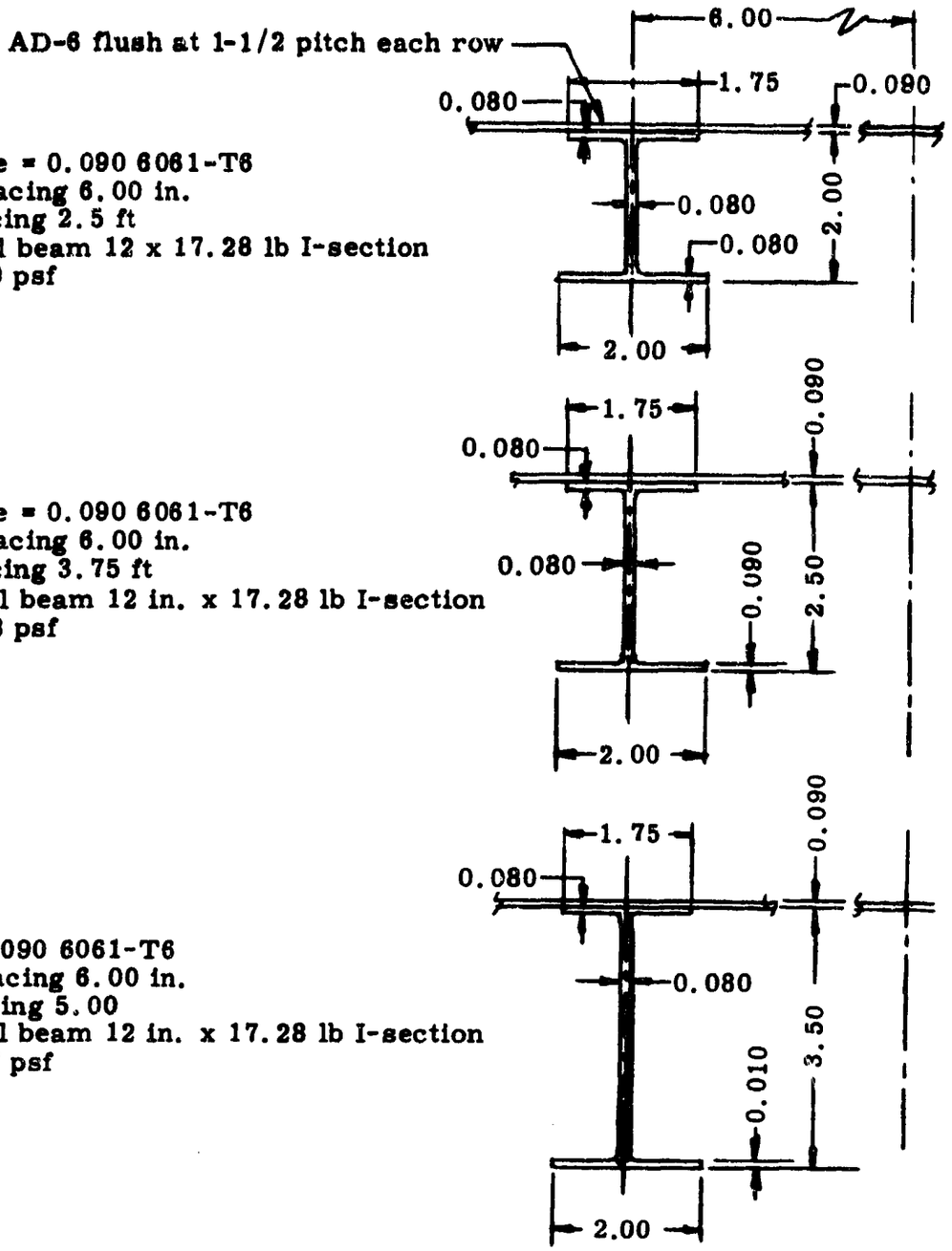

Fig. 5-36. Plate--Stringer Design--Rivet and Bonded, Use FM-47 Bond

I	Plate Thickness	0.090 6061-T6
	Stringer Spacing	6.00 in.
	Frame Spacing	2.50 ft
	Longitudinal Beam	12 in. x 17.28 lb I-beam
	Weight	2.08 psf

II	Plate Thickness	0.090 6061-T6
	Stringer Spacing	6.00 in.
	Frame Spacing	3.75 ft
	Longitudinal Beam	12 in. x 17.28 lb I-beam
	Weight	2.22 psf

III	Plate Thickness	0.090 6061-T6
	Stringer Spacing	6.00 in.
	Frame Spacing	5.00 ft
	Longitudinal Beam	12 in. x 17.28 lb I-beam
	Weight	2.46 psf

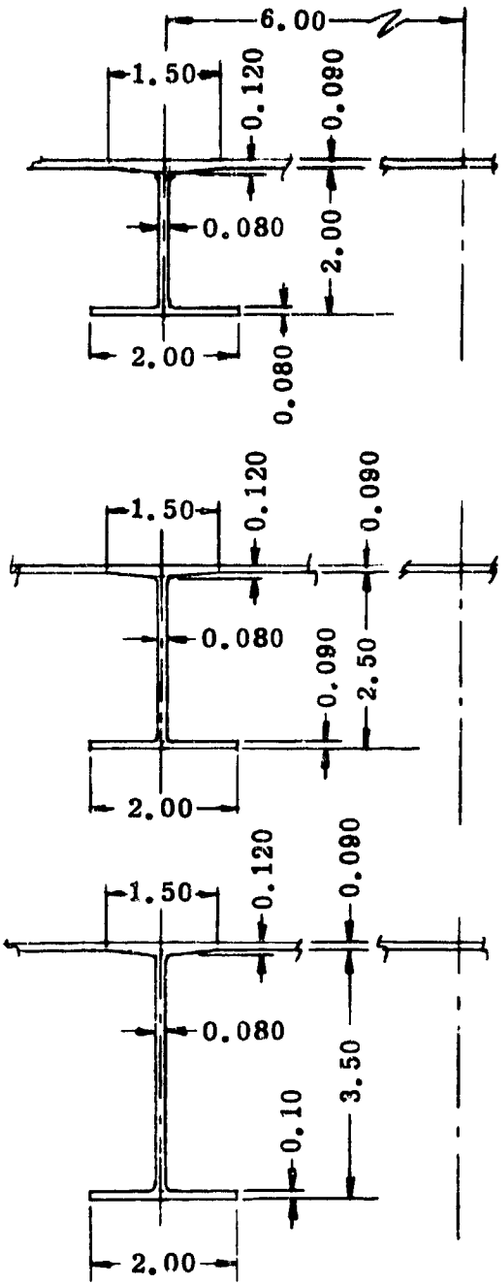

Fig. 5-37. Plate Stringer Design Integrally Stiffened Extrusion

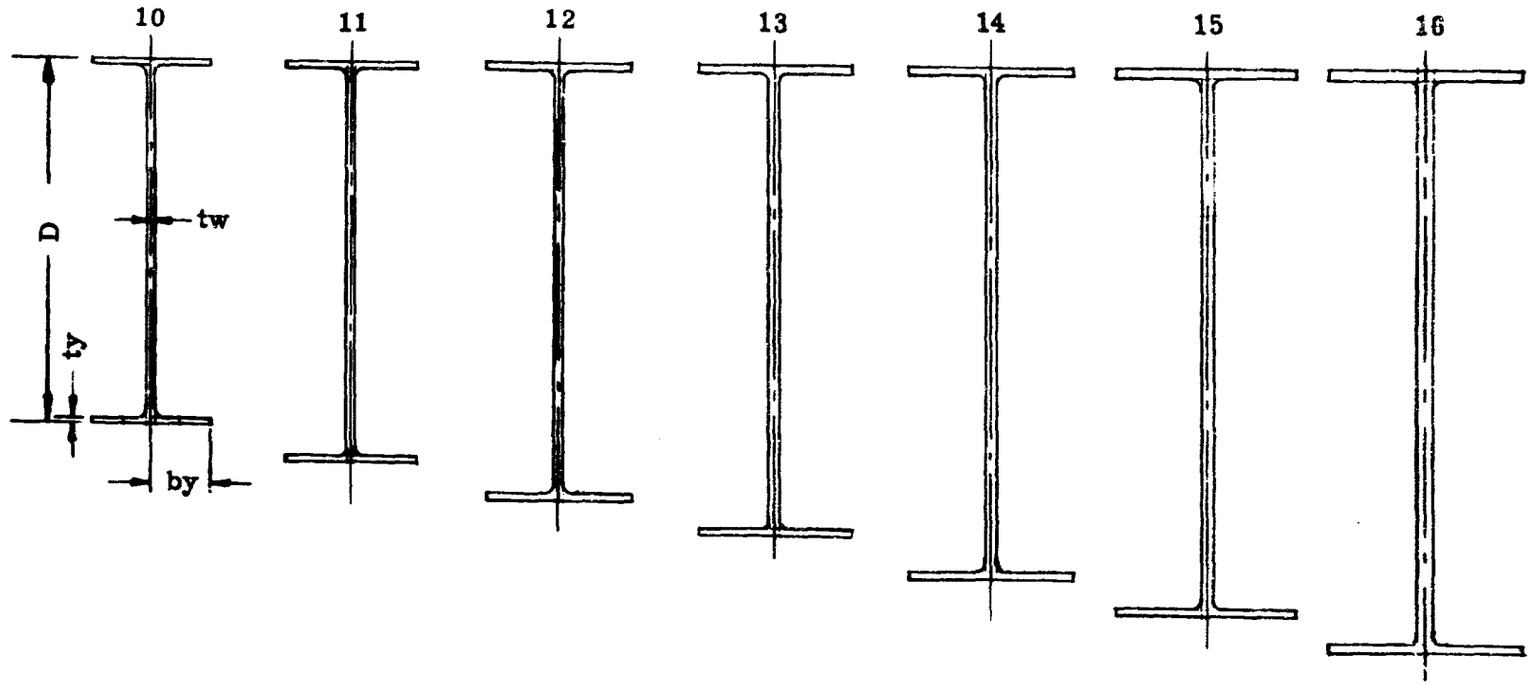

D	tw and ty	by	weight
10	0.167	1.67	3.28
11	0.183	1.83	3.95
12	0.200	2.00	4.70
13	0.217	2.17	5.54
14	0.233	2.33	6.40
15	0.250	2.50	7.35
16	0.267	2.67	8.38

	$M = 0.125\ wl^2$	$= 0.125\ Pbd^2$	$= 122\ bh^2$	$p = 975$ psf
	5 ft	3.75 ft		2.50 ft
L-8	12 x 4.70	11 x 3.95		10 x 3.28
L-9	13 x 5.54	12 x 4.70		11 x 3.95
L-10	14 x 6.40	13 x 5.54		12 x 4.70
L-11	15 x 7.35	14 x 6.40		13 x 5.54
L-12	16 x 8.38	15 x 7.35		14 x 6.40

Fig. 5-38. Deck Supporting Structure (special I-beams)

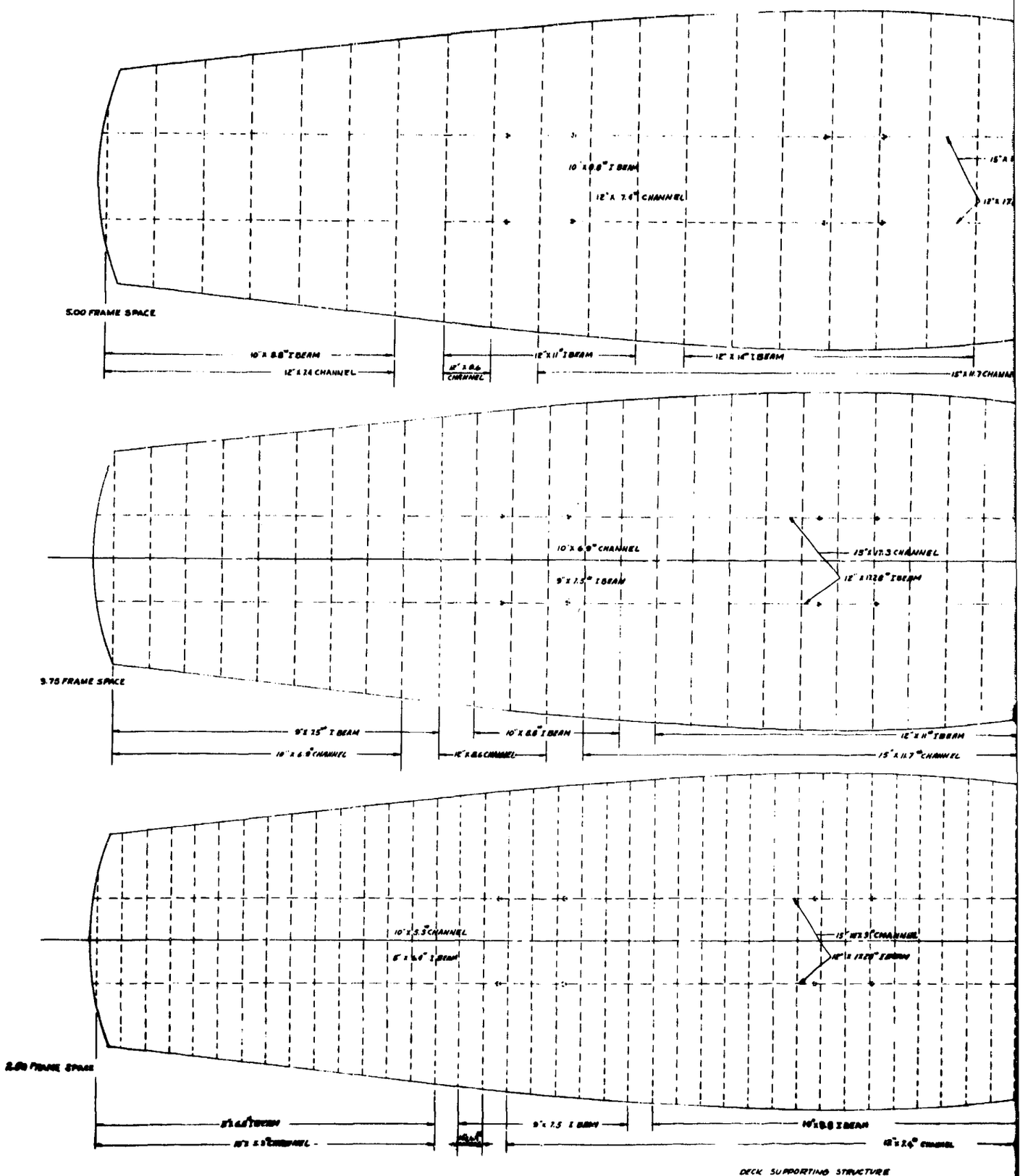

DECK SUPPORTING STRUCTURE
(STANDARD I BEAM & CHANNEL)

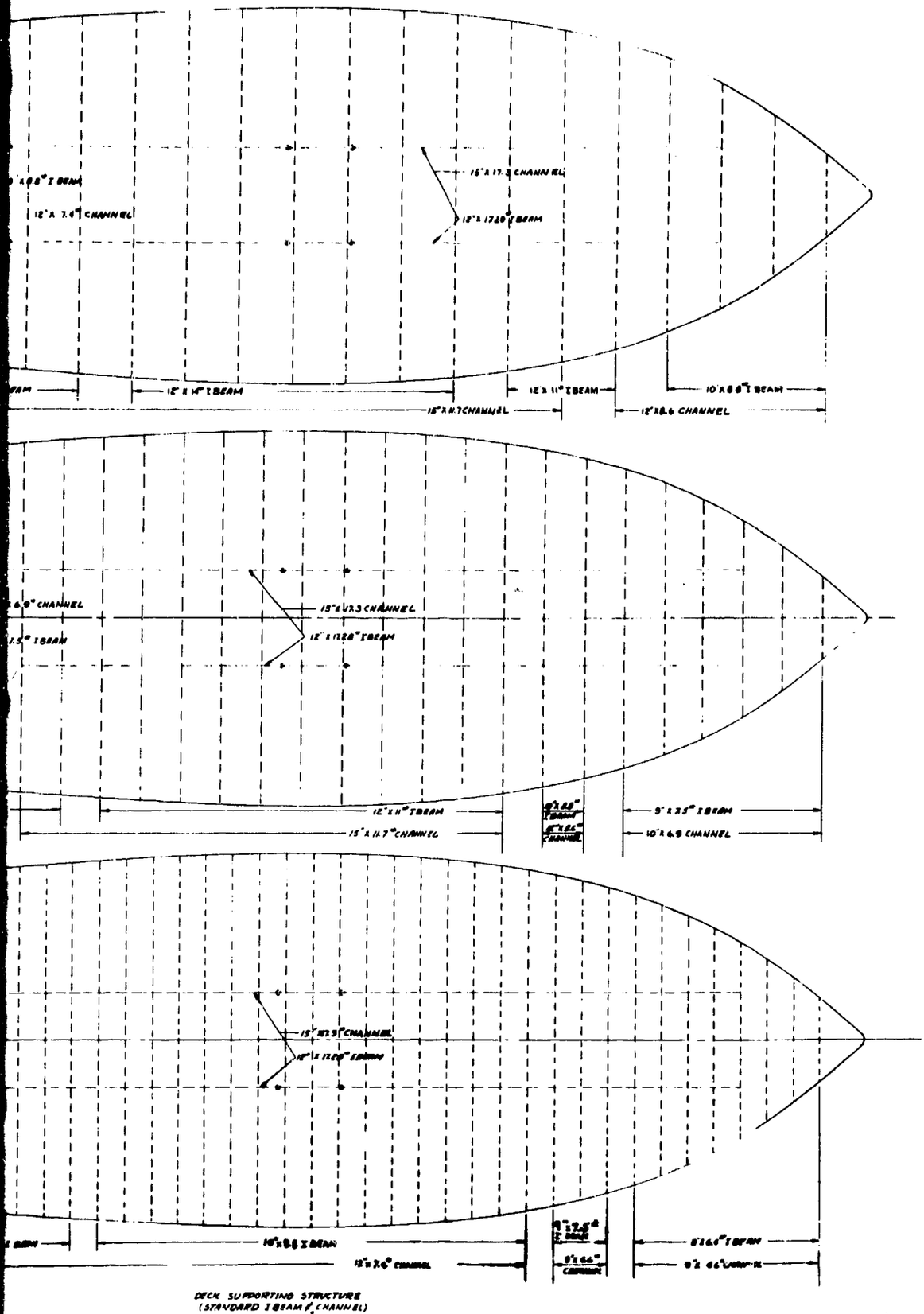

Fig. 5-39. Deck Support Structure (standard I-beam and channel)

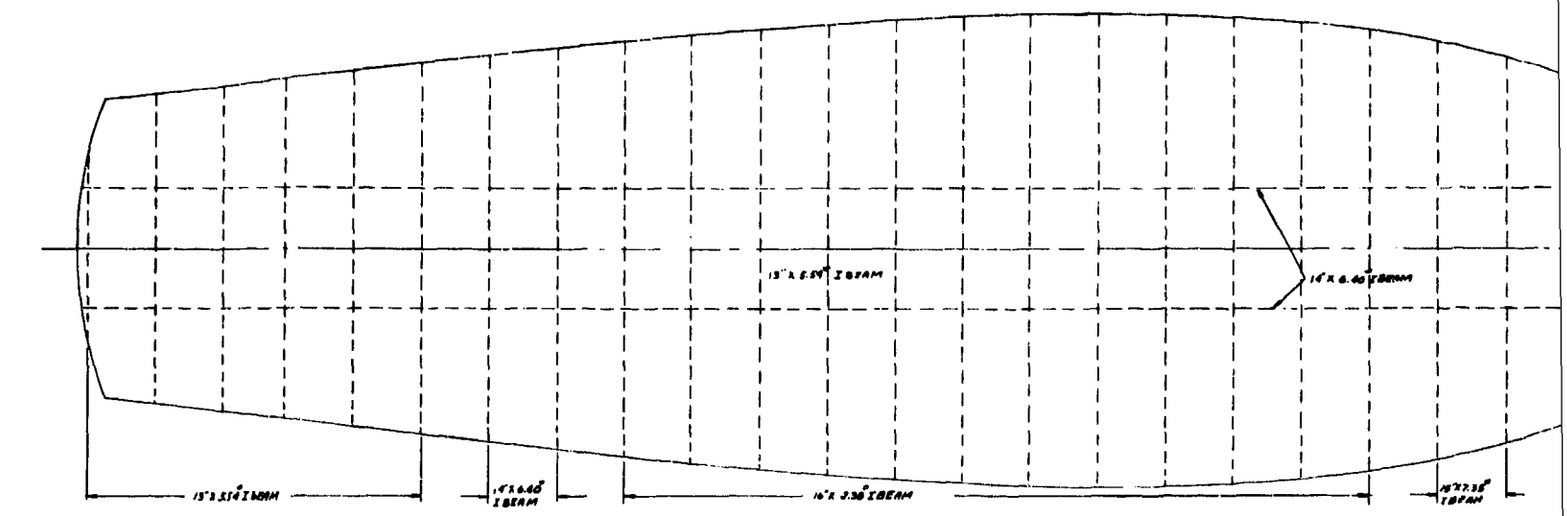

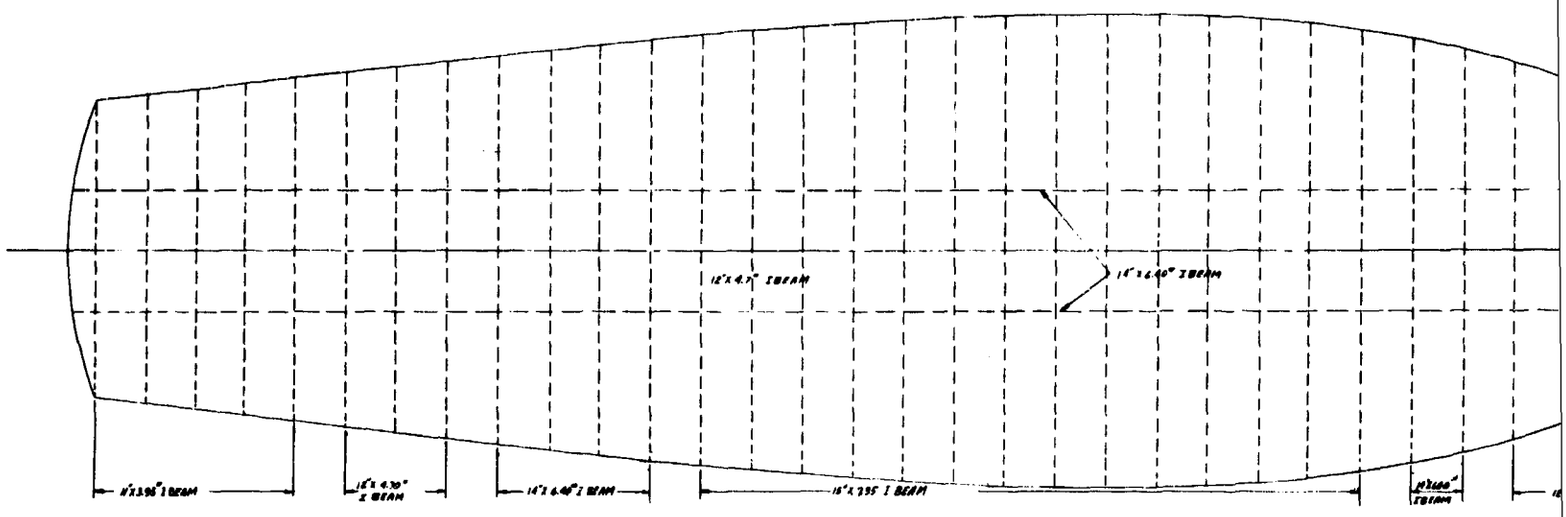

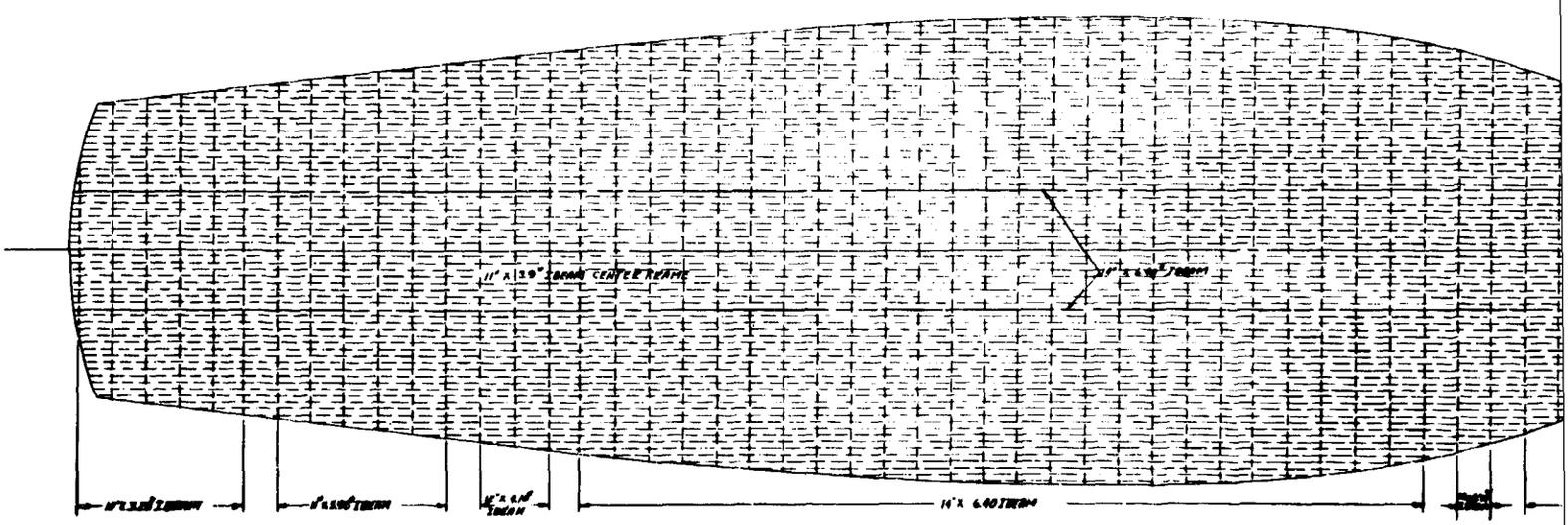

DECK PLATE STRUCTURE
(SPECIAL I BEAM)

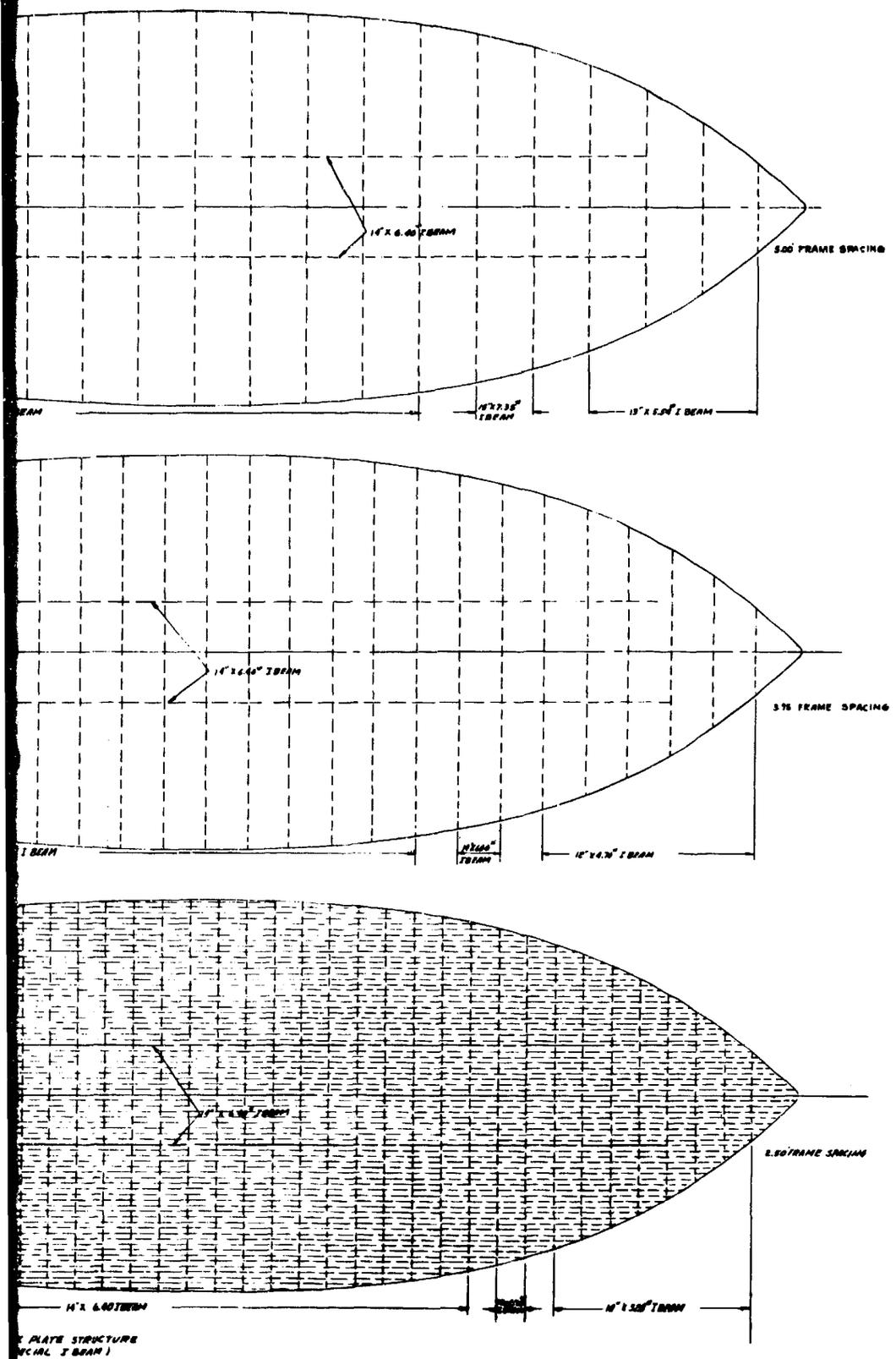

Fig. 5-40. Deck Plate Structure (special I-beam)

2

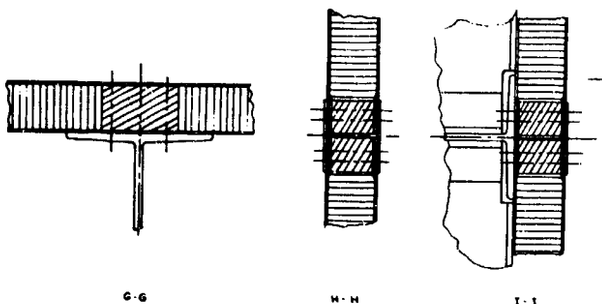

G-G
FACES .060 CORE 1/16 CELL .001 FOIL TOTAL THICKNESS 1.85
SCALE 1½" = 1"

H-H

I-I
Z-Z SIMILAR

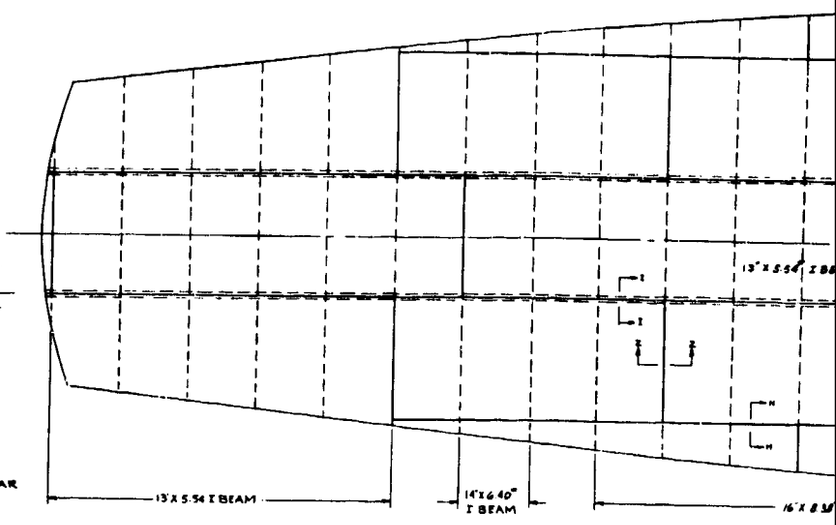

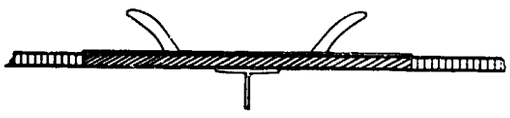

K-K
TYPICAL ATTACHMENT OF DECK FITTING HARDWARE
SCALE 1½" = 1"

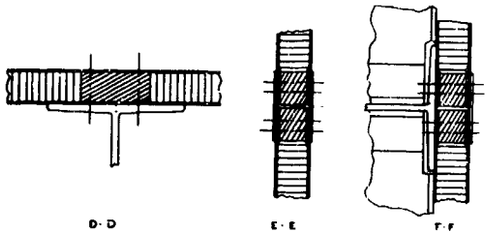

D-D

E-E

F-F
FACES .060 CORE 1/16 CELL .001 FOIL TOTAL THICKNESS 1.25
SCALE 1½" = 1"
Y-Y SIMILAR

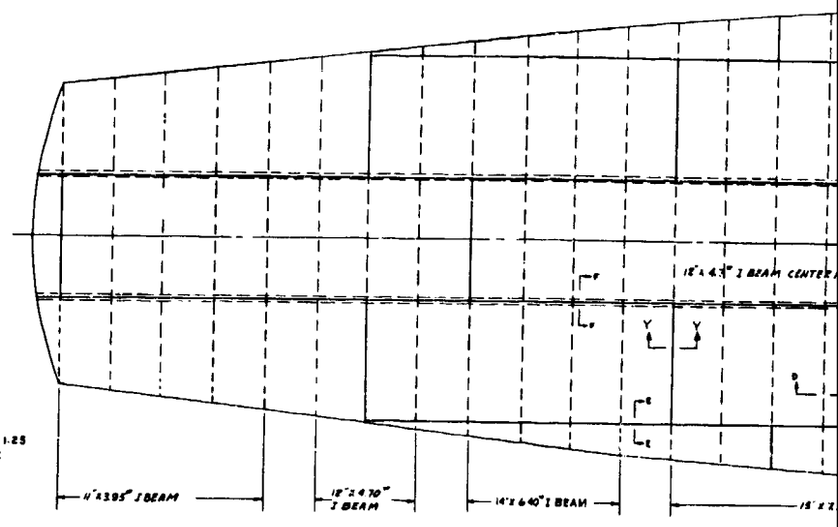

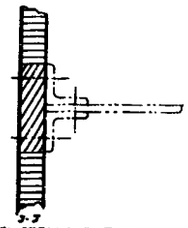

J-J
TYPICAL ATTACHMENT OF SUPER-STRUCTURE

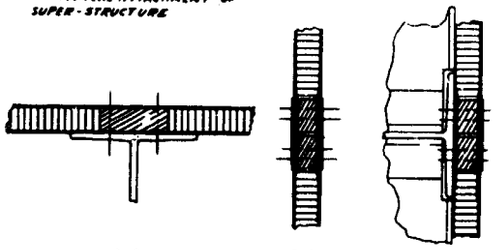

A-A
FACES .060 CORE 1/16 CELL .001 FOIL TOTAL THICKNESS 1.00
SCALE 1½" = 1"

B-B

C-C
R-R SIMILAR

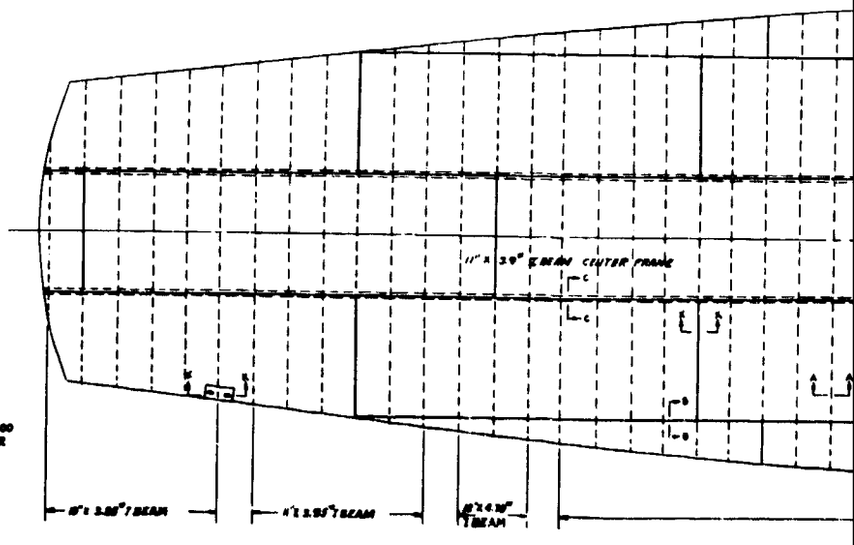

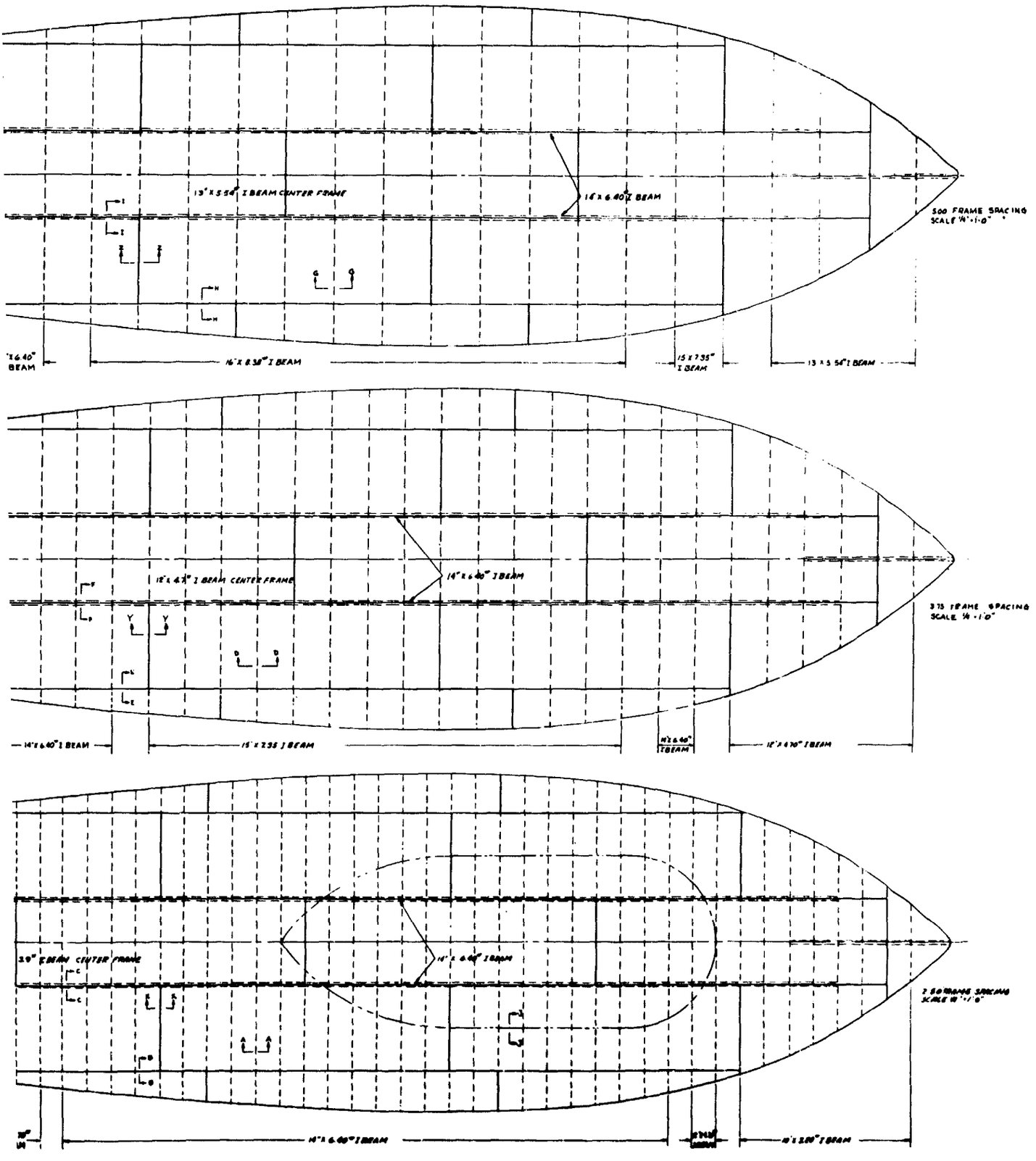

Fig. 5-41. Deck Plate Structure (honeycomb)

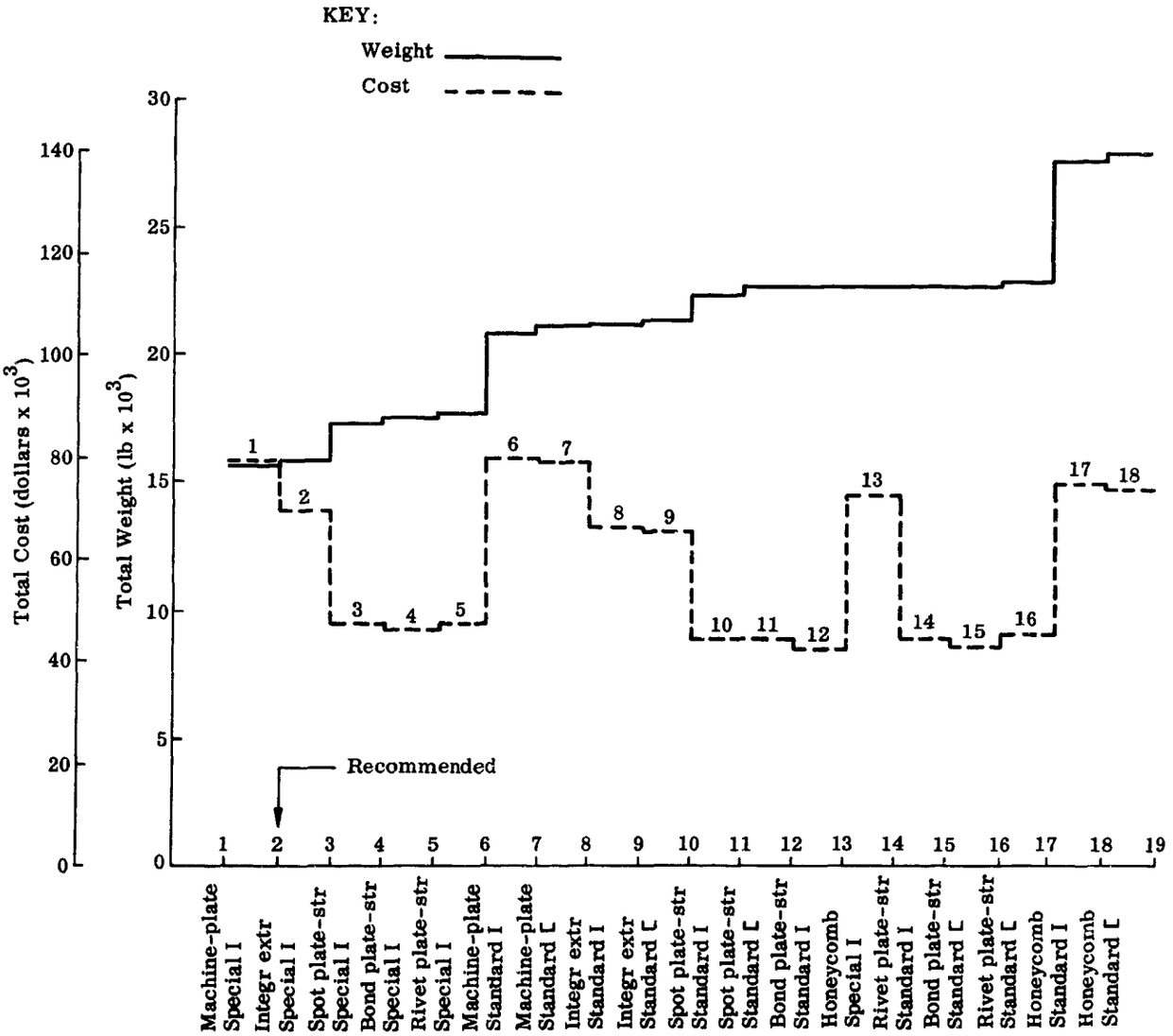

Types of Structure (6061 material)--See Figs. 5-36 to 5-41

Fig. 5-42. Weight and Cost Relationship for Different Types of Decking and Supporting Structure at 3.75-Foot Frame Spacing

6.0 CONCLUSIONS AND RECOMMENDATIONS

A rational method of determination of structural design criteria for hydrofoil ships has been developed. Although the particular analyses are based upon specific environment and example ship design characteristics, the specific results of the study may also have general application. It is concluded that:

(1) A rational estimate of pressure and load occurrence can be developed for both hullborne and foilborne operational modes of a specific hydrofoil ship design.

(2) The magnitude of the pressures and loads can be represented as a continuous function of the cumulative number of occurrences.

(3) Seaplane experience confirms the need for rational determination of the loadings on a statistical basis.

(4) Low dead rise angles on the hull (5° to 6°) lead to extreme pressures and loads which make landing a critical condition for the overall strength of the hull as well as for the local hull bottom.

(5) At moderate hull dead rise (12° to 17°) the critical condition for overall hull bending is the fatigue life in the hullborne conditions.

(6) The forward portion of the hull structure may be critical for either yielding to occasional loads (permanent set) or fatigue failures under the cumulative occurrence of lesser loadings, depending upon the material characteristics.

(7) The midship and after hull bottom structure is critical for the permanent set criteria.

(8) A controlled load factor submerged foil system will not generate critical vertical loads in the hull if the foil arrangement does not cause excessively large 1-g moment in the flight condition.

(9) Substantial side loads are generated on the struts in passing through wave systems. Unless the response of the hull can alleviate these loading conditions, the side load experienced on a strut may be from 3 to 7 times the side loads required for steady turn.

(10) Increase in foilborne speed from 45 to 100 kn tends to make all regions of the hull structure critical for the landing loads rather than hullborne, particularly at low dead rise angles.

There are many more detailed conclusions which might be drawn from the analyses. However, it must be noted that the study has been primarily directed to a limited evaluation of a method for development of structural design criteria

for hydrofoil ships. The next steps in this criteria development should be experimental and operational evaluation of some of the critical areas in the analysis. Three items in particular would seem to require experimental work and one, operational experience.

(1) Low dead rise is desirable from a performance standpoint but theoretically yields extreme pressures and loads on impact. The possibility of lower-than-theoretical peak pressures, low average effective pressure and local structural response have been noted, but there is a lack of experimental confirmation. It is recommended that the low dead rise impact problem be investigated on structurally representative models--if possible on an actual hull. (This would also be applicable to the impact of higher dead rise surfaces in the rolled condition.)

(2) The moderate yield allowable materials which will be used in hydrofoil ship structures may have appreciably greater life than the referenced seaplane hull structures. It is recommended that a brief life program be implemented to test a number of typical hull structure assemblies under repeated loads to determine their fatigue characteristics relative to seaplane or other structures which have been evaluated.

(3) In all of the analyses it must be recognized that the basic operation of the ship has been assumed. The two characteristics which most need substantiation--since they are most important to the final composite loads--are slamming behavior and sinking speed in the landing approach. It is recommended that occurrences of slamming and the landing approach conditions be measured under various simulated ASW tactical methods in several wave conditions.

7.0 REFERENCES

1. "Climatological and Oceanographic Atlas for Mariners," Vol. I, North Atlantic Ocean. Prepared by The Office of Climatology, U. S. Weather Bureau and Division of Oceanography, U. S. Navy Hydrographic Office, August 1959.

2. Pierson, W. J., von Newmann, G. and James, R. W., "Practical Methods for Observing and Forecasting Ocean Waves by Means of Wave Spectra and Statistics," Dept. of Meteorology, Research Division, New York University, New York, N. Y., July 1953.

3. "Martin Model 270, Water Loads Investigation, Hull Bottom Pressures and Impact Loads," ER 7516, the Martin Company, November 1955.

4. Pierson, J. D., Dinger, D. A.,and Neidinger, J. W., "A Hydrodynamic Study of the Chines--Dry Planing Body," ETT Report 492, SMF Fund Paper No. FF-9, May 1954.

5. Pierson, J. D., "On the Pressure Distribution for a Wedge Penetrating a Fluid Surface," ETT Report No. 336, SMF Fund Paper No. 167.

6. "Study of Permanent Set Behavior of Seaplane Hull Bottom Plating," Martin Company Report ER 7135, 1954.

7. "A Study of Fatigue Life and Structural Behavior of Seaplane Hull Bottom Plating," Martin Company Report ER 6659, April 1955.

8. Haire, Emory T., "Quantitative and Systematic Attack on Fatigue" (Fig. 5), Third Pacific Area National Meeting, ASTM, October 11 to 16, 1959.

9. Van Dyck, R. T., "Model Tests of Three 1/36-Scale Hydrofoil Hull Configurations in Calm Water and in Waves," Davidson Laboratory Report LR-825, 16 January 1961.

10. Lewis, E. V., "Ship Speeds in Irregular Seas," Paper presented at the Annual Meeting of the Society of Naval Architects and Marine Engineers, New York, N. Y., November 9 through 12, 1955.

11. Lewis, E. V., Numata, E., "Ship Motions in Oblique Seas," Paper presented at the Annual Meeting of the Society of Naval Architects and Marine Engineers, New York, N. Y., November 17 through 18, 1960.

12. Rossell and Chapman, "Principles of Naval Architecture, Vol. I," The Society of Naval Architects and Marine Engineers, 1947.

13. "Ships and Waves," Council on Wave Research and Society of Naval Architects and Marine Engineers (Chapter 18, Fig. 2), 1954.

14. "Analysis of Acceleration and Water Pressure Data Obtained on a P5M-2 in Moderately Rough Water," Martin Company Report ER 9918, March 1958.

15. Pauken, Julius E., "Statistical Analysis of Seaplane Fatigue," Aerospace Eng, Vol. 18, No. 11, November 1959.

16. Widmayer, E., "M-270 Water Loads Investigations--Structural and Impact Loads," Martin Company Report ER 7515, July 1955.